The interactions of cosmic ray neutrinos

Craig, R.

The Interactions of Cosmic Ray Neutrinos

A Thesis submitted to the University of Durham for the Degree of Doctor of Philosophy

by

R. Craig, Dip. Tech. Grad. Inst. P.

June, 1969

Frontispiece

SPECTROGRAPH 2

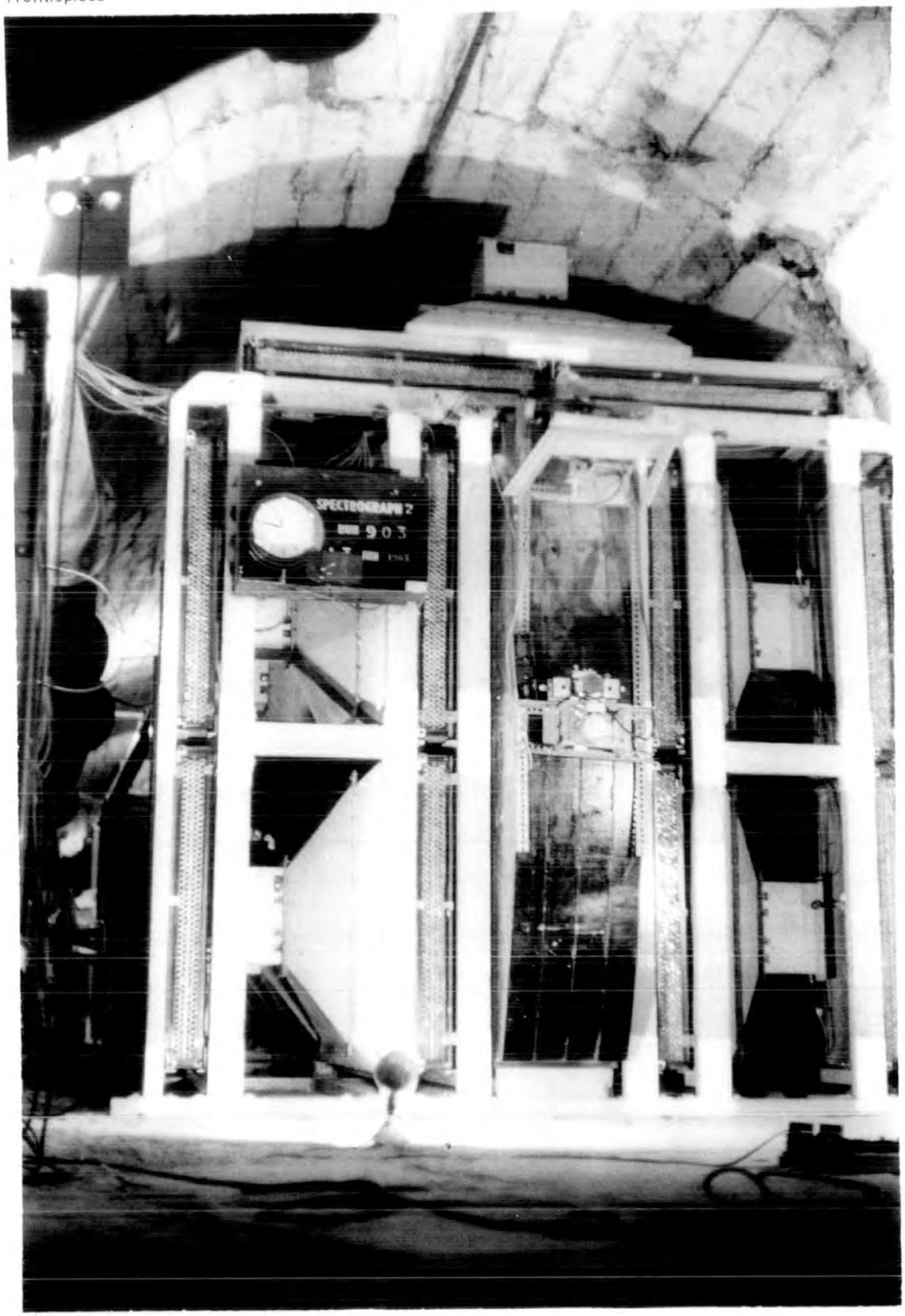

Abstract

A collaboration experiment between Tata Institute, Bombay, Osaka City University and Durham University has been performed underground at a depth of 7500 m.w.e. in Kolar Gold Fields, South India, primarily to study muons produced by the interactions of cosmic ray neutrinos. The results obtained are described and analysed.

The rate of neutrino-induced muons has been found to be less than predicted for several widely different assumptions made about the inelastic interaction cross section above 10 GeV (the limit of the machine data). However the results clearly show the importance of the inelastic interaction and suggest that the cross section continues to rise to $\gtrsim$ 30 GeV/c whilst the fraction of energy taken by the muon falls.

The energies of two neutrino-induced muons have been measured with magnetic spectrographs and neutrino interactions inside the detectors have been recorded along with unambiguous examples of upward moving muons.

Muons of atmospheric origin have also been detected and both their intensity and angular distribution have been established and described by appropriate expressions. Their energy spectra and mean energies have been predicted and compared with those derived from observations made of their electromagnetic accompaniment.

The celestial co-ordinates of the arrival directions of neutrino-induced muons may be suggestive of a possible point source of extra-terrestrial neutrinos and those of the atmospheric muons have shown a possible large scale anisotropy in the southern celestial hemisphere, the implications of which are discussed.

These results are compared with those of other workers and the future plans for cosmic ray neutrino studies are discussed.

Preface

The work reported in this thesis has been carried out by the author, between September, 1965 and September, 1968, as a member of an international team of scientists and technicians from Tata Institute of Fundamental Research, Bombay, Osaka City University, Japan, and Durham University. During this time, the author has been a research student working under the supervision of Professor A. W. Wolfendale.

Whilst in India, the author, along with his colleagues, was responsible for the construction, maintenance and operation of the apparatus and the improvements and refinements made to the techniques and methods used. The author's main contribution was to the erection and commissioning of the magnetic spectrographs with particular reference to the alignment of the spectrographs' flash tubes.

The calculations of atmospheric muon energy spectra were made in Durham along with the co-authors of the two papers by Craig et al. (1967; 1968a). The calculation of the mean energies, electromagnetic shower observation probabilities and telescope's apertures were made by the author and the interpretation of the results, calculation of rates, angular distributions, celestial co-ordinates and mean energies of detected results reported and those from the other underground experiments are also the author's responsibility.

The combined reports made by the international team after the author joined the group are those published by Menon et al. (1966; 1967a,b) and Krishnaswamy et al. (1968; 1969). The results and observations reported in those publications are revised using the data available to the end of

1968 and are given in the present work.

The study of the possibility of charged particle tracks in mica, summarised in Appendix 5, was made in Durham together with the co-authors of Craig et al. (1968c).

CONTENTS

CHAPTER 1

Introduction.

Throughout the development of modern physics, the researches of the physicist have steadily revealed the complexity of the sub-atomic particles. Increased energies and fluxes of particles, produced in accelerators, have lead to more and more intriguing observations in high energy nuclear physics.

The existence of particles was beginning to be apparent by 1895. Perrin showed that the cathode rays in the Crookes tube were charged particles in motion and Thomson was able to measure their charge to mass ratio.

Although the Crookes tube may be regarded as the ancestor of the modern accelerators, most progress in the field throughout the first half of the twentieth century came from the study of natural phenomena. In the early 1900's, not long after the study of natural radioactivity had lead to the identification of α , β and γ radiation, it became apparent that there was a radiation of extra-terrestrial origin - the cosmic radiation. Several of its properties were discovered and between 1930 and 1940 rapid progress was made through the discovery of both the positron and the muon. Following the Second World War, the existence of the pion, the kaon and the hyperons was established. In particular, the discovery of the pion, in 1947, was a great step forward as it confirmed Yakawa's theory of 1935, in explanation of the strong nuclear force.

The importance of this field of research had then become apparent and the development of the accelerating machines progressed rapidly.

Throughout the 1950's and 1960's, bigger and bigger machines have been constructed, the largest ones in operation at present being the proton accelerators at CERN, Brookhaven and Serpukhov. The high flux of accelerated particles, made available in machines such as these, have lead to the discovery of about two hundred sub-atomic particle-like resonances.

This combined work of physicists, studying natural and artificially-induced phenomena on the sub-atomic scale, has opened the door to a most interesting, and perhaps the most basic, field of study in Science.

1.1 Neutrinos and Weak Interactions

Not the least simple conception in this field is that of the neutrino, a particle which can possess very high energies, penetrate astronomical distances without interaction and have so small a mass, if any, that it cannot be measured. Since its postulation by Pauli in 1931, the neutrino has proved to be a most interesting particle. For its direct discovery, the physicist had to wait until 1956 when Cowan et al. finally confirmed it via inverse beta decay interactions in a multilayer target and scintillation counter assembled under one of the Savannah River nuclear reactors.

The first role assigned to the neutrino was to explain the shape of the beta decay spectrum by taking away the missing mass. The process was described by Fermi in 1933 in the first weak interaction theory. The same weak force is now known also to be responsible for the interaction of neutrinos and for the long-lived decays of a number of particles.

As Weak interaction theory is still being developed, there remains

doubt as to whether the intrinnic interaction has any energy dependence before modification by strong interactions. Two approaches may be made to this problem. One is to study purely leptonic processes and the other is to measure leptonic properties in mixed interactions, such as the scattering of neutrinos by nucleons, as has been done in the accelerators.

Following the predictions of Lee and Yang (1955), Wu et al. (1956) discovered the non-conservation of parity in the beta-decay of Co^{60}. As a consequence, weak interactions may be identified not only by their control of the behaviour of the neutrino but also by their violation of parity conservation.

After this important discovery, rapid progress was made in the study of the weak nuclear force which lead to the development of the V - A theory of weak interactions by Feynmann and Gell-mann. The V - A theory successfully describes the known processes at low energies in which strangeness is conserved. At higher energies, however, it breaks down. For example, the cross sections for interactions such as $\nu_e + e \rightarrow \nu_e + e$ and $\nu_e + e \rightarrow \nu_\mu + \mu$ are predicted to be greater than the limit set by unitarity for neutrino energies above 300 GeV.

One means of overcoming this difficulty at high energies is by the mediation of weak interactions through a vector boson of finite mass, such as the intermediate (W) boson proposed by Lee and Yang (1960). Any such mediating boson is predicted to be of large mass since studies of beta decay, polarisation of weak decay products and low energy reactor-neutrino interactions show that the weak force is of very short range.

So far, machine experiments have only shown that the mass of the

intermediate boson, if it exists, must exceed about 2 GeV. Future experiments, either in larger accelerators or in colliding beam arrangements for lepton- lepton scattering or nucleon - nucleon interactions, may well throw light on the existence or otherwise of this particle apart from giving a more complete understanding of the whole field of weak interactions.

1.2 Natural Sources of Neutrinos

Since the suggestion of Bethe and Critchfield in 1939, the fusion chain as the mechanism of energy production in the heart of hydrogen-burning stars has been widely accepted. Several of the reactions involved lead to the emission of neutrinos and the value to astronomers of the detection of these neutrinos is easily appreciated.

The neutrino experiment of Danby et al. (1962), carried out at the Brookhaven National Laboratory, in which the existence of two types of neutrino, the muon neutrino and the electron neutrino, was shown, has affected the approach to the field of neutrino astronomy. The electron neutrinos, produced in stellar interiors, can only give rise to electrons in their interactions (unless the reaction $\nu_e + e \rightarrow \nu_\mu + \mu$ is found to be possible) and, as a result of the low energies of such neutrinos, < 14 MeV, their presence can only be detected via processes such as $n + \nu_e \rightarrow p + e^-$ The identifications of the pair $p + e^-$ is not as easy as the identification of the pair $n + e^+$ via secondary γ rays as in the case of detecting reactor-produced antineutrinos.

A technique involving this interaction in Cl^{37} is being employed by Davis (1964) of Brookhavan in an attempt to detect solar neutrinos but as yet no significant rate has been recorded.

On the other hand, muon neutrinos, particularly at high energies, are more easily detected, as their interactions give rise to penetrating muons which can be detected by the conventional techniques of Cosmic Ray Physics. Very few muon neutrinos, however, are expected to be produced outside the Earth's atmosphere and it seems unlikely that a study of them in the cosmic radiation could be of any use to neutrino astronomy. That is not to say that a study of muon neutrinos in cosmic rays reaching sea level and below would be of little use. On the contrary, as the accelerating machines are restricted to low energies in comparison with cosmic rays, a study of cosmic ray neutrinos and their interactions at high energies is essential in extending our present knowledge, particularly with regard to the cross sections for neutrino interactions.

The production of atmospheric neutrinos is best understood with regard to the overall propagation of primaries and secondaries through the atmosphere.

From the results of experiments, in mountain research laboratories, aircraft, rockets, satellites and particularly balloons carrying nuclear emulsions, it has been possible for the composition of the primary cosmic rays incident upon the Earth's atmosphere to be established. Other than the extra terrestrial neutrinos previously mentioned, the vast majority of primaries are protons with about 6% alpha particles and much smaller fractions due to heavier nuclei, electrons and γ -rays.

Interactions of the primaries with air nuclei nearly all occur in the first 200 gm/cm^2 of the atmosphere and, if the primary energy is high enough ($\gtrsim 10^{14} eV$), they can produce a few tens of hadrons in one collision. Of the particles created $\sim 80\%$ are pions, and $\sim 20\%$ are

kaons along with a smaller number of baryons.

Proceeding to greater depths, nucleons continue to undergo nuclear interactions in which more pions are produced, the neutral pions decay very rapidly into γ - rays, which give rise to electromagnetic cascade showers, and the charged pions either interact with nuclei to produce more hadrons or decay to muons and muon neutrinos.

By virtue of their weak nuclear interactions and their time-dilated lifetimes, many muons survive to sea level and below. Consequently the charged cosmic radiation reaching sea level is primarily composed of muons to the extent of almost 80%, the remainder being made up of electrons with $\lesssim$ 1% protons and pions. (Those muons decaying before reaching sea level produce both electron and muon neutrinos.) At depths greater than a few meters underground only the muons remain along with the neutrinos.

Thus, it can be seen that the atmosphere and the Earth's surface can provide a natural filter for neutrino detectors situated deep underground. Only one main problem remains, that of removing or identifying muons of atmospheric origin.

1.3 The Nature of Particles Underground.

The early workers performing experiments for the detection of cosmic rays underground were well aware of the background radiation from local radioactive decay. The fractional contribution to the measured rates, on account of this background, increases with depth as the muon intensity decreases. Anomalous results recorded by some workers using only two or more unshielded layers of geiger counters have since been explained in terms of successive Compton scattering of γ - rays in the counter trays. To avoid the same effect, more recent workers have used lead-shielded

detectors and by and large the results obtained at various depths are consistent with one another.

Barrett et al.(1952) were the first to describe the angular distribution of underground atmospheric muons by the $\cos^{n}\theta$ form which follows from the depth intensity expression $I_v = Ad^{-(n+1)}$, where d is the depth. The establishment of such an expression was necessary for the calculation of effective aperture of the earlier apparatus, which did not include visual detectors.

A series of intensity measurements was made at various depths by Miyake et al.(1964) in a collaboration between Tata Institute of Fundamental Research, Bombay and Osaka City University. This series, which included the operation of telescopes at a depth greater than ever before, was followed by a similar series in the same mines by a team from Tata Institute and Durham University. This second series employed flash tubes to clarify the results, particularly with regard to electromagnetic accompaniment. The results were in good agreement with those of Miyake et al.and provided a useful contribution to the composite depth intensity relation built up over the years from the results of various experiments.

One of the most important results of this work was that the experiment of Miyake et al.recorded no events whatsoever at the greatest depth of 8400 m.we.(K.G.F. rock). It thus became obvious that at great depths it might be possible to detect muons produced in neutrino interactions in the surrounding rock.

1.4 The Cosmic Ray Neutrino Experiments

Two cosmic ray neutrino experiments were commissioned in the period late 1964 - early 1965, one as a collaboration between the Case Institute,

Ohio and the University of Witwatersrand situated in the East Rand Proprietry Mines, South Africa and the other as a collaboration between Tata Institute Bombay, Osaka City University and Durham University situated in the Kolar Gold Fields, South India.

The basic principles behind both experiments are the same, as well as their situations in Gold Mines. Operating sufficiently deep underground with detectors giving some degree of angular information, it is possible to identify near-horizontal penetrating particles which have been produced in the surrounding rock by neutrino interactions. Atmospheric muons, incident from near vertical directions, can easily be distinguished with the angular information available.

At this point the two experiments diverge. To have as large a detecting area as possible, to compensate for the low rate of neutrino events expected, the Case-Wits experiment originally consisted of two parallel walls of scintillators extending along each side of one of the mine tunnels. The K.G.F. experiment on the other hand, although covering a smaller area, was of a more sophisticated design, involving visual detectors interspaced with lead absorbers to give more information about the events.

Both groups reported the detection of the products of the first identified natural neutrino interactions in 1965. The K.G.F. group confirmed without doubt, through flash tube photographs, that one event was an example of an inelastic neutrino interaction (Achar et al., 1965), convincingly demonstrating the value of visual detectors in such an experiment. (The accumulation of more flash tube records has shown the complexity of many events detected which would have lead to ambiguity if visual detectors had not been employed.)

Still continuing, these two experiments have been extended both to detect more neutrino interaction products through larger detectors and to give more information about the events.

Another experiment designed to detect neutrino muons was commissioned in 1967 by the University of Utah group. Although no results on neutrino-induced muon events have yet been published, the apparatus is expected to provide useful information in this field. The principle behind the design is different from the other two experiments in that it is situated at a shallower depth employing Cerenkov detectors to identify upward-moving muons, presumed to be neutrino-induced.

1.5 The Development of the K.G.F. Experiment

The choice of location for the neutrino experiment was not a difficult one. The experiments of Miyake et al. and Achar et al. (Tata/Durham collaboration) had given useful data on atmospheric muon intensities underground in the Kolar Gold Fields. One of the difficulties of interpretation of underground results has been the normalisation of the depth of operation to an equivalent depth in standard rock. Bearing in mind the possible errors in this conversion, it was clearly desirable to perform the neutrino experiment under rock with known attenuation power, in order to have as accurate an estimate as possible of the atmospheric muon background.

The cross cut to Heathcote Shaft at 80th level in Champion Reef Mine, K.G.F. was chosen as an ideal site. Being over 10 ft. high and 12 ft. wide, supplied with electricity at 25 c/s and situated in the down cast ventilating air stream, usually at less than 35°C and 85% humidity, it provided ample space and comparatively good working conditions under 7600 ft. ($\equiv$ 7500 m.we. standard rock) of well studied rock.

Telescopes 1 and 2, fully described in the next chapter, were constructed initially for the main purpose of detecting unambiguously neutrino-indueed muons and pions.

Following the successful detection of the products of an inelastic neutrino interaction and at least two other possible neutrino-induced events, the experiment was expanded in the form of three additional telescopes, the purpose of which was two fold. Firstly, the increased aperture of the apparatus would increase the rate of events and enable a more accurate estimate of the intensity of neutrino-induced muons to be made. Secondly vertically mounted flash tubes were introduced along with the horizontal ones as used in Tels 1 & 2, interspaced between thicker layers of iron absorber. The resultant increased angular resolution and increased penetration required of the particles was to give a better estimate of the interaction points in the rock for multiparticle events and to help to distinguish between muons and pions. These telescopes were commissioned in March 1966 and operated along with Tels 1 & 2.

It became obvious, from the electromagnetic accompaniment of the events recorded in the five telescopes, that the neutrino-induced events were, as expected, of much lower mean energy than the atmospheric muon events, being most probably in the range of a few GeV to a few tens of GeV. Thus the operation of spectrographs came to mind as a workable proposition. However, the cost of building spectrographs of sufficient aperture to measure the momentum of, at the most, a few neutrino-induced muons, did not seem to be justified when at the same cost a much larger array of telescopes of the Tels 1 & 2 type could be constructed. Fortunately, before the decision was taken, a generous offer was made by

the Yawata Iron and Steel Co. Ltd. of Japan, to donate the required magnet iron. The offer was accepted.

Spectrographs 1 & 2 became operative in mid - 1967. Their design is essentially for the detection of neutrino-induced muons but also includes sets of scintillators to aid the detection of atmospheric muons, the nature of which is of great importance at such depths.

The final development in the experiment was partly triggered by the manifestation of one of the difficulties of operating an experiment in such a remote situation, namely the lack of a high flux of background cosmic radiation for testing the apparatus. Throughout the first 10 - 11 months of 1967, Tels 3, 4 and 5 failed to yield any events to add to the total of 6 recorded during 1966. Regular maintenance tests were made on the apparatus but, without any penetrating cosmic rays to simulate genuine events, there was doubt about whether or not the apparatus had been functioning correctly.

Beginning in January 1968, Tels 3, 4 & 5 have been operated successfully on a 2 - fold coincidence (one side triggering) arrangement as opposed to their original 4 - fold operation as in the other detectors. Essentially the same circuitry has been employed, as before, and, in the absence of definite evidence regarding the erficient or inefficient 4 - fold operation in 1967, the running time for that year has been rejected.

The present situation may be briefly summed up as follows. Tels 1 & 2 and Specs. 1 & 2 are recording events, as they have always been, on 4 - fold coincidence triggering, whilst Tels 3, 4 and 5 are yielding a higher rate of events operating on 2 - fold coincidence triggering. Since the commissioning of the experiment in 1965, well over 200 events

have been recorded in all, of which at least 14 were neutrino-induced.

The following chapters describe the apparatus involved in the K.G.F. Neutrino Experiment, its construction, efficiency and monitoring, the results obtained and the interpretation put upon them. Comparisons are given between intensities and angular distributions of muons expected and observed and between the expected and observed mean energies of muons underground. The celestial co-ordinates, calculated from the directions of the observed events are examined and finally, in Chapter 9, the information gained from the experiment is assessed, compared with that from similar experiments and used as a guide in anticipating future work and the contribution it may make to our knowledge of the phenomena under study.

CHAPTER 2

The Experimental Apparatus.

2.1 The Design of the Detectors.

2.1 1 Telescopes 1 and 2

The construction of the first 2 telescopes can be seen in the diagram fig. 2.1. Two walls of plastic scintillater 3m high and 2m wide are split into 1m ^{2} sections, each section being viewed by a pair of 5" diameter photomultipliers. The enclosure for each scintillator element is in the form of a 4 sided pyramid with scintillator blocks, $4 \times (0.5\ m^2)$, being held in the base and the photomultipliers mounted on a light tight box at the apex. The internal surface of the pyramids are painted white to allow diffuse scattering of the scintillator light.

Separated by 80 cms, the two 5 cm. thick walls of scintillator enclose 3 layers of neon flash tubes separated by 2 walls of 2.5 cm thick lead absorber. The flash tube layers are composed of 3 trays, each containing a total of 214 tubes packed in 4 columns, mounted one above the other. The flash tubes 2m long, lying horizontally parallel to each other in each tray, are arranged such that the two inner columns are staggered by $\frac{1}{2}$ tube diameter to those in the outer columns to reduce to a minimum the effect of the dead space between tubes. An aluminium sheet 2m x 1m between the inner columns of tubes, positioned by teflon insulators, serves as the high voltage electrode and two similar sheets, one outside each of the outer columns of tubes, provide the earthed electrode.

The two lead absorber layers are of the same height and width as the

FIG 2.1: Front View of Telescopes 1&2

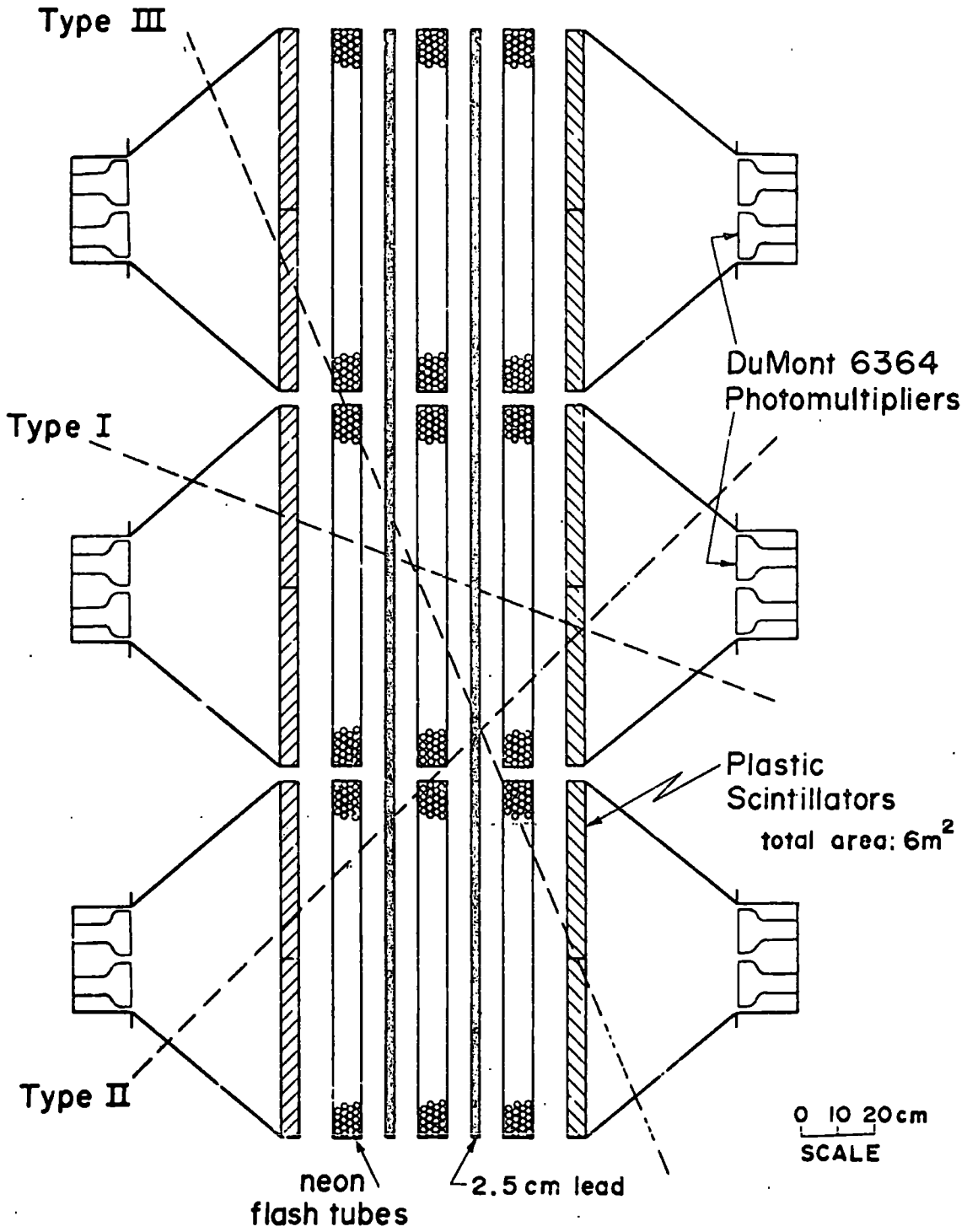

scintillator walls such that a particle creating a 4 - fold coincidence by passing through both walls must have penetrated all three layers of flash tubes and 2 layers of lead also.

Telescopes 1 & 2 face each other separated by a distance of $\sim$ 6 m. 3 cameras are mounted on the front of each, arranged so as to view the other telescope. The top and bottom cameras are mounted so that each view about $\frac{2}{3}$ of the telescopes flash tubes. The middle cameras view the complete telescopes but lie at a large angle from the axes of the most extreme flash tubes and thereby receive a reduced intensity. For this reason the middle cameras were regarded as reserves in case of failure of one or both of the others.

2.1 2 Telescopes 3, 4 and 5

As already mentioned, the reason for building telescopes 3, 4 and 5 was not only to increase the size of the detecting area but also to have detectors giving more information regarding the nature of the neutrino induced events.

Basically of the same design as the first two telescopes, 3, 4 and 5 incorporated 2 layers of vertically mounted flash tubes and four layers of 7.5 cm iron absorber instead of lead. The construction can be seen in fig. 2.2. The need for a reasonable optical path length above the telescopes for viewing the vertically mounted azimuthal flash tubes necessitated the reduction in height to 2 m. The width of the scintillator walls is the same, 2 m.

Partly to keep the space required to a minimum and partly to enable the use of only one camera per telescope without viewing the flash tubes at large angles, mirror systems were arranged for each telescope. These

FIG 2.2: Front View of Telescopes 3,4 &5

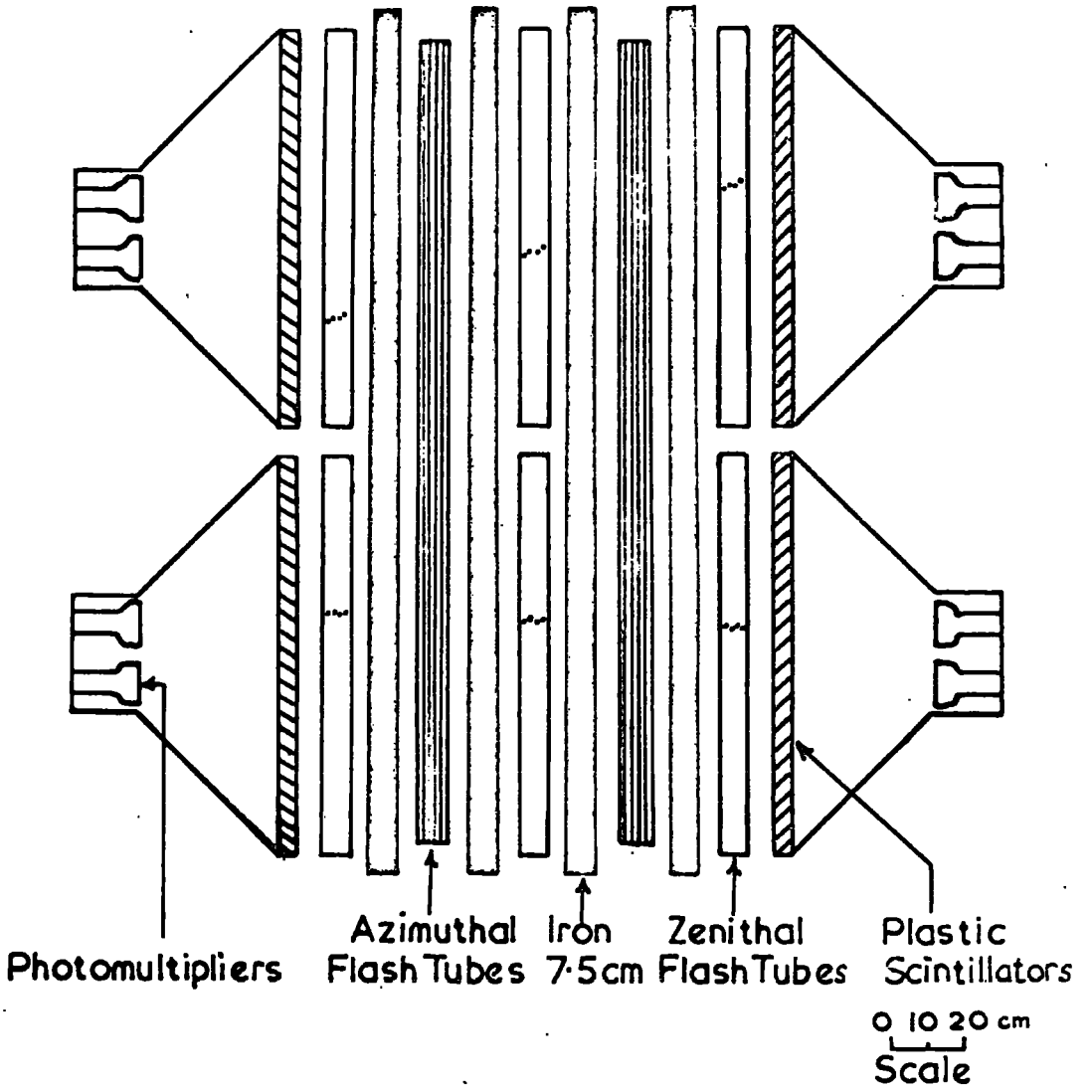

were very successful for the horizontally mounted (zenithal) flash tubes but involved 3 reflections of flash tube light at a large angle for the azimuthal tubes. The use of the fastest film available (Ilford H.P.S.) and large aperture cameras (Cannon) helped to overcome the consequential difficulty of lack of brightness. Recently, perspex prisms have been fitted so as to enable the tubes to be viewed virtually along their axes. This has greatly improved the image brightness.

2.1 3 Spectrographs 1 & 2

The Spectrographs are intended for measuring the energy of neutrino induced muons. They have, therefore, been designed to present their greatest aperture to particles travelling in the horizontal direction as can been seen in fig. 2.3.

Two layers of flash tubes on each side of the magnet enable the estimate of track location to $\sim 0.2^{o}$ projected zenith angle.

To provide additional information on atmospheric muons, four scintillator elements were positioned on top of the spectrographs, together with a layer of flash tubes, such that 4 - fold coincidences are accepted between North and South side scintillators and top and either side scintillators also.

It was not expected that the energy of atmospheric muons would be measured with these spectrographs firstly because of the estimated high mean energy of the former and secondly because of the poor geometry presented to near-vertical particles.

The scintillator boxes, for space conservation, are not so deep as those used in the other detectors but have been shown at Tata Institute

FIG 2.3 Front View of Spectrographs 1&2

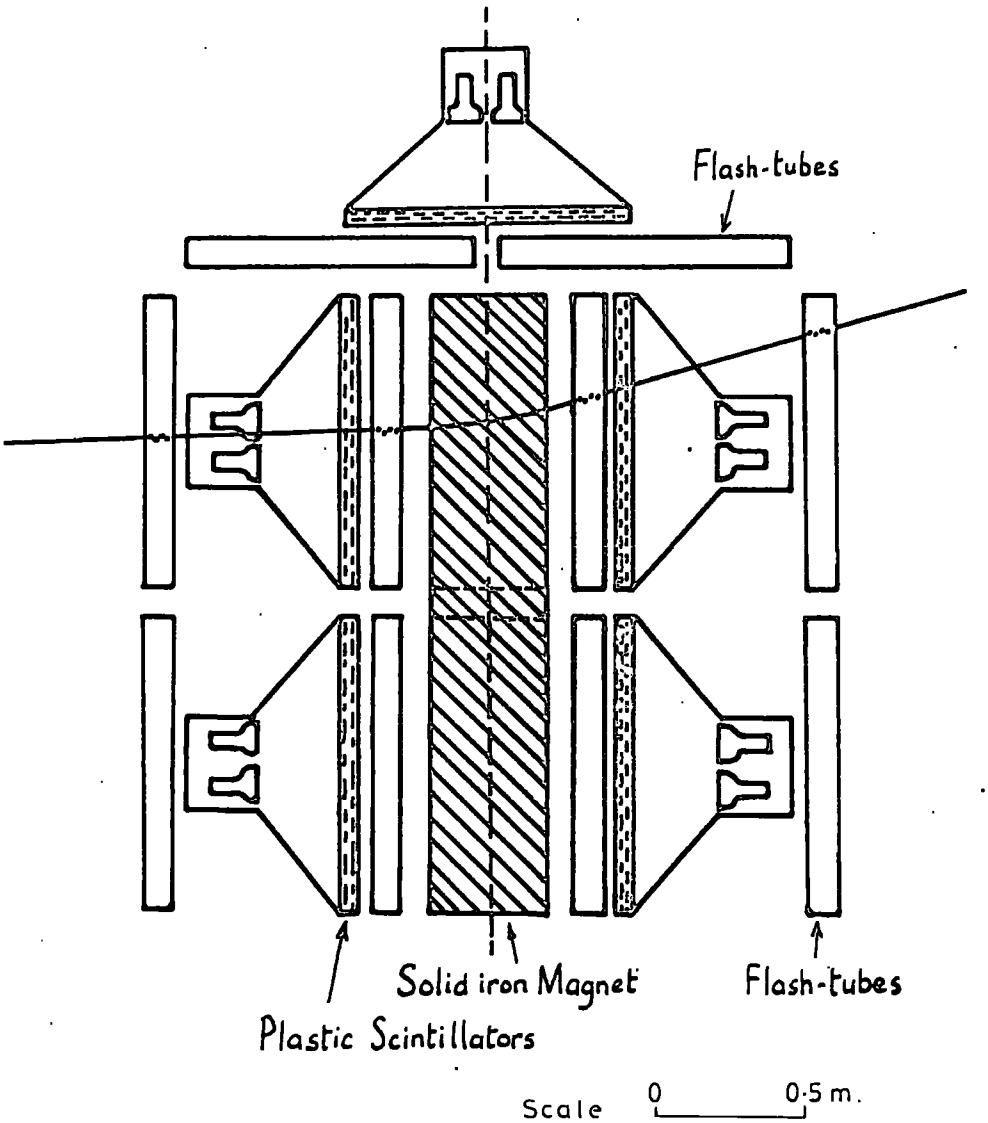

to have virtually as good light collecting efficiency. They also have a base 1 m^2 housing 4 scintillator blocks 5 cm thick.

Each spectrograph is $\sim$ 4 meters long and incorporates 'back to back' 2 m flash tubes. It has, therefore, to be viewed from both the front and the back. This is achieved via mirrors for the Spectrograph 'backs' and directly for the 'fronts' which face each other with about 11 m separation.

The magnets themselves consist of about 40 tons of iron blocks ($< 0.1\%$ carbon). 40 sections are welded together to give each magnet the dimensions 2.1 m high, 4 m long and .4 m thick. A slot 10 cm high, for taking the windings runs 35m along the centre of each magnet. Welded to the ends of the magnets are curved end pieces for maintaining a smooth flux shape.

Aluminium strips 5 cm wide and 0.5 cm thick are used for the coil winding in the two sections of each magnet, one for the upper arm and one for the lower. The power supplies provide currents of 0 - 300A at a voltage 0 - 10V. A study of the magnetic induction in the two arms of the magnets showed that it saturated at $\sim$ 14.5 kilogauss for $>$ 220A. The fringing fields of the magnets were used as a guide to the uniformity of the flux throughout the magnet. The field was found to be quite uniform along the region covered by the winding but of reduced intensity near the extremeties of the two arms. To eliminate the complication of estimating the energy of muons deflected in these regions, the adjacent scintillators were partly blanked off, as shown in fig. 2.5.

The maximum detectable momentum (m.d.m.) not only depends on the strength of the magnetic field and the distance between the 2 flash tube layers in each arm but also on the configurations of the flashed tubes. Some configurations permit a large variation both in angle and position

of the particle trajectories themselves whereas others, usually by virtue of the particle passing through inter-tube gaps, do not. The average m.d.m. has been estimated to be $\sim$ 20 GeV/c but under certain circumstances it may approach 30 GeV/c.

The complete arrangement of detectors in the laboratory is shown in fig. 2.4.

2.2 Spectrographs flash tube alignment

In the construction of Telescopes 1 - 5, the flash tubes were optically insulated from each other via a continuous sheet of 'fablon' black plastic sheeting. The flash tubes were inserted into the trays enwrapped by the fablon in a continuous 'figure 8' manner. This method was somewhat crude and did not give very uniform packing as regards the horizontal and parallel positioning of the tubes. The tendency was for the tubes to form a fan shape being closer at the back than the front.

For the construction of the spectrographs, individual fablon sleeves were used for each flash tube. Careful packing enabled the horizontal alignment of all tubes to better than $\sim$ 0.4 cm back to front difference with respect to the base support of the tray. (In most cases the error was 0 - 0.2 cm).

The heights of every 10th tube in the inner columns of flash tubes in every tray were measured above the base level at both the front and back (See fig. 2.5). The height of a sighting bracket at the back was also measured.

A system of Cartesian Co-ordinates was marked on the spectrograph framework such that the 'horizontal' base line was the same height with respect to the magnet at the front and the back (The magnets were not

FIG 2.4: The Laboratory Arrangement

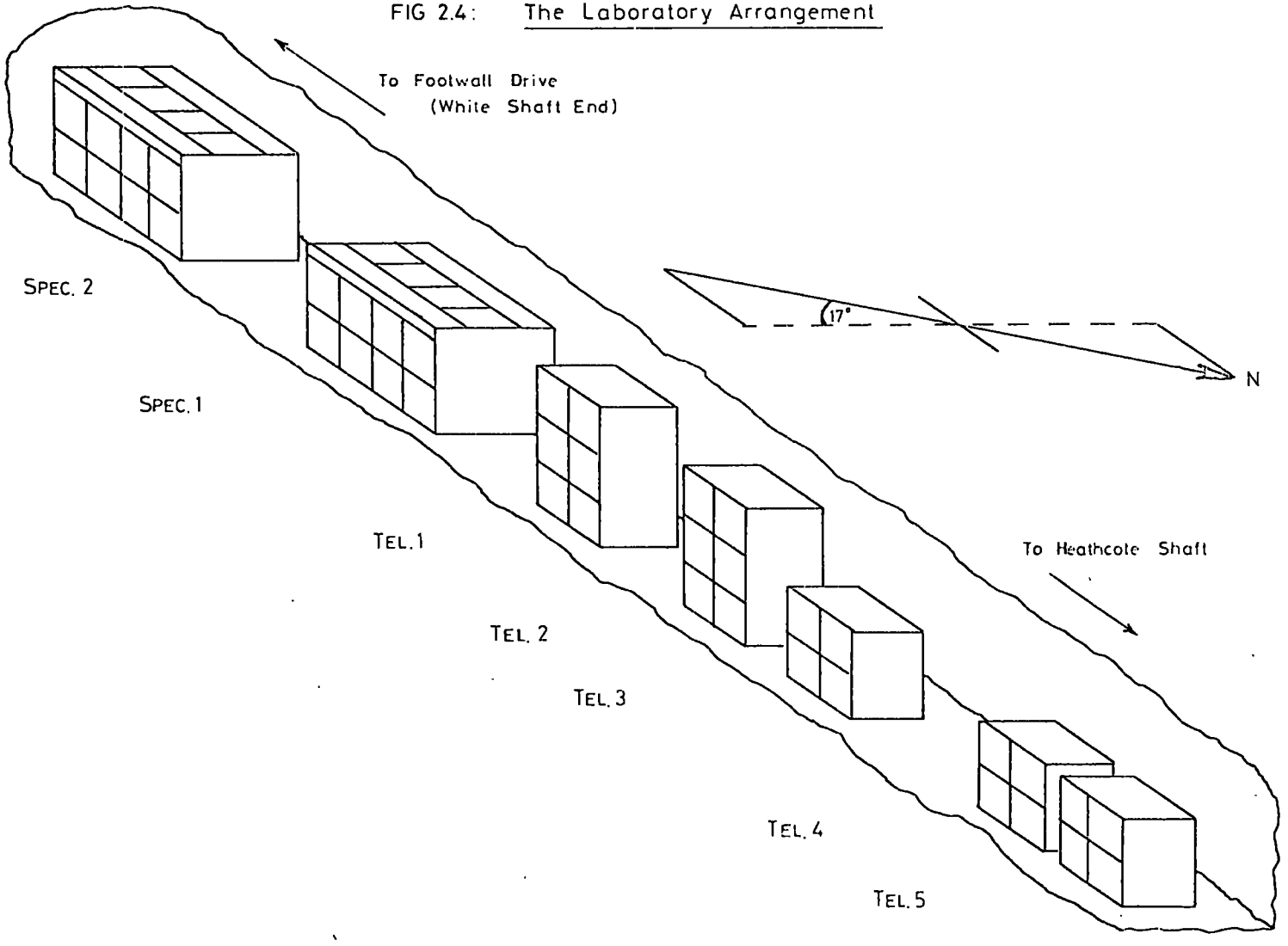

FIG. 2.5: Spectrographs' Flash Tube Alignment

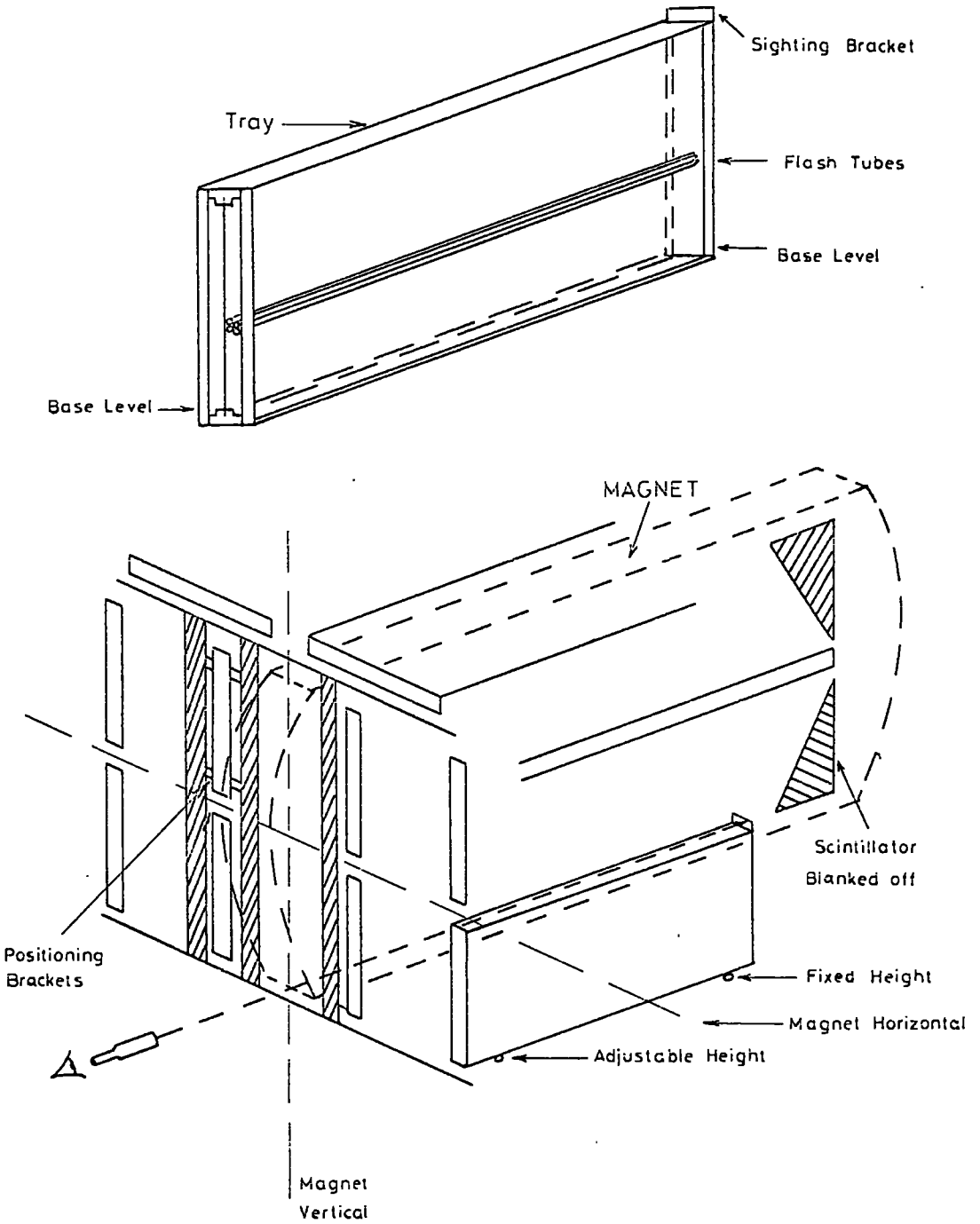

positioned truely horizontal.) The vertical base line was a true vertical,

As the flash tube trays were moved into position, a cathetometer was used to site the bracket of the rear of each tray so that, with the previous measurements of the tubes in each tray known, the tray could be raised or lowered at the front until the majority of the tubes were parallel with the magnet. (Although there was a variation from tube to tube in each tray, the majority could be aligned correctly and the ones which were not were of known deviation.) The trays involving the greatest packing errors $\epsilon > 0.2$ cm were installed in the horizontal positions where accuracy is not so important.

Through - sighting with the cathetometer was used for the vertical alignment and back - to - back alignments of the trays. They were, thereafter, held rigidly in these positions both at the front and back by templates extending to the adjacent frame work girders.

For each of the measured flash tubes it was possible to establish co-ordinates of their positions. Interpolation can then give the co-ordinates of any of the 8500 tubes.

The extent of bowing of the tubes along their length has been investigated and is estimated to give an error of $\pm$ 0.5 m m. The greatest error arises in the uncertainty of the position of transit of a particle across the tube in cases of tubes which are higher at one end than the other. The crude scintillator azimuthal information can be useful in these cases. Thus sometimes the tube height error for the vertical trays may be $\pm$ 1 m.m. and in others $\pm$ 0.5 m.m.

The possibility of some tubes settling into position over a period of time has been investigated but no changes $>$ 0.5 m m have been measured.

2.3 The System and its Operation.

The linking of the ciruitry associated with each telescope has been continuously improved and modified during the development of the experiment. The description which follows is of the final arrangement after the commissioning of the one side triggering of Tels 3, 4 & 5. The more fundamental aspects of the system have remained unchanged. Only the interconnections and associated circuits have been modified.

Fig. 2.6ais a block diagram of the circuitry from photomultiplier pulse to 4 - fold coincidence generation between scintillator elementsin each wall of Tels 1 & 2 and Specs 1 & 2.

From the photomultipliers (Du Mont 6364 and E.M.I. 9579 B), the signals are preamplified in the photomultiplier boxes. The signal from each preamp. is fed to the main amplifier which gives two outputs, one linear and one shaped after discrimination. The discriminator outputs of the two channels from each photomultiplier box pass into the 2 - fold coincidence unit where they are combined with those from the other boxes in the same scintillator wall. The 2 - fold coincidence output is then combined with that from the other scintillator wall of the telescope in an A N D gate in the 4 - fold coincidence circuit. (In the case of the Spectrographs this A N D gate has 3 inputs.)

The linear outputs of each pair of photomultipliers are added and fed through a delay line to an O R gate mixer when all the pulses from one wall of scintillator are combined before amplification for display on an oscilloscope. The delay lines are so arranged as to delay the added pulses from each pair of photomultipliers by successive multiples of $5\mu s$.

FIG 2.6a: Telescopes 1&2 and Spectrographs 1&2 Coincidence Circuitry

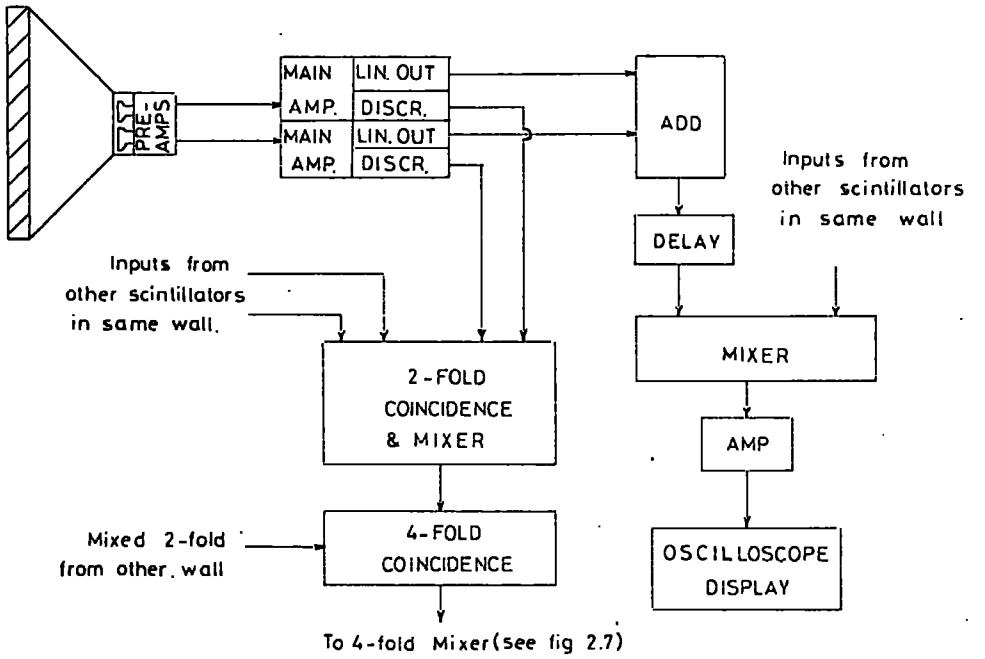

FIG 2.6b: Complete Circuitry of Telescopes 3,4&5 O.S.T.

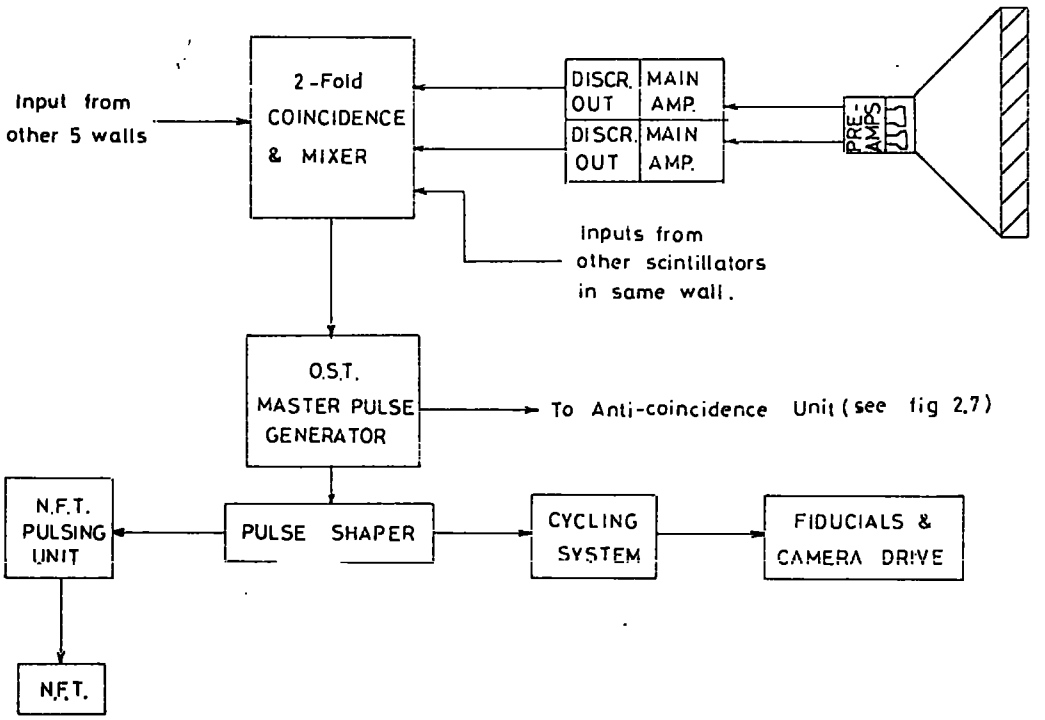

FIG 2.7: Master Pulse Generation & Distribution (Tels 1&2, Specs 1&2)

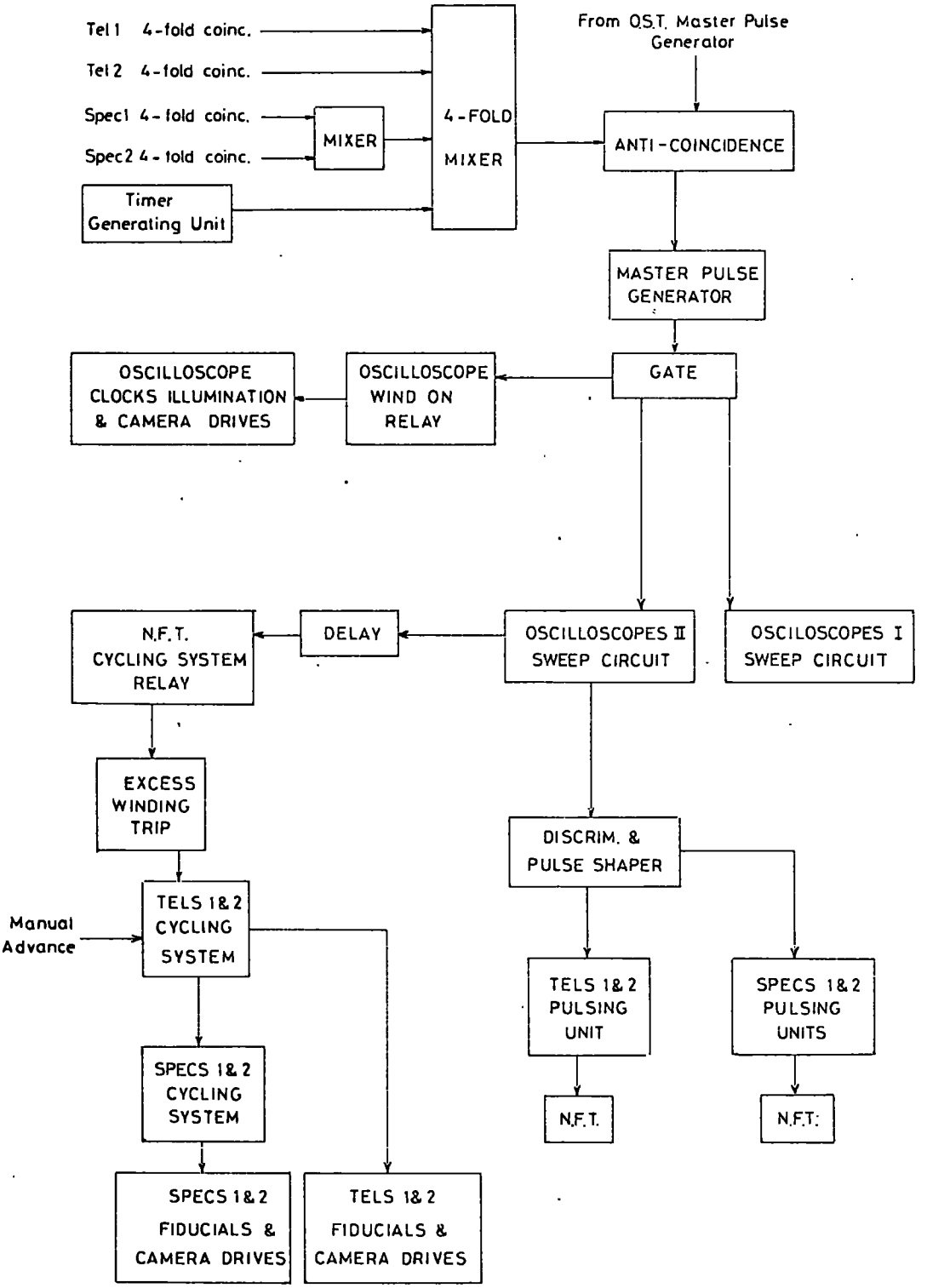

As the complete sweep of the oscilloscope time base is $\gtrsim 30\,\mu s$, the pulses observed can be identified with different photomultiplier pairs according to their positions. The 0 R gate does not operate selectively in cases of several pairs giving pulses but accepts them all for display as individuals by virtue of their various time delays. Continuing in fig. 2.7, the 4 - fold coincidence pulses from Specs 1 & 2, Tels 1 & 2 and the 'timer unit' are fed through an 0 R gate into the Master Pulse Generator. In this way a coincidence in any of these detectors gives rise to a master pulse which ultimately leads to the pulsing of the neon flash tubes in all four detectors. (The 'timer unit' is a seperate system which generates artificial 4 - fold coincidences once per 2 - 3 hrs. The unit is employed because of the necessity to trigger the camera wind on system as light leakage begins to fog the film in the open shutter cameras when it is exposed for $\gtrsim$ 3 - 4 hrs.)

The output of the Master Pulse Generator passes through an anti-coincidence circuit (described later) to the gate circuit. This rejects all 4 - fold pulses for the succeding 8 sec. whilst the wind on operation takes place.

Three outputs are taken from the gate circuit, one to trigger the oscilloscope wind on relay, one to trigger the sweep of the oscilloscopes displaying Tels 1 & 2 2 - fold pulses and the other to trigger the sweep of the oscilloscopes displaying Specs 1 & 2 2 - fold pulses. A delayed output from the latter unit is used as a trigger for both the neon flash tube pulsing units and the flash tube camera wind-on trigger relay. This enables the 2-fold pulse shapes to have been recorded before being obliterated by the severe pick up resulting from the high voltage

flash tube pulse. The pulsing units, described in section 2.6, require a long pulse of $\geq$ 10 μs. and $\geq$ 30 volts in order to ensure the firing of the thyratrons. This is provided by a pulse shaper unit which includes a discriminator to eliminate spurious triggering from O.S.T. pick up.

The oscilloscopes are arranged in two groups, each viewed by a camera. The four corresponding to the four scintillator walls of Tels. 1 & 2 are housed in a viewing box which also contains an illuminated clock. The illumination is triggered by the oscilloscope wind on relay and immediately afterwards the camera winds the film to a clean frame. The same arrangement is used for recording Specs 1 & 2 scintillator pulses which are displayed on 6 oscilloscopes, each with 4 different delay times for the 2 - fold pulses. The limited number of oscilloscopes available necessitate the adding, for display, of the 2 - fold pulses of vertically adjacent photomultiplier boxes in the vertical scintillator walls of the spectrographs. The loss of information resulting from this is of no importance as the flash tube information provides the projected zenith angle from which the upper or lower scintillator giving the 2 - fold pulse can be identified.

All of the telescopes are also provided with clocks and date boards. The 'flash tube' wind-on relay operates a cycling system based on a low geared d.c. motor operating microswitches through a camshaft. The first microswitch completes the fiducial light, clock and date boards illumination to be followed shortly afterwards by the second which winds on the cameras. Two such winding systems are employed, one for the Tels. 1 & 2 and one for Specs. 1 & 2. The former is connected to be the master and contains a trip circuit with a maximum of 45 pulses to prevent the loss of film through

repeated cycling caused by a fault elsewhere. Manual wind-on switches are fitted at the two exits to the laboratory to enable clean frames to be brought into position at the start of each run.

For the one side triggering of Tels 3, 4 & 5, the master pulse is generated immediately after the 2 - fold mixing circuit. (See fig. 2.6b) No oscilloscopes are available for displaying the pulses and the flash tube cameras, fiducials etc. are operated directly by a relay - driven cycling system triggered by the gate circuit output.

The greater number of one side triggering coincidences results in many more flash tube pulsings than in the other detectors. The pick up from the few pulses in the latter is accepted by the OST coincidence circuitry and results in typically an additional 10 - 15 frames per night, most of which are created by the 'timer'. This is negligible compared with the total of about 200.

On the other hand the pick up of the OST flash tube pulsing by the other detectors is much greater and cannot be tolerated in terms of film wastage. The anticoincidence overcomes this by rejecting any 4-fold pulse in Tels 1 & 2 and Specs 1 & 2 which is accompanied by an OST master pulse.

2.4 Coincidence and associated circuits

Both the preamplifier and main amplifiers are transistorized Japanese commercial products. The former consists of 2 cascaded emitter followers, followed by 2 main stages of amplification, and ends with a further 2 emitter followers. Feedback is built in throughout to preserve the pulse shape. With a gain of 30 x the pulse is fed to the main amplifier which is directly coupled with 4 main stages split into 2 sections of 2 stages. Each section ends in an emitter follower with feedback to the first stage

of the section. The output, amplified 100 x, is then split. One, the linear output, leads to the oscilloscope display and the other serves as an input to a Schmitt trigger. The latter is included so as to give a fixed output pulse for any input signal over the triggering level. It therefore acts as a discriminator.

The 2 - fold coincidence circuit adds the pulses from each pair of photomultipliers, passes the combined pulse through an OR gate along with the other 2 - fold pulses, from the same scintillator wall of the telescope concerned, and on to the discriminator. This method of 2 - fold coincidence generation is based upon the fixed outputs of the Schmitt triggers. A single channel pulse would have a voltage of ~ 3 volts and a double would have nearly twice this. Setting the discriminator at 4 - 5 volts satisfies the coincidence demands.

The master pulse circuit consists simply of a monostable multivibrator followed by a pulse amplifier.

The gate circuit uses the master pulse input to trigger a bistable multivibrator which feeds a monostable multivibrator. The former rejects all input pulses until the long time constant pulse decay in the latter reaches a bias level required to reset it. As mentioned previously, the time constant of the monostable section leads to a dead time of ~ 8 sec.

The delay circuit, used to withhold the flash tube pulse trigger, is built into one of the oscilloscope sweep generator circuits. It is a monostable multivibrator followed by a rectified differentiating circuit which only gives an output on the return sweep of the multivibrator. The time constant used gives a delay of $\sim 35\,\mu s$ which easily covers the sweep time of the oscilloscopes.

2.5 Neon Flash Tubes

The neon flash tube was first introduced by Conversi and Gozzini in 1955 and its properties have been well studied since then (e.g. Coxell, 1961.) Nevertheless, some aspects of its behaviour are not fully understood when it is operated with different types of pulsing systems particularly at very high voltages. (see section 2.7.) The efficiency variation with field given by Coxell is shown in fig. 2.8 together with the angular variation of the light output intensity.

The tubes used in the present experiment are 2 m long 1.76 mm external and 1.59 mm internal mean diameter. They are painted black at the seal end and white at the window end to enhance the light output. They are filled to a pressure of 60 cm Hg with commercial neon (98% Ne, 2% He).

Their successful operation depends upon a rapid rise time of the high voltage pulse to avoid clearing the ion pairs before the breakdown potential is reached, as high a field as possible for maximum efficiency without excess spurious flashes and a short delay time between the traversal of the charged particle and the pulse application. The time delay of $> 30\mu s$. demanded by the oscilloscope display system only results in an efficiency drop of a few percent from the value with no time delay for 60 cm Hg pressure tubes. The other requirements can only be met by the pulsing units and discharge circuitry used.

Care over the angle of observation of the tubes has been taken and no tubes are viewed at an angle greater than 8° from their axes.

2.6 U.H.T. Pulsing Units

The most common pulsing unit used in the experiment is the M K III shown in fig. 2.9. It consists of a 2 - stage R - C coupled amplifier

FIG. 2.8a: Flash Tube Efficiency - Field Characteristics

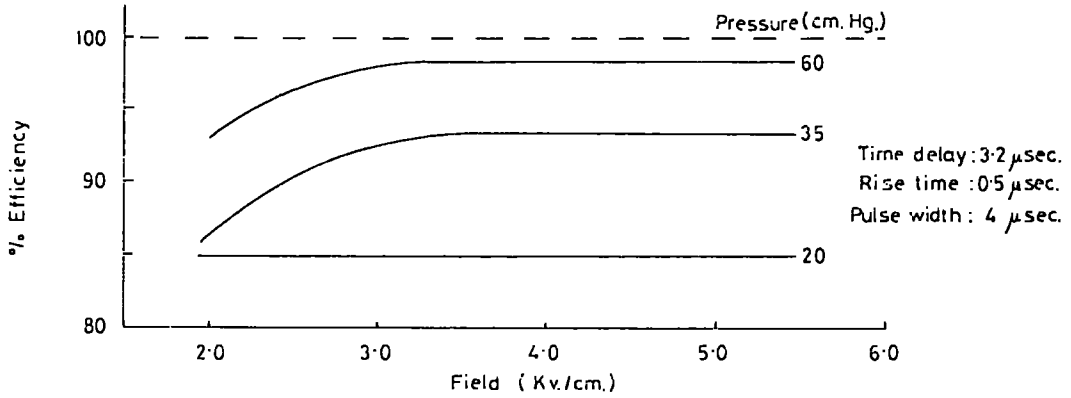

FIG. 2.8b: Angular Variation of Flash Tube Light Intensity

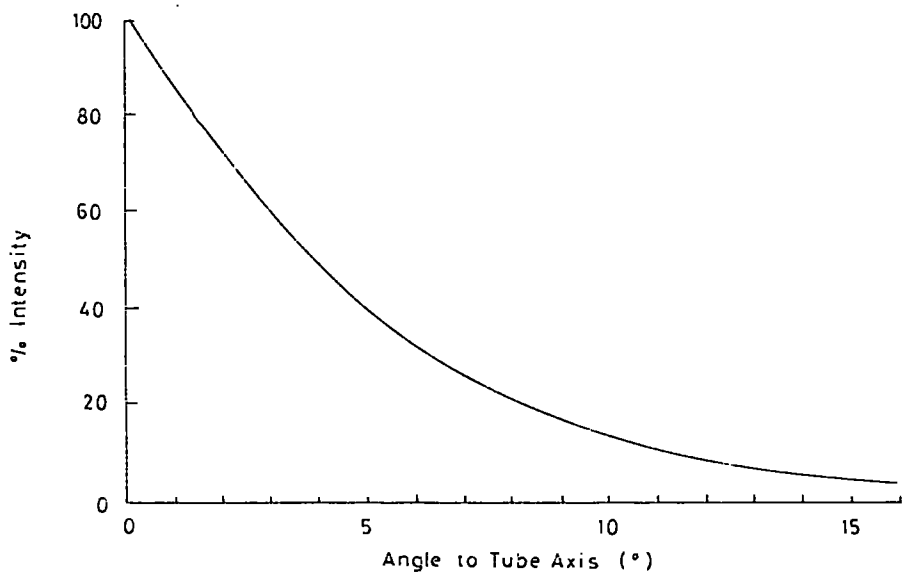

FIG. 2.8c: Layer Efficiency Variation with Load Capacitance

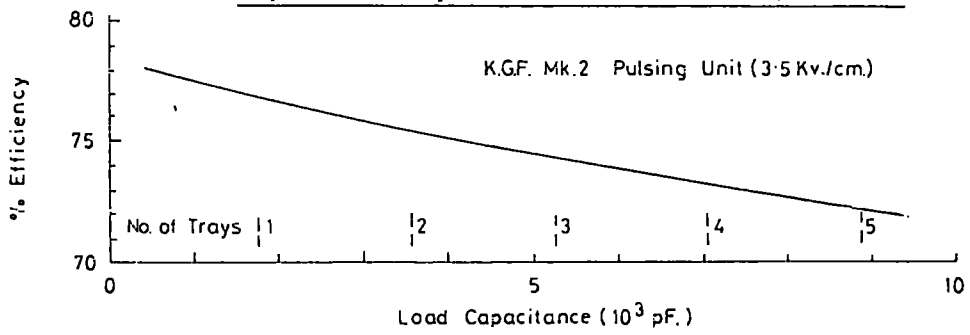

with a cathode follower to supply the pulse to the thyratron grid. The thyratron only switches ~ 4 KV which is used as a trigger for the surge diverter. The surge diverter is a cold cathode tube capable of passing ~ 2000 amps. This property makes it most useful for the discharge of up to 16 discharge circuits, 4 of which are shown.

Previous circuits (MK II) used the thyratron directly as the switch for the discharge circuit but the current restriction of 200 amps only permitted the discharge of one discharge circuit and several units were required.

More recently some circuits have been modified to use a high ratio pulse transformer to trigger the surge diverters. These have the advantage of not needing the bulky high current heater transformer required by the thyratrons.

The variation of flash tube layer efficiency with the number of K.G.F. flash tube trays being pulsed from one discharge circuit has been studied using a MK II unit with TCC Visconol 0.04 μF High Voltage condensers. The variation for a standing voltage of $12 \cdot 5$ KV on the condenser is shown in fig 2.8. (The maximum value of the layer efficiency depends on the flash tube dimensions and is $\sim 80\%$ for the K.G.F. tubes.) Although the efficiency of tubes tested using the Visconol condenser does not fall very rapidly with increased load (i.e. no. of trays pulsed), the brightness falls off more rapidly and the effective efficiency as recorded on the film is reduced. For this reason Visconol condensers were never used to pulse > 4 trays from the same discharge circuit.

The inductance in the discharge circuit has been shown to have a large effect on the efficiency and brightness of the tubes. Much of this

FIG. 2.9: K.G.F. Mk III Pulsing Unit

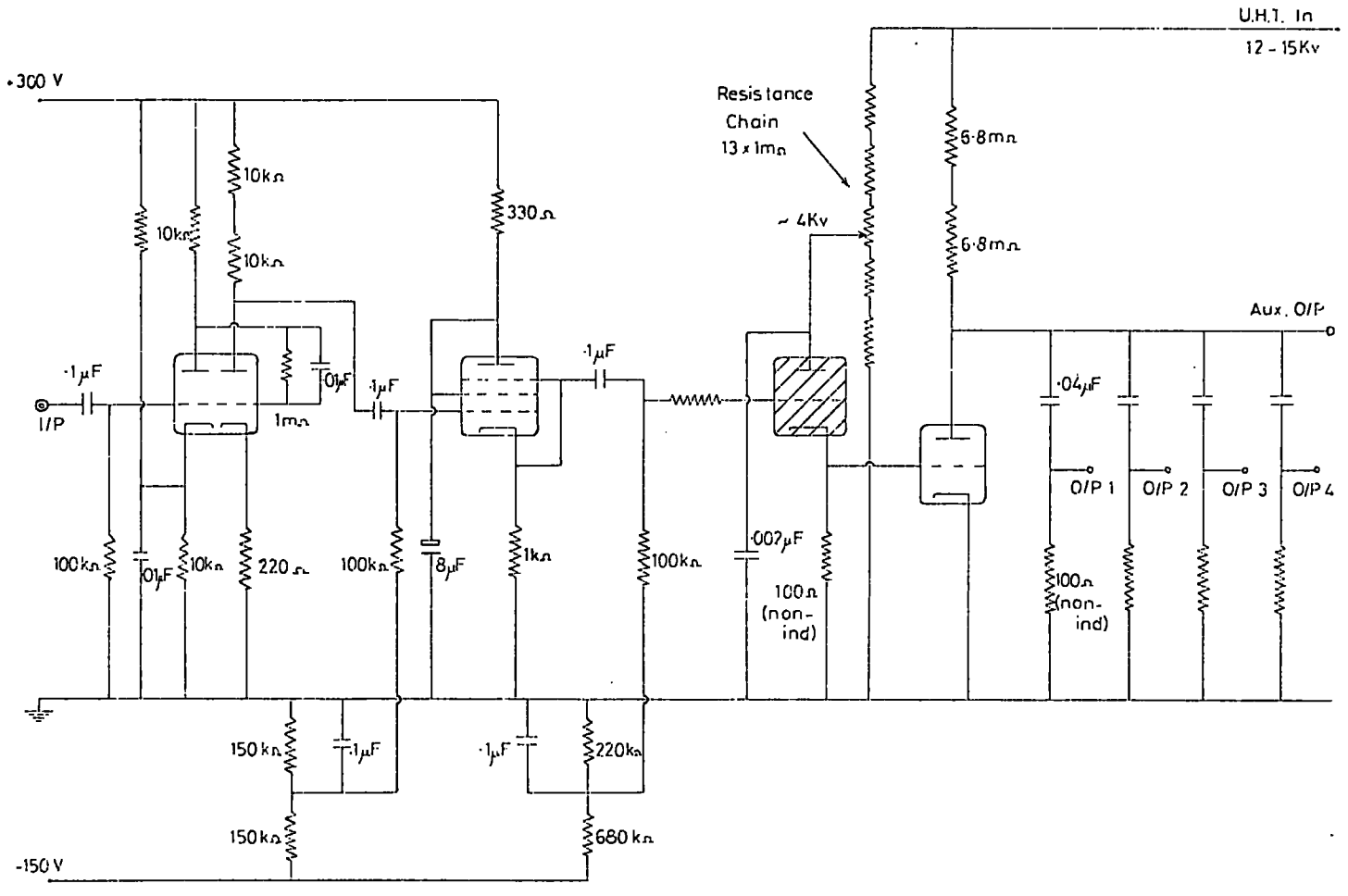

inductance is estimated to be in the condensers themselves. Variations in brightness and efficiency have been observed in the same trays pulsed by the same unit at the same voltage with only a different type of condenser being used. P.C.I. 0.05 μF condensers have been found to be very satisfactory in this respect and have been used successfully to pulse up to 6 trays from one discharge circuit whilst still maintaining a high brightness and efficiency. Hivotronic 0.13 μF condensers, coupled to a 50 Ω non-inductive resistance, have also been shown to give good results.

Therefore, according to the components and cable used in a given section of the detectors, the U.H.T. supply voltage has been adjusted over the range 12 - 15 KV to give high efficiency coupled with a low rate of spurious tubes.

2.7 Operation and Testing Procedures

Before the commencement of each run all flash tube trays were pulsed and observed for spurious flashes to ensure that all circuits concerned were on. The cameras were all wound on via the 'manual' switch at least one frame to ensure that the motors were operational. The triggering circuitry was checked to be on and the run was started by giving 2 winds-on pulses from the laboratory gate. During the run, timer-initiated master pulses were generated about every $2\frac{1}{4}$ hrs. along with any master pulses generated from 4 - fold coincidences. In the one side triggering section, 2 - fold coincidences occurred so frequently that it was not necessary to induce artificial master pulses for winds-on. The run was terminated by 2 winds-on, as it was started, and the oscilloscope films were developed

and analysed on site. Any faults which had developed and were apparent on the film could be remedied then. Usually the run films were composed of timer frames, accidental 4 - fold frames and genuine 4 - fold frames when an event had been recorded. The development of the flash tube film was done on surface to avoid the loss of running time, as this usually involved processing ~ 25 m of film (20 m from OST).

As mentioned previously, the problems of operation of the apparatus of this great depth are headed by the lack of cosmic rays for testing purposes. A long running time without events can be indicative of both a low intensity and fault conditions in the detectors. Therefore effective testing proceedures had to be devised.

The monitoring and testing proceedure for the coincidences circuitry is given in section 2.8 and that for the flash tube circuitry was as follows. Everyday the mirrors were cleaned and the electronic circuits were checked for obvious faults such as a cracked high voltage condenser. (This fault although drastic occurred several times as a result of over-heating. The shutting down of the mines ventillation system for a few hours could cause the laboratory temperature to rise by several degrees.)

About twice per week the circuits and cables were cleaned of dust and the U.H.T. voltages on the discharge condensers were measured for comparison with the voltage when the last event occurred.

As a weekly check, photographs were taken of each flash tube tray pulsed with a Co^{60} radio-active source positioned near its base. The test photographs were examined for significent variations in the number of tubes flashed. The theory behind these tests is that all tubes would flash in which ionisation had occurred but total recombination was

not completed prior to the high voltage pulse application. If the rise time is longer, more recombination and clearing of the ion pairs would occur resulting in the flashing of fewer tubes. Although the absolute number of flashes expected is difficult to predict, a steady change in rise time over several tests would be obvious. As another test, the number of spurious flashes and 'glow' tubes (repetatively spurious) in each tray on each frame of every run was recorded for Tels 1 & 2 and Specs 1 & 2 whilst the same was recorded for a sample of frames for Tels 3, 4 & 5 O.S.T. The variation of numbers of 'glow' tubes is a good indication of the variation in voltage reaching the tray. The variation in the number of spurious tubes is more subject to statistical error.

An interesting observation worthy of mention was made during the radioactive source tests. If a second pulse was given to a flash tube tray with the source present within a period of $\lesssim 20$ mins. after the first pulse, a less than usual number of flashes occurred. This observation agrees with the findings of Pickersgill (private communication.) He found a similar effect using a similar type of discharge circuit for pulsing trays traversed by a single muons at sea level. A possible explanation that has been given is the temporary polarisation of the flash tube glass. Presumably this would be analogous to the slow rise time situation in which the ion pairs diffuse before the critical voltage is applied.

In the observed case the effect only occuredwhen the first pulse was applied with the source in position, indicating that a discharge is necessary to produce the memory. It, therefore, seems unlikely that the effect could affect the ordinary running of the apparatus as only very few spurious and glow tubes flash when the pulse is applied.

It is considered that the test proceedures used were sufficient to establish the efficient running time of the experiment. The only period of doubtful running time was that of Tels 3, 4 & 5 4 - fold coincidence operation discussed in Chapter 1. This running time occurred when less rigorous checking techniques were employed.

2.8 4 - fold Coincidence Triggering

The setting up procedure and monitoring system of the scintillator elements, to ensure high efficiency for the detection of minumum ionising particles with low noise background, has been described in full by Narasimham (1967). Briefly, the methods used were as follows:-

Before incorporating the scintillator elements into the Neutrino Experiment, a preliminary experiment was performed at a depth of 824 m.we. st. rock. Here the muon rate was high enough to perform the tests quickly and the local radio-active decay background was comparable to that in the experimental site. The composition of the apparatus was the same as is shown in Fig. 2.10.

The 2 - fold counting rate from either pair of photomultipliers viewing their respective scintillator blocks was the total of the counting rates from cosmic ray muons, local radio-active decay and noise created in the photomultipliers. The rates observed were high enough for the latter to be neglected at this shallow depth as the resolving time for a coincidence was only 2 μs .

The 4 - fold counting rate was considerably less than the 2 - fold rate as radio-active decay coincidences were eliminated by the lead absorber between the scintillators. The fraction of the 4 - fold rate attributable to the detection of the soft component accompanying out -

of - geometry' muons was shown to be $\lesssim 5^{\circ}$ by putting the scintillator elements side by side for some time.

The forms of the 2 - fold and 4 - fold rates were similar to those shown in Fig. 2.10. The rapid rise in the 4 - fold rate with photomultiplier voltage in the lower voltage region indicates the rise to maximum efficiency for muon detection. The slower rise beyond the critical voltage for maximum efficiency for muons is due to increased efficiency of detection of the muon - accompanying soft component. The rapid rise in the natural 2 - fold rate above the critical voltage comes from increased efficiency of detection of local radioactive decay. 2 - fold rates taken with a radio-active source at a given distance from the scintillator are also shown in Fig. 2.10.

The same tests performed at the experimental site at 7500 m.we. st. rock showed an overall reduction in the 4-fold rate caused by the fall off of muon intensity with chance coincidences of photomultiplier noise and/or local radio-active decay being responsible for most of the counts. Similarly the 2 - fold rate was also reduced at photomultiplier voltages below the level necessary for high efficiency detection of the local radioactivity.

On the basis of these tests, a calibration procedure was established to facilitate regular checking of the efficiency of the scintillator elements. For an efficiency of $\sim 100\%$ for the detection of minimum ionising particles, it was deemed necessary to have a 2 - fold rate for each scintillator element of > 10/hr, or alternatively, with the radioactive source, a 2 - fold rate of > 30/hr and an individual channel rate (i.e. 1 photomultiplier's output) of 500/min.

During running time of the detector array, the 2 - fold counts of each scintillator element were recorded on message registers to allow a check to be made on the rates at the end of each run. At the same time, the 2 - fold rates from each scintillator element, together with the mixed 2 - fold rates of all scintillator elements in one wall of a telescope, were sampled for 10 minutes every $4\frac{1}{2}$ hours by means of a uniselector triggered by an electronic timer.

Finally, as a regular procedure, about once per two weeks the 2 - fold rates of each scintillator element were measured manually with and without the radioactive source in position near each scintillator.

2.9 One Side Triggering Efficiency

The triggering coincidence arrangement of Telescopes 3, 4 & 5 was changed in January 1968 from 4 - fold with the intention of increasing the aperture so as to accept more atmospheric muon events. The 2 - fold coincidence requirements were for any 2 photomultipliers viewing the same scintillator in any of the 6 walls of scintillators in the 3 telescopes. As was stated in the previous section, during the 4 - fold coincidence operation of the detectors, the photomultiplier voltage was adjusted to give a 2 - fold rate $>$ 10/hr per scintillator element. This gives a total 2 - fold rate for the 3 telescopes of $>$ 240/hr which is clearly too high for 2 - fold triggering where photography of flash tubes is involved. The photomultiplier voltage was, therefore, reduced to give a total 2- fold rate of $\sim$ 10/hr in the 3 telescopes. Although this reduced the number of 'chance' coincidences and the amount of film used in photographing the flash tubes, it also reduced the detection efficiency, the photomultiplier voltage being below the critical value for 100%.

An estimate of the variation of efficiency for muons passing through the scintillators at different angles was obtained from a test performed at the site of the contemporary experiment of Krishnaswamy et al. (1968) at a depth of 1545 m.w.e. st. rock in Edgar's Shaft in the same mines. This test described later, indicated that the efficiency for detecting muons incident perpendicularly on the scintillator (as is the case for neutrino-induced muons in the telescope arrangement) was quite low. Those incident at very oblique angles were detected with good efficiency.

From previous experience it was thought that E.M.I. photomultipliers were more efficient at lower voltages than du Mont photomultipliers. So as to reduce the possibility of chance coincidences wholly or partially caused by photomultiplier noise, all du Mont photomultipliers in Telescopes 3, 4 & 5 were inter-changed with E.M.I. photomultipliers in the spectrographs. The consequential reduction in the chance 2 - fold rate of the 3 telescopes enabled the E.H.T. voltage to be increased and the efficiency along with it. (N.B. The resultant increase in 2 - fold rate to the Spectrographs gave only a very small increase in the rate of 4 - fold coincidence triggers.)

Following the interchanging of photomultipliers in July 1969, a more prolonged efficiency test was carried out. This time the New Trial Shaft site of Krishnaswamy et al. at $\sim$ 900 m.w.e. was used. The test was made on photomultiplier pairs used in the one side triggering arrangement both before and after the interchanging.

The tests and their results were as follows:-

2.9 1 <u>The Edgar's Shaft Test: Angular Variation of Efficiency</u>

The apparatus of Krishnaswamy et al. was used with two of the scintillator elements replaced by 2 elements from Telescope 5. The two

remaining triplets of photomultipliers of Krishnaswamy et al. were run at their usual high voltage to give 100% efficiency wheras those from Telescope 5 were run with a reduced voltage as during the operation of the one side triggering arrangement. The apparatus was, therefore, effectively split into two, one half running at 100% triggering efficiency and the other at < 100%. Analysis of the crossed flash tube photographs enabled the true zenith angles of detected single muons to be measured. The ratio of number detected in a given angular cell by the Telescope 5 photomultiplier pairs to the number detected by the 100% efficiency photomultiplier triplets was taken as the efficiency of the telescope 5 scintillator elements in that angular range.

The variation of efficiency with zenith angle found for the horizontally mounted scintillators is shown in Fig. 2.11.

The EHT voltage on the photomultipliers and gain of the amplifiers for this test were, overall, less than those used in the operation of the one side triggering arrangement for Telescope 5. As a consequence fig. 2.11 underestimates the efficiency of the detectors in operation in situ. However, the most important result of this test was the shape of the angular variation of efficiency for this type of detector element. This was clearly established.

2.9 2 The New Trial Shaft Test: Overall Efficiencies

For this test six photomultiplier pairs used in the one side triggering of Telescopes 3, 4 & 5 were chosen to be representative of all of the photomultipliers used. (Time did not permit the testing of all of the photomultipliers.) The selection of the photomultiplier pairs was on the basis of numbers of O.S.T. events detected by them to date.

FIG. 210: O.S.T. Scintillator Element Characteristics at ~ 900 m.w.e.

(Tel. 5 - Element N3)

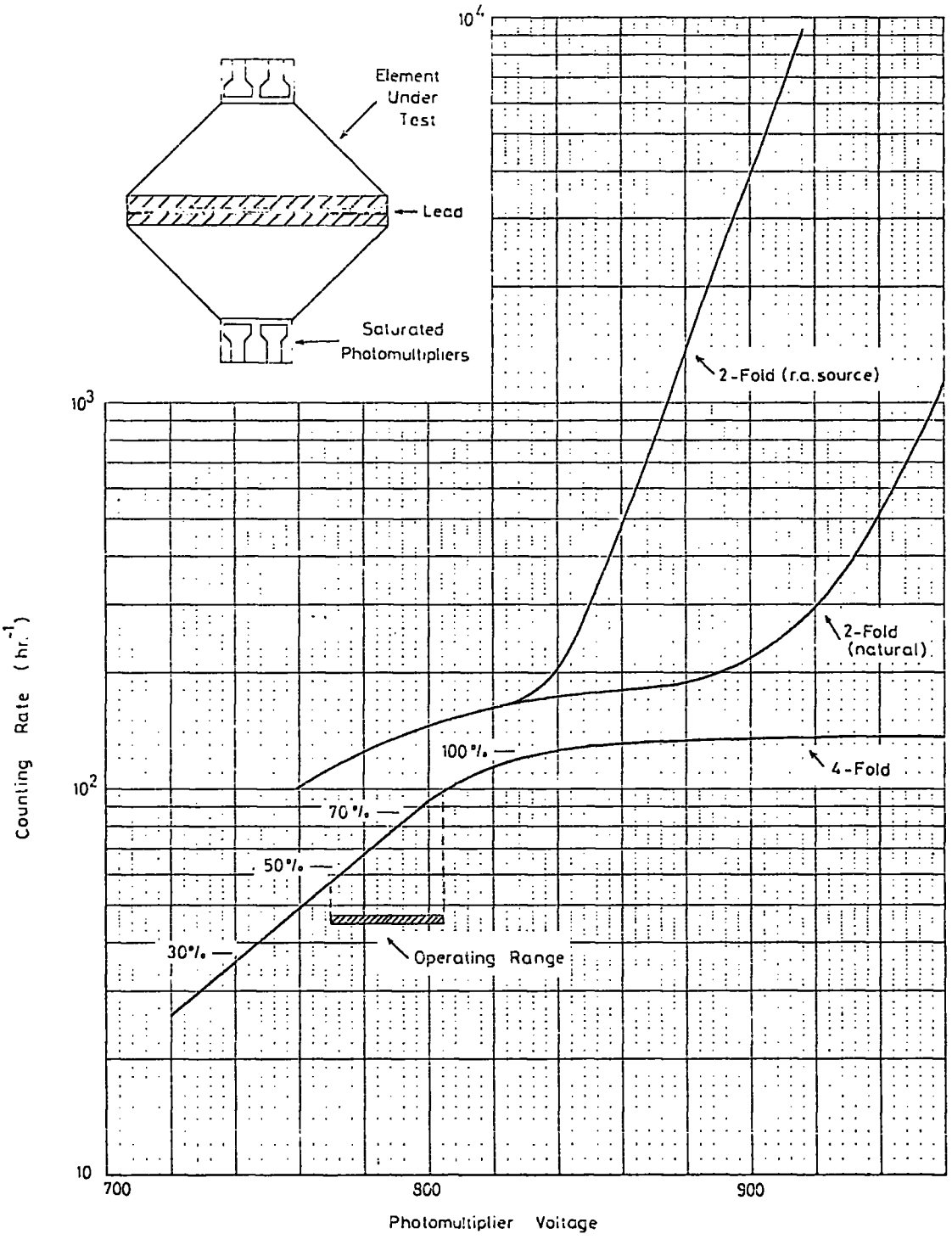

FIG. 211: Detection Efficiency of Scintillator Element (Horizontally Mounted)

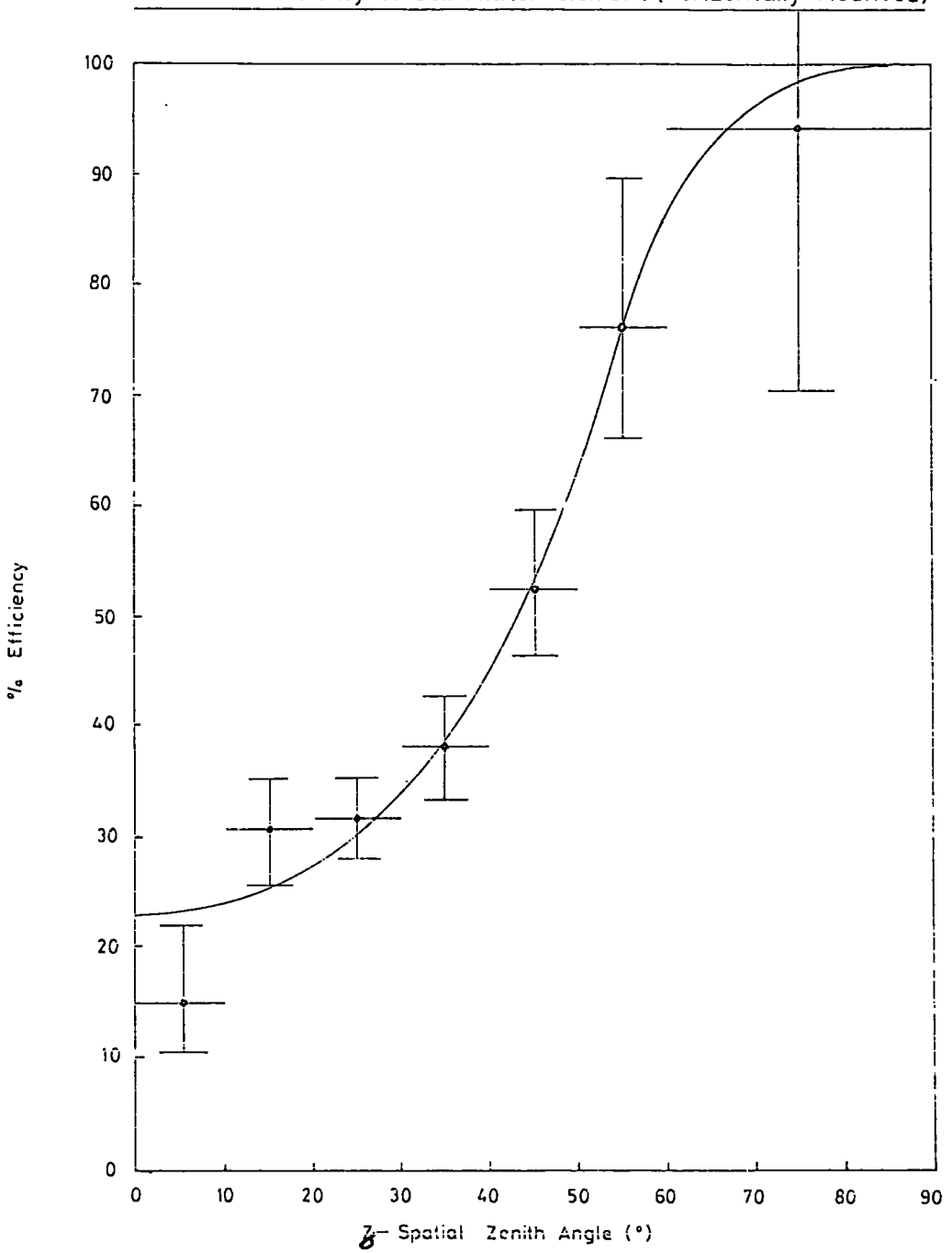

Using a telescope basically the same as that used by Miyake et al. (1964) consisting of two layers of horizontal scintillators seperated by 5 cms of lead (See fig. 2.10), the overall efficiency of the 6 photomultiplier pairs were estimated over a range of photomultiplier E.H.T. voltages as follows.

The lower pair of photomultipliers were saturated by applying a voltage above the critical level for 100% efficiency, whilst the upper pair, being the ones under test, were operated at several different voltages. By assuming that 100% efficiency was achieved at a photomultiplier voltage slightly above the 'knee' in the 4 fold rate characteristic, it was possible to estimate the efficiencies at lower voltages as being proportional to the reduced count rate. The 2 - fold rate characteristics, using the radioactive source, were corrected for the difference in natural counting rates between the test site and the experimental site. This enabled the photomultiplier voltage variation over the running time to be estimated from the regularly measured 2 - fold rates. By applying the photomultiplier voltage ranges, thus obtained, to the 4 - fold rate characteristics, a range of efficiencies were obtained for each photomultiplier pair tested.

The efficiency ranges of the untested photomultiplier pairs were assumed to be the same as the tested pairs with the same photomultiplier combination. (i.e. 2 E.M.I., 2 Du Mont or 1 E.M.I. + 1 Du Mont.)

The overall efficiencies of each of the 3 telescopes, assuming an average value over the individual detector elements, were used to estimate an angular variation of the same basic shape as that observed in

FIG. 2.12: Detection Efficiency of O.S.T. Scintillator Elements (Vertically Mounted at 7500 m.w.e.)

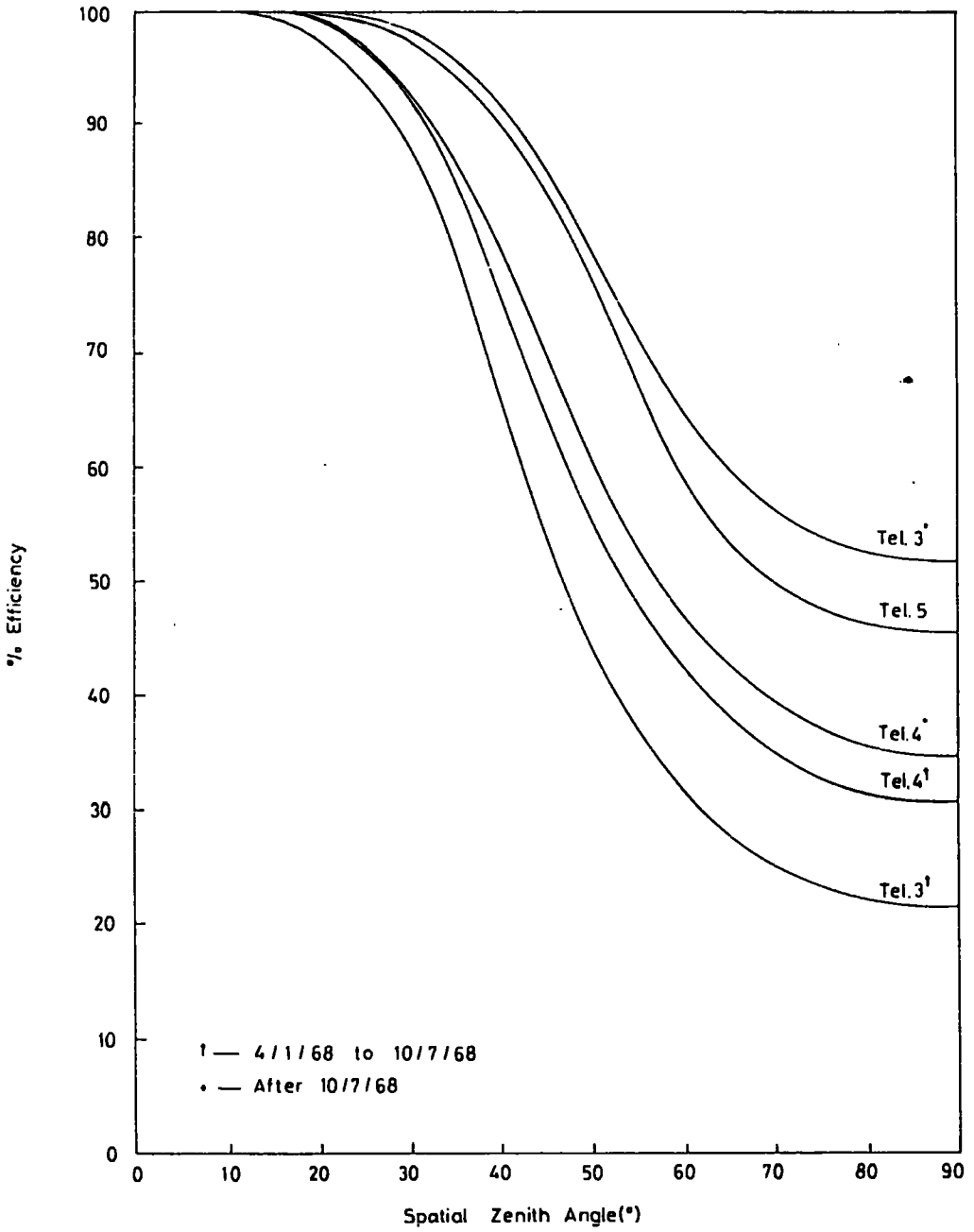

the Edgar's Shaft Test. For this, the spatial zenith angular distribution of muons at the test site was taken to be of the form $\cos^2\theta$.

The best estimates of the efficiency variation with zenith angle are shown in fig. 2.12.

CHAPTER 3

The Energy Spectrum of Atmospheric Muons Underground.

3.1 Introduction

The mass composition and spectrum of high energy primary cosmic rays are still very uncertain. Together with the characteristics of high energy interaction mechanisms, these parameters may be studied, to some extent, via the energy spectra of atmospheric muons penetrating deep underground, in so far as a change in any one of them affects the resulting muon spectra.

There are two basic approaches to the calculation of atmospheric muon energy spectra underground. One is to work from an assumed sea level energy spectrum via the range - energy relationship, making appropriate corrections for energy loss fluctuations. The other is to use the depth intensity relationship for greater depths, working back to the energy of the muons in passing the depth in question, again via an appropriate range energy relationship.

Both methods have their limitations. Using the sea level spectrum there is, first of all, doubt about its form at high energies and, secondly, there is doubt about the energy loss parameters in the range-energy relationship, again at high energy. On the other hand, the measured depth intensity curve incorporates naturally the effects of energy loss fluctuations, but statistics are so poor, at great depths and large zenith angles, that there are large errors on the observed intensities.

Miyake et al. (1964), operating at a depth of 8400 m.we. K.G.F. rock, were only able to establish an upper limit to the intensity of 10^{-11} cm.$^{-2}$ sec.$^{-1}$ st.$^{-1}$. The Case - Wits group (Reines et al., 1966) have given an

intensity at 8800 m.w.e. East Rand rock, but this measurement also has relatively large errors, such that an extrapolation of the measured depth intensity relation to greater depths could vary considerably within the range of uncertainty.

The energy spectra of atmospheric muons underground have been calculated by Craig et al. (1968), using both sea level spectra and depth intensity relations, and mean energies have been calculated as a function of depth. Details of the calculations are given in this chapter and a comparison with the experimental results is made in Chapter 6.

3.2 The Sea Level Muon Spectrum

The review by Osborne et al. (1964), of the sea level energy spectra derived by earlier workers, explains the observations made to that date. The discrepancies between the earlier Durham spectrum of Hayman et al. (1963), based on the spectrograph data at energies < 1000 GeV, and the spectra of Higashi et al. (1964) and Krasilnikov (1962), derived from burst measurements, have in the main been overcome.

An analysis of δ cascade measurements, using nuclear emulsions, by Osborne and Wolfendale (1964), was used with the best estimate K/π ratios, at different energies, to give a better estimate of the sea level spectrum at energies in the range 1000 - 7000 GeV. Coupled with revised sea level intensities derived from underground measurements, using a corrected Z^2/A value for the Kolar rock and a different ratio of the fluctuating to non-fluctuating energy proportional parameters in the range - energy relation, the modified sea level energy spectrum of Osborne et al. agreed well with those derived from the burst measurements.

Menon and Ramana Murthy (1967), however, using the shallow depth intensity data with an average range energy relation supported by the fluctuations correction of Zatsepin and Mikhalchi (1962), have derived a sea level spectrum which is greater than the 'O.P.W.' spectrum (i.e. the spectrum of Osborne et al.) at higher energies. These authors suggest that the reason may be that the O.P.W. spectrum has been affected by an underestimation of the high energy intensity by Hayman and Wolfendale whose spectrograph results excluded shower and knock on events in which the particle trajectory could not be established. On account of the increase in probability of knock-on and shower production with muon energy, the bias would lead to the greatest errors in the high energy region. Although Osborne et al. had in fact made a correction for the bias, its value is difficult to estimate and its accuracy is in doubt.

It may be concluded that the O.P.W. spectrum is the best estimate at energies $\lesssim$ 1000 GeV but at higher energies there is still uncertainty. Of course, it is at just such high energies that the sea level spectrum is required for the calculation of the energy spectra of muons deep underground, energies in the range 10^4 to 10^6 GeV being of prime importance. Clearly an extrapolation of the best estimate sea level spectrum at $<$ 7000 GeV to 10^6 GeV must be made with reference to the muon production mechanisms, if working downwards, or the high energy range - energy relation, if working upwards from depth intensity data.

3.2 . 1 Derivation from Primary Spectra.

The primary cosmic ray spectrum, for energies above 10^{13} eV, has been estimated from the size spectrum of extensive air showers. Thus obtained, in terms of energy per nucleus, the spectrum must be converted to terms of

energy per nucleon for the calculation of the pion, kaon and muon spectra. There is still considerable doubt about the primary mass composition at energies above 10^{15} eV but there is better agreement at lower energies (i.e. $\lesssim 10^{14}$ eV), the composition being approximately 93% protons, 6% α-particles, 0.4% for medium mass nuclei and less for other nuclei. A widely held view is that the 'kink' in the primary spectrum in the region $2.5 - 3 \times 10^{15}$ eV (see Khristiansen et al., 1966) represents a cut - off in the primary rigidily spectrum which is attributable to galactic modulation.

To make the conversion to energy per nucleon, as no clearly preferred primary mass composition is available, it is necessary to use different models to cover the possibilities.. These have been taken as,

M - The spectrum, in energy per nucleus, of Adcock et al. (1967), assuming the mass composition at lower energies, as stated above, and a much increased contribution from heavy particles at $> 10^{15}$ eV.

U.1 - The spectrum, in energy per nucleus, of Adcock et al., assuming only proton primaries.

U.2 - The spectrum, in energy per nucleus, of Griesen (1966), assuming only proton primaries.

These spectra, in terms of energy per nucleon, are shown in fig.3.1.

Using the method outlined by Brooke et al. (1964), the primary spectra were used in the calculation of the sea level spectra assuming the C.K.P. relation (Cocconi et al.,1961) to hold good up to the energies concerned.

The C.K.P. relation gives the number of pions emitted in the forward direction in the C system as,

$$N(E_\pi)dE_\pi = \frac{A}{T_p} \cdot \exp\left(-\frac{E_\pi}{T_p}\right) dE_\pi \qquad 3.1$$

FIG 3.1: Comparison of Primary Spectra.

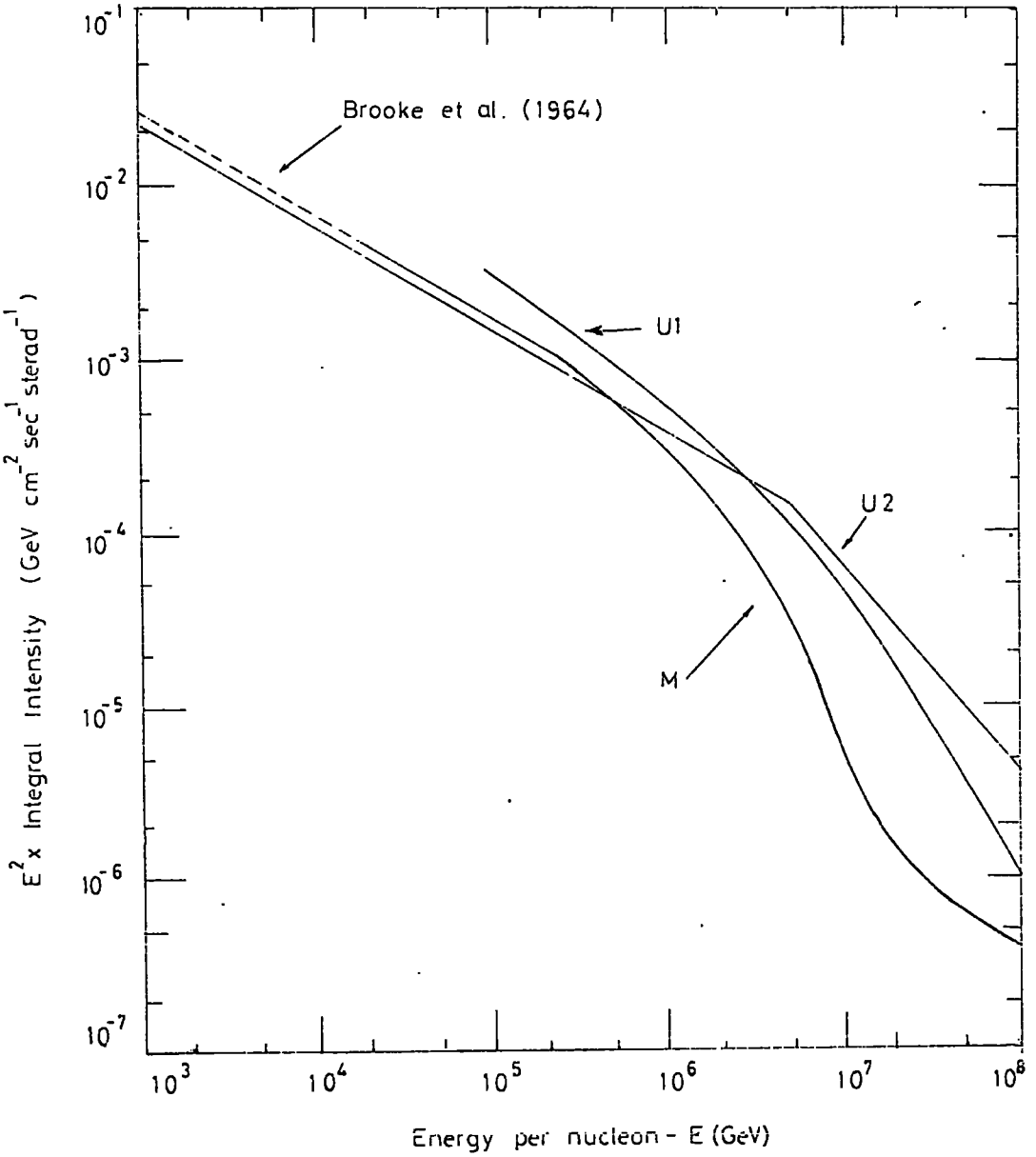

where E_π is pion energy in the L system, A is the mean multiplicity of pions emitted in the forward direction in the C system (assumed to vary as $E_p^{\frac{1}{4}}$, where E_p is the primary energy) and T_p is mean energy of the pions.

The contribution from kaons having been included, the spectra obtained to 10^6 GeV have been normalised to the O.P.W. spectrum at 2000 GeV. The 'K' and 'U2' spectra are a good indication of the limits to the true spectrum and are shown in fig. 3.2.

3.2.2 Extension of Muon Spectra from Sea Level to 7500 m.we.

The problem of range fluctuations of muons penetrating underground has been studied by several authors, starting with Bollinger (1951). Making similar assumptions about the various cross - sections and using computers for Monte Carlo methods, the most recent workers, notably Oda & Murayama (1965), Menon & Ramana Murthy (1967), Kobayakawa (1967) and Osborne et al. (1968), are in quite good agreement over the survival probabilities of muons to different depths underground.

Osborne et al. have extended their calculations to depths greater than the others for application to the neutrino experiments at great depths and high sea level muon energies. Their survival probabilities have, therefore, been used, in connection with the sea level spectra derived previously, to predict the depth intensity relation to 15000 m.we.* (see fig 3.3).

---

* Throughout this thesis, unless otherwise stipulated, the unit 'm.we' means meters water equivalent of 'standard rock' with $Z^2/A = 5.5$ and of average density 2.65 gm. cm.$^{-3}$.

FIG. 3.2: Differential Muon Spectra at Sea Level.

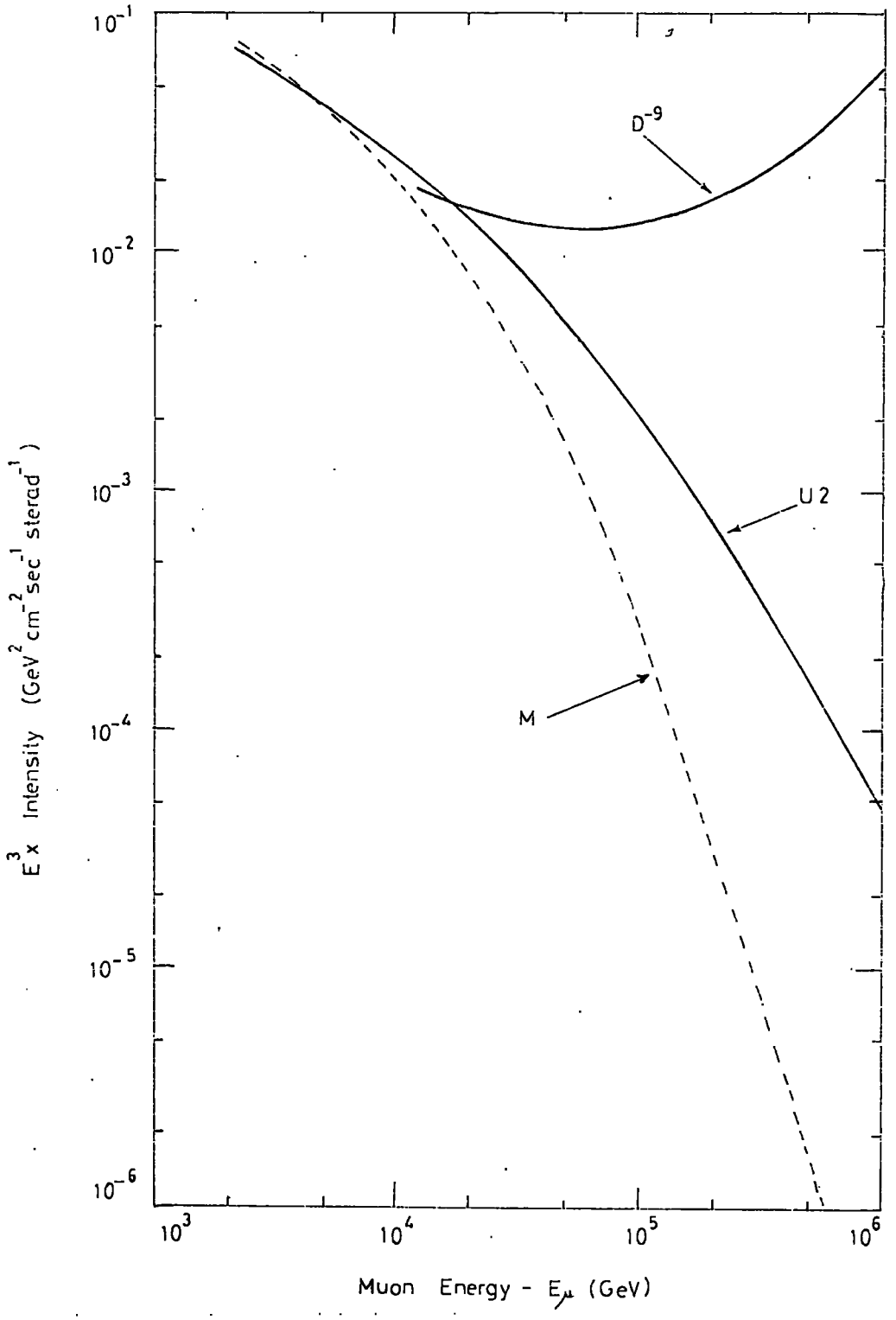

The extended depth intensity relations were used to calculate the differential muon spectrum at 7500 m.we.by a relaxation method. As a first approximation, a muon range - energy relation, neglecting fluctuations, was assumed up to 10^4 GeV so as to derive the integral muon spectra at 7500 m.we.from the depth intensity forms. These spectra were differentiated and applied to the survival probabilities to give further depth intensity curves which could be relaxed to agree with the original yielding relaxation factors for energies over the spectral range. The first approximation spectra were modified, according to the relaxation factors which gave consistency between the depth intensity curves, and are shown in fig. 3.4.

3.3 The 7500 m.we.Muon Spectra from the Depth Intensity Relation

Although the muon depth intensity variation has been well established experimentally at depths less than 4000 m.we. and quite well at depths between that and 7500 m.we., as already mentioned, it is still quite uncertain at greater depths.

The interpretation of the early results of K.G.F. Neutrino Experiment, in terms of equivalent vertical intensities at greater depths, has been discussed by Menon et al. (1967c). This paper proposed a depth intensity relation, neglecting range fluctuations and assuming a constant exponent of the sea level spectrum, which was normalised to the observed depth intensity relation at 4000 m.we. and 7500 m.we.

The angular distribution of the K.G.F. results, however, suggested a less steep fall off of intensity with depth, being better represented by a $\cos^8\theta$ variation up to $\sim 50^\circ$. Consequently the depth intensity relation is $I_v(D) \propto D^{-9}$ (where D is the depth.)

Extrapolations of the two depth intensity relations, discussed by Menon

et al. are also shown to 15000 m.we.in fig. 3.3 denoted by 'exponential' and 'D^{-9}'. (The validity of such extrapolations is, of course, doubtful.) These depth intensity relations have been used with the survival probabilities, to calculate the muon spectra at 7500 m.we., as described in section 3.2, and are also shown in fig 3.4.

Reversing the procedure, the sea level spectrum corresponding to the D^{-9} depth intensity relation to 15000 m.we.has been derived, for comparison with those derived from the primary spectra (fig. 3.2).

3.4 The Mean Energy of Vertical Atmospheric Muons Underground

The measurement of the muon energy spectrum deep underground presents many difficulties and has not yet been undertaken. The mean energy, however, can sometimes be estimated and in connection with this, the expected mean energies are derived below.

The calculation of the mean energies of atmospheric muons underground is best divided into two parts, the first being for great depths where range fluctuations effects must be considered and the second for shallow depths where they may be neglected.

The differential spectra, derived previously, were divided into 20 energy cells up to 5×10^3 GeV and a mean intensity over the cell range was attributed to the median energy of each cell.

The mean energy of muons in each spectrum was then taken as,

$$E_\mu (o,h) = \frac{1}{I(o,h)} \left\{ \sum_{k=1}^{20} \left[N(E)_k \cdot E_k \right] + \frac{\gamma}{\gamma - 1} A E_o^{-\gamma} \right\} \qquad 3.2$$

FIG. 3.3 Depth-Intensity Variation at Greater Depths

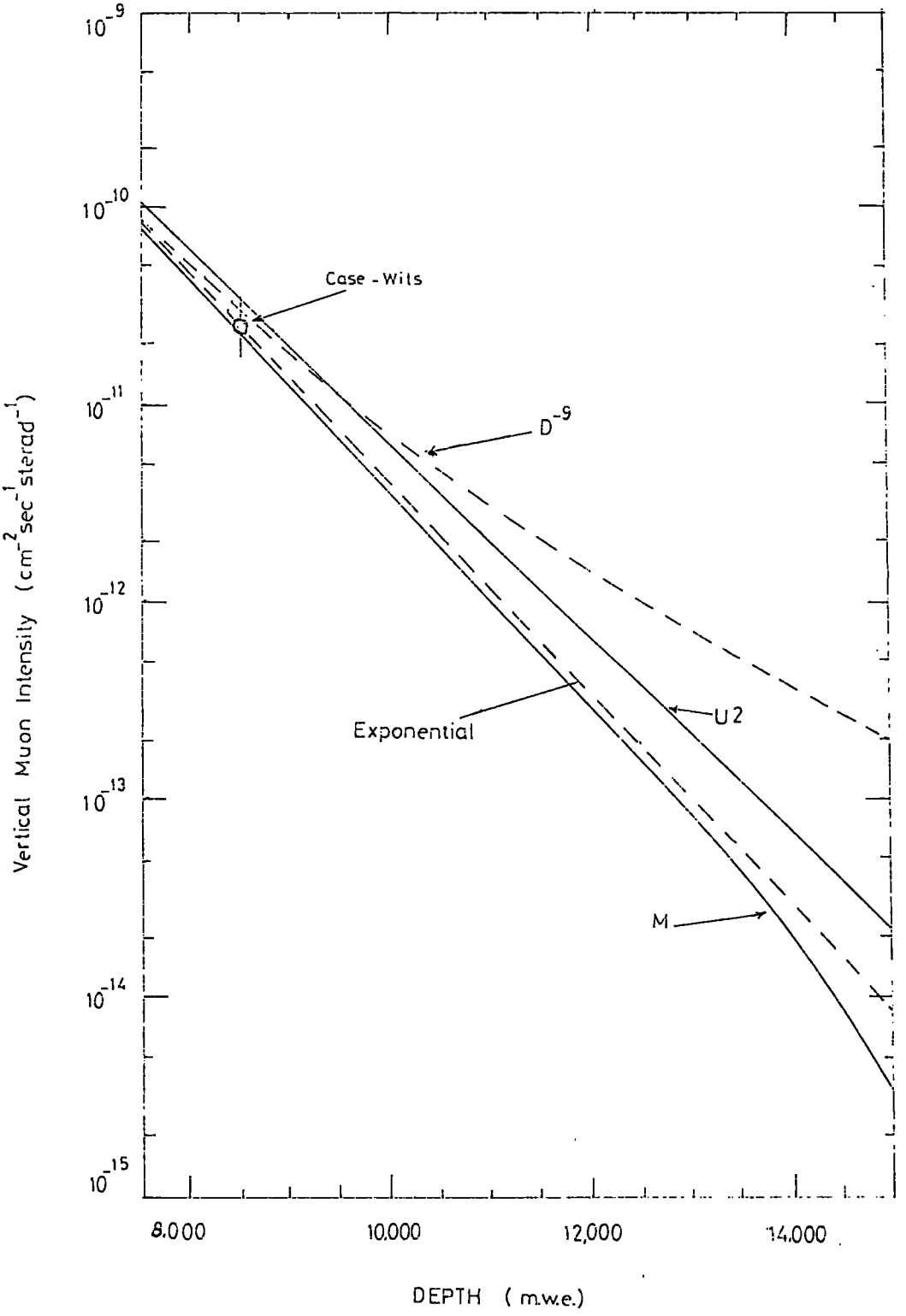

FIG. 3.4: Vertical Spectra of Atmospheric Muons at 7500 m.w.e.

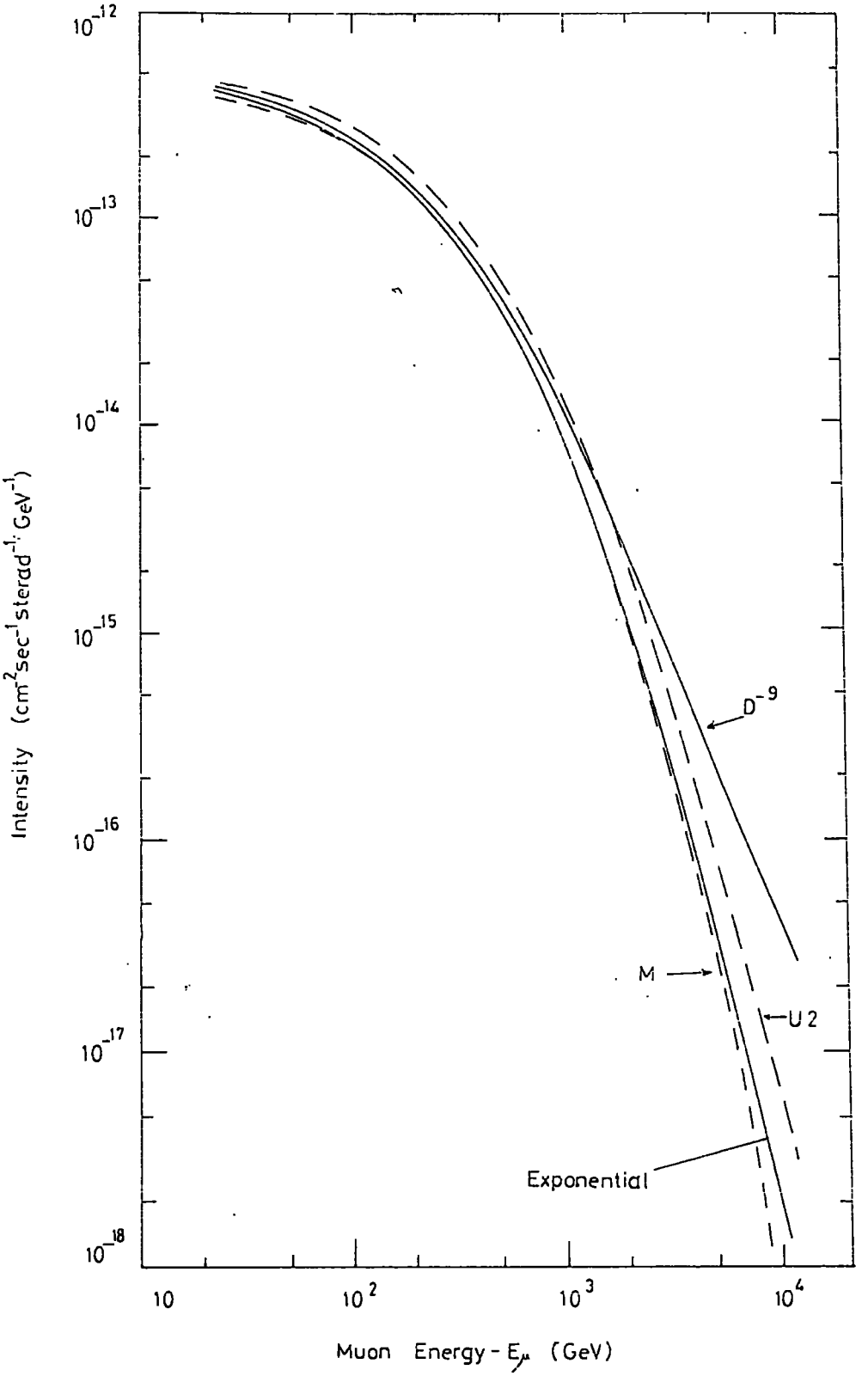

where $N(E)_k$ is the mean cell intensity, E_k is the median energy of the cell and $I(o,h)$ is the vertical intensity at the depth h.

$AE_o^{-\gamma}$ is a correction term which approximately accounts for the contribution from muons of energy $> 5 \times 10^3$ GeV on the assumption of a constant exponent of the energy spectrum at those energies.

The mean energies calculated for muons reaching 7500 m we are shown in table 3.1.

Table 3.1 : Mean Energy of Vertical Atmospheric Muons at 7500 m we

Depth Intensity Relation	Primary Spectrum	$\bar{E}_\mu$(GeV)
exponential	-	287
D^{-9}	-	393
-	M	286
-	U2	336

A further set of mean energies has been calculated from the depth intensity curves via differential spectra for a depth of 10,000 m.we. These values, together with those for 7500 m we, are shown in fig. 3.10 as a continuous variation of mean energy with depth greater than $\sim$ 4000 m.we.

A point of interest is that the adoption of an exponential depth intensity relation leads to a constant mean energy of atmospheric muons at all angles and at all depths. This, of course, only applies to depths where the intensities are adequately described by such an exponential form.

The effect of range fluctuations may be overlooked for vertical depths

FIG. 3.5: Integral Muon Spectra at Sea Level

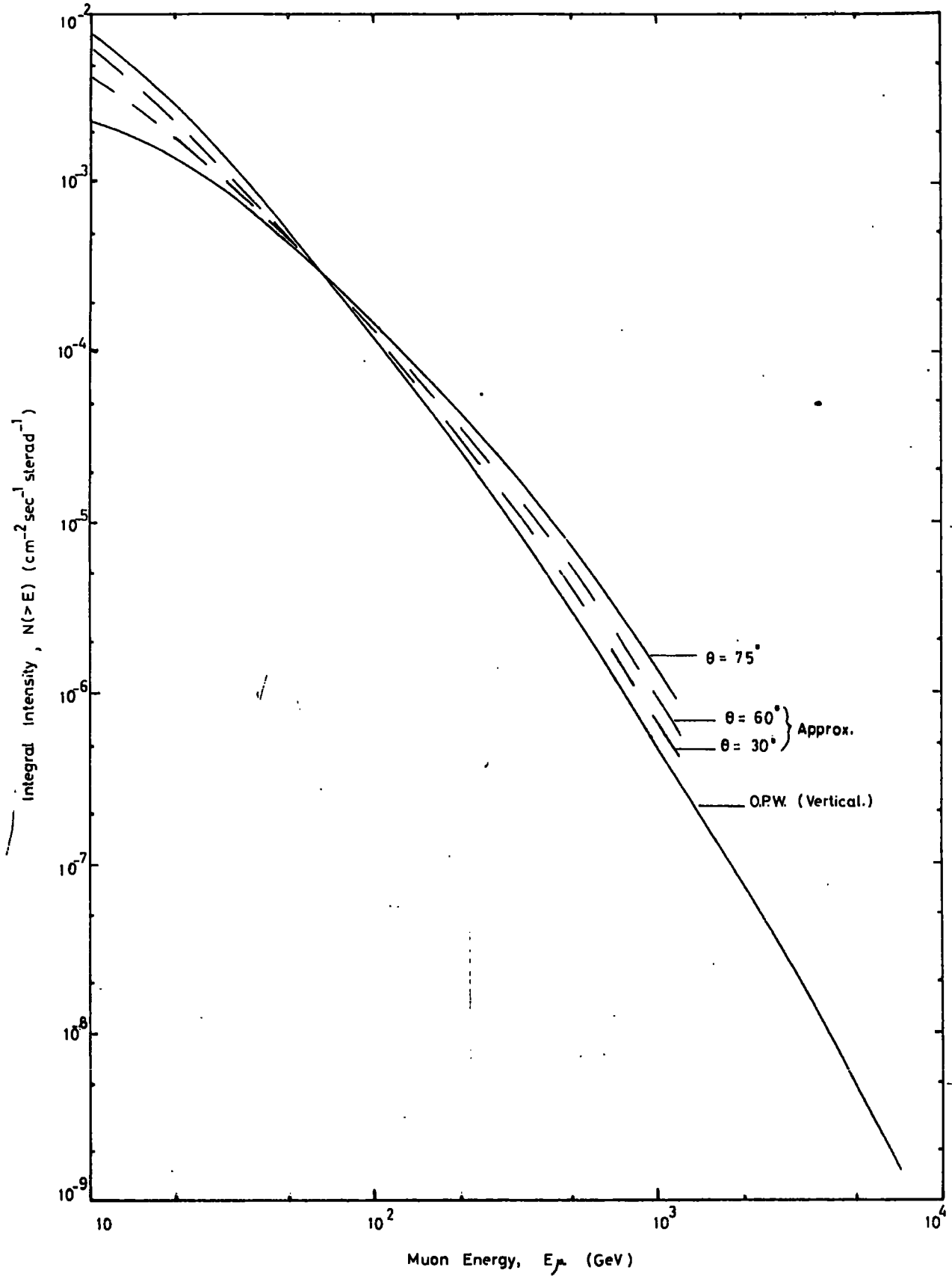

FIG. 3.6: Average Range Energy Relationship for Muons ($b = 4 \cdot 0 \times 10^{-6}$ gm^{-1} cm^{-2})

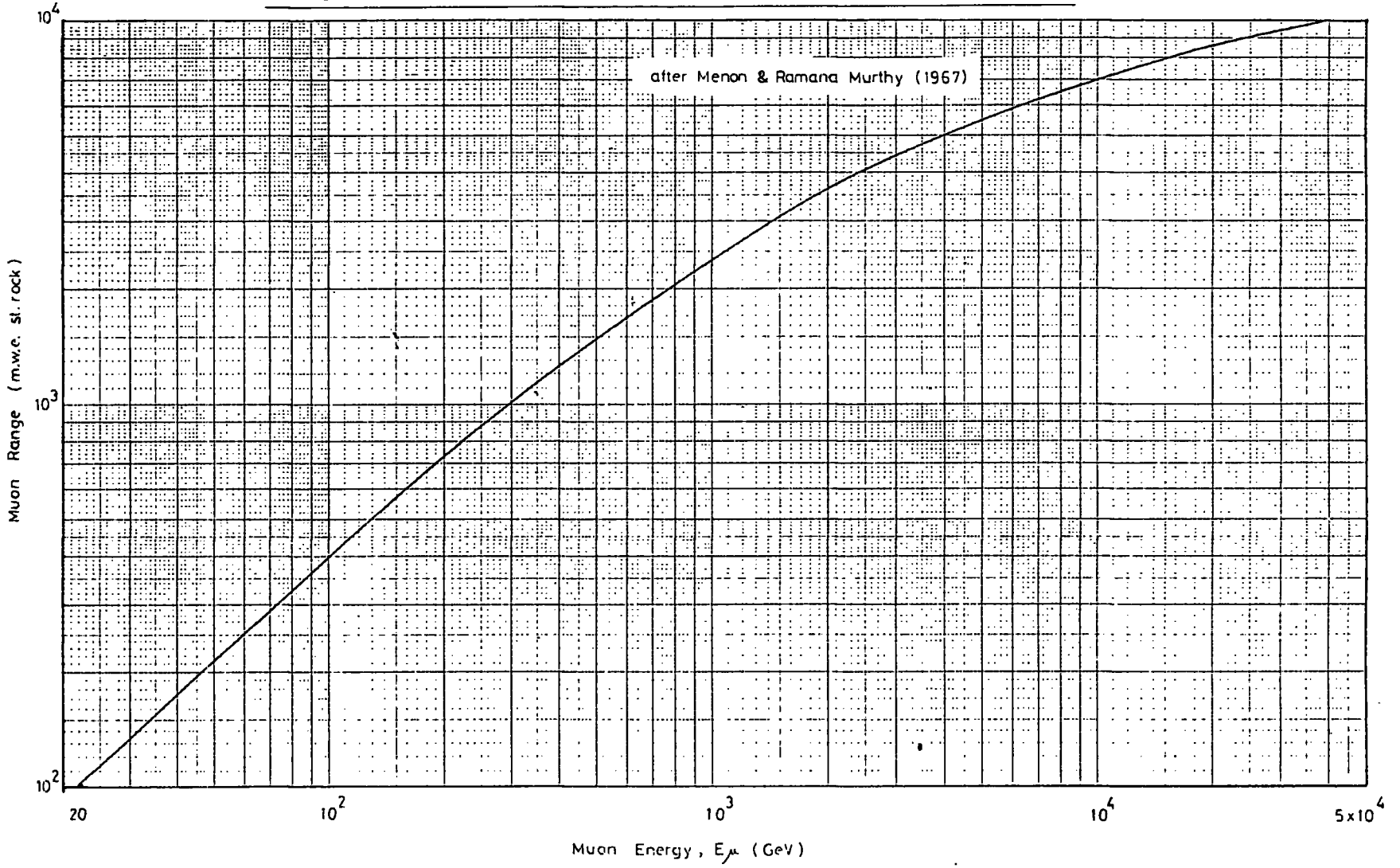

$\lesssim$ 2000 m.we. and the vertical differential spectra at 25 m.we., 300 m.we. and 1871 m.we. have been obtained from the O.P.W. sea level spectrum and the range energy relation (neglecting fluctuations) derived by Menon and Ramana Murthy for $b = 4.0 \times 10^{-6}$ $cm^2 gm^{-1}$.

The integral spectra, so obtained, have been differentiated numerically and the mean energies calculated, by the above method. The spectra are shown in figs. 3.7a and 3.7b and the mean energies are given in table 3.3.

3.4 1 Previous Estimates of Mean Energy

Stockel (1967) has also calculated the mean energy of vertical muons to about 3000 m.we. A sea level differential spectrum was obtained, in much the same manner as in section 3.4, and the muon energy loss equation was applied, with $b = 4.0 \times 10^{-6}$ gm^{-1} cm^2, to muons of different discreet energies. Using both the O.P.W. spectrum and that of Menon and Ramana Murthy (M.R.M.), Stockel established the differential spectra at several depths and used them to calculate the intensity for comparison with the measured intensity. Both spectra were found to underestimate the intensity when used as described above, the O.P.W. spectrum by more than the M.R.M. with increasing depth. To overcome this discrepancy, an artificial spectrum (A) was created which gave close agreement with the depth intensity observations.

Using the A and the O.P.W. spectra, the mean energy was found to vary with depth as shown in fig. 3.8.

It seems, however, that, if fluctuations had been taken into account, at least some of the descrepancy between the spectrum and the depth intensity relation could have been overcome for the O.P.W. spectrum and almost all for the M.R.M. spectrum. (See table 3.2).

On account of the relative insensitivity of the mean energy to the exact

FIG. 3.7a : Underground Vertical Integral Muon Spectra

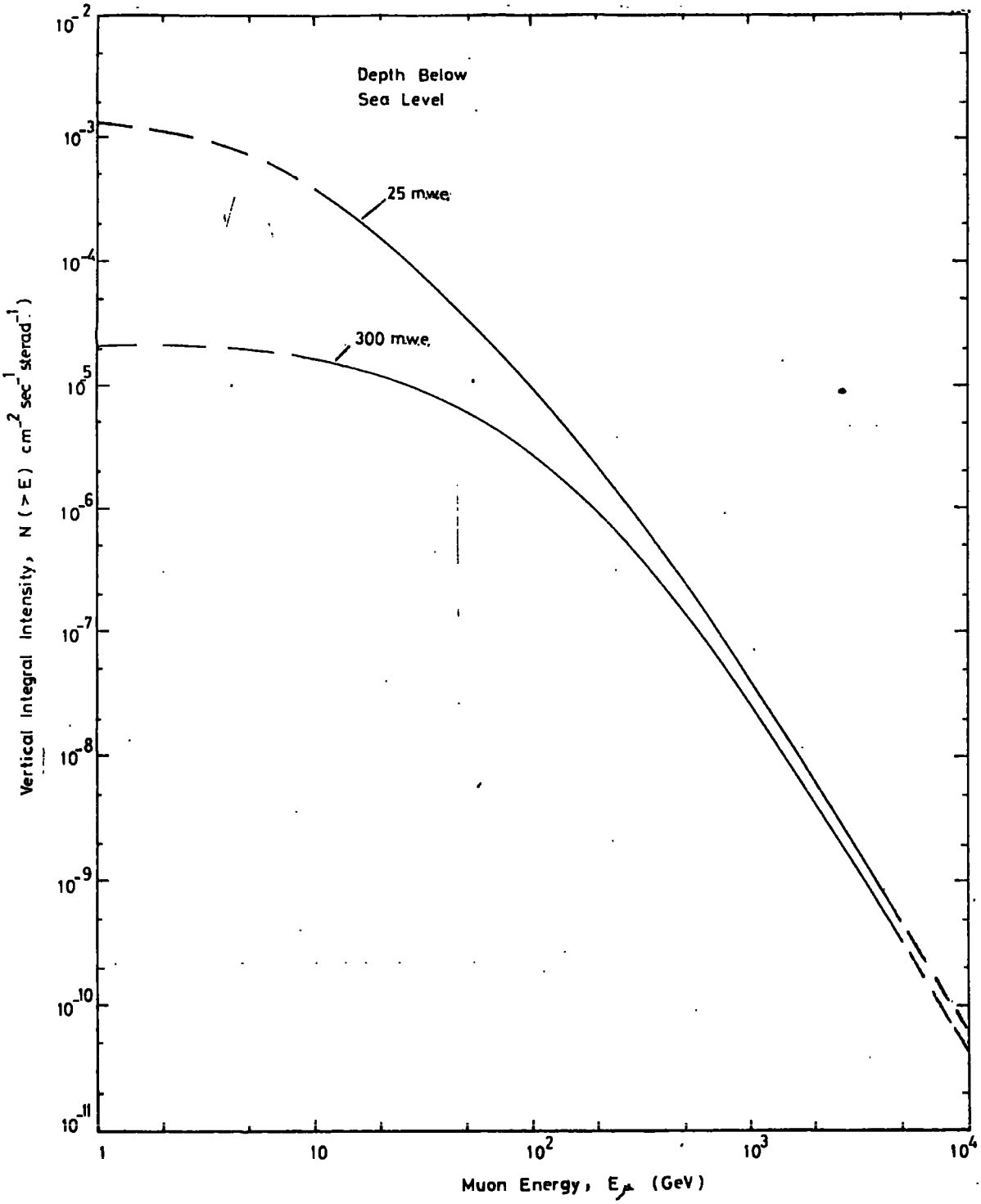

FIG. 3.7b : Vertical Integral Muon Spectrum at 1871 m.w.e.

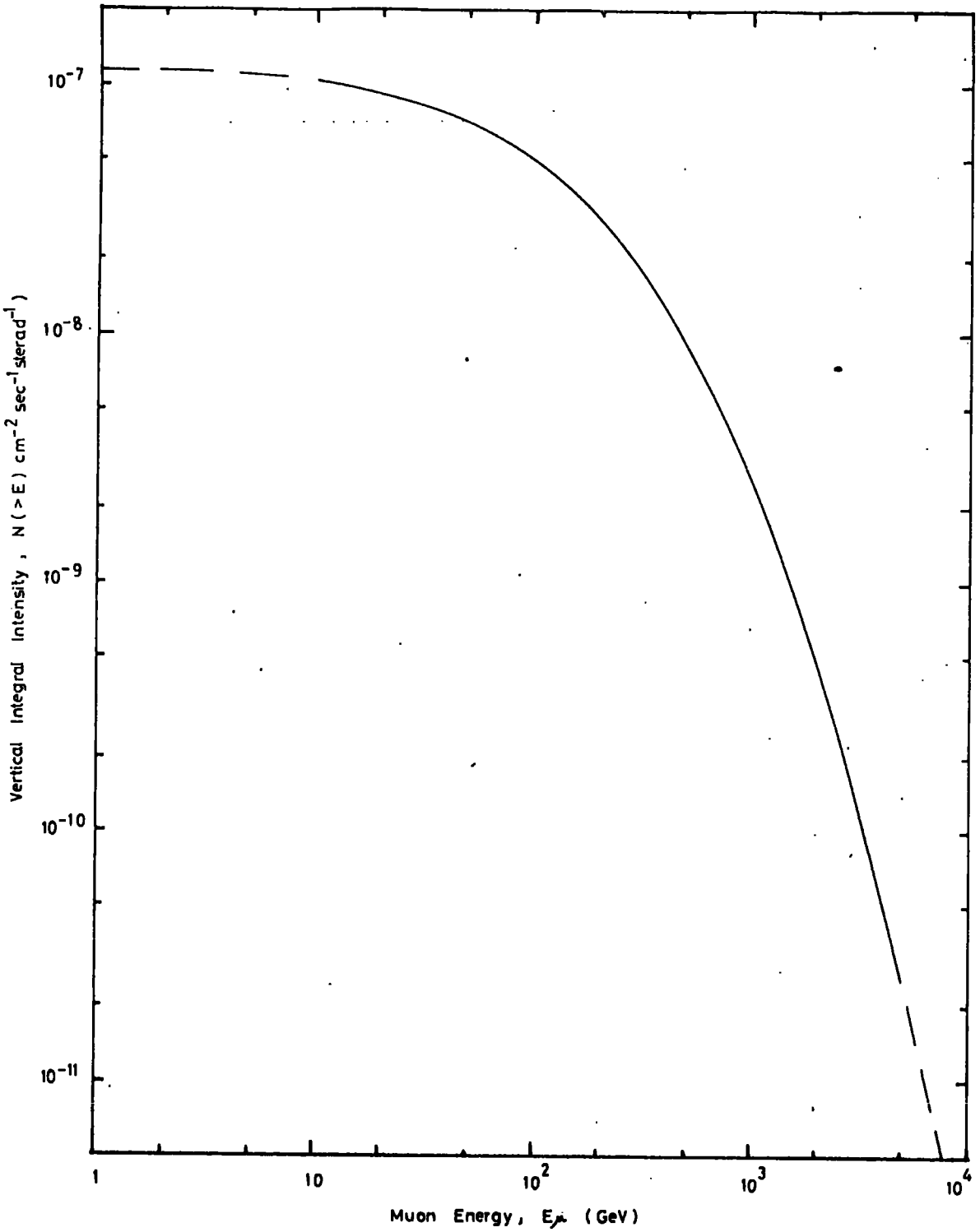

FIG. 3·8: Comparison of Variations of Vertical Muon Mean Energy with Depth

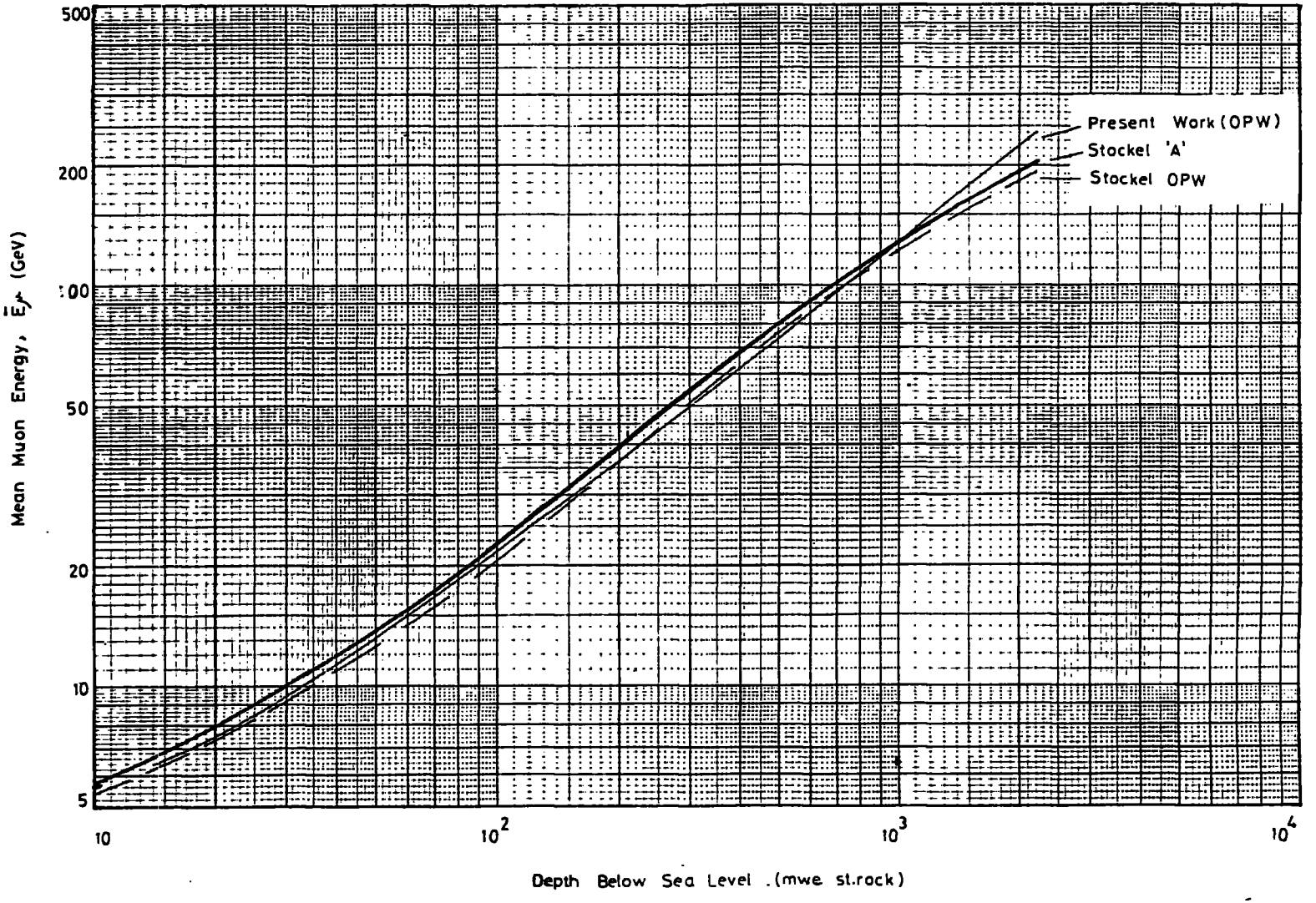

sea level spectrum used, it is not unreasonable to assume that the mean energies derived via the A spectrum are similar to those which would have been derived using the M.R.M. spectrum corrected for fluctuations, particularly at depths > 1000 m.we. This is not surprising as the M.R.M. spectrum at energies in excess of 100 GeV is based mainly on underground intensity measurements.

Table 3.2 : Comparison of calculated integral intensities at 3162 m.we.

Source	Vertical Integral Intensity ($cm^{-2}sec^{-1}st.^{-1}$) neglecting fluctuations	including fluctuations
O P W Spectrum	1.35×10^{-8}	1.69×10^{-8}
M R M Spectrum	1.56×10^{-8}	1.95×10^{-8}
'A' Spectrum	-	2.03×10^{-8}
best fit I/D curve	-	2.09×10^{-8}

The fluctuations corrections used are those of Osborne et al. (1968), for $\gamma = 2.7$.

3.5 The Mean Energy of Atmospheric Muons at all Zenith Angles

For non-vertical muons, the equivalent vertical depth is given by h secθ for a flat surface. The increase in the minimum muon energy, for penetration to the depth h from a zenith angle θ , must be taken into consideration in the calculation of the differential spectra as the effect of fluctuations now becomes important at shallower vertical depths.

A muon from a zenith angle as great as 75° need only have a minimum sea

level energy of about 350 GeV to reach a vertical depth of 300 m.we. Such muons are only slightly affected by fluctuations, so the effect may be neglected for the depths 25 m.we. and 300 m.we.

It is not possible, however, to neglect the effect of μ - e decay at large zenith angles and shallow depths. This affects the O.P.M. sea level spectrum as shown in fig. 3.5 for zenith angles of 30°, 60° and 75°.

Using the Menon and Ramana Murthy range energy relation, as before, the spectra and mean energies at the two depths 25 m.we. and 300 m.we. have been calculated for zenith angles of 30°, 60° and 75° from the sea level spectra of fig 3.5.

For the depth 1871 m.we, the depth intensity method has been used for different zenith angles. The measured relationship was taken to 4000 m.we. and thereafter the exponential form of Menon et al. was used.

The variations of mean energy with zenith angle for the 3 depths are shown in fig. 3.9.

$\bar{E}_{\mu}(g,h)$, the mean energy of all atmospheric muons (i.e. 'global mean') detected at a depth h, is given by,

$$\bar{E}_{\mu}(g,h) = \frac{\int_{0}^{\pi/2} \bar{E}_{\mu}(\theta,h) \cdot 2\pi \sin\theta \cdot I(\theta,h)\, d\theta}{\int_{0}^{\pi/2} 2\pi \sin\theta \cdot I(\theta,h)\, d\theta} \qquad 3.3$$

Where $\bar{E}_{\mu}(\theta,h)$ is the mean energy, at depth h, of muons arriving from a zenith angle θ and $I(\theta,h)$ is the muon intensity at an angle θ and depth h.

The mean energies for all muons given by equation 3.3, and for vertical muons only are shown in table 3.3 and fig. 3.10.

FIG. 3·9: Variation of Mean Muon Energy with Zenith Angle.

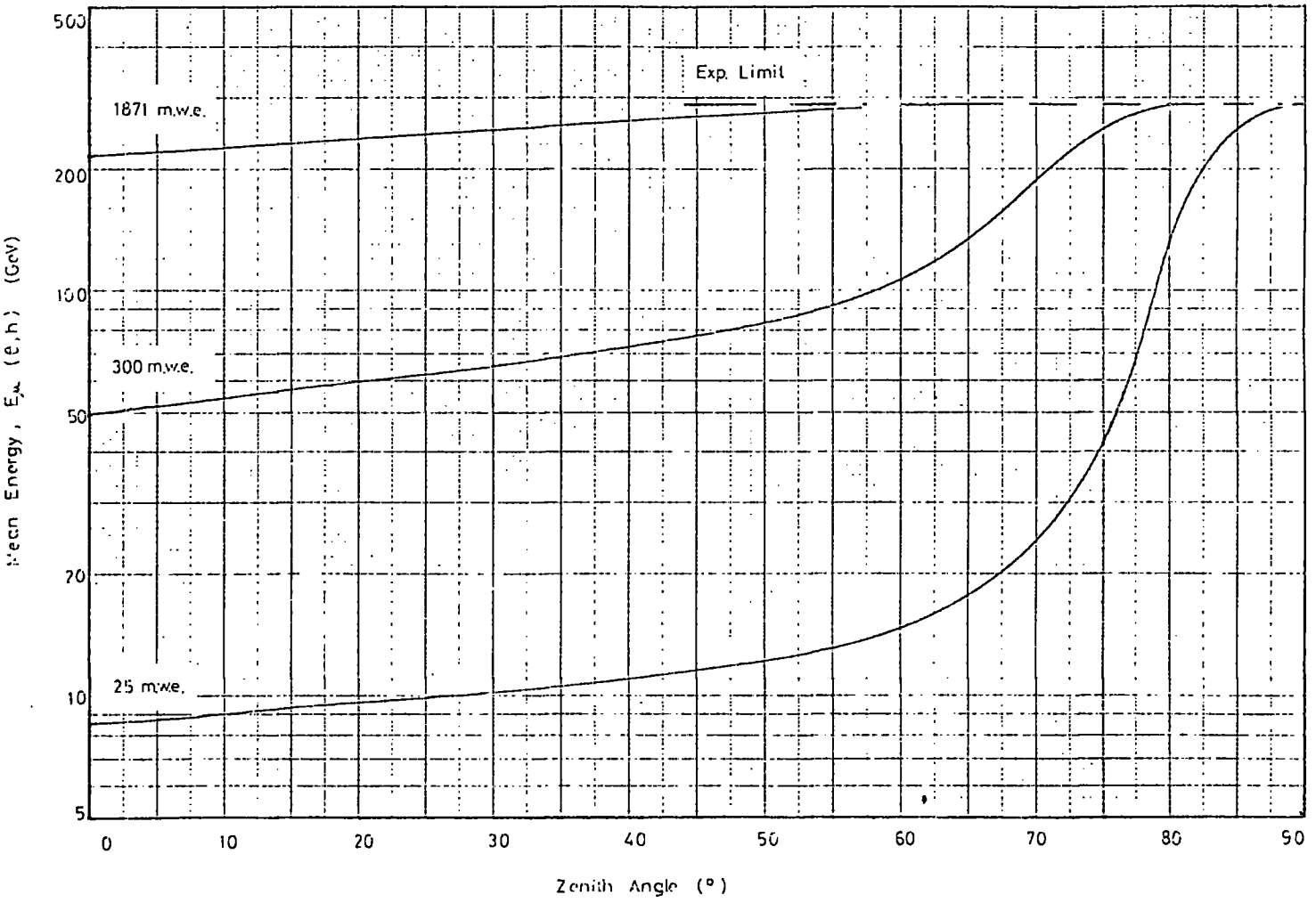

The use of the depth intensity curve for the calculation of the mean energies at depths $>$ 1871 m.we. leads to different results according to the depth intensity model assumed. The curve for vertical muons has been allowed to diverge at large depths in accordance with the use of the different expressions. The global mean has been calculated only from the exponential depth intensity relation at great depths and consequently reaches the asymptotic limit at $\sim$ 4000 m.we. For the other depth intensity models the curve would slowly approach the value for vertical muons with increasing depth, as a result of the increasing fall off of the angular distribution, but would not tend to a constant limiting value.

Table 3.3 : Mean energy of atmospheric muons underground

	25 m.we.	300 m.we.	1871 m.we.
$\bar{E}_\mu(o,h)$ - vertical muons	8.5	49.5	214
$\bar{E}_\mu(g,h)$ - all muons	13.5	79	259

3.6 Mean Energies in the B.D. Experiment

Using the detector apertures and atmospheric muon angular distributions at the depths of operation, the expected mean energies have been estimated for the B.D. experiment (Achar et al., 1965a). The points are shown in fig. 3.10.

The significance of the calculated mean energies is that the detected muons are from all zenith angles but restricted by the detector aperture. As the vertical and global curves run closer together at greater depths, the aperture effect of the apparatus becomes less important with the result that

FIG. 3·10: Variation of Mean Muon Energy with Depth.

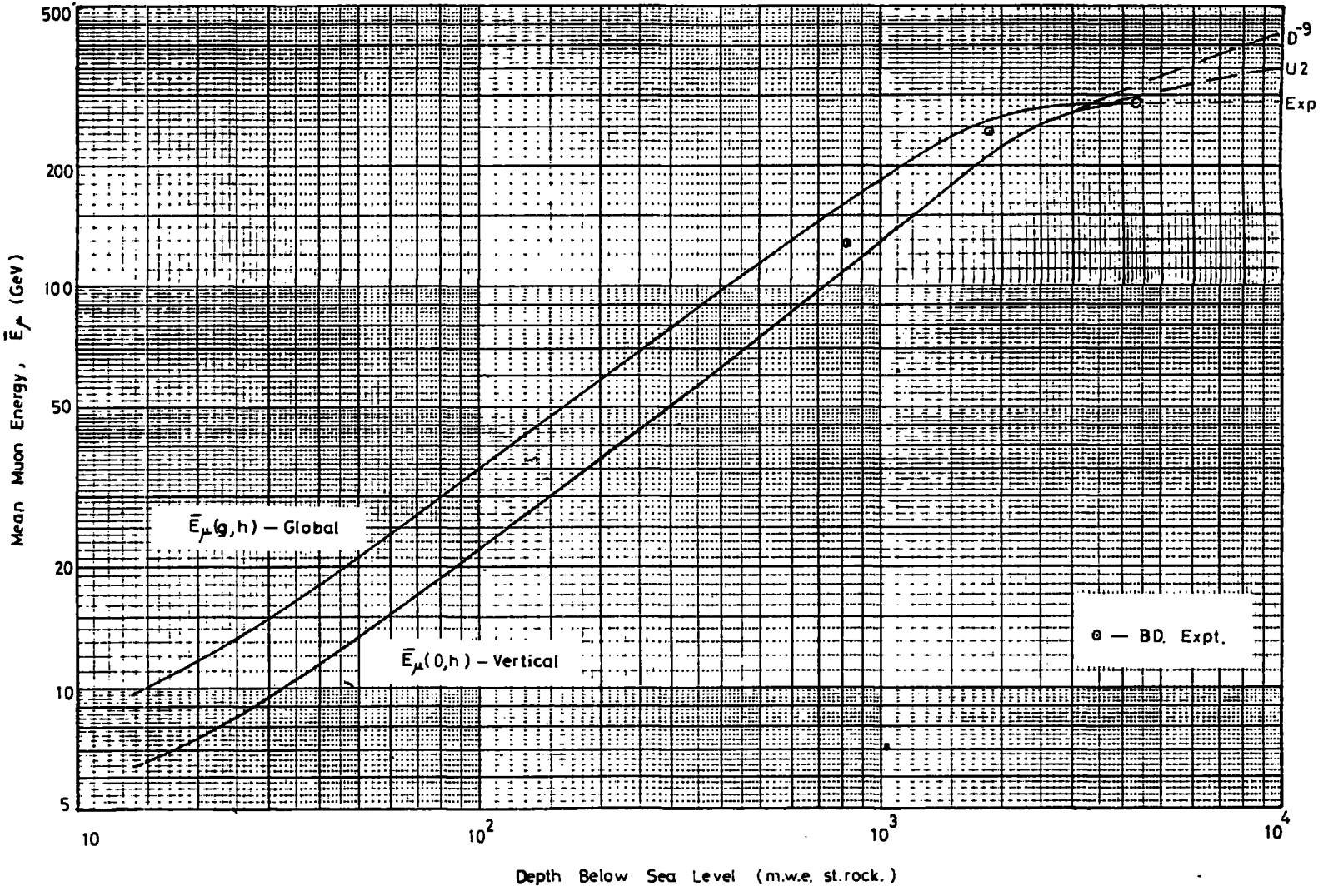

the effective mean energy is closer to the global mean. The 4361 m.w.e. point is at a depth where the calculated curves are dependant upon the extrapolation of the depth intensity curve and are, therefore, in doubt.

The effect on the calculated mean energy of the use of different values of the energy loss parameter b has been considered by Stockel. The error arising from the use of a non-realistic value of b for energies less than 1000 GeV, where the energy loss processes are quite well understood anyway, should give only a small error in the underground mean energy estimate. At higher energies, the errors may be larger. However, the sea level spectrum and the depth intensity relation for the equivalent depths are also doubtful so that even if a more accurate estimate of b was available, there would still be considerable uncertainty about the mean energy.

3.7 Shower Size probabilities

The mean energy of muons detected underground is reflected in the degree of electromagnetic accompaniment. There is, therefore, the possibility of determing the mean energy from measurements on this accompaniment. The probability of observing showers of more than a given number of electrons produced in the lead absorber of Tels. 1 & 2 has been calculated for different shower-initiating muon energies.

3.7 1 Knock On Interactions

The probability of a knock on collision of an incident particle of spin $\frac{1}{2}$ has been derived by Bhabha (1938) as,

$$\phi(E,E')dE' = \frac{2C m_e c^2 \gamma^2}{\beta^2} \cdot \frac{dE'}{(E')^2} \left[1 - \beta^2 \frac{E'}{E'_m} + \frac{1}{2} \left(\frac{E'}{E + mc^2} \right)^2 \right] \qquad 3.4$$

where $\phi(E,E')dE'$ is the probability per gm. cm.$^{-2}$ of a particle of kinetic energy E, charge z, and rest mass mc.^{2} creating a knock-on electron with energy between E' and $E' + dE'$. $C = 0.15\ Z/A$ cm.^{2} gm.$^{-1}$, Z is the atomic number and A the atomic weight of the absorber, $m_e c.^2$ is the electron rest mass and E'_m is the maximum transferable energy.

E'_m is given by Bhabha, as quoted by Sternheimer (1952) as,

$$E'_m = \frac{E^2 - m^2c^4}{mc^2\left(\frac{m}{2m_e} + \frac{m_e}{2m} + \frac{E}{mc^2}\right)} \qquad 3.5$$

For the case of an incident muon, m is the muon mass.

The energy transfer probabilities to knock on electrons from muons of incident energies 90, 200 and 400 GeV, given by equation 3.4, are shown in fig. 3.11.

3.7 2 Pair Production

Roe (1959) has calculated the electron pair production interaction probability for muons in typemetal ($\bar{Z} = 81$). Using the somewhat lengthy formula of Murota et al. (1956), he has calculated the probability curves, for 90, 200 and 400 GeV muons, which are shown in fig. 3.12. for values of the constants α and 'a' of 2 and 3 $m_e c^2/\mathcal{E}$ respectively. ($\mathcal{E}$ is the total energy of the electron + positron.)

The adoption of the curves derived for these values of the constants is merely for convenience in the present work. The significance of 'a' can be understood in terms of the energy division between the pair. At high energies, the probability of the pair taking very high and very low fractions of the energy is considerably increased. The limit of integration given by 'a' (= $nmc^2/\mathcal{E}$ where n is an integer) becomes important on account of the enhanced

FIG. 3·11: Ionisation and Collision Interaction Probabilities.

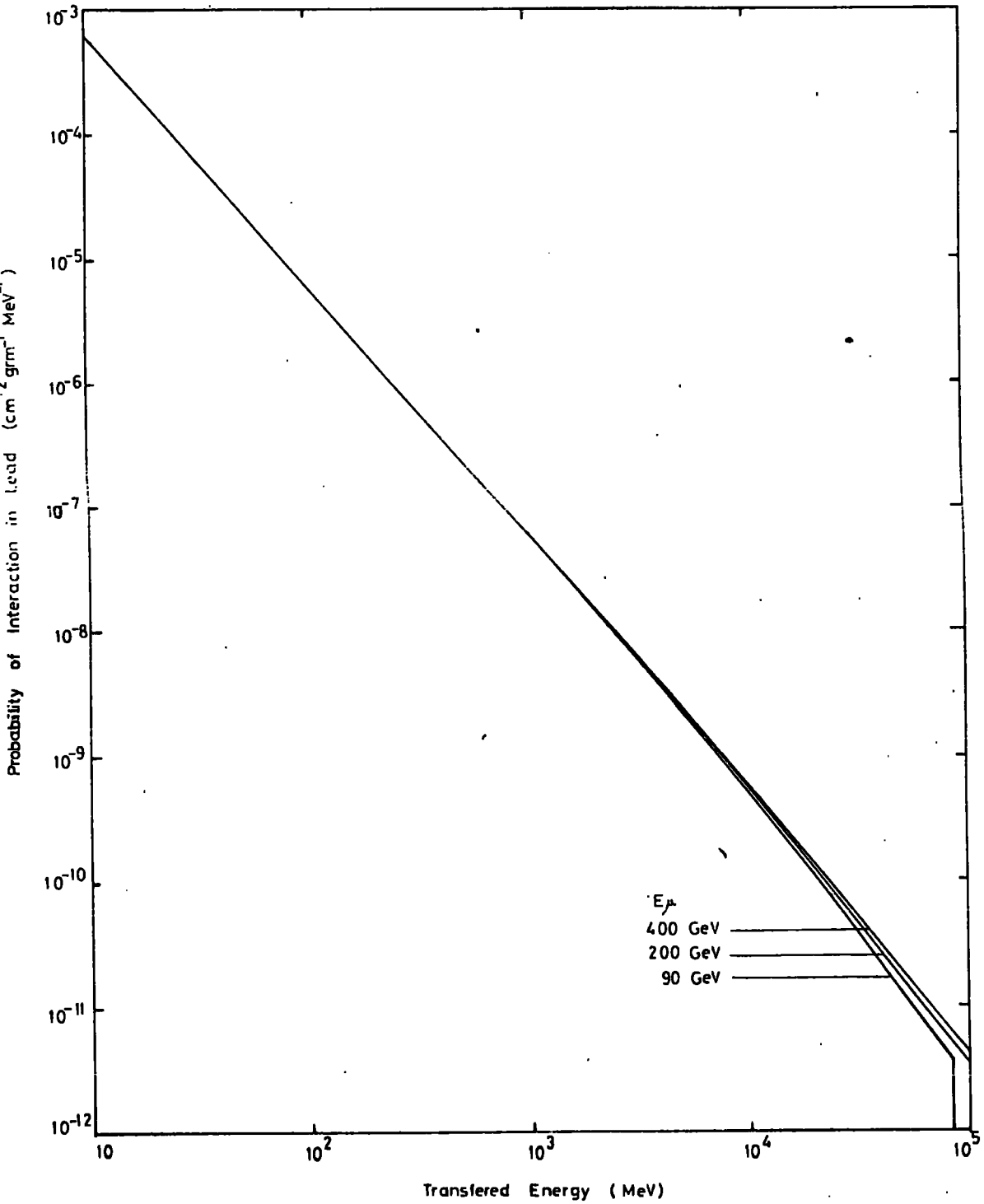

FIG. 3·12: Pair Production Interaction Probabilities.

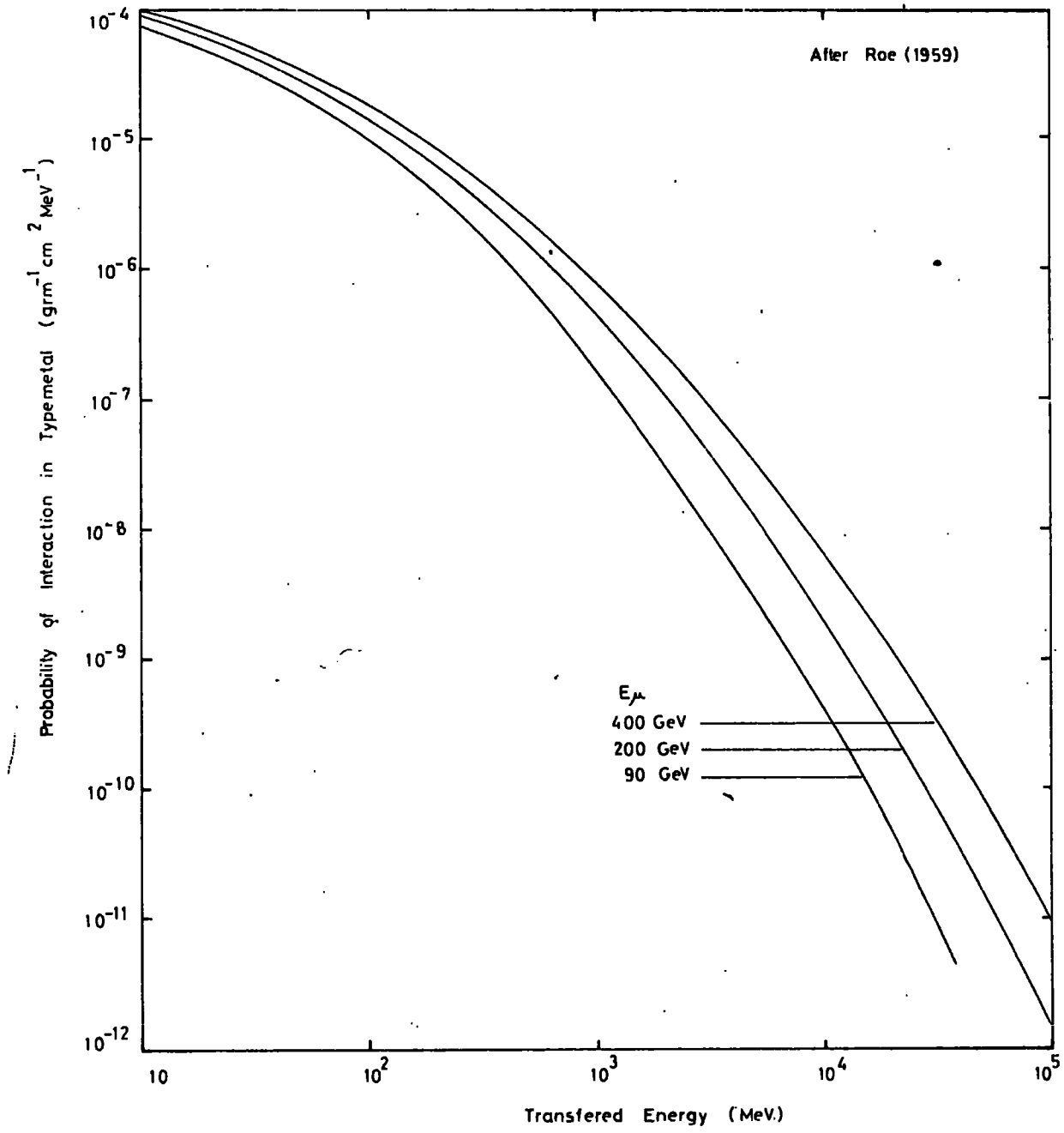

FIG. 3·13: Bremsstrahling Interaction Probabilities.

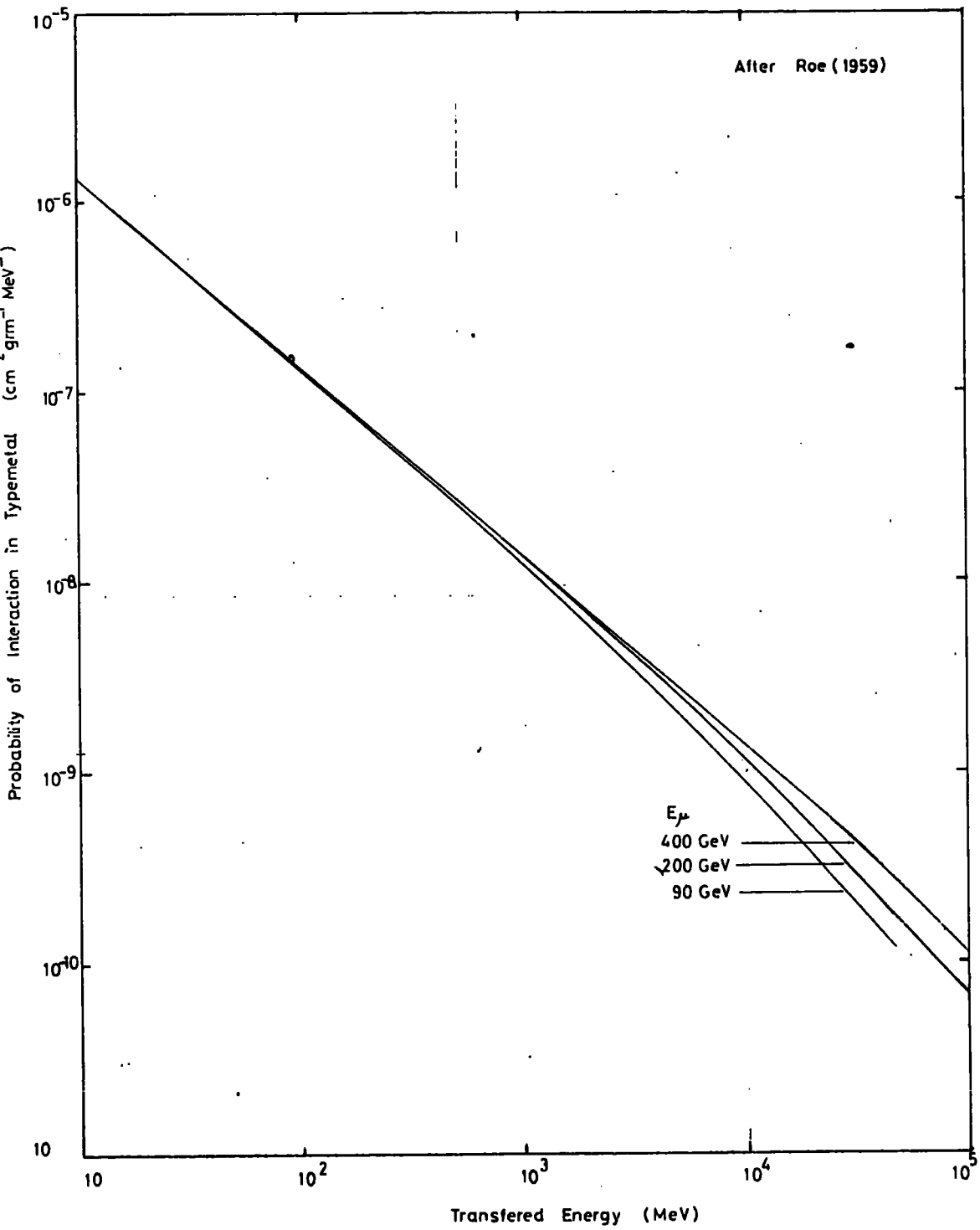

probabilites of the pair taking these extreme energy fractions.

For application to the shower rate expected in the K.G.F. experiment, a relatively large value of 'a' would be appropriate. The error arising from the use of n = 3, and not 10 or more, is not significant for the present analysis as only the low energy transfer probability is effected and it is in this region that the knock on process contributes considerably more than pair production to the total interaction probability.

The significance of 'α' is not clear, however, for the same reason, any error in the value adopted is not significant in the present analysis.

3.7 3 Bremsstrahlung

The probability of a muon, of energy E, emitting a quantum of energy between E′ and E′ + dE′ has been given by Rossi (1952) as,

$$\phi_{rad}(E,E')dE' = 4\alpha \frac{N}{A} Z^2 r_e^2 \frac{dE'}{E'} F(U,v) \qquad 3.6$$

where N is Avogrado's number, r_e is the classical radius of the electron $\alpha = e^2/hc = \frac{1}{137}$ and the other symbols are as previously designated.

F(U, v) is the electron screening correction factor and has been calculated by Bethe and Heitler (1934).

Using equation 3.6 with the screening correction factor appropriate to the γ and muon energies, Roe has calculated the bremsstrahlung interaction probabilities and these are shown in fig. 3.13, again for muon energies of 90, 200 and 400 GeV.

The total interaction probabilities, for the 3 processes considered above, are as shown in fig. 3.14. (Although Roe's calculations were made for interactions in typemetal, the probabilities have been assumed to be

FIG. 3·14 : Total Electromagnetic Interaction Probabilities.

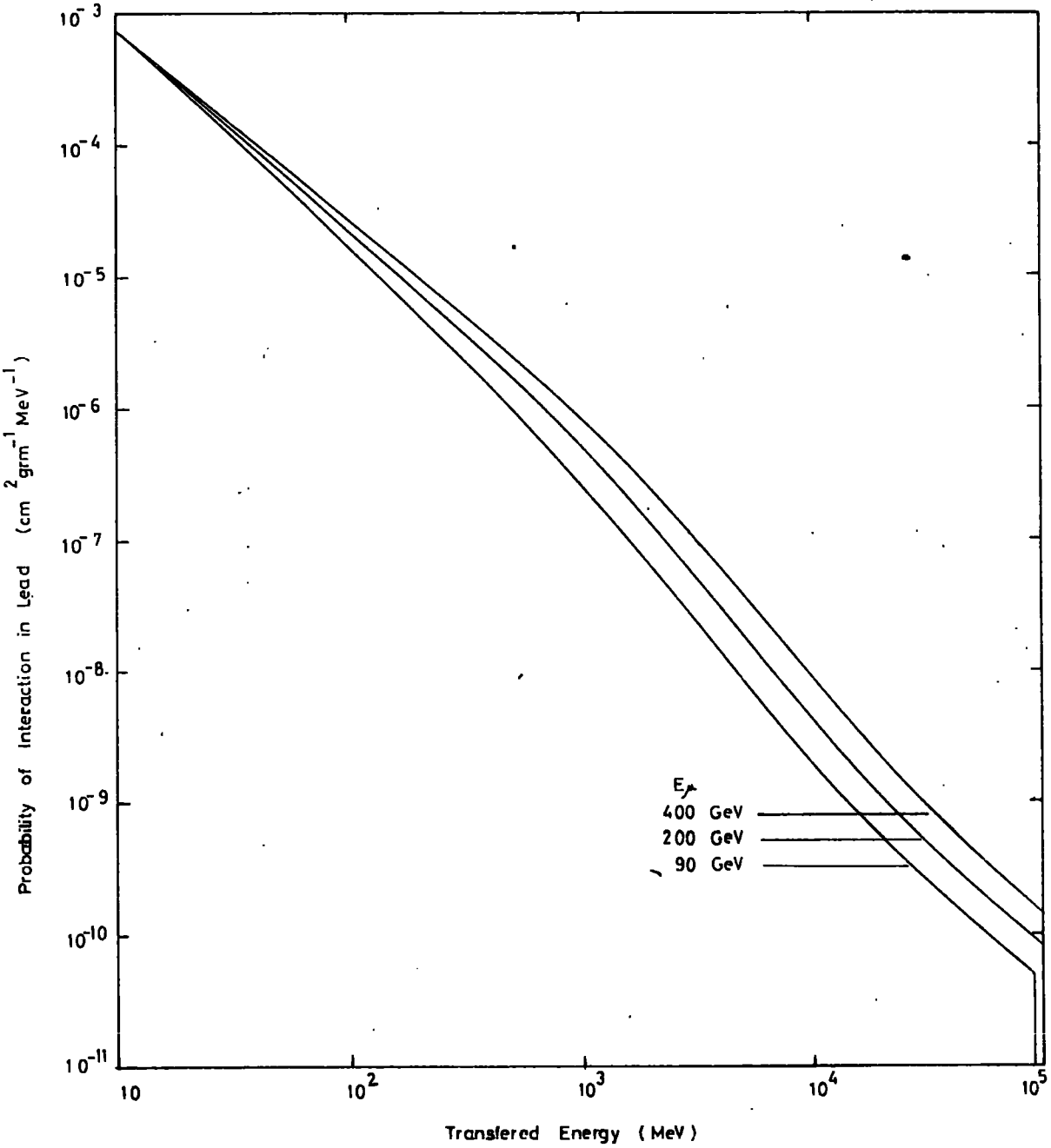

applicable to lead which has almost the same Z and A.)

3.7 4 Shower Observation Probability

Having established the probability of the production, by a muon, of an electromagnetic shower - initiating primary, it is necessary to estimate the probability of observing, in a flash tube tray, such a shower from a primary produced in the lead absorber.

Rogers(1965) has given shower curves, from the calculations of Crawford and Messel (1962), for shower - initiating primary electrons, in lead, of energies 0.1 - 1 GeV. For the higher range 1 - 100 GeV, the shower curves of Buja (1963), as quoted by Rogers, are suitable. The composite shower curves from these two sources are shown in fig. 3.15.

The parameter ϵ may be defined as representing the probability of a shower, having been produced in the absorber, consisting of more than n electrons on passing through the following flash tube tray layer.

Thus,

$$\epsilon = 1 - \frac{1}{t}(b - a) \quad \text{for } b > t$$

$$\epsilon = \frac{a}{t} \quad \text{for } t > b$$

where t is the total absorber thickness, a is the thickness of absorber over which the shower consists of $>$ n electrons and b is the thickness of absorber from the primary production point to the depth where the shower is reduced to n electrons.(see fig. 3.15.)

Assuming an effective absorber thickness t of 10.8 radiation lengths in lead, this being a median value for atmospheric muons expected in Tels. 1 & 2, the values of ϵ have been estimated from the cascade shower curves

FIG. 3·15: Electron-initiated Cascade Shower Curves.

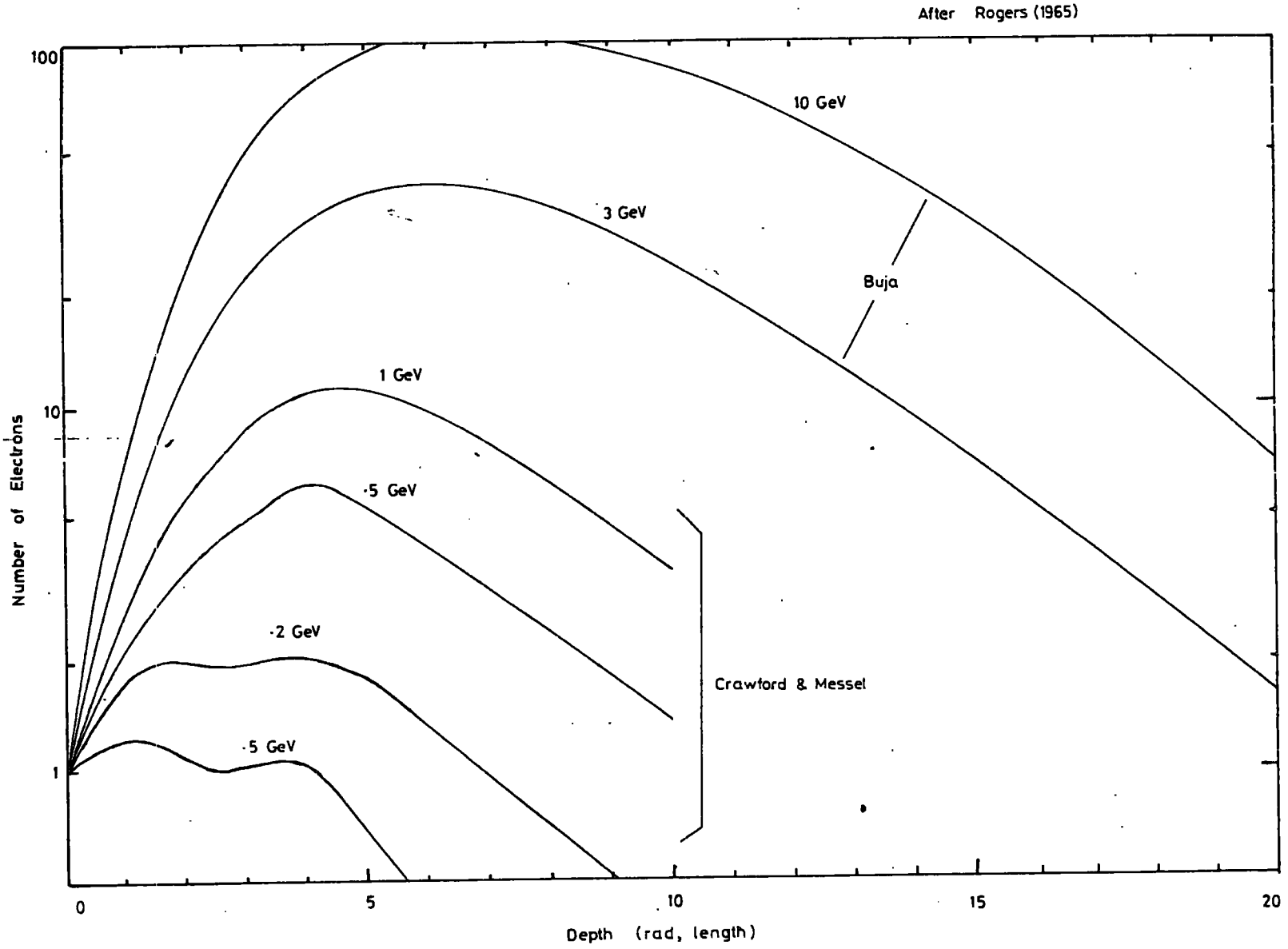

for different electron primary energies and different minimum numbers of electrons observed in the showers.

If the total interaction probability derived in the previous section is P_E then ξP_E represents the probability of observing, in a flash tube tray layer following a lead absorber, a shower of more than n electrons from a primary electron of energy Ep produced by a muon of energy E_μ.

Consequently $\int \xi P_E . dE_p$ is the probability required, i.e. the probability of observing more than n electrons in a shower, per muon of energy E_μ traversing a lead layer in Tels. 1 & 2.

The probability of observing different numbers of electrons in showers can be seen from the variation of $\xi P_E . E_p$ with E_p, for 200 GeV muons in fig. 3.16.

3.7 5 Correction for γ - Initiated Showers

Throughout the calculation, the shower curves for electron initiated showers have been used. Clearly this is not valid for higher energy shower primaries which are mainly γ - initiated from bremsstrahlung interactions.

Cascade shower curves for both electron and photon - initiated showers for muons incident on lead (E. Mamidzhanian - private communication) have been used to estimate the ratio, $\bar{n}e/n_\gamma$, of electron to γ - initiated showers for different shower primary and muon energies. Figure 3.17 shows the variation of $\int \xi P_E \, dE_p$ with n, the number of electrons observed, corrected for $\bar{n}e/n_\gamma$. The probability curves are as calculated for 90, 200 and 400 GeV and these have been extrapolated and interpolated for other muon energies.

FIG. 3·16: Variation of Observation Probability with Shower Primary Energy

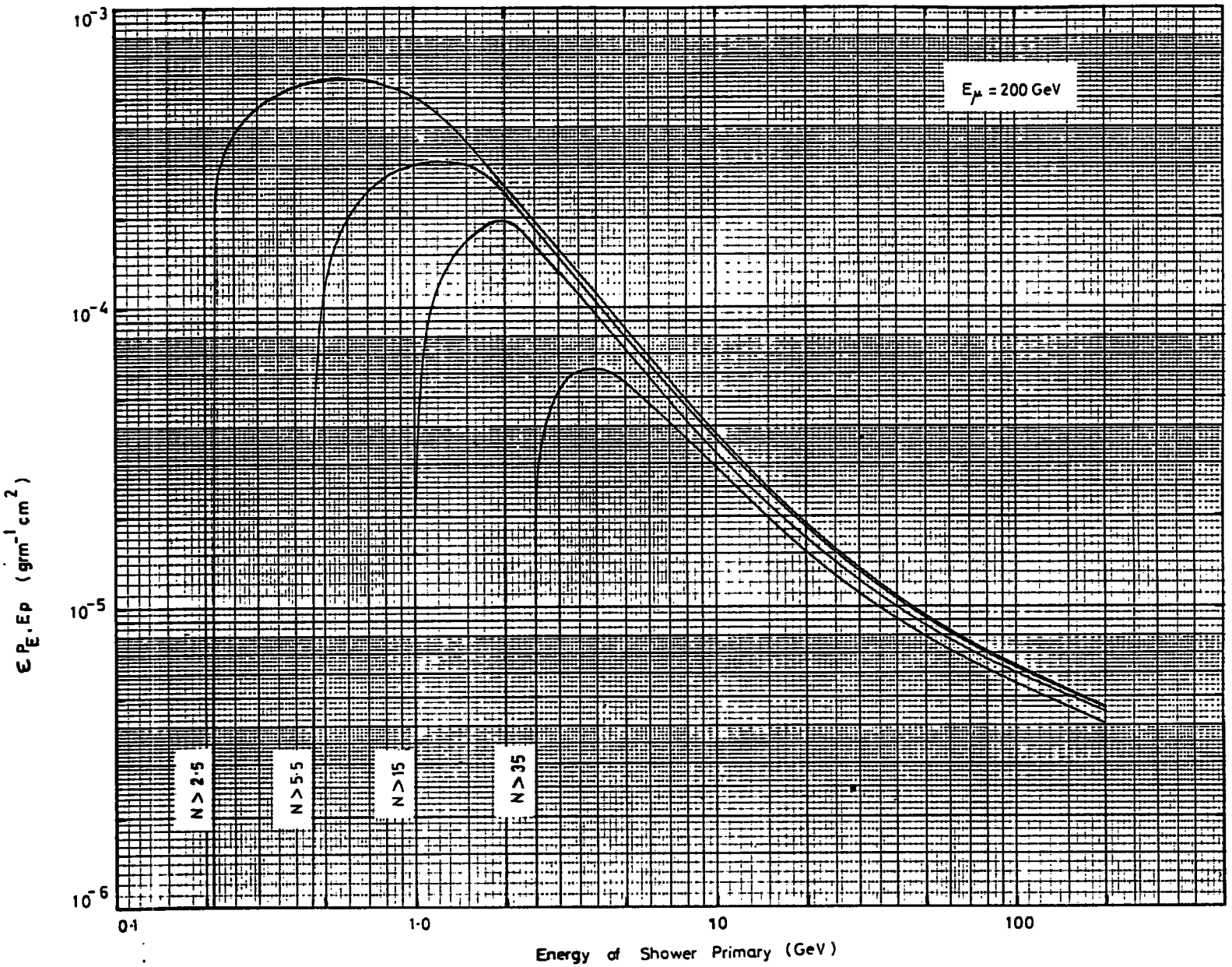

FIG. 3·17: Probability of Shower Observation in Telescopes 1 & 2.

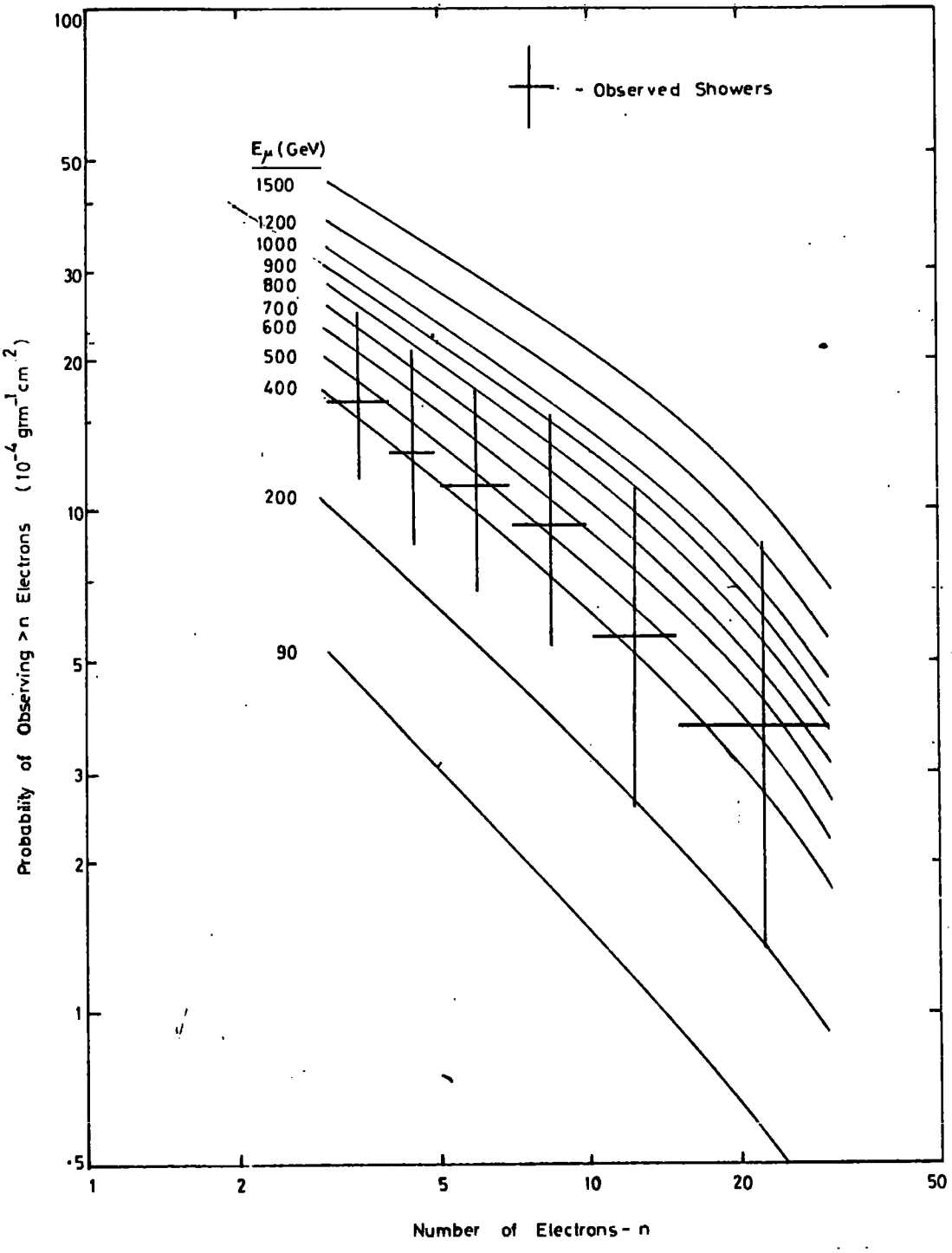

CHAPTER 4

Neutrino Interactions.

In order to estimate the intensities and energy spectra of those muons detected underground which have been produced in neutrino interactions, it is necessary to know; firstly, the neutrino production mechanisms; secondly, the neutrino interaction cross sections and; finally, the energy taken by muons produced in such interactions.

The neutrino energy spectra calculated by Osborne et al. (1965) have been used together with the best estimates of the cross-sections and muon energies, both predicted and measured in accelerator experiments, to estimate the energy spectra of neutrino-induced muons.

4.1 The Energy Spectrum of Atmospheric Neutrinos

The present energy limitations of the particle accelerators for neutrino production, result in great importance being attached to cosmic ray studies of neutrino interactions at energies $\gtrsim$ 10 GeV. With this in mind, several workers since Greisen (1960) have made estimates of the sea level energy spectra* of neutrinos produced in the atmosphere. Some workers have only considered certain production mechanisms; for example Markov and Zheleznykh (1961), who considered pion decay only, and Zatsepin and Kuzmin (1962) who considered muon and pion decay only. The most comprehensive works are those of Osborne et al. (1965) and Cowsik et al. (1963, 1966).

---

* The underground spectra of neutrinos is virtually the same as the sea level spectrum if no resonances exist in the cross-sections.

The spectra of Osborne et al., described below, were derived for neutrinos produced in the decay of muons, pions and kaons. (Kaon decay modes with a branching ratio $< 1\%$ were neglected). Basing their model of neutrino parent propagation in the atmosphere on the measured sea level muon spectrum at different zenith angles and on the propagation of γ cascades in the atmosphere (Osborne & Wolfendale, 1964), these authors calculated the vertical and horizontal neutrino spectra for K/π ratios of 0, 20 and 40%. They used the neutrino energy spectra expressions of Zatsepin and Kuzmin, together with the spectrum of decaying muons, to calculate both the electron and muon neutrino spectra from this source. On the basis of the O.P.W. sea level spectrum, they worked back to a pion production spectrum and used it to calculate the neutrino spectra from pion and kaon decay. The spectra obtained by Osborne et al. for the horizontal direction are shown in fig. 4.1.

Differences arise between the vertical and horizontal spectra for several reasons. Firstly, the neutrino spectrum from muon decay in the vertical direction falls rapidly as less muons decay at higher energies. In the horizontal direction, where the path lengths are greater, more high energy muons are able to decay and the neutrino spectrum is accordingly enhanced. Secondly, the horizontal intensity of neutrinos from pion decay is enhanced principally because the pions have a higher probability of decaying in the upper atmosphere. The effect is greatest at high energies. The same effect is emphasised in the case of kaons on account of their greater rest mass, such that, even though kaon decay produces less neutrinos than pion decay at low energies, it becomes the more important process at higher energies.

The ratio of the total intensities of muon neutrinos in the horizontal

FIG. 4.1: Energy Spectra of Horizontal Atmospheric Neutrinos

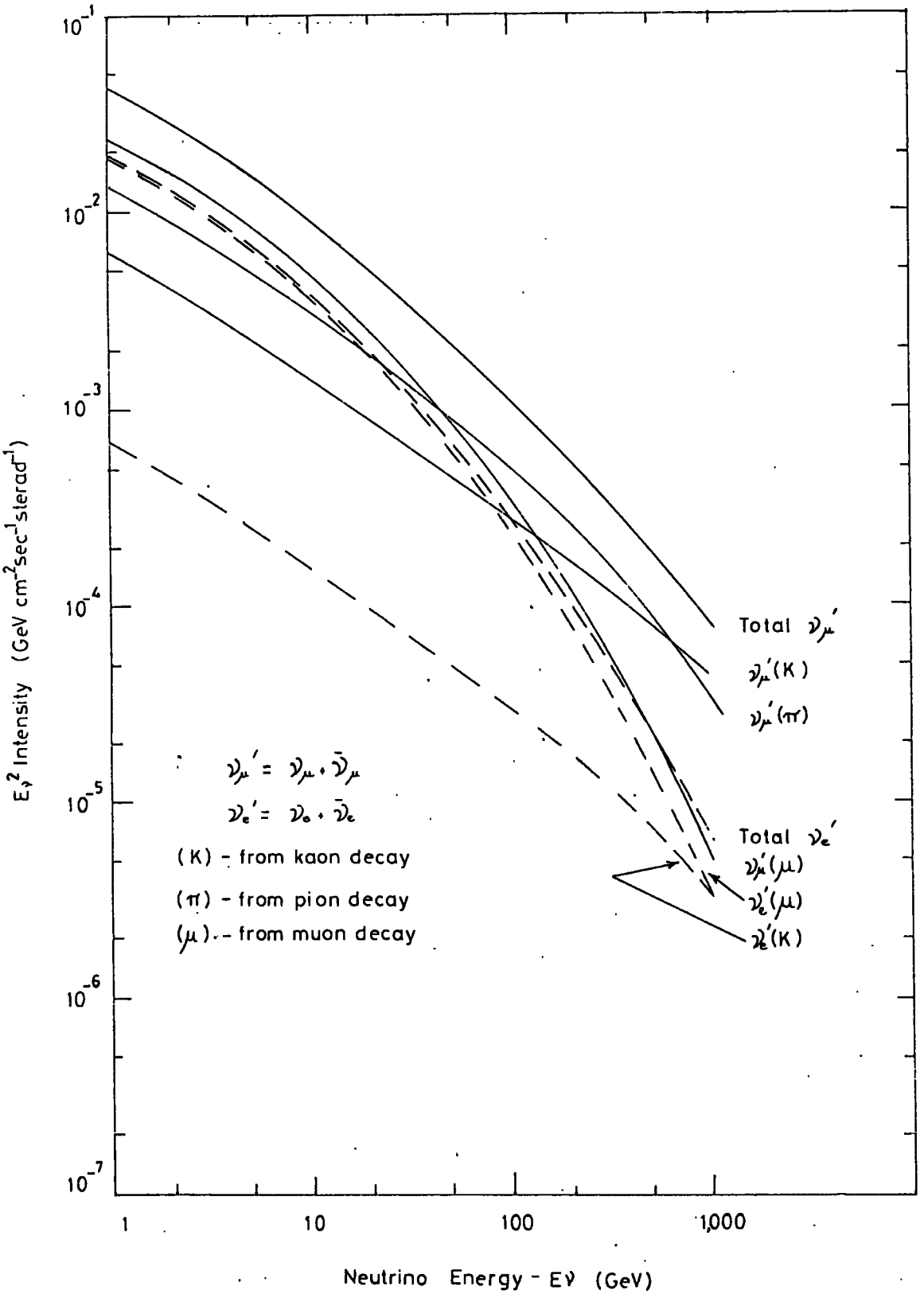

and vertical directions was found to be 1.43 at 1 GeV increasing to 3.7 at 1000 GeV.

The uncertainties regarding the value of the K/π ratio have their greatest effect in the vertical direction, the latter being about twice as great as that in the horizontal. As the spectra of Osborne et al. are in quite good agreement (i.e. $\sim$ 20% difference) with other workers, these neutrino spectra are considered to be quite adequate and suitable for use in connection with the K.G.F. Experiment, the errors arising from the doubt about the K/π ratio being reduced on account of the acceptance bias towards horizontally-incident particles.

4.2 Neutrino Interactions.

The neutrino interactions which can be detected by the K.G.F. detectors are those producing at least one muon with $\geq$ 100 MeV kinetic energy. Four types of interaction could satisfy this requirement.

4.2 1 Elastic Interactions

Elastic interactions are those in which no additional hadrons are produced and the lepton number is conserved. The following neutrino interactions fall in this category.

$$\nu_\mu + n \rightarrow p + \mu^- \quad : \quad \bar{\nu}_\mu + p \rightarrow n + \mu^+ \qquad 4.1$$

Yamaguchi (1961) has calculated theoretical cross-sections for the above reactions and has found that they increase linearly with energy to about 1 GeV where the effect of form factors is to suppress the rise. The cross-sections for both interactions tend to the asymptotic value of 0.75×10^{-38} cm.$^{-2}$. Below 1 GeV, the cross-section for $\nu_\mu + n$ is about three times as great as

that for $\bar{\nu}_\mu$ + p and falls slightly, after the initial increase, to level off at the asymptote.

The 1963/64 CERN experiments, on neutrino interactions in freon, which have been reported by Block et al.(1964), showed that there is no reason to doubt the value predicted by Yamaguchi. More recently at CERN, neutrino interactions in propane have been studied up to $\sim$ 10 GeV. These results give an asymptotic value to the cross-section of 0.6×10^{-38} cm.$^{-2}$ (Young, private communication and Perkins, 1969). This value has been taken for the calculation of the neutrino-induced muon rate at K.G.F.

The fraction of energy taken by the muon has been given by Block et al. and Young as 1.0 and 0.9 respectively. Again, the latter value has been adopted. The most recent CERN propane results (to be published) indicate that, at energies < 10 GeV, $E_\mu/E_\nu \approx 0.8$. However the ratio increases with energy to 10 GeV and a ratio of 0.9 remains the best estimate for the K.G.F. neutrino spectrum which is thought to have a mean energy of a few tens of GeV.

4.2 2 Inelastic Interactions

Particularly at higher energies, neutrino interactions may result in the creation of one or more hadrons. Such interactions are termed 'inelastic'. Those interactions mediated by vector bosons, however, are not included. The interaction can be represented by,

$$\nu_\mu + N \rightarrow N' + \mu + \pi + \ldots\ldots \qquad 4.2$$

Experiments using the large accelerators have shown that most inelastic neutrino interactions below 10 GeV proceed via single pion production channels. Berman and Veltman (1965) have proposed that the single pion production proceeds via the manifestation of the $N^*\left(\frac{3}{2},\frac{3}{2}\right)$ resonance at 1238 MeV. They have

calculated the cross-section for this interaction and, on the assumption of the same form factors, have found it to be of similar form to the elastic cross-section, but saturating at a higher energy.

As the neutrino energy is increased, the number of available inelastic channels increases also. The K.G.F. apparatus does not permit much distinction between these different channels and it is the total inelastic cross-section that is of primary interest.

The total cross-section for the CERN freon and propane runs has been given by Perkins (1969) with the inelastic contribution expressed as

$$\sigma_{inel} = 0.6 \times 10^{-38} \; E_\nu \qquad \text{cm.}^2/\text{nucleon.}$$

This is an increase over the value of $0.45 \times 10^{-38} \; E_\nu$ given by Block et al. and agrees well with the predicted value of $0.7 \times 10^{-38} \; E_\nu$ due to Berman and Veltman for single pion production.

Lee and Yang (1962) pointed out that on the assumption of a local nature of the leptonic current, the cross-section could be, at the most, quadratically dependent on the neutrino energy. Although the earlier freon runs at CERN showed that the cross-section could be described by $\sigma_{inel} = 0.19 \times 10^{-38} \; E_\nu^{\,2}$ cm.^{2}/nucleon, the additional propane results are better described by the linear form above.

The experimental data obtained to date does not show any evidence for saturation of the inelastic cross-section and clearly its behaviour above 10 GeV must be taken as a variable for calculating the expected rates at K.G.F.

The fraction of energy taken by the muon in inelastic interactions is not well known from the machine experiments on account of the possible missing mass in the form of neutrons and γ-rays. In calculating the neutrino-induced muon spectra at K.G.F., Achar et al. (1965e) and Osborne (1966)

assumed the fraction to be 0.5. This figure was increased to 0.67 in the report by Menon et al. (1967b) on the strength of more recent data from CERN. This latter value has been supported by the latest CERN data (Ramm., private communication).

4.2 3 Boson mediated interactions

The possible mediation of weak interactions through bosons have been considered by several authors since Yukawa (1935). Lee and Yang (1960) presented the intermediate boson in its present form in which it must exist in both positively and negatively charged states, with spin 1 and magnetic moment $(e/2M_W)(1 + k)$. The short range of the weak interactions necessitates its being of large mass.

If the intermediate boson exists, its production and decay must increase the rate of neutrino-initiated events expected at K.G.F. At lower energies, not much in excess of the critical energy for its production, the boson would be mainly produced by the incoherent interaction,

$$\nu_\mu + N \rightarrow N + \mu + W \qquad 4.3$$

At higher energies on the other hand, the interaction would be more likely to occur with the whole nucleus in the coherent reaction,

$$\nu_\mu + Z \rightarrow Z' + \mu + W \qquad 4.4$$

A fourth type of interaction which may be produced by a neutrino is the resonance type. Such a resonance was proposed by Glashow (1960) as,

$$\bar{\nu}_e + e^- \rightarrow W^- \qquad 4.5$$

The cross-section for elastic lepton-lepton interactions is about 3 orders of magnitude down on the nucleon-lepton interactions 4.3 & 4.4. If a W boson is produced, a resonance occurs in the $\bar{\nu}_e + e^-$ cross-section with a peak

value of 10^{-28} cm.^{2}/electron. The motion of the target electrons reduce this value to 10^{-31} cm.^{2}/electron with a finite width of $E_t/10$ GeV. Although the threshold laboratory energy for the reaction is $Mw^2/2me$, the size of the resonance could partly compensate the rapidly falling $\bar{\nu}e$ spectrum to give a noticable contribution to the total events detected at K.G.F.

Bosons produced in the above reactions could decay through the following modes.

$W \longrightarrow \mu + \nu_\mu$)
$W \longrightarrow e + \nu_e$) Leptonic modes
)

$W \longrightarrow \pi$, K etc. Non-leptonic mode.

As yet, the neutrino experiments performed at CERN, Brookhaven and Argonne have failed to produce intermediate bosons. The CERN freon data (Bernadini et al. 1965), which was analysed for non-interacting particles from leptonic decays, did not give a result above the expected background of penetrating pairs from inelastic interactions. This set the minimum boson mass limit of 2.2 GeV. Non-leptonic decay mode analysis for several mesons yielded five events which could qualify for boson decay and these led to a minimum mass limit of 1.7 GeV. The Brookhaven and Argonne approach (Burns et al., 1965 and Lamb et al., 1965) was to study the angular distribution of muons from boson decay. These experiments, too, were only able to establish a lower limit of $\sim$ 2 GeV for the boson mass.

4.3 Cross Sections for Neutrino Interactions

The energy spectrum of neutrino-induced muons at the K.G.F. site was first calculated by Osborne (1966). This calculation has subsequently been modified according to the current best estimates of the assumptions

made, by Menon et al. (1967b) and Craig et al. (1968). The spectra presented here are those of Craig et al. modified only by the increased inelastic cross section reported by Perkins.

For the uninvestigated region above 10 GeV, two forms for the variation of cross section with energy have been considered: (a) $\sigma_{inel} \propto E_\nu$ to 10 GeV and constant at higher energies and (b) $\sigma_{inel} \propto E_\nu$ to 10^4 GeV and constant at higher energies. The horizontal muon spectra have been calculated for both of these forms.

Similarly, 3 cases have been considered for intermediate boson production, Mw = 1.8, 2.5 & 3.0 GeV via the incoherent and coherent interactions (equations 4.3 & 4.4).

Burns et al. (1965) quote the cross-sections for boson-mediated interactions as calculated by Wu et al. These cross sections were used by Osborne to the upper limit of their validity, 20 GeV. (The cross-sections of Wu et al. are for interactions in aluminium ($\bar{Z}$ = 13, A = 27) but as K.G.F. rock is very similar (mean $\bar{Z}$ = 12.9, mean A = 26.3), they are taken as being applicable to that too.) Thereafter, Osborne interpolated for values of the cross sections to 100 GeV, above which the asymptotic limit of von Gehlen (1963) becomes applicable. On the basis of these cross-sections, the coherent interaction becomes dominant above 50 GeV.

The energies taken by the 'prompt' muon (that produced with the boson) and the boson itself have been considered by Veltman (1963), for Mw = 1.8 GeV & $E_\nu \sim$ 10 GeV, and have been shown to be peaked at energies proportional to their masses. The muon spectrum is, therefore, peaked at $E_\nu M_\mu / (Mw + M_\mu)$ which corresponds to the minimum momentum transfer of $Mw^2/2 E_\nu$. Thus, near the threshold energy for the interaction, the muon has been assumed to

take on energy of E_ν /20.

The asymptotic case at high energies has been considered by Lee et al. (1961), who found that the prompt muon then takes on energy of E_ν /2.

Osborne has taken a value of 40% for the muonic decay mode of the boson. The energy of the decay muon has been deduced from the work of Bell and Veltman (1963) and Uberall (1964) who calculated that the intermediate boson is almost 100% circularly polarised. The muon energy was shown to be, consequently, 0.25 of the boson energy.

Therefore, for the near threshold case, the decay muon has an energy 0.95 $E_\nu/4$ and for the asymptotic case 0.5 E_ν /4.

Table 4.1 shows the cross-sections for the various interactions and the number of events expected from each.

4.4 The Energy Spectrum of Neutrino-Induced Muons.

By virtue of the much greater penetration of muons than electrons, the effective target thickness of rock presented to muon neutrinos is much greater than that presented to electron neutrinos (except in the case of the Glashow resonance type interaction). The latter may, therefore, be neglected when considering the total spectrum and event rate expected underground in the K.G.F. experiment.

The general expression for the intensity of neutrino-induced muons, from a zenith angle θ , is given by Osborne as,

$$I_\mu(\theta) = \frac{N_A}{A} \int_{E_{min}}^{\infty} N_\nu(E_\nu, \theta) \cdot R_{eff}(E_\nu) \sigma(E_\nu) \, dE_\nu \qquad 4.6$$

where N_A is Avagadro's Number, A is the Atomic Weight, $N_\nu(E_\nu, \theta)$ is

TABLE 4.1 : Neutrino cross-sections and number of events expected to 31/12/68.

Interaction	Cross-Section	Fraction of Energy taken by Muon	Total+ No.of events	No.of+ events at $> 50^{o}$	Approx. median neutrino energy (GeV)
Elastic	0.6×10^{-38} per n-p pair	0.9	3.5	3.1	2.5
Inelastic					
(i) $E_\nu < 10$ GeV	$0.6\ E_\nu \times 10^{-38} cm^2$ per nucleon	0.67	7.7	6.7	-
(ii) $E_\nu > 10$ GeV	(A) $0.6\ E_\nu \times 10^{-38}$ for all E_ν	0.67	17.7	15.5	25
	(B) 0.6×10^{-38}	1.0	7.3	6.2	9
Boson production					
	Mw = 1.8 GeV	(a) near threshold*	19	16.6	100
		(b) asymptotic	67	59	
	Mw = 2.5 GeV	(a) near threshold	8.6	7.5	200
		(b) asymptotic	31	27	
	Mw = 3.0 GeV	(a) near threshold	5.6	4.9	300
		(b) asymptotic	22	19	
Glashow resonance	Mw = 1.8 GeV	0.25	5.8	-	3000
	Mw = 2.5 GeV	0.25	1.3	-	6000
Total of all interactions	(Upper limit, Mw = 1.8 GeV & case (A)		54	~46	
	(Lower limit, Mw 1.8 GeV & case (B)		18.5	16.0	

+ Totals include O.S.T. events corrected for detection efficiency.

* The cross section for boson production varies with energy as described in section 4.3. Cases (a) & (b) represent the upper and lower limits.

the intensity of neutrinos of energy E_ν, R_{eff} is the effective range in rock of muons produced by neutrinos with energy E_ν and $\sigma(E_\nu)$ is the total cross-section per nucleus for the particular interaction.

This equation has been used by Craig et al. to predict the horizontal muon spectra of 7500 m.w.e. st. rock for all of the various interactions and cases described previously except the Glashow resonance. These are shown in fig. 4.2 calculated from the neutrino spectra in fig. 4.1 to 1000 GeV. At higher energies, they are calculated from neutrino spectra based on the U2 primary spectrum described in Chapter 3.

Table 4.2 shows the mean energy of horizontal muons, with energy above 0.5 GeV, for various cross-section assumptions.

A comparison of neutrino-initiated muon intensities from the inelastic interaction expected for different zenith angles is shown in fig. 4.3.

Both the rate of neutrino-induced muons and their mean energy are sensitive to the various assumptions made about the cross-section and boson mass. The relation between the two parameters is shown in fig. 4.4. It is clear that the event rate is very sensitive to the boson mass at small mass values. The rate is less sensitive to the inelastic cut off energy. On the other hand, the mean energy is quite sensitive to the cut off energy. Lee (private communication to Wolfendale) has pointed out that at higher energies, the energy fraction taken by the muon in the inelastic interaction may not be valid. If the fraction falls with energy, the mean muon energy would be less sensitive to the saturation energy and it may not be possible to distinguish between, (a) a continuously increasing cross-section with falling fraction of energy taken by the muon and (b) a saturating cross-section and a constant energy fraction.

FIG. 4.2: Horizontal Spectra of Neutrino Induced Muons.

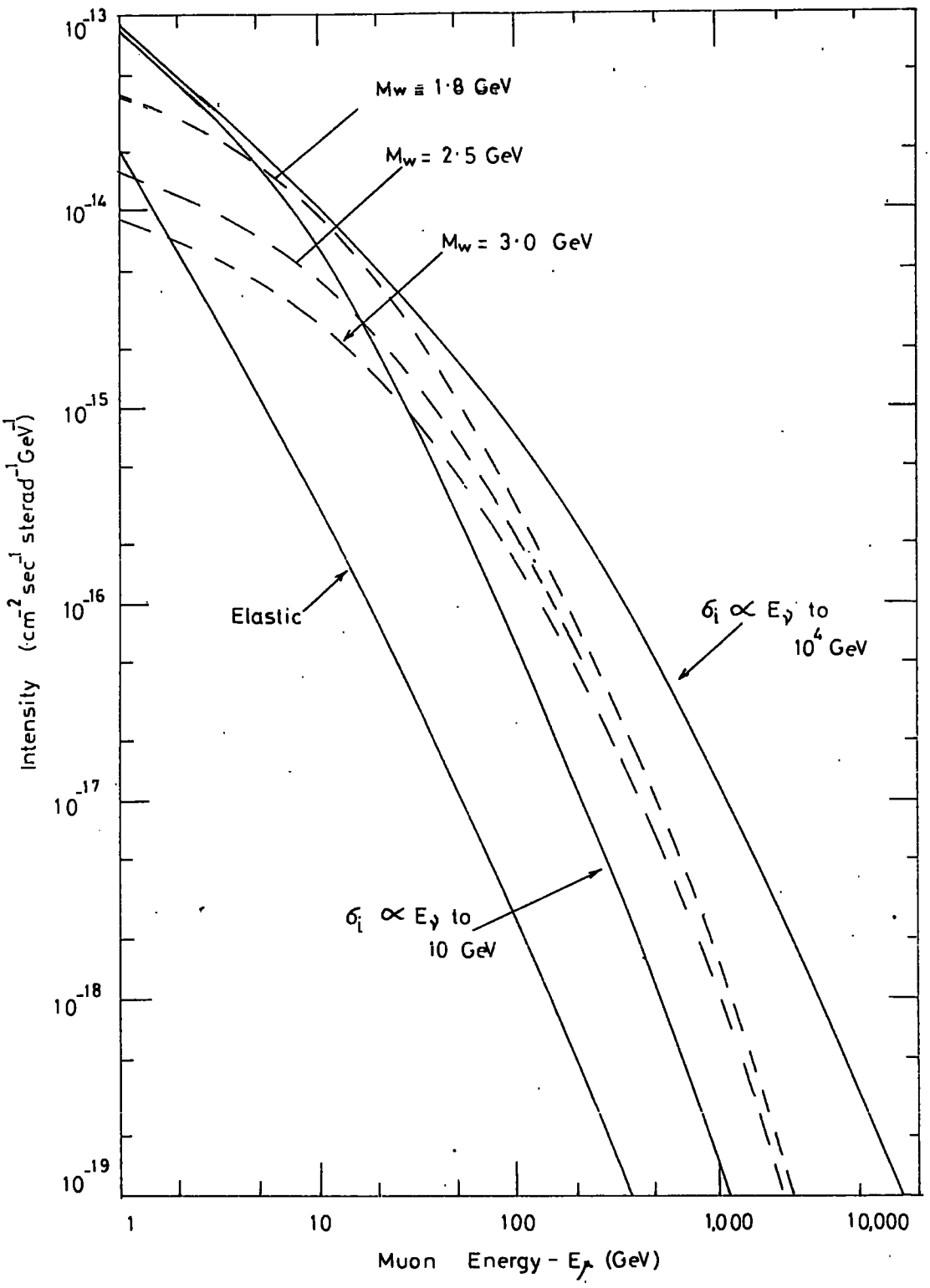

TABLE 4.2 : Mean energies of muons from neutrino interactions.

Interactions and Cross Sections	Mean Energy (GeV)
(a): elastic + $\sigma_{inel} \propto E$ to GeV, then constant	8.8
(b): elastic + $\sigma_{inel} \propto E$ to 10^4 GeV, then constant	80
(c): (a) + boson production, Mw = 1.8 GeV	28
(d): (a) + boson production, Mw = 3.0 GeV	27
(e): (b) + boson production, Mw = 1.8 GeV	60
(f): (b) + boson production, Mw = 3.0 GeV	76

FIG. 4·3: Energy Spectra of Muons from Inelastic Neutrino Interactions at different Zenith Angles

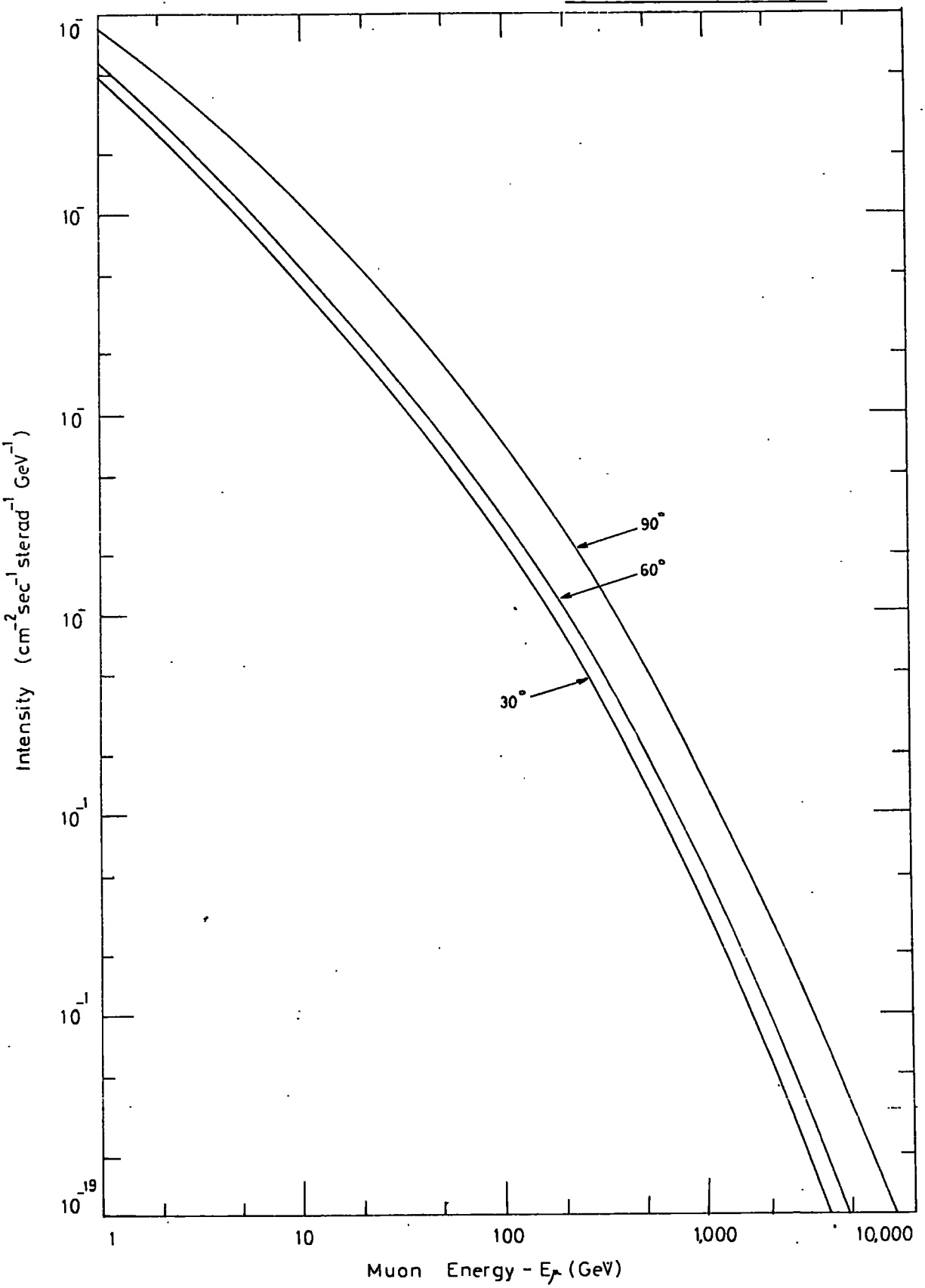

FIG. 4.4: The Rate and Mean Energy of Neutrino-induced Muons

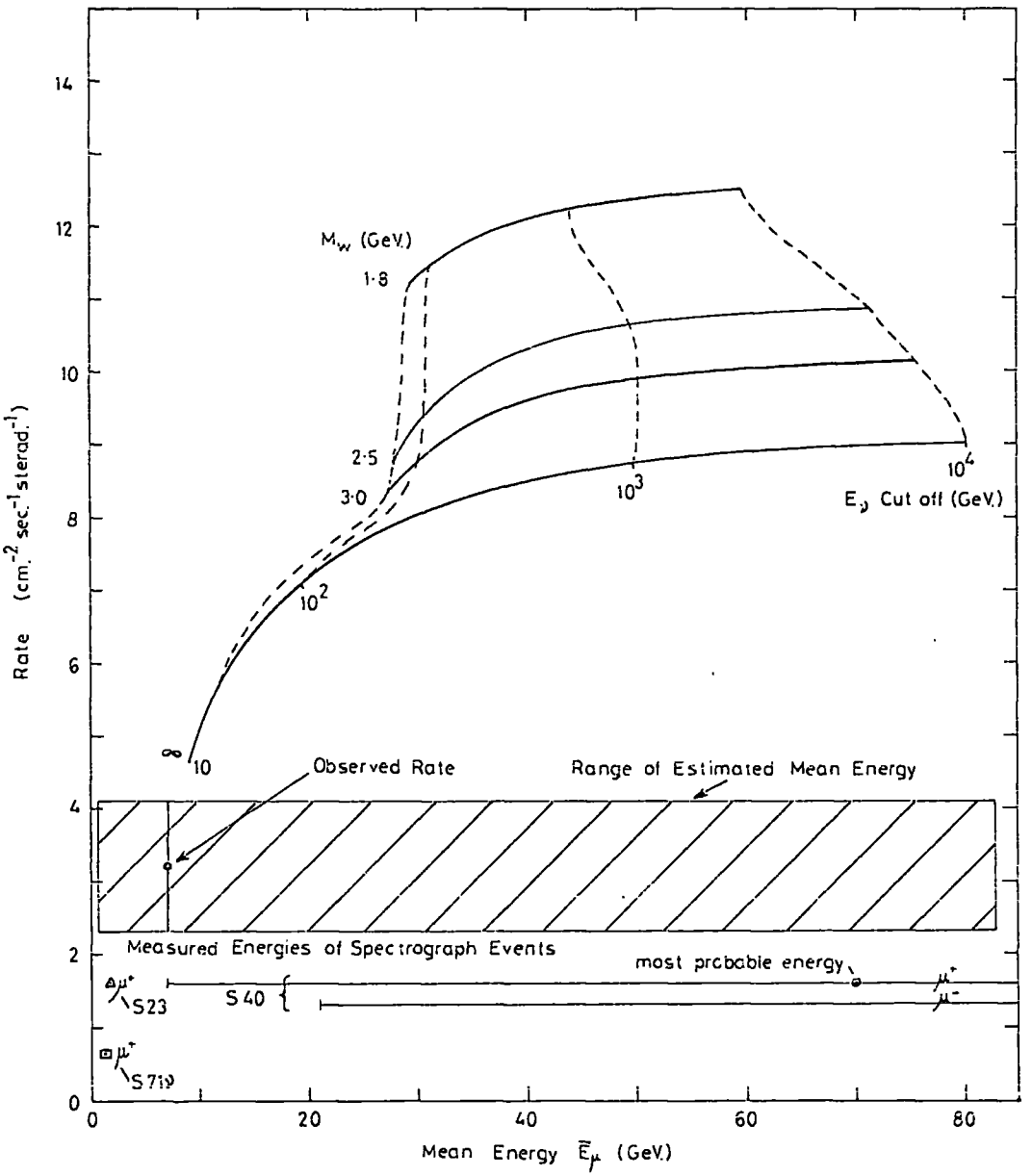

CHAPTER 5

The Experimental Results.

5.1 Introduction

The operation of the present experiment deep underground using visual detectors partly overcomes the problem of identifying the source of the detected particles. The intensity of atmospheric muons detected above a zenith angle of 60° is negligible and, thus, muons detected in the range 60° - 90°, together with upward moving muons, can be assumed to be neutrino - induced. In the intermediate angular range 50° - 60°, the majority are of neutrino origin but identification is less certain. Muons from zenith angles below 50° are thought to be predominantly of atmospheric origin with a smaller number of neutrino origin and the identification of muons from each source requires a more detailed analysis of the results.

Upward moving knock on electrons have been seen to accompany some muons at zenith angles below 50° and it is considered that some of these were created by upward moving muons. Although the number is small (less than 4 for Tels. 1 & 2), it may be supposed that other unaccompanied upward moving muons have also been detected. The expected symmetry of neutrino-induced muons about the horizontal suggests that a similar number of downward moving ones may have been observed.

It is clear, on the basis of this arguement, that whereas only a small number of upward moving neutrino-induced muons have produced knock ons, the implication is that several times this number of neutrino-induced muons have been detected at small angles. This possibility contributes a systematic error to the intensity and angular distribution of atmospheric muons.

(There is also a possibility that some of the events in the range 30° - 50° are of a somewhat different origin. This possibility is discussed in Chapter 6).

In order to make a reasonable assessment of the intensities and angular distributions of both atmospheric and neutrino-induced muons, the following analysis has been made.

5.2 The Basic Results.

Table 5.1 shows the basic results from all of the detectors recorded to the end of 1968.

TABLE 5.1 : Basic results to 31/12/68

	Tels. 1 & 2	Tels.3,4 & 5 4-fold trigger	Tels.3,4, & 5 O.S.T.(2-fold trigger) $\geqslant$ 2 layer events	Specs. 1 & 2
Total no. of 'in geometry' events	54	4	42	61
No. at zenith angles $> 50^{\circ}$	6	2	5	2
Exposure time (hr.)	43,722	14,203	18,452	18,946

A notable feature of the events in Tels. 1 & 2 is the high degree of electromagnetic accompaniment of the muons. Several events involve knock on electrons or small showers and several 'out of geometry' events were triggered by this accompaniment. (An 'out of geometry' event is one in which the muon has not passed through both scintillators giving the coincidence, the trigger

being provided, in part at least, by the accompanying particles.)

At large angles several multiple-particle events have been seen which suggests the importance of non-elastic interactions, Event 4 being a good example. Two of these events seem to have been created by neutrino interactions within the structure of the telescopes frameworks, the tracks in Event 29 originating from an upright support girder of Tel. 1 and those in Event 061 from the iron absorber of Tel. 5. (see figs. 5.1 & 5.2).

The Spectrograph and Tels. 3, 4 & 5 O.S.T. events have shown the importance of the inclusion of absorber between the coincidence detectors. Some of these events have consisted only of unconnected short tracks probably caused by γ - e showers which would most probably have been misinterpreted without absorbers.

Finally a few large showers have been detected. (e.g. Event 018 - fig. 5.3). These were probably produced by very energetic atmospheric muons. The largest shower event, however, Event 13, when analysed, seemed to have been produced by a shower primary travelling at a large zenith angle and this event was therefore probably neutrino-induced.

5.3 Measurement of Zenith Angle

As Tels. 1 & 2 are viewed directly by cameras with small lens distortion, the event films could be scanned by direct projection. By a method of superposition , the projected zenith angles of event particles could be measured with respect to a previously photographed plumb line suspended in front of the telescope.

For some events, it was not possible to construct an undeflected trajectory through the flashed tubes. This was, in several cases, the result of slipping of the rear ends of the flash tubes within the trays.

FIG. 5.1: Event 29

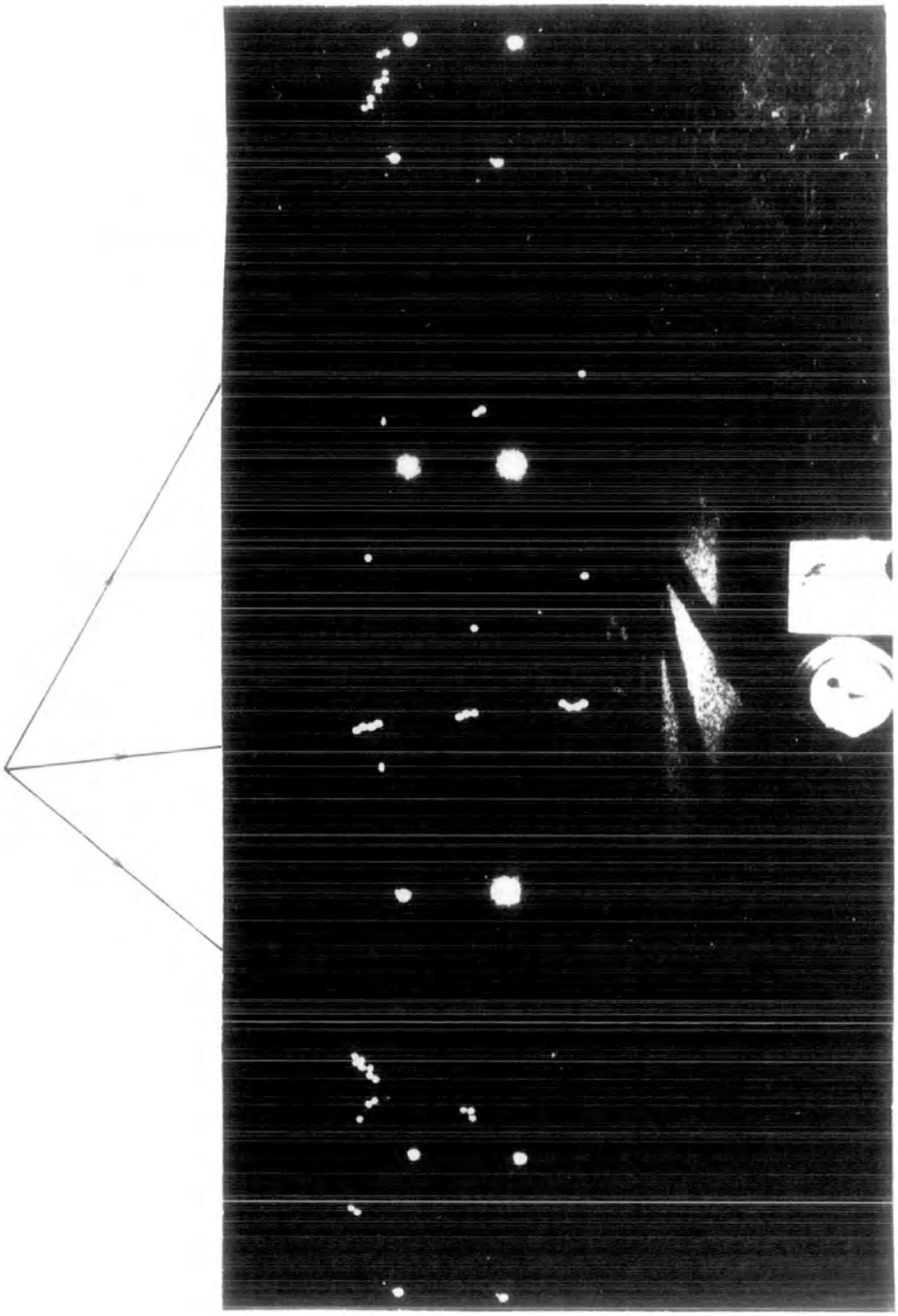

FIG. 5.2 Event 061

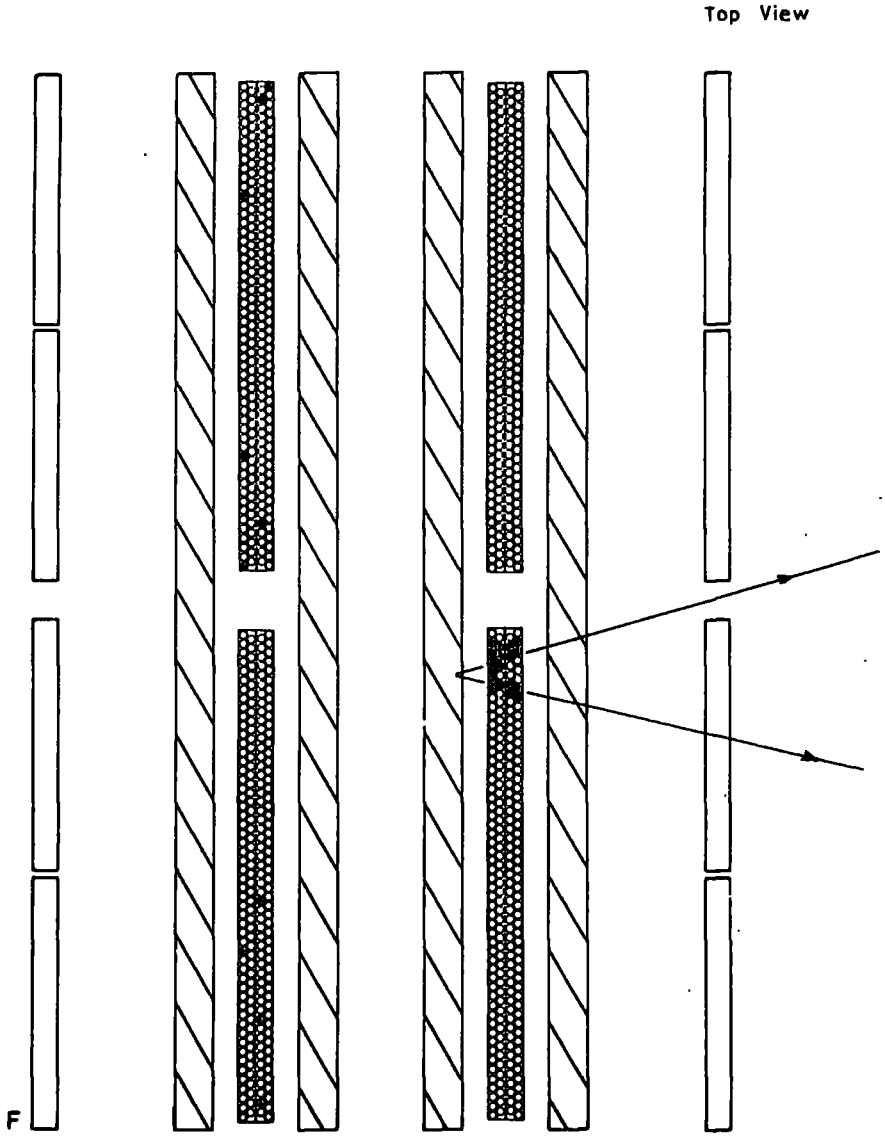
Top View
F

FIG. 5.2 Event 061

Run No. ϑR 970 Date 3/9/68

Telescope 5 Time 14-30 I.S.T.

13-03 M.S.T.

Projected Zenith Angle : $98^{\circ} \pm 10^{\circ}$

Azimuth Angle : $\sim 0^{\circ}$

Spatial Zenith Angle : $98^{\circ} \pm 10^{\circ}$

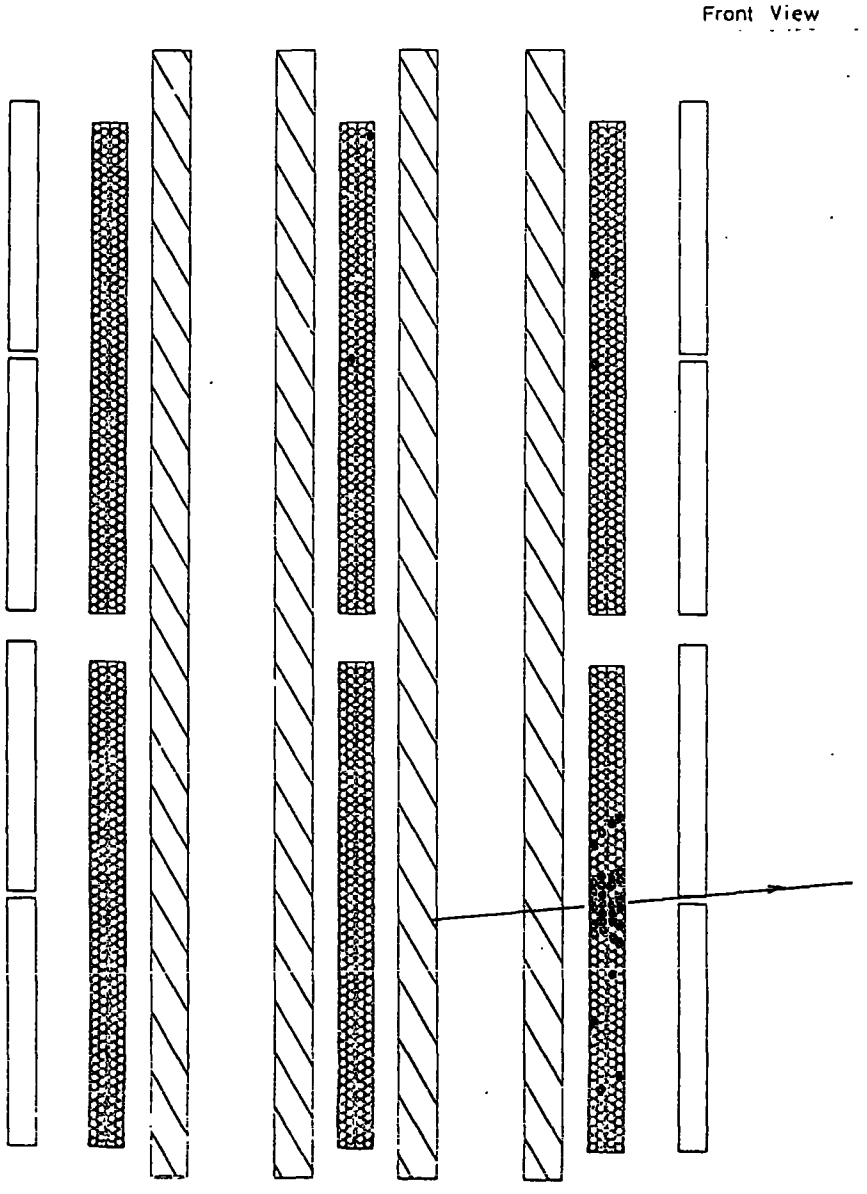

FIG. 5.3 Event 018

Top View

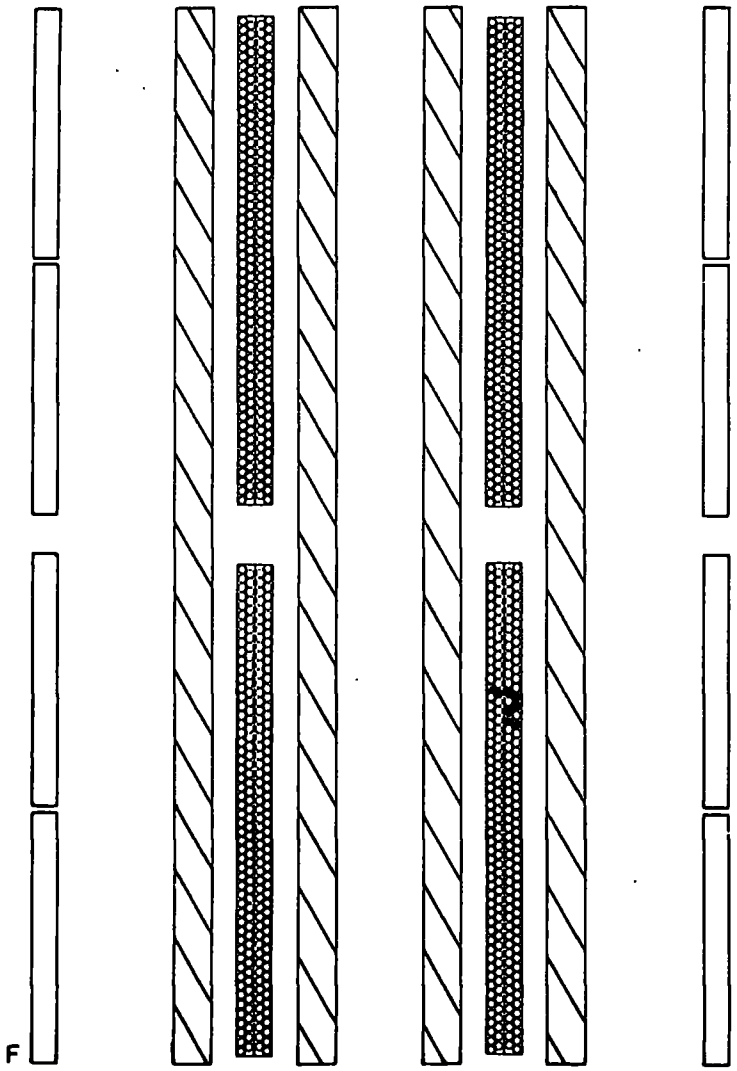

FIG. 5.3 Event 018

Run No. ϑR 815 Date 29/2/68

Telescope 4 Time 04-12 I.S.T.

14 - 26 M.S.T.

Projected Zenith Angle : Probably ~ 44°

Azimuth Angle : 26° ± 20° E of Tel N

Spatial Zenith Angle : 48° ± 4°

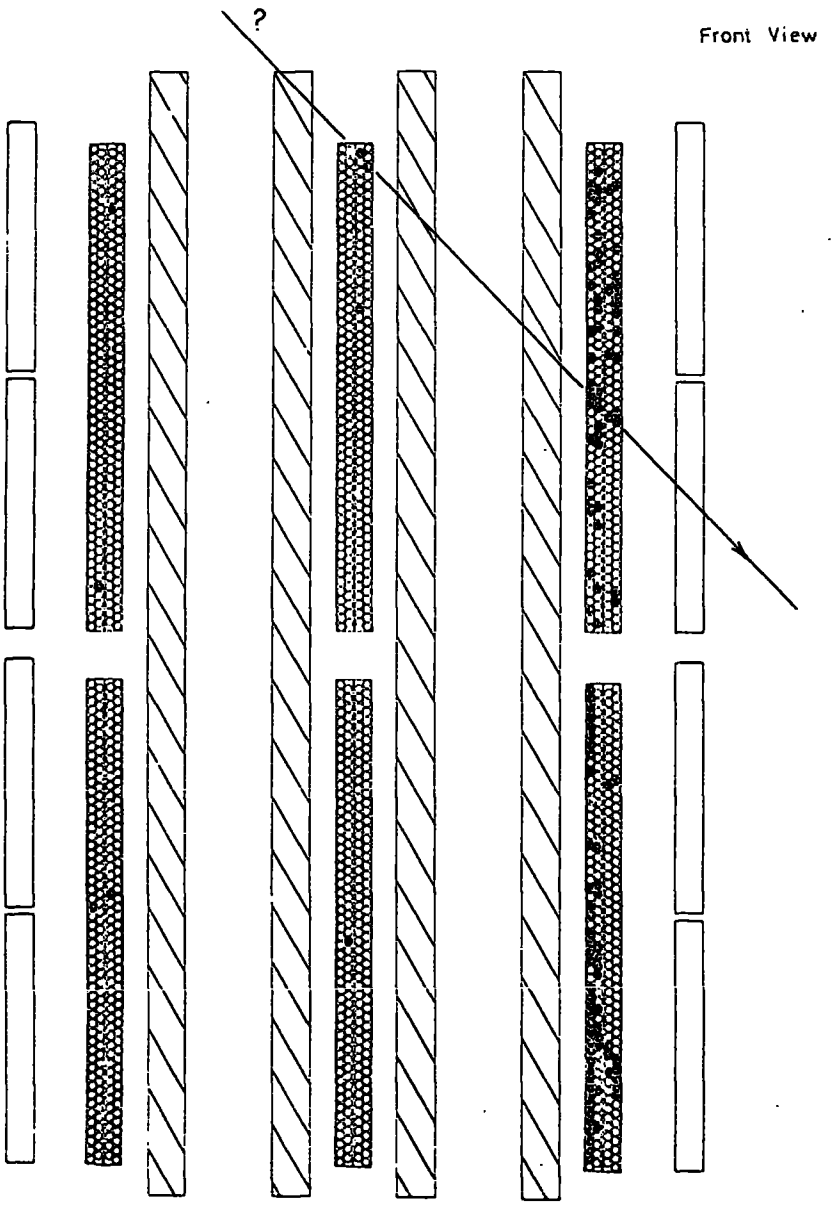

Taking the slipping into consideration some events still seemed to involve scattering in the lead layers. In these cases, it was assumed that the projected zenith angle of the upper part of the trajectory was the incident angle. In most cases the error in the measured projected zenith angle was $\pm 1^{\circ}$.

Tels. 3, 4 & 5 all incorporate mirror systems between the flash tubes and the cameras making the event angular measurement more difficult. However, as above, the method evolved was based on the superposition technique. Key fiducial lights were made visible in both mirrors viewing the zenith trays and it was possible to relate the track section visible through one mirror with that visible through the other and to measure the angle with respect to the plumb line as before. For the azimuthal trays, 4 seperate inclined mirrors were used. The event was, therefore, scanned for identification of flashed tubes and the azimuthal angle of the best line through the latter was subsequently measured on a mimic diagram. Depending upon the configuration of the flashed tubes, the azimuth angles could be measured with an accuracy of $\sim \pm 3^{\circ}$.

As already described, the spectrograph flash tubes were carefully aligned to maintain a high maximum detectable momentum. Using the measured tube co-ordinates, the projected zenith angles of the early events were calculated. Almost all events could be described by an undeviating trajectory. However the traversal line error and configuration of the flashed tubes enabled the estimation of minimum momenta for + ve and - ve particles for each event. Greater numbers of events having been accumulated, it was deemed not useful to estimate such minimum momenta for particles which were, in the main, of high energies beyond the m.d.m. of the system. Thereafter,

the projected zenith angles were measured directly from the film projections as for the other detectors and only events of special interest were analysed via the co-ordinate system. The projected zenith angles could be measured with accuracy ranging from 0.2° to 1.5° according to the method of analysis used, the track length in the flash tubes and the flashed tubes configuration.

The total 'in-geometry' events listed in Table 5.1 are shown in figs. 5.4, 5.5 and 5.6 for the different detectors.

5.4 Telescopes 1 & 2 Events

A detailed description of neutrino-induced events is now given. The commonly non-elastic nature of neutrino-interactions is easily seen. This is followed by an examination of the doubtful events in an attempt to make a more accurate estimate of the intensity of neutrino-induced muons.

5.4 1 Definite Neutrino-Induced Events.

(a) Event 4 has been thoroughly discussed by Achar et al. (1965d). The event consisted of two near-horizontal tracks, one at $99.2^{\circ} \pm 0.3^{\circ}$ and the other at $96.2^{\circ} \pm 0.8^{\circ}$. The penetrating nature of the two particles, together with the lack of cascade multiplication enabled the identification of the particles concerned as muons or pions. The large zenith angles of the tracks eliminated the possibility of the particles being atmospheric muon induced leaving the two possible explanations as, (a) The production and decay of an intermediate boson; or (b) The production of a pion in an inelastic neutrino interaction.

(b) Event 29, shown in fig. 5.1, consists of 3 clear tracks. The

FIG. 5.4: Angular Distribution of Tels, 1 & 2 Events.

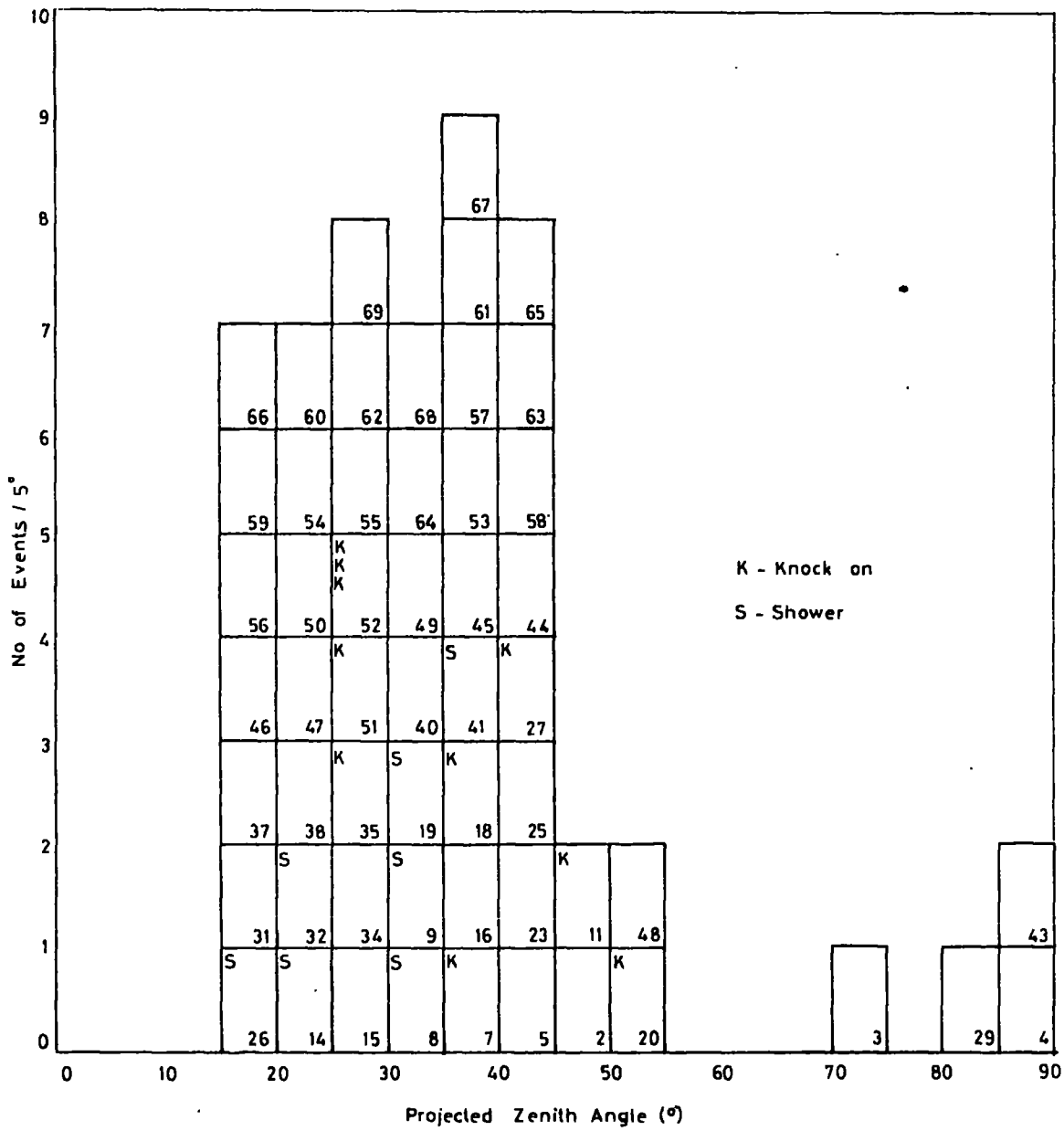

FIG. 5.5: Angular Distribution of Specs, 1 & 2 Events.

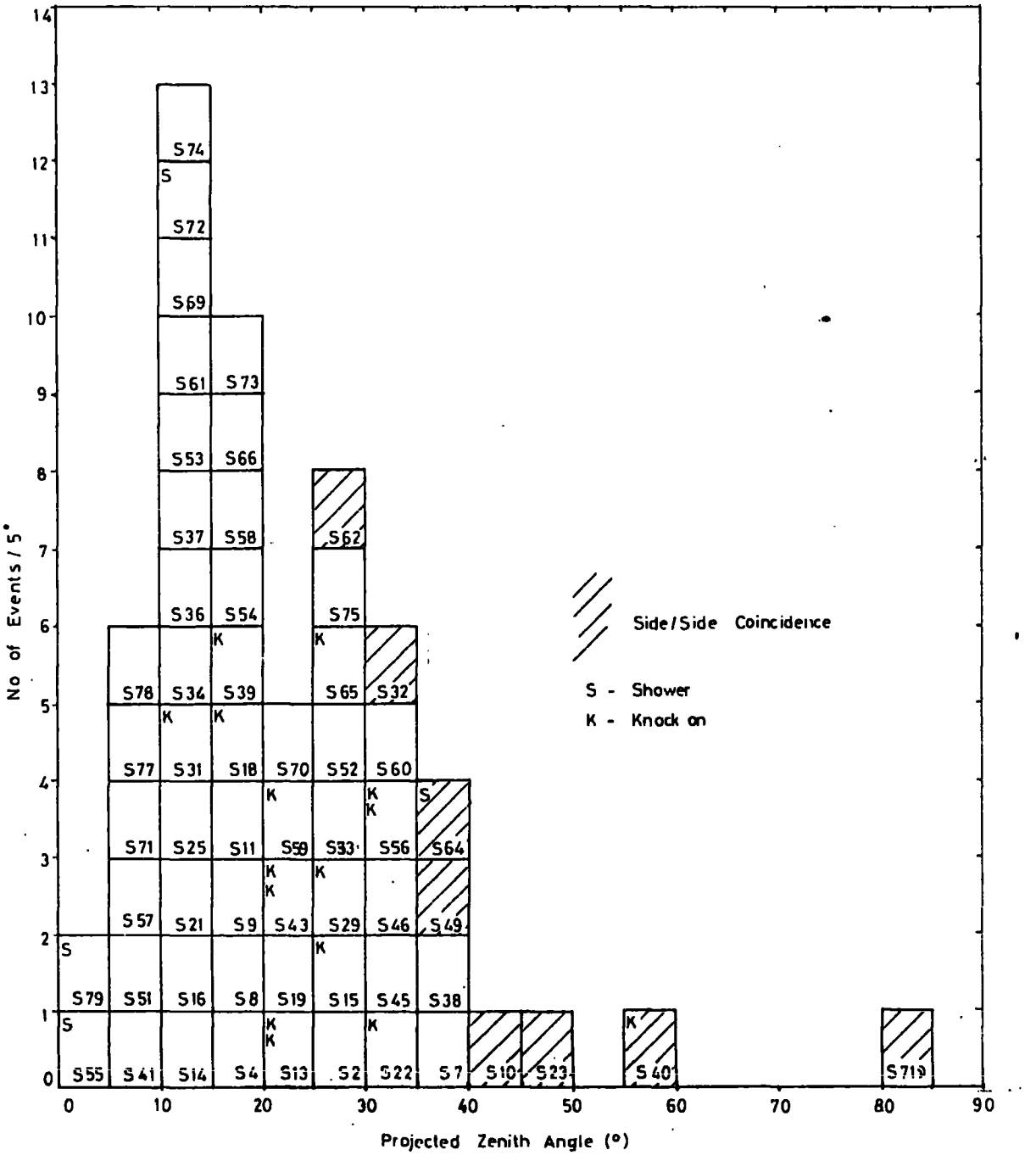

FIG. 5.6: Angular Distribution of Tels 3,4 & 5 Events.

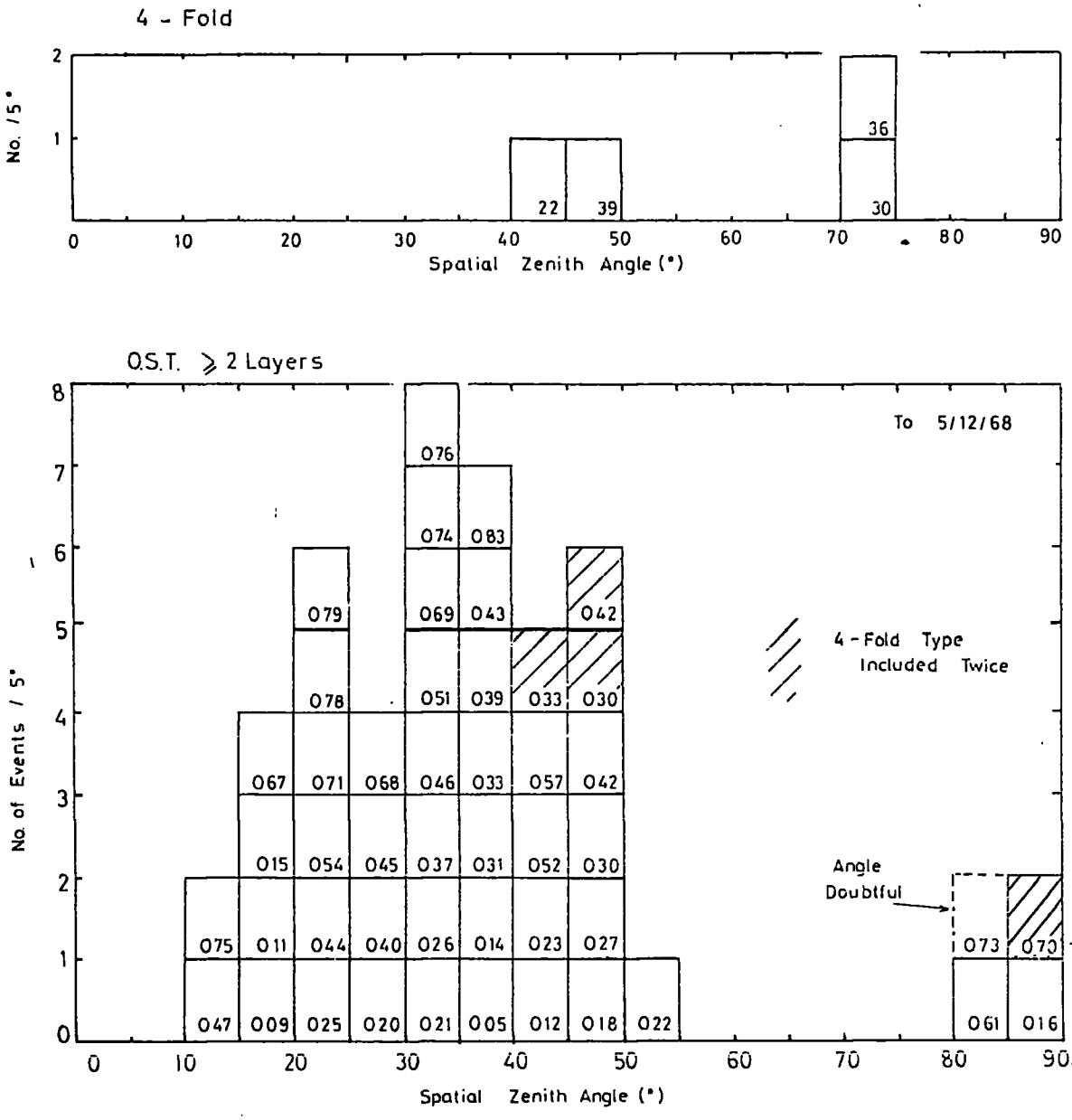

middle track, at a projected zenith angle of 96.5°, penetrates at least 8 radiation lengths in the lead absorber without multiplication and can be taken as caused by a muon or pion. The upper track, of p.z.a. 155°, intersects with the middle track in a girder of the telescope framework. The track does not pass through the lead absorber, but leaves the geometry of the telescope after crossing one flash tube tray. Signs of knock on electrons accompany the upper track. The lower track either stops in the lead absorber or leaves the geometry of the telescope. This track, which is suggestive of a pion interacting in the lead, when projected back, intersects the other two at the same point.

If the event was the result of the nuclear interaction of an atmospheric muon, then the upper track could, although not necessarily, have been the track of the incident muon. However, the probability of an interaction producing a backward moving particle giving the middle track is negligibly small. So is the possibility of a very large angle atmospheric muon, incident out of geometry, creating interaction products, which followed all three observed tracks, because of the rapid fall off of atmospheric muon intensity with zenith angle.

The most likely explanation is t hat the middle track was a muon or pion resulting from a neutrino interaction and that the lower track was a pion. The upper track could have been caused by an electron. However, this possibility is greatly reduced by the fact that the penetration is suggestive of a fairly high energy and this would not be consistent with the large angle of emission.

It, thus, seems that the event is the result of the non-elastic interaction of a neutrino in the girder and the three tracks observed are those of the products of the interaction. If so, then at least one of the products

may be a muon and at least one of the others a pion. The two most likely explanations are,

(i) Production and decay of an intermediate boson,

$$\nu_\mu + Z \rightarrow Z' + \mu + W \hookrightarrow \pi + \ldots\ldots \text{(non-leptonic mode)}$$

or (ii) Pion production in an inelastic interaction

$$\nu_\mu + N \rightarrow \mu + N' + \pi + \ldots\ldots$$

The middle track could then be a muon and the lower track a pion stopped or scattered in the lead.

(c) Event 43 (Appendix 4, fig. A4.1) is another example of a neutrino interaction. The flashes in the centre trays form a track at 85.5° which crosses the full width of the telescope and seems to have been responsible for saturated pulses in the scintillators N3 and S3 or S4. The other flashes indicate complex electromagnetic accompaniment. The short tracks in the lower trays suggest a divergence from the North. This is substantiated by the possible knock on electrons in the centre middle tray. It is not possible to deduce the nature of the neutrino interaction which produced the near-horizontal muon or pion.

5.4 2 Intermediate Angle Events.

Doubt about the intensity of neutrino-induced muons and the angular distribution of atmospheric muons leads to uncertainty in the angle at which the expected numbers of events from the two sources are equal. This angle could be as low as 45° or higher than 50°. Four events fall in this region. It is most unlikely that they are all of atmospheric origin, and some, at least, must be of neutrino origin.

(d) Event 2 was a simple case of an unaccompanied muon at 48° and

(e) Event 11 a case of a muon, at 47° p.z.a., accompanied in one tray by a knock on (or χ -ray) of doubtful direction.

(f) Event 20 also consisted of a single muon (p.z.a. - 51.5°) accompanied by a knock on electron which was clearly downward moving.

(g) Event 48 is shown in fig. 5.7. The two penetrating tracks at 53.7° & 48.7° p.z.a., pass through the rear scintillators on the North side and the front scintillators on the South side. The resultant path length in the lead is enhanced such that the penetration was probably at least 12 radiation lengths. They were, therefore, most probably caused by muons or pions and appear to intersect at the photomultiplier box of scintillator N3.

The two tracks in the lower North tray are less clearly identifiable. They were caused either by particles which stopped or which left the telescope geometry. They cannot be made to intersect at the point of intersection of the two main tracks nor can they both be made to intersect either one of them unless scattering is assumed to have taken place. There are two most likely explanations,

(i) The lower track is that of a particle produced by one of the two penetrating particles and produced, itself, a knock on electron which gave the upper track

(ii) Three particles were produced in the interaction in the photomultiplier box. Two were penetrating particles and the third was either lost in the production of two other particles in the scintillator or scattered in the production of one other particle.

Other atmospheric muon events suggest that the probability of detecting

FIG. 5.7: Event 48

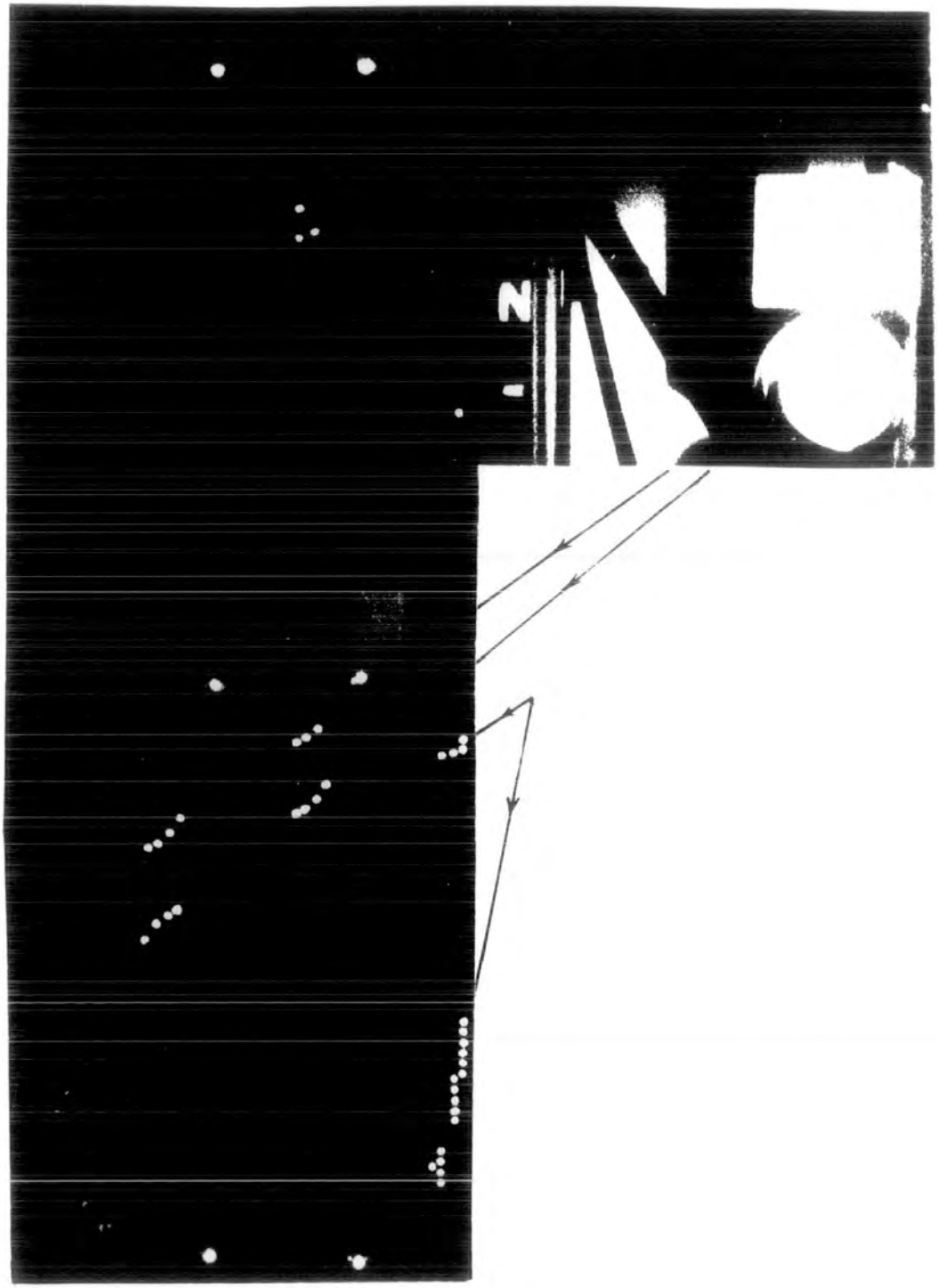

the products of the photonuclear interaction of a muon is $\lesssim 3\%$ whereas other neutrino-induced events indicate that $\gtrsim 50\%$ of detected neutrino interaction products are from non-elastic interactions. As the probabilities of neutrino and atmospheric events at this zenith angle are similar, it seems much more likely that the event was neutrino initiated.

It is not possible to distinguish between the possibilities (i) and (ii). However, the lower of the two doubtful tracks is more likely to have been a pion than an electron at the angle observed and the required energy of ~ 40 MeV. The event is another example of the importance and the nature of non-elastic neutrino interactions.

In view of the doubt about Events 2, 11 & 20, a reasonable estimate is to assume that two are of atmospheric origin and the other, along with Event 48, is of neutrino origin.

5.4 3 Small Angle Muons with Upward Moving Accompaniment

As mentioned in the previous section, the knock on electron accompanying Event 11 may have been upward moving. Similar phenomena have been observed in five other events. These events are now examined in an attempt to distinguish between the three possible explanations,

(i) Downward moving muon with a scattered knock on.

(ii) Downward moving muon with a backward knock on.

& (iii) Upward moving muon with a forward knock on.

(h) Event 15 consisted of a muon scattered in one lead layer with two non-adjacent tubes flashed in the flash tube layer nearest the wall. The event could be explained in terms of (ii) or (iii) above or, more probably, as spurious flash tubes.

(i) Event 35 includes the track of a knock on electron parallel to, but separated from, the muon track. The knock on could be upward of downward moving falling in any of the three categories. If the knock on was upward moving, it must have been scattered before crossing the flash tubes. Case (i) seems the most likely.

(j) Event 18 shown in Appendix 4, fig. A4.2, consists of a straight track in the centre and North side trays with two tracks diverging upwards in the South side trays. It is not possible to construct an undeviating track through the flashed tubes on the diagram but there is a slight doubt about the alignment of the tubes in the middle tray and, thus, the penetrating particle may not in fact have been deflected. The short upper track could well have been that of an upward moving knock on which stopped in the flash tube tray so that cases (ii) or (iii) could be the explanation.

(k) Event 51 also shown in Appendix 4 (fig. A4.3) involves the upward divergence of two particles in one tray. The penetrating track is that of a muon but it is not possible to identify the other. The small opening angle could indicate that the second particle was a knock on electron although there is no multiplication to support this. This event could also be in categories (ii) or (iii).

(l) Event 54 is the most interesting in this group and is shown in fig. 5.8. Tracks A,B & C can be aligned as an undeviated penetrating particle. The best line through track D can be taken to a vertex at point F from which a line can be drawn through track E. If tracks D & E are the primary products of an interaction at F, then the event could involve the photonuclear interaction of an upward moving neutrino-induced muon. However,

FIG. 5.8: Event 54

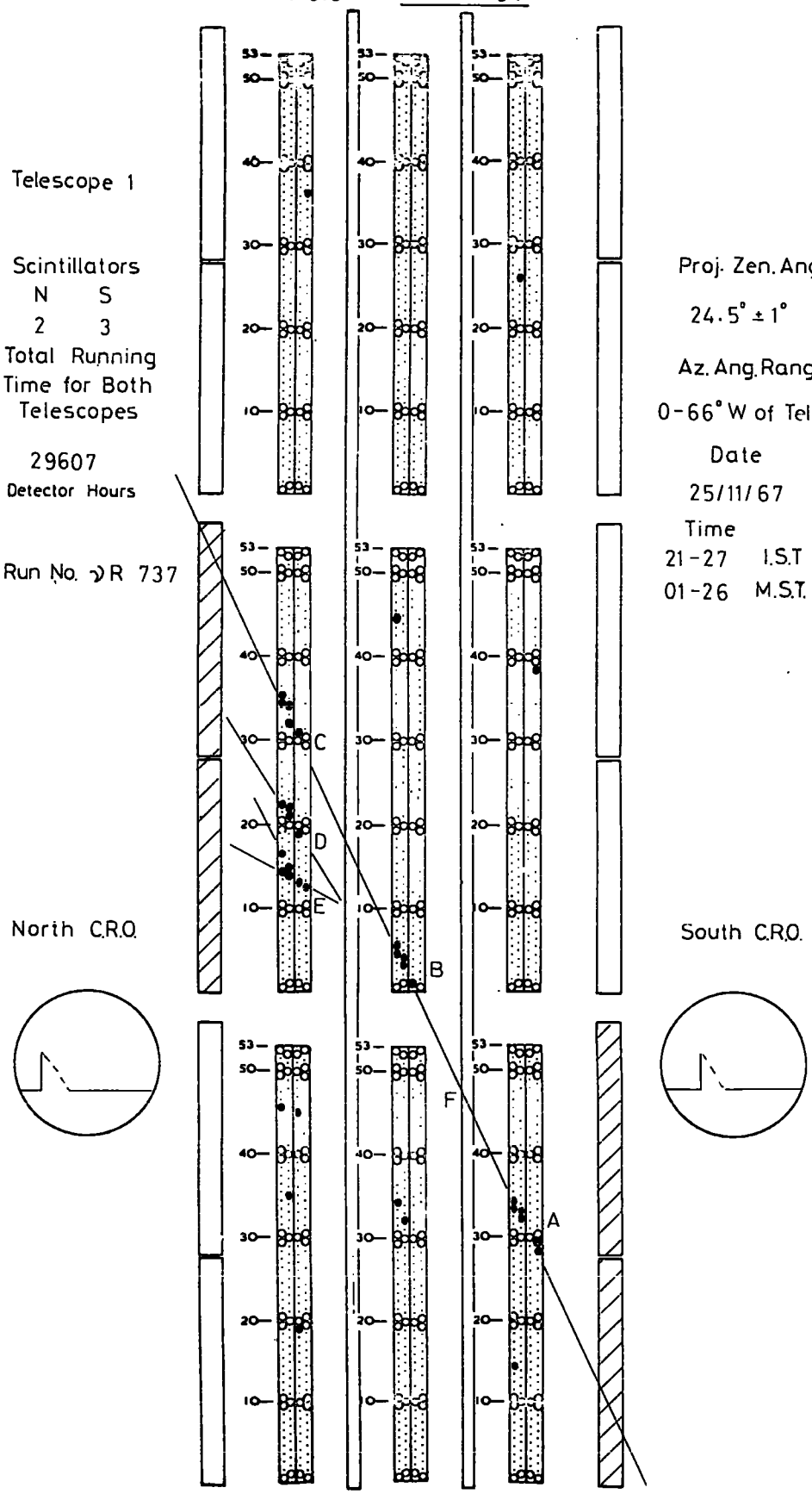

the probability of this being the explanation is small.

Still considering an interaction at F, track D could be a knock on electron, produced by an upward moving muon, which multiplied in the second lead layer giving track E.

Alternatively, if D & E were downward moving, it would have been necessary for the particles concerned to have been scattered. In this case, track D may have stopped in the third column of flash tubes or may have traversed inefficient flash tubes. (The latter possibility is supported by the inefficiency in track C.) However, the flashed tubes of track E suggest the production of an upward moving knock on, in the centre electrode of the tray, which would have to be explained as backward moving. Also the scintillator, through which the downward moving knock ons would have passed, did not give a very large pulse.

On balance the most likely explanation seems to be the second. i.e. An upward moving neutrino-induced muon produced a high energy knock on electron which gave rise to multiplication in the second lead layer.

Using flash tubes, Pickersgill (1968) has studied the rates of knock on electrons produced by muons in iron absorber at sea level. The results indicate that about 1 in 10 knock ons is backward moving. Of the muons detected in Tels. 1 & 2, 13 have produced knock on electrons. On the basis of Pickersgill's findings, '1.3' of these may be expected to have been backward moving. But, of the 5 events just examined, 3 clearly involve upward moving knock ons. Thus a best estimate of 2^{+2}_{-1} events may be taken as having been caused by upward moving muons.

5.5 Spectrograph Events.

Apart from the purely electromagnetic events mentioned already, the

spectrographs have yielded at least two events in which a near-vertical muon has initiated an electromagnetic shower in the magnet iron. Showers produced in the overhead rock have also been detected, Event S12 (fig.A4.4) being a good example. One event was probably the result of the nuclear interaction of a near-vertical out of geometry muon in the magnet iron and another was very probably a pair of muons from an extensive air shower.

Since the acceptance of the spectrographs is much higher than that of Telescopes 1 & 2 at small zenith angles, the proportion of neutrino-induced events at zenith angles less than the cross-over angle, of equal intensities from both sources, should be less than in the case of Tels. 1 & 2.

The lack of absorber makes muon identification difficult as well as the estimation of the particle directions from the accompaniment divergence. The identifiable neutrino events consequently tend to be those at large zenith angles and those which are magnetically deflected.

5.5 1 Deflected Events.

(m) Event S23 was the first event in which the momentum of the particle was measurable. It is shown in fig. 5.10. Unfortunately only one tube flashed in one of the flash tube trays traversed, due probably to the alignment of the inter-tube spacings in the direction of the track. However there is no doubt about the authenticity of the event. Assuming energy loss in the magnet, the particle was found to be downward moving, of positive charge and deflected by 9.4°.

Ashton and Wolfendale (1963) give the relationship

$$\Delta\theta = -\frac{300\,B}{\alpha}\,\ell_n\left(1-\frac{\alpha\ell}{P_i}\right) \qquad 5.1$$

for the deflection of a particle with energy loss in a solid iron magnet. B is the magnetic induction, α the mean momentum loss per unit

FIG. 5.9

EVENT NO S 40 RUN NO 796 DATE 7/2/68 TIME 03-39 IST 12-26 MST

SPECTROGRAPH
1 B

SCINTILLATORS
S 4 T- N 3

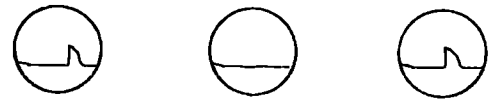

TOTAL RUNNING TIME (SPECTROGRAPHS) 7520 hr.

AZIMUTH ANGULAR RANGE
2·9° E to 31·3° W of Spec N

DIRECTION
Upwards ?

PROJECTED ZENITH ANGLE
Incident Upwards 58·9°-59·3°
Leaving Upwards 57·8°-59·4°

SPATIAL ZENITH ANGULAR RANGE
Incident Upwards 59·0°- 63·1°

MAGNET CURRENT
220 A

MAGNETIC DEFLEXION
+1·5°
0
-0·55°

MOMENTUM
For Upward μ^+ P_{min} 7 GeV/c
For Upward μ^- P_{min} 21 GeV/c

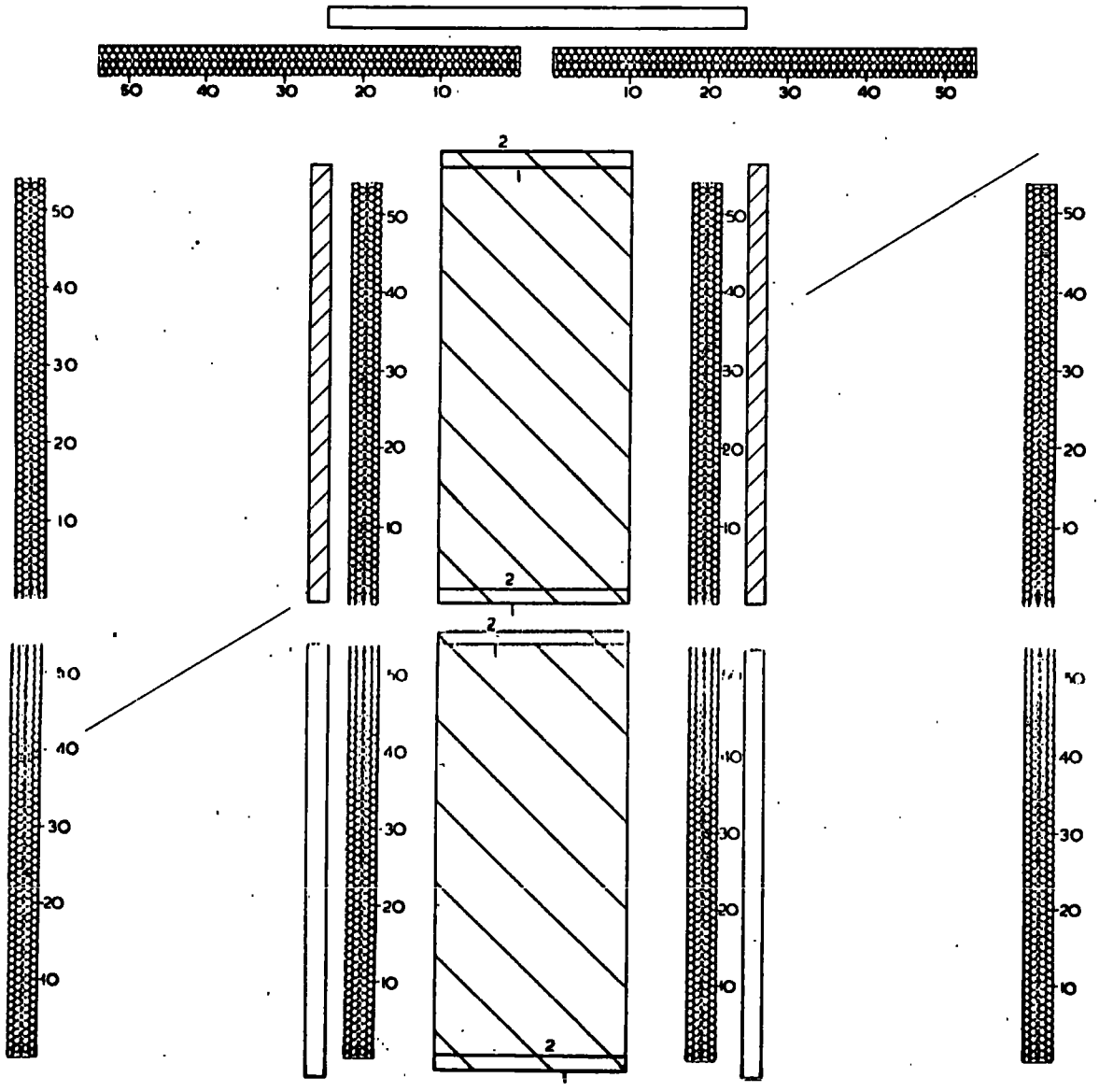

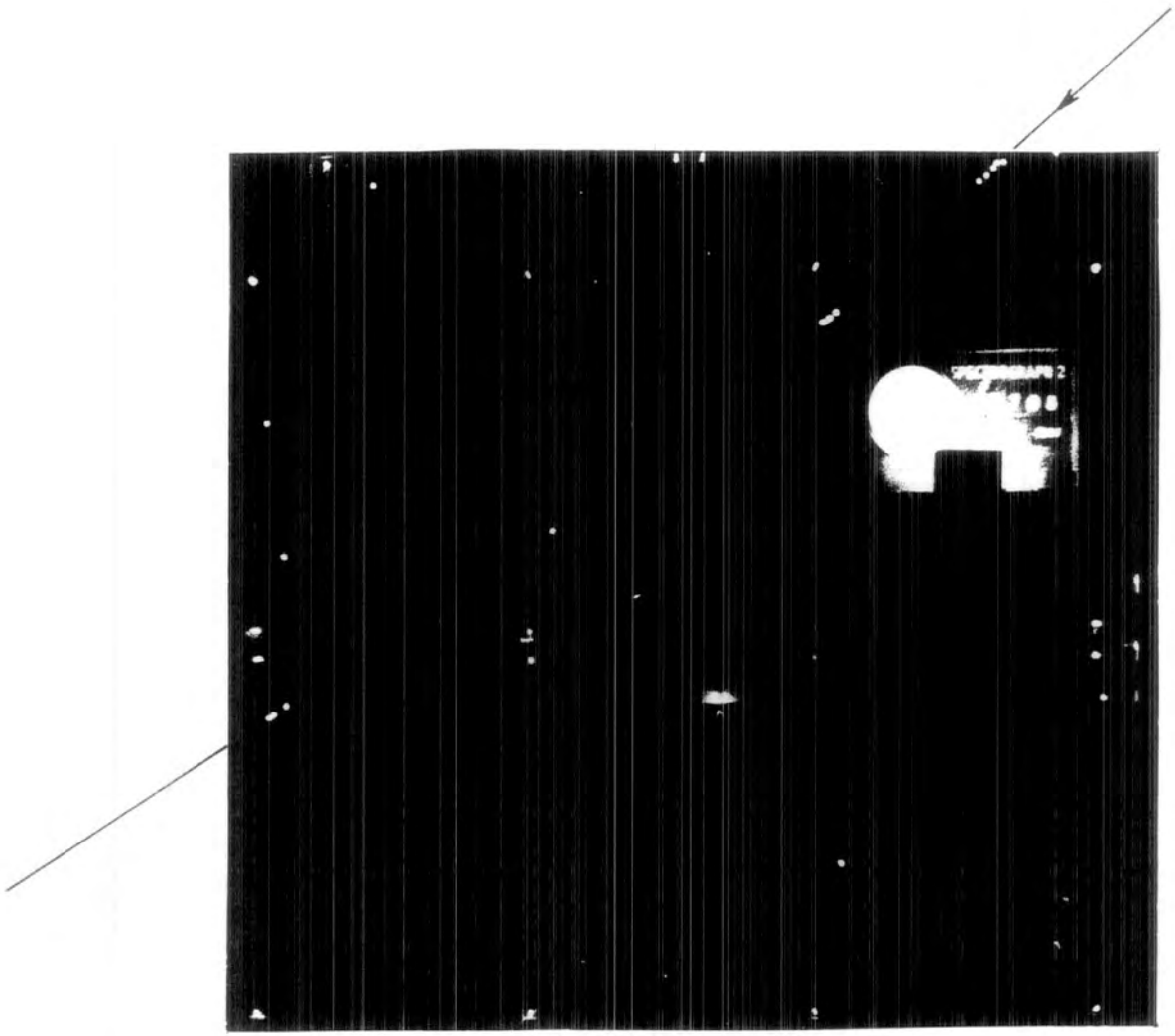

FIG. 5.10: Event S 23

path length ℓ and P_i is the incident momentum.

For this event and using this relation, the momentum is found to be 1.8 ± 0.5 GeV/c where the error is due largely to multiple coulomb scattering.* No allowance has been made for the increased path length with azimuth angle, as the most probable angle over the azimuth range for this event was zero.

This event has been accepted as a neutrino-induced muon on account of its incident zenith angle of 48.5°.

(n) Event S40 (fig. 5.9) is also accepted as being neutrino-induced by virtue of its zenith angle of $\sim 59^{\circ}$. An upward moving knock on electron was produced in one flash tube tray but an undeflected trajectory is just possible and it cannot be established if the muon responsible was upward or downward moving. The reason for this is that there is poor location of the upper arm due to the passage of the muon between the flash tube trays. Considering the neutrino spectrum, the most probable muon energy has been estimated to be ~ 70 GeV/c for an upward moving μ^+.

The absolute range using the flash tube restrictions only for an upward moving particle is μ^+, P min = 7 GeV/c; μ^-, P min = 21 GeV and vice versa for a downward moving particle.

(o) Event S71 (fig. 5.11) is another definite neutrino-induced event. Although the trajectories are such that the numbers of tubes flashed are small, the scintillator pulses were clear and indicative of a genuine event.

---

* The ratio of magnetic deflection to R.M.S. coulomb scattering for the K.G.F. spectrographs is given by, $\theta/\alpha = 0.38\, t_m/\sqrt{t_s}$, where tm is the projected path length perpendicular to the direction of magnetic flux and ts is the true spatial path length. The minimum value of $\frac{\alpha}{\theta+\alpha}$ for these spectrographs is $\sim 25\%$. For horizontal particles the minimum is $\sim 30\%$.

FIG. 5.11

EVENT NO S 71 RUN NO 1015 DATE 16/11/68 TIME 20-29 IST 00-05 MST

SPECTROGRAPH
2 F & B

SCINTILLATORS
S 3 T - N 2

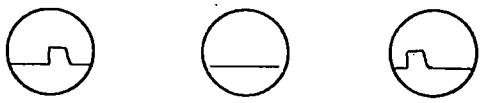

TOTAL RUNNING TIME (SPECTROGRAPHS)

AZIMUTH ANGULAR RANGE
0°-63° E of Spec N

DIRECTION
Downwards

PROJECTED ZENITH ANGLE
83° ± 1°

SPATIAL ZENITH ANGULAR RANGE
83°-86°

MAGNET CURRENT
220 A

MAGNETIC DEFLEXION
23° (or ~ 34°)

MOMENTUM
1-2 GeV/c

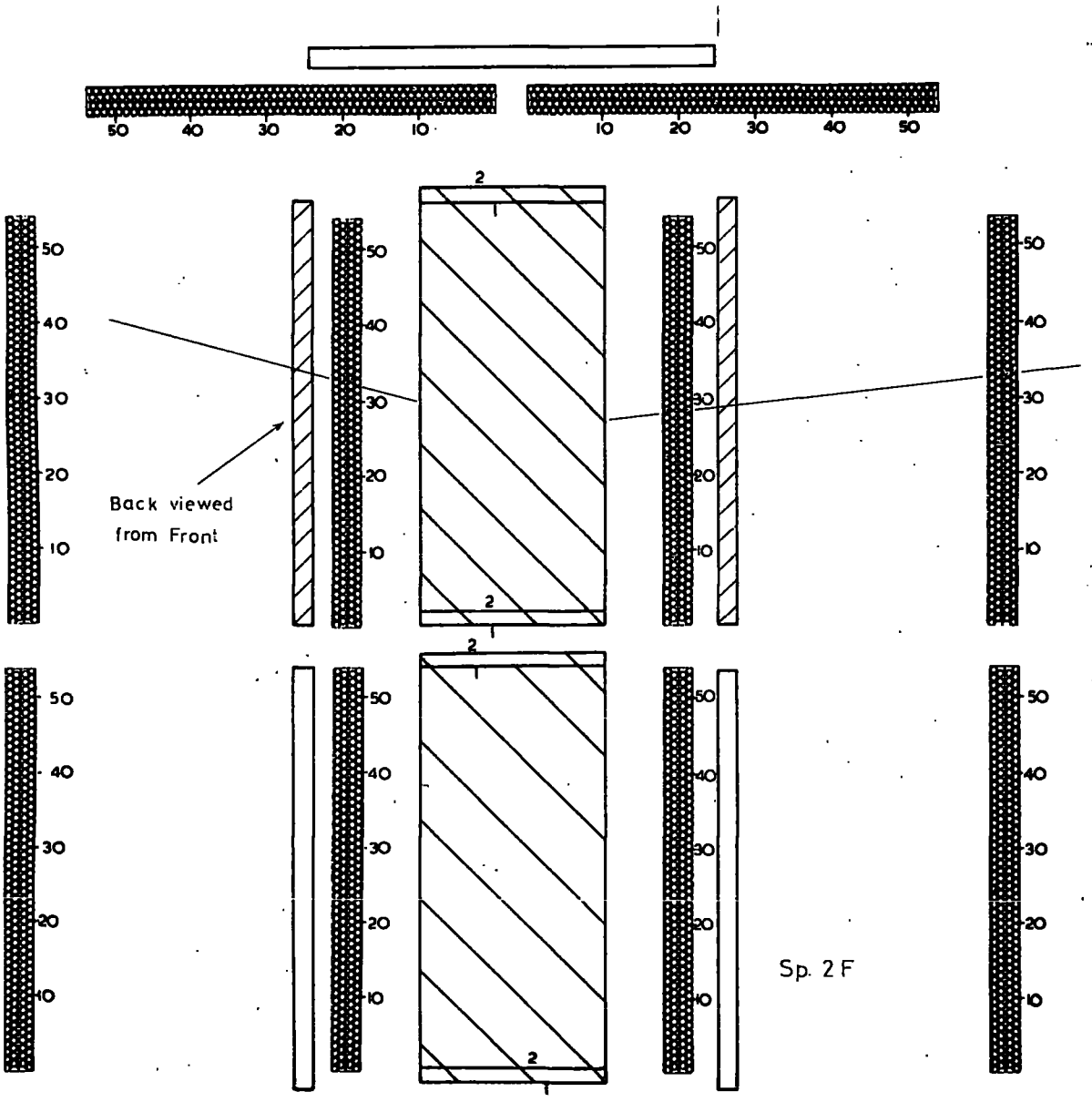

The deflection in the magnet was so great ($\sim 34^{\circ}$) that the energy of the muon must not have been much greater than that required to penetrate the magnet iron. Again using the equation of Ashton & Wolfendale, the energy of the incident muon has been estimated to be ~ 0.9 GeV/c (assuming zero azimuthal angle). As can be seen in the diagram, since no track was visible in the southernmost flash tube trays, the muon either passed between the trays, stopped before reaching them or left the telescope geometry. If the latter was the case, then the deflection would have been $\sim 23^{\circ}$ with a consequential increase of the incident energy to ~ 2 GeV/c. However the increased path length in the magnet would have reduced the emergent energy to a similar value as in the first case.

A reasonable estimate for the incident energy is 1 - 2 GeV/c for μ^{+} incident from the North. The multiple coulomb scattering error ranges from 30 - 45%.

5.5 2 Small Angle Events

(p) Event S48 (fig. A4.5) is the only spectrograph event showing a small zenith angle track with upward moving accompaniment. The additional flashed tubes in the top tray are best explained by an upward moving knock-on electron but could conceivably be explained by two downward moving ones.

It may be concluded that as the identification of neutrino induced events at angles $< 45^{\circ}$ is almost impossible only those at $> 45^{\circ}$ are useful for intensity estimates and 3 such events have been recorded. However the possible upward events are analysed in Chapter 7 from the standpoint of consistency, or otherwise, with the large angle data.

5.6 Telescopes 3, 4 & 5

5.6 1 Four-fold triggering

Four 'in geometry' events were recorded during the 4-fold coincidence operation of Tels. 3, 4 & 5, as can be seen in fig. 5.6.

In spatial zenith angle the atmospheric and neutrino events 'cross over angle' is greater than in the projected case and the 4 events are divided equally between the two origins.

5.6 2 One Side Triggering.

The one side triggering events can be divided into two sections, those seen to penetrate absorber in the telescope and those not doing so. The latter group, although containing muons principally incident at such zenith angles as to leave the bottom of the telescope before penetrating the absorber, also contains electromagnetic accompaniment of undetected muons, and is consequently of little use in the estimate of muon intensities.

The former group ($\geqslant$ 2 layer events) contains 4 events in which both scintillator walls were traversed, one of these events consisting of 2 seperate particles each crossing one wall which would have been classified as an out-of-geometry event during 4-fold coincidence operation.

The allowance which must be made for the efficiency of the scintillators, on account of the enhanced probability of detecting a particle with electromagnetic accompaniment traversing the scintillator, or a particle passing through two scintillator walls, is described in Chapter 6.

5.6 3 Large Zenith Angle Events

(q) Event 061 shown in fig. 5.2 is one of the most important events recorded in the experiment. It is considered to be an example of a neutrino

interaction actually inside one of the iron absorbers. It is not possible to identify the individual particles involved but, their number suggests that some, at least, are electrons (presumably from $\pi^{o} \rightarrow \gamma \rightarrow e^{+}e^{-}$). Again the complexity of the interaction is a striking feature showing the importance of visual detectors.

(r) Event 016 shown in fig A4.6 was clearly produced by a new horizontal neutrino-induced muon. Electromagnetic accompaniment was produced in the last two absorbers.

(s) Event 070 is sketched in fig. 5.12. The interpretation placed upon the flashed tubes is that they represent the products of an upward-moving neutrino which interacted within the apparatus. Three particles were detected, two of which penetrated one layer of absorber. If only three particles were produced in the interaction then the incident direction of the neutrino was as shown in the sketch (i.e $\sim 125^{\circ} + 30^{\circ}$ zenith angle). Only the particle designated 'A' which penetrated the scintillator has been included in the angular distribution.

There is one further event (073), the zenith angle of which is in doubt, which may be at a sufficiently large angle to have been neutrino induced.

5.7 The Division of Events.

The 3 events described in section 5.4 1 and one other large angle event detected in Tels. 1 & 2, Event 3, may be taken with 2 of the intermediate angle events to give a total of 6 neutrino-induced muons detected in Tels. 1 & 2 at projected zenith angles greater than 45°.

FIG. 5.12: Event 070

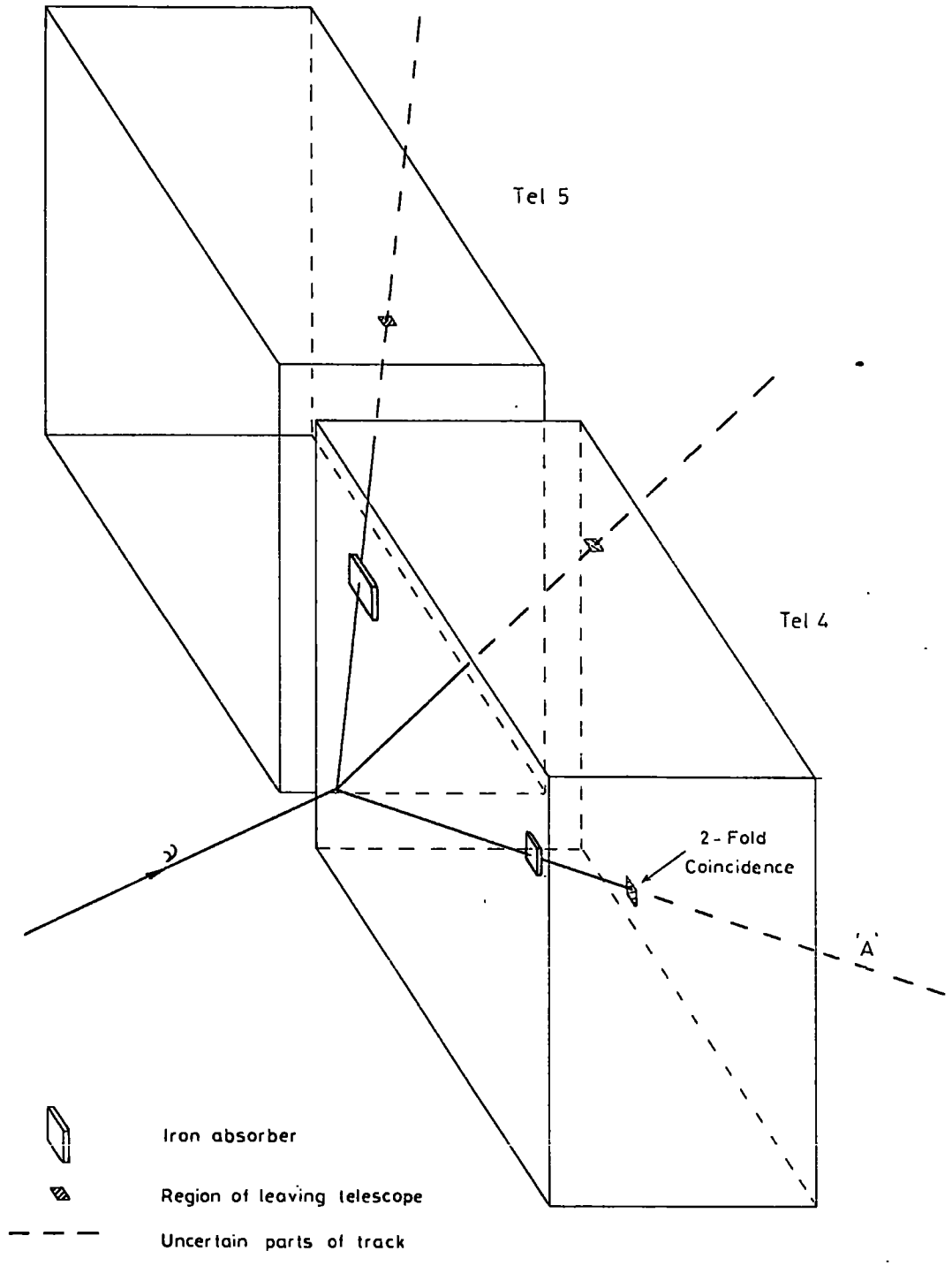

Specs. 1 & 2 have recorded 3 neutrino-induced muons at greater than 45° p.z.a., the data at smaller angles being unsuitable for making an estimate.

Tels. 3, 4 & 5 have yielded 2 neutrino events at spatial zenith angles greater than 50° on 4-fold coincidence and at least 3 on 2-fold coincidence.

Thus the total number of identified neutrino events detected in the experiment is 14.

CHAPTER 6

The Intensity and Angular Distribution of Atmospheric Muons Underground

6.1 Angular Distribution Expressions

The nature of muons at great depths underground (i.e. $\gtrsim$ 2000 m.w.e. standard rock) has been studied by several workers, namely Miyazaki (1949), Bollinger (1951), Barton (1961), Castagnoli et al. (1965), Miyake et al. (1962, 1964), Achar et al. (1965a,b) and also in the three neutrino experiments in India, South Africa and Utah, U.S.A.

Since the review of the early underground experiments, most of which were performed at shallow depths, given by Barrett et al. (1952), the angular distribution of atmospheric muons has usually been represented by the essentially empirical relation,

$$I(\theta, h) = I(0, h) \cos^{n}\theta \qquad 6.1$$

where $I(\theta, h)$ is the intensity at a depth h and a spatial zenith angle θ and the index n is a slowly varying function of depth.

This expression follows from the assumption of a depth intensity relationship of the form,

$$I(0, h) = Ah^{-m} \qquad 6.2$$

and a $\sec\theta$ enhancement of non-vertical muons from π-μ decay.

Miyake et al. measured the muon intensities at several depths. However, their apparatus could only measure the total rate and did not give any information on the angular distribution of the detected muons. Using an iterative procedure involving equations 6.1 and 6.2 and assuming n =

m -1 on the basis of the validity of the sec θ enhancement, they estimated the index n from the values of m measured at their different depths of operation.

The use of a $\cos^n \theta$ form of the angular distribution for $\theta \not\gtrsim 60^\circ$, by Miyake et al. was justified by Achar et al. who used flash tubes at similar depths to measure n directly.

The justification for using a $\cos^n \theta$ form to describe the results in the early shallow depth experiments was in the fact that n changes only slowly with depth near the surface and so n is not a function of θ until a large angle ($\theta \gtrsim 60^\circ$) is reached.

At great depths, however, the rate of change of n with depth becomes greater such that the assumption of constant n at a given depth falls down at zenith angles $\gtrsim 40^\circ$. This is apparent in the work of Achar et al. who found fractional discrepences in the values of n between using a maximum angle, θ max, of 60° and 45° amounting to 6%, 9.5% and 8% at their depths of 824, 1871 and 4361 m.w.e. st. rock respectively. Their best estimate values of n were for effective depths given by h sec θ_{eff} , θ_{eff} being the effective discreet zenith angle of all detected muons.

At 824 m.w.e., the exponent n varies very little with θ and even at 60° has increased only by about 10%. At 1871 m.w.e., n increases by about 70% between the vertical and 60° and the value of n obtained from the experiment is thus for an effective vertical depth greater than 1871 m.w.e. At 4361 m.w.e., a different aspect of the same effect counteracts the increase in effective depth, namely the rapid fall off of intensity with θ . Consequently the effective zenith angle for all muons is reduced and the effective depth of the measured n is not so much different from the vertical

depth.

Workers at greater depths are thus posed with the problem of deciding what form of angular distribution to assume for their results bearing in mind the deficiencies of the $\cos^n \theta$ form outlined above. One solution to the problem would be to use a varying n over the range of zenith angle but this runs into difficulty immediately as the value of n is not known at greater vertical depths and, therefore, large zenith angles at the operating depth. To use the observed angular distribution to predict the value of n for greater vertical depths is not much more satisfactory since at great depths, where the intensity of neutrino-induced muons is becoming comparable to that of atmospheric muons, the identification of the latter is difficult.

The solution given by Menon et al. (1967c) is to use a more accurate form of depth intensity relationship and consequently a different angular distribution. They proposed the depth intensity form,

$$I(0, h) = B \exp(-m) \qquad 6.3$$

where $m = h/\lambda$, h is the depth and λ a constant; the corresponding angular distribution being,

$$I(\theta, h) = I(0, h) \sec\theta . \exp\left[-m(\sec\theta - 1)\right] \qquad 6.4$$

This relation is valid for small zenith angles at 7500 m.w.e. and for larger zenith angles at shallower depths, for example to $\sim 60^\circ$ at 4000 m.w.e.

Creed (1967) points out that the exponential form is a poor fit at large zenith angles at 7500 m.w.e. and that the depth intensity variation at depths $>$ 7500 m.w.e. appears to follow more closely a power law decrease.

Such a deduction, however, cannot be conclusive on account of the weakness of the evidence for the variation of intensity of atmospheric muons with depth $>$ 7500 m.w.e. The exponential form can be neither confirmed or refuted on the basis of results in which there is doubt about which of the detected muons are of atmospheric origin.

Clearly there are disadvantages in applying either of the forms 6.1 and 6.4 to the muons detected in the K.G.F. Experiment with zenith angles $< 50^{\circ}$. Bearing in mind these limitations, both expressions (6.1 using constant n) have been used in calculating the distributions which may be expected to be observed in the detectors operating at the 7500 m.w.e. site.

6.2 The Apertures of the Detectors

The derivation of the angular distributions of muons expected in the K.G.F. neutrino Experiment has been discussed by Osborne (1966) and Narasimham (1967).

The equations for the differential aperture of horizontally orientated telescopes given by Osborne have been applied to the four types of detector in use. The differential aperture is given by the product of the solid angle and the area of the 'shadow' of the first scintillator wall on the second wall presented to incident muons from various zenith angles.

The differential aperture in terms of projected zenith angle is given by,

$$\frac{d\Omega}{d\beta} = 4\int_{0}^{\tan^{-1}X/Z} f(\beta,\phi)\, d\phi \qquad \text{for } \pi/2 \geqslant \beta \geqslant \tan^{-1}Z/Y \qquad 6.5$$

where $$f(\beta,\phi) = (X - Z\tan\phi)(Y - Z\cot\beta)\frac{\cos^2\phi \sin^2\beta}{(\cos^2\beta\cos^2\phi + \sin^2\beta)^2} \qquad 6.6$$

for the upper hemisphere.

Y is the telescope height, X its length and Z the width between the scintillator elements. β is the projected zenith angle (i.e. zenith angle projected onto the plane of the front windows of the flash tubes) and ϕ is the azimuth angle.

(N.B. $\tan^{-1} Z/Y$ is the minimum zenith angle acceptable by a telescope for an 'in geometry' event.)

It is necessary to integrate equation 6.5 numerically and fig 6.1 shows $d\Omega/d\beta$ obtained for Tels. 1 & 2 and Tels. 3, 4 & 5 O.S.T. $\geqslant 2$ layer events.*

The differential aperture in terms of spatial zenith angle ($d\Omega/d\theta$) can be obtained from equations A3.2 & A3.3 in Appendix 3. Fig. 6.2 shows the spatial apertures obtained from these equations for Tels 3, 4 & 5, O.S.T. & 4-fold coincidence and Specs. 1 & 2. (The aperture presented to top/side coincidences in the spectrographs has been calculated by Osborne using a different expression - private communication.)

The 'effective aperture' of a telescope is that presented to a non-isotropic radiation such as atmospheric muons and is given by

$$\left(\frac{d\Omega}{d\beta}\right)_{eff} = 4\int_{0}^{\tan^{-1} X/Z} \frac{I(\theta,h)}{I(0,h)} f(\beta,\phi)\, d\phi \qquad 6.7$$

$$\text{where} \quad \theta = \tan^{-1}\left(\frac{\tan\beta}{\cos\phi}\right) \qquad 6.8$$

---

* The criterion for a $\geqslant 2$ layer event is that the particle must traverse a minimum of 3 flash tube diameters in the horizontal direction in an azimuth tray as well as pass through the trigger-giving scintillator wall outside the adjacent zenith tray.

FIG. 6.1: Differential Apertures in Projected Zenith Angle.

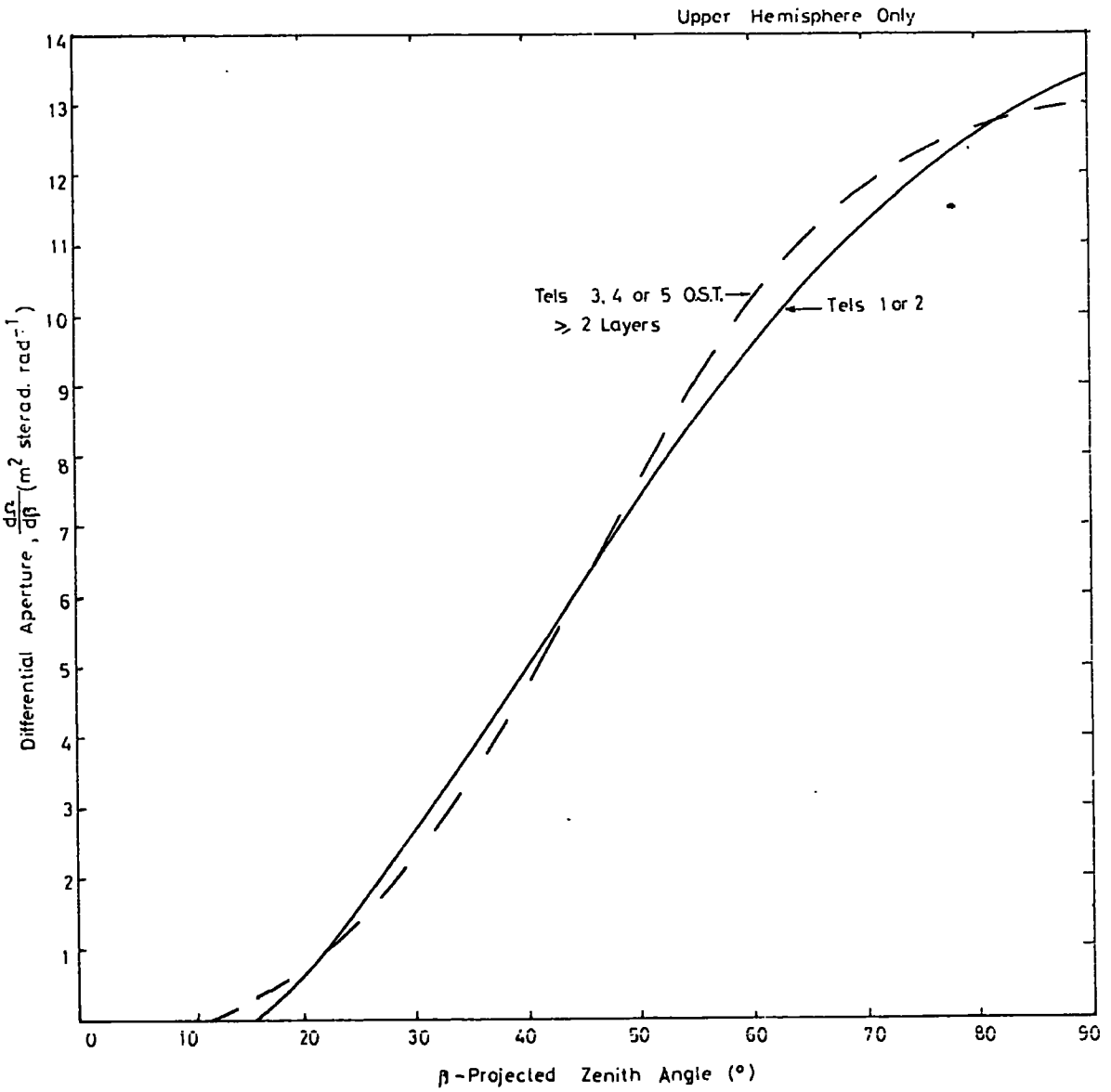

FIG. 6.2: Differential Apertures in Spatial Zenith Angle

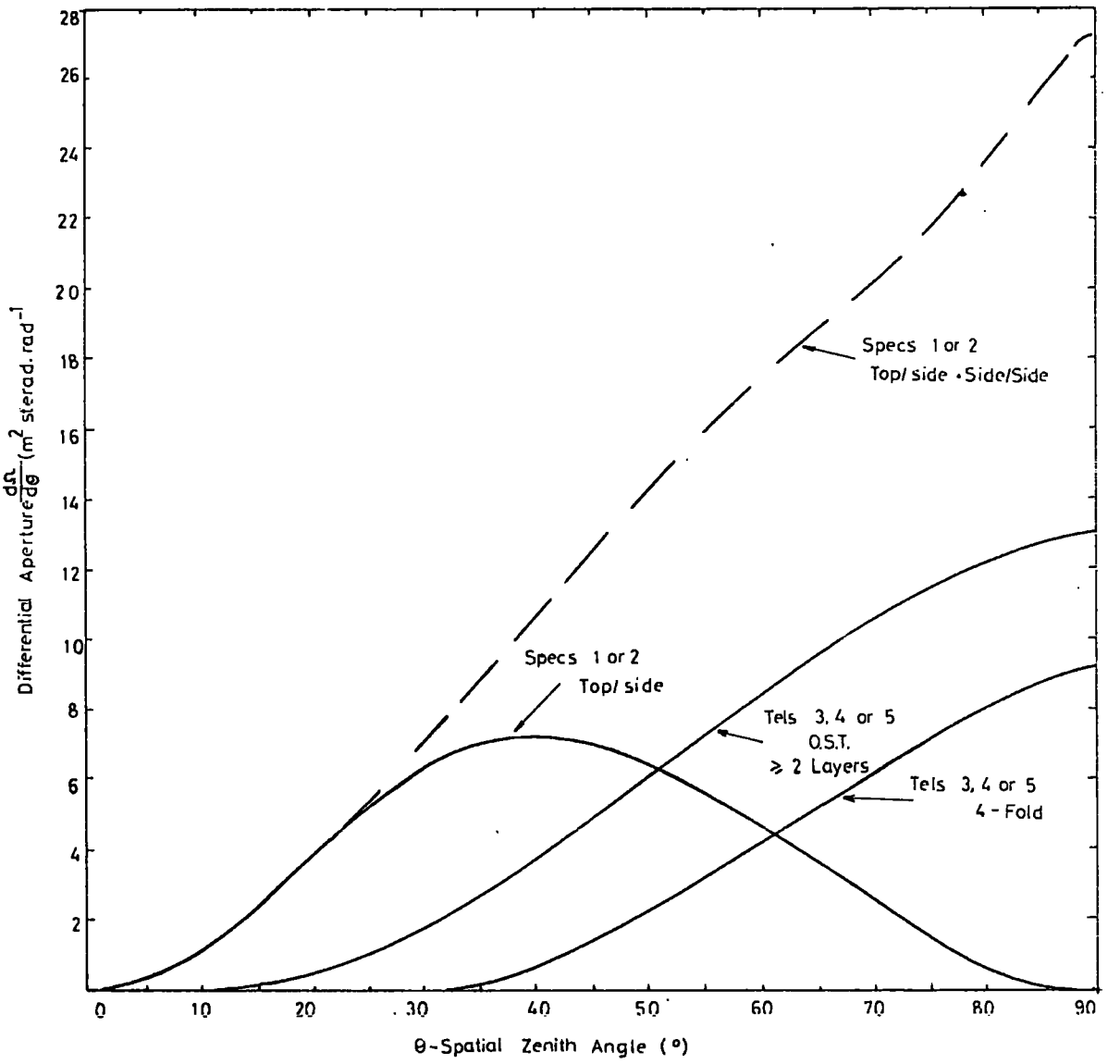

$I(\theta,h)/I(0,h)$ depends upon the assumed form of the angular distribution and has been taken as given by equations 6.1 & 6.4 for n = 6, 7, 8, 9 & 10 and m = 7, 8, 9 & 10 respectively.

Although the shape of the effective differential apertures for different values of the parameters n amd m are similar, particularly at small zenith angles, the integral apertures vary quite considerably (See Table 6.1). Consequently the accurate establishment of a best fit distribution is of prime importance in any estimate of the vertical intensity.

Table 6.1 : Integral Effective Apertures of Tels. 1 & 2 for Atmospheric Muons.

	Integral Aperture (0° - 50°) per telescope. m^2st.								
Angular Distribution	$\cos^n\theta$					$\sec\theta.\exp(-m(\sec\theta-1))$			
Index	n=6	n=7	n=8	n=9	n=10	m=7	m=8	m=9	m=10
Tels. 1 & 2	0.46	0.36	0.28	0.23	0.19	0.34	0.27	0.21	0.18
Specs.1 & 2	1.39	1.22	1.07	0.95	0.83	1.25	1.08	0.95	0.86

The effective differential apertures derived from equation 6.7 for Tels. 1 & 2, Tels. 3, 4 & 5 4-fold and O.S.T. $\geqslant$ 2 layer atmospheric events are shown in figs. 6.5, 6.7a and 6.7b respectively.

For Specs. 1 & 2, the differential aperture (fig. 6.2) is in terms of θ but it is required in terms of β as only limited azimuthal information is available in the results. On the assumption of a $\cos^8\psi$ variation of the angular distribution in projected zenith angle, where ψ

is the zenith angle projected on the vertical plane parallel to the axes of the flash tubes, the variation of the median value of ψ for θ in the range $0 - 60^{\circ}$ has been calculated on the assumption of the detector aperture being constant over ϕ . Now,

$$\sin\phi = \tan\psi / \tan\theta \qquad 6.9$$

which enables ϕ median to be estimated. The transformation of the differential aperture from being in terms of θ to terms of β is then achieved through applying ϕ median to equation 6.9. The spectrographs effective differential apertures, calculated as above, are shown in fig. 6.6.

The method used is an approximation in so far as the assumptions made are not strictly true. However, the difference between ψ median for a $\cos^{8}\psi$ distribution and the true distribution (not yet established here) has been shown to be small and the length of the spectrographs, 4 m , is enough not to introduce much error in the assumption of constant aperture over ϕ .

(N.B. The integral effective aperture for the spectrographs must be taken as $\int_{0}^{\theta_{max}} I(\theta,h)/I(o,h) \cdot d\Omega/d\theta \cdot d\theta$)

6.3 The Effect of Scattering in the Overhead Rock.

In their passage through matter, muons incur energy loses and are scattered in electromagnetic interactions. By far the most important is the continuous process of multiple coulomb scattering for which the mean square angle of scatter is given by,

$$\overline{(\delta\phi)^2} = \left(\frac{E_s}{\beta c p}\right)^2 \frac{dx}{X_o} \qquad 6.10$$

where dx/X_o is the depth of absorber in radiation lengths and p is the muon momentum. E_s = 21 MeV for the true angle of scatter and 14.8 MeV for the projected angle of scatter. The latter is more useful for the K.G.F. results, as in most cases only the projected zenith angle of the muon can be measured.

Muons penetrating the telescopes are virtually all of relativistic velocities and, assuming a linear energy loss over short elements of depths, 6.10 may be rewritten, integrated, as

$$\overline{\theta}^2 = \frac{14.8^2}{X_o} \int_o^{x_1} \frac{dx}{E_o} \qquad 6.11$$

where $E_o = E_1 + \alpha x$ is the energy of the muon entering the cell. E_1 is its energy leaving the cell after penetrating a distance x_1 . It follows that,

$$\overline{\theta}^2 = \frac{7.7 \times 10^{-4}\, x}{E_1 \; E_o} \qquad 6.12$$

where x is in m.w.e. standard rock and E_o & E_1 are in GeV.

Applying this to muons reaching 7500 m.w.e., it is clear that at shallow depths, and therefore high muon energies, the scattering is very small. Only the scattering in the last few m.w.e. of relatively low energy muons makes a significant contribution to the total. For example, the scattering in the first 5000 m.w.e. of rock is less than one tenth of the scattering in the last 250 m.w.e. for a muon reaching 7500 m.w.e. with an energy of 300 GeV.

The variation of root mean square projected angle of scatter with energy for muons reaching 7500 m.w.e. st. rock is shown in fig. 6.3. This curve is true for most depths underground below a few tens of m.w.e.

FIG. 6.3: Muon Scattering Variation with Energy.

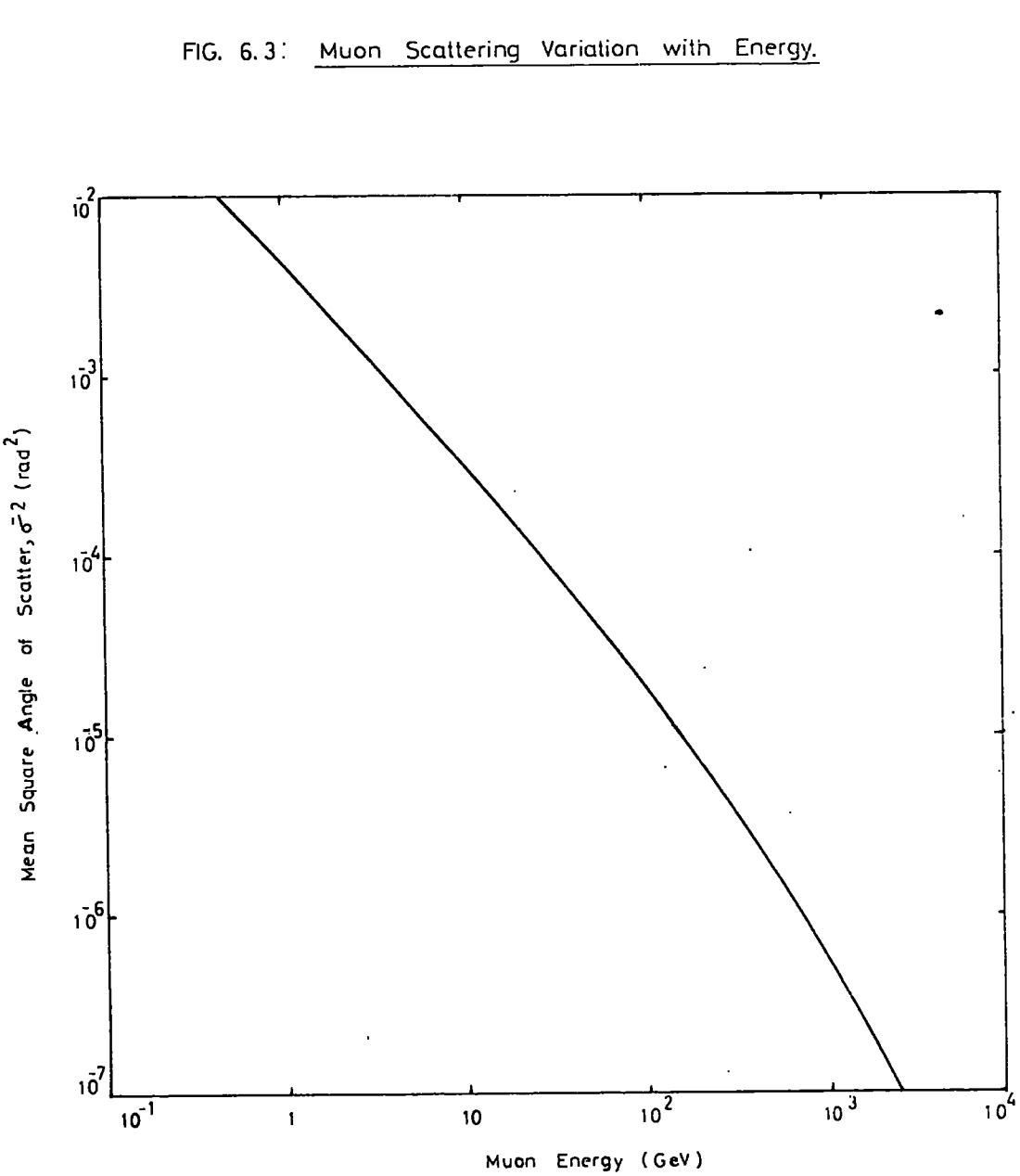

FIG. 6.4: Approximate Differential Intensity of Scattered Vertical Muons reaching 7500 m.w.e.

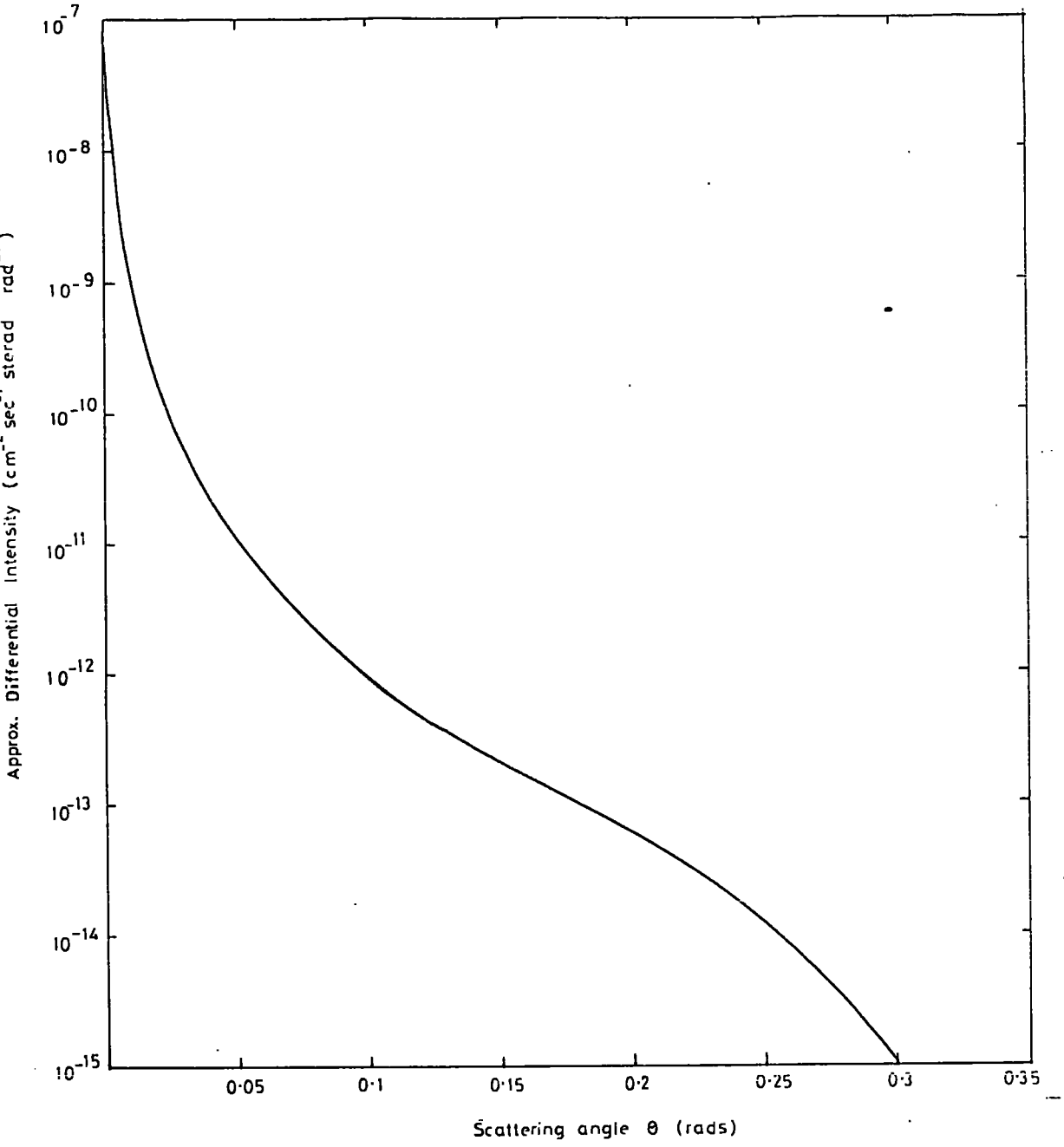

Multiple coulomb scattering is approximately described by a normal distribution if, as above, large angle single deflections are ignored. As the standard deviation is a function of muon energy, the normal distribution may be represented by the function $\phi(\theta, E)\,d\theta$ which is the probability of a muon of energy E being scattered to an angle θ. If N(E)dE is the differential muon spectrum, then

$$\overline{\theta^2} = \frac{\int_0^\infty \int_0^\infty N(E)\,dE \cdot \theta^2 \cdot \phi(\theta,E)\,d\theta}{\int_0^\infty N(E)\,dE} \qquad 6.13$$

where $\overline{\theta^2}$ is the mean square angle of scatter of all muons.

For the 7500 m.w.e. differential spectrum derived from the U2 primary spectrum (Chapter 3, fig. 3.4) $\sqrt{\overline{\theta^2}}$ has been calculated to be $< 1^\circ$. The overall scattering distribution is shown in fig. 6.4. The probability of a muon being scattered by $> 3^\circ$ is 4×10^{-3} and by $> 5^\circ$ is 10^{-4}.

It can, therefore, be safely assumed that scattering alters the angular distribution of the detected muons by $< 1^\circ$.

6.4 Intensity and Angular Distribution

The angular distribution of muons detected in the three telescope groups to 30/11/68 have been used to establish best fit expressions of the forms described in section 6.2. The statistics, however, are not good and the application of a goodness of fit test, of theoretical expressions of similar form to the histograms made up of the events observed, could easily give a misleading result as a consequence of the chance selection of the cells used. In an attempt to overcome this difficulty, an error of $\pm 2.5^\circ$ was attributed to the best estimate projected zenith angle of each event and its

contribution to the histogram was distributed over the two 5^{o} cells covered proportionately to the error spread in each. This approach can be critisized on the basis of alteration of the statistical nature of the experimental data. For this reason, a best fit distribution having been estimated in this way, true χ^2 tests were applied to the original observed data in which each event contributed to one cell only.

The true χ^2 tests showed clearly that the similarity between the expressions leads to χ^2 not being very sensitive to the index n or m. For Tels. 1 & 2, the observed distribution does not differ significantly (with 95% confidence) from both forms applied within the index ranges $11 > n > 6$ and $10 > m > 5$. Similarly for Specs. 1 & 2 the ranges are $12 > n > 7$ and $11.5 > m > 7.5$. For both Tels. 1 & 2 and Specs. 1 & 2, the variation of χ^2 with the index n for the $\cos^n\theta$ form had a lower minimum than that with the index m of the exponential form.

Table 6.2 : Atmospheric Muon Results.

	Angular Distribution $\cos^n\theta$ form : exp. form				Vertical Intensities ($cm^{-2}\ sec^{-1}\ st^{-1}$)	
	best fit n	best est.n	best fit m	best est.m	assuming $\cos^9\theta$	assuming $\sec\theta$. $\exp(-8.5(\sec\theta - 1))$
Tels 1 & 2	8.3	~9	7.5	~8.5	$< 1.3 \times 10^{-10}$	$< 1.2 \times 10^{-10}$
Specs. 1 & 2	9.6		9.8		$< 9.2 \times 10^{-11}$	$< 8.6 \times 10^{-11}$

N.B. The intensities quoted in the table are given as upper limits as the number of muons included not of atmospheric origin is not known. It seems unlikely that such muons would give more than a 15% contribution to the intensity.

FIG. 6.5: Comparison of Observed and Expected Angular Distribution of Atmospheric Muons - Tels 1&2

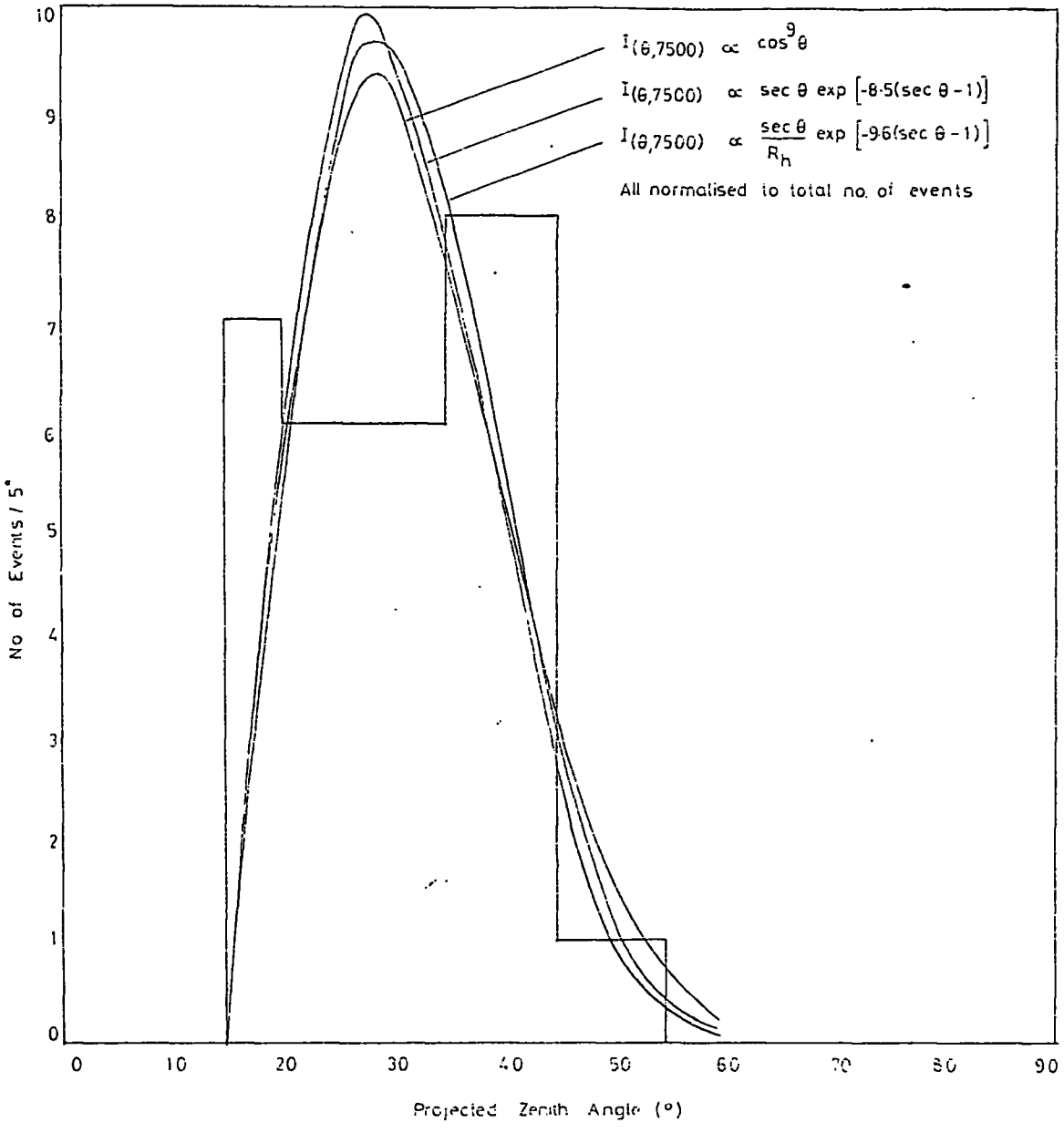

FIG. 6.6: Comparison of Observed and Expected Angular Distribution of Atmospheric Muons - Specs 1&2

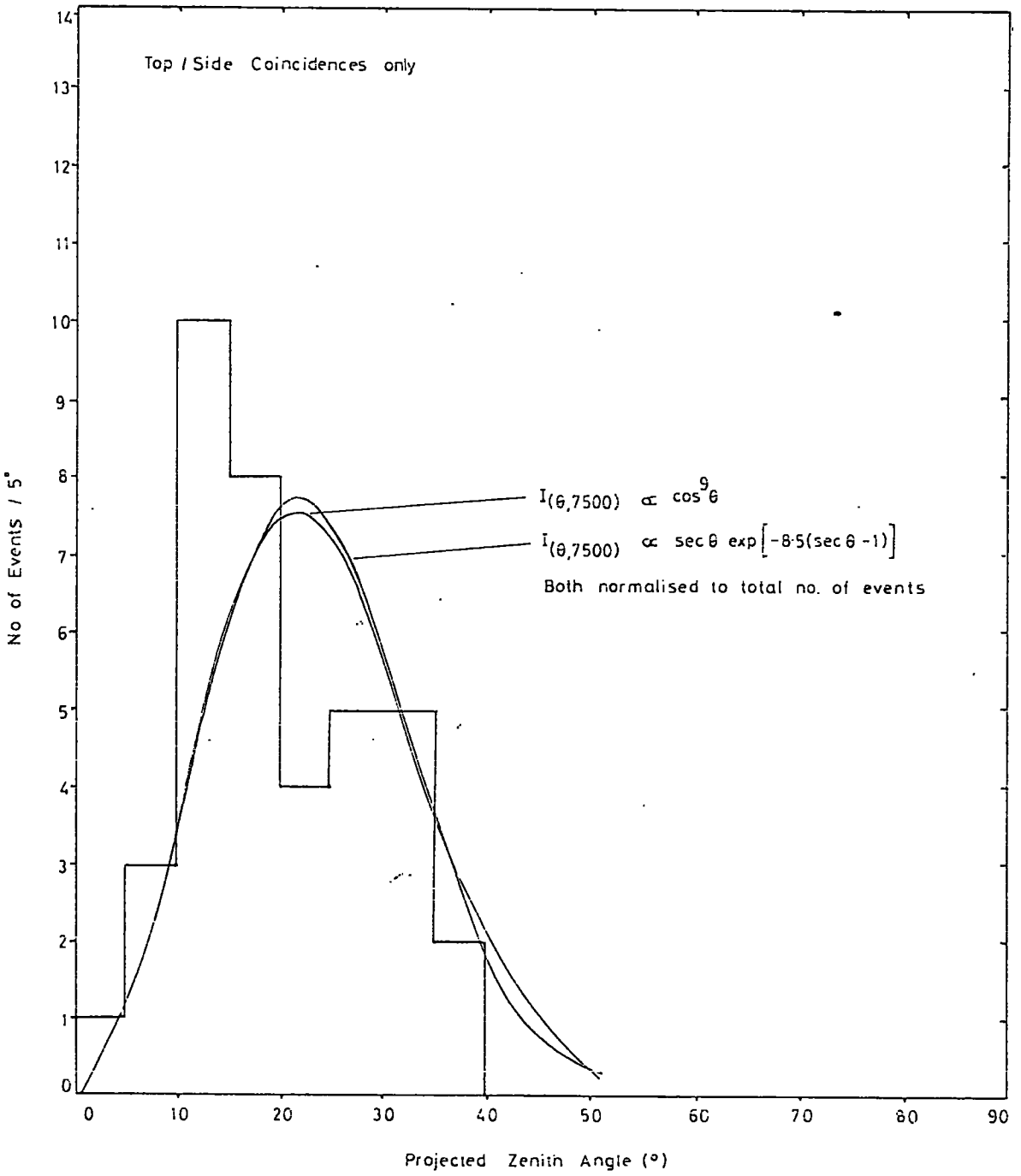

Comparison of Observed and Expected Angular Distribution of Atmospheric Muons

– Tels 3,4 & 5.

FIG. 6·7a : 4 - Fold

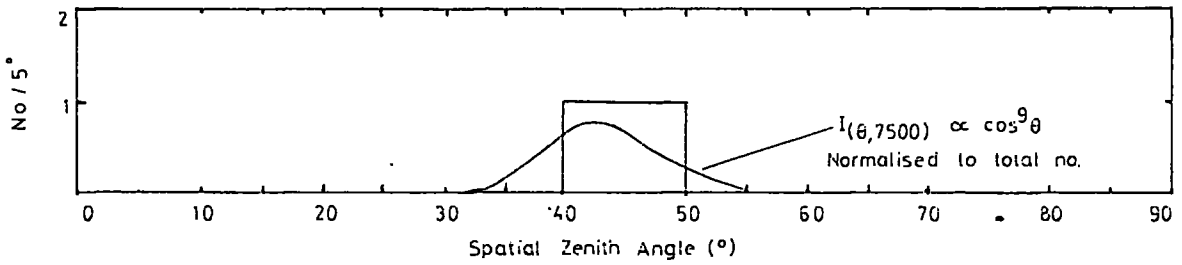

FIG. 6·7b : O.S.T. ≥ 2 Layers

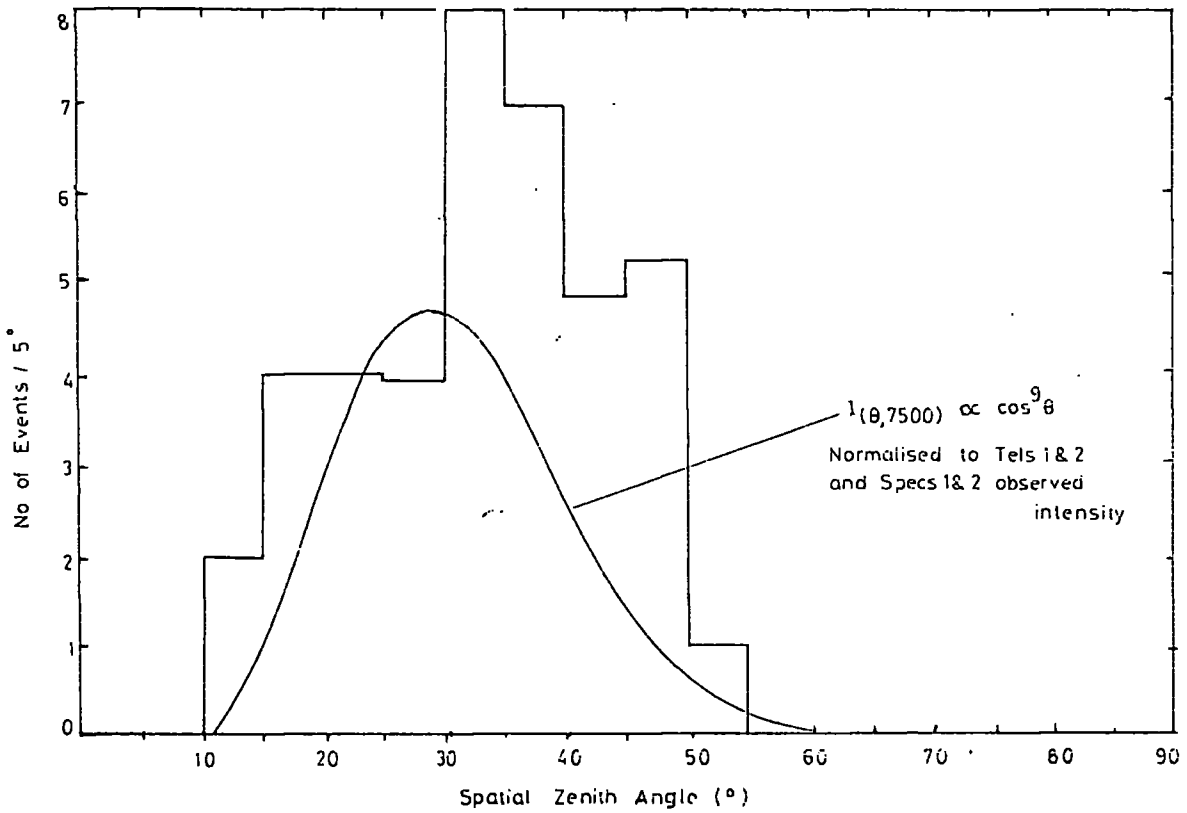

This is because there has been an excess of events in the 30° - 50° region which is better covered by the comparatively broad distribution of $\cos^{n}\theta$ with constant n.

The best fit values of n amd m, to the 'smoothed' data are given in table 6.2.

The expected angular distribution of $\geqslant$ 2 layer events in Tels. 3, 4 & 5 O.S.T. operation, calculated on the basis of the best estimated distribution from the other detectors namely,

$$I\ (\theta\ ,\ 7500) = 10^{-10}\ \cos^{9}\theta \qquad cm^{-2}\ sec^{-1}\ st^{-1} \qquad 6.15$$

is shown in fig 6.7b* together with the observed distribution.

6.4 : 1 Interpretation of the Results

Somewhat unexpectedly, the observed intensity of O.S.T. $\geqslant$ 2 layer events has been found to be about double the predicted value. It is not possible to explain this result in terms of an underestimation of the scintillator efficiencies. In view of the previous discussion (Menon et al. 1967a,b) concerning the excess of events in the 30° - 50° region in Tels. 1 & 2, this result could be important.

* Events caused by single particles (assumed to be muons) are plotted as full contributors to the histogram. Events in which accompanied particles have passed through the scintillator, and increased the detection efficiency to an assumed 100%, have been counted as fractional contributors, the fraction being the efficiency at the appropriate zenith angle in the telescope concerned.

4-fold type events have been counted as two events because they passed through two scintillator walls. However, as it cannot be assumed that they would have been detected in both walls individually 100% contribution has been assumed in one wall and the efficiency fraction in the other.

The possible explanations considered previously are,

(a) Topographical effects, including rock density variation and mining excavation voids.

(b) Scattering of atmospheric muons.

(c) Muon neutrinos produced near polar regions.

(d) Muons from W - decay as a result of the Glashow resonance interaction.

(e) Interaction products of nuclear interaction and pair production by high energy muons.

The effects under (a) are estimated to lead to $< 10\%$ error in the intensity measurement at any angle. Approximately equal numbers of events have been detected from North and South, which supports this.

The possibilities under (b) and (c) have been estimated to have a negligible effect, (d) also seems unlikely on the basis of the currently predicted cross-section. Only one or two events would be expected as a result of the resonance and any peak resulting from it would be expected at about 60°.

The possibility of the events being pions from nuclear interactions has also been considered. However, taking the current best estimates of the photonuclear cross section, only about 1 in 1000 particles detected are expected to be from this source.

6.4 : 2 Modification of the Exponential Form

The large angle enhancement may be accomodated in the angular distribution expression if the expression itself is modified. For equation 6.3, Menon et al. established the values of the constants B and λ from the known intensities at 4000 and 7500 m.w.e. Whereas B is a

constant, dependent on the muon intensity, λ is a function of the energy loss processes. This can be seen in the expressions of Kilhalchi and Zatsepin (1965) for the vertical depth intensity relation including bremsstrahlung fluctuations,

$$I(h) = A \frac{\exp\left[-\gamma(1 + \kappa b')ah\right] \exp(\phi(h))}{\left[1 - \exp\left\{-(1 + K_1 b')ah\right\}\right]^{\gamma}} \qquad 6.16$$

where γ is the slope of the sea level integral spectrum, κ is a slowly varying function of γ, b' is the ratio of the fluctuating to non-fluctuating energy loss parameters, a is the non-fluctuating energy loss parameter, K_1 is a function of b and γ, and ϕ accounts for the effect of fluctuations.

For great depths the expression reduces to,

$$I(h) = B \exp\left[-(1 + \kappa b')ah\right] \qquad 6.17$$

Comparing this with 6.3, it can be seen that $1/\lambda = a\gamma(1 + \kappa b)$. Therefore, clearly, any changes in the slope of the sea level spectrum or in the nature of the energy loss parameters can result in a change in λ.

If we define $\lambda = \lambda' y(h)$ where λ' is constant and equal to the value attributed to λ by Menon et al. and $y(h)$ is a function of h, then the depth intensity relation becomes,

$$I(0,h) = 9.8 \times 10^{-7} \exp\left(-\frac{h}{\lambda' y(h)}\right) \qquad 6.18$$

and the corresponding angular distribution is,

$$I(\theta,h) = I(0,h) \sec\theta \cdot \exp\left[\frac{h}{\lambda}\left(\frac{1}{y_{(h)}} - \frac{\sec\theta}{y_{(h\sec\theta)}}\right)\right] \qquad 6.19$$

The Tels. 1 & 2 observed angular distribution has been used to

establish the following rough expression for y(h) at depths > 8500 m.w.e.

$$y_{(h)} = 1 + (1.5 \times 10^{-5})h \qquad 6.20$$

where h is the depth below 8500 m.w.e. st. rock.

For shallower depths, $y_{(h)} = 1$.

On the basis of 6.19 and 6.20, the rate of events in the 30° - 50° region of Specs. 1 & 2 and Tels. 3, 4 & 5 O.S.T. must be considered to be downward and upward statistical fluctuations.

If the increase in λ is real, it could either be the result of a reduction in slope of the sea level spectrum or a decrease in the energy proportional term of the fluctuating energy loss processes. If the latter is considered alone, the effect might not be fully explained by the complete termination of the photonuclear cross-section. A fall in the bremsstrahlung term could also be required. (See Appendix 1)

The depth intensity relation for greater depths given by equations 6.18 & 6.20 are shown in fig. 6.8 along with that derived from the U2 spectrum for comparison.

6.4 : 3 The Effect of Fluctuations on the Angular Distribution

Fluctuations in energy loss of muons penetrating deep underground result in an enhancement of the muon intensity over that predicted by a unique range energy relation. Although it would be more meaningful to express the fluctuations effect in terms of a varying 'b' in equation 6.17, workers making theoretical studies of range fluctuations have often presented their results in the form of fluctuations correction factors for the intensity of muons at different depths underground. (Appendix 2).

The depth intensity curve of Menon et al., equation 6.3, has been

FIG. 6.8: Comparison of Depth Intensity Relations

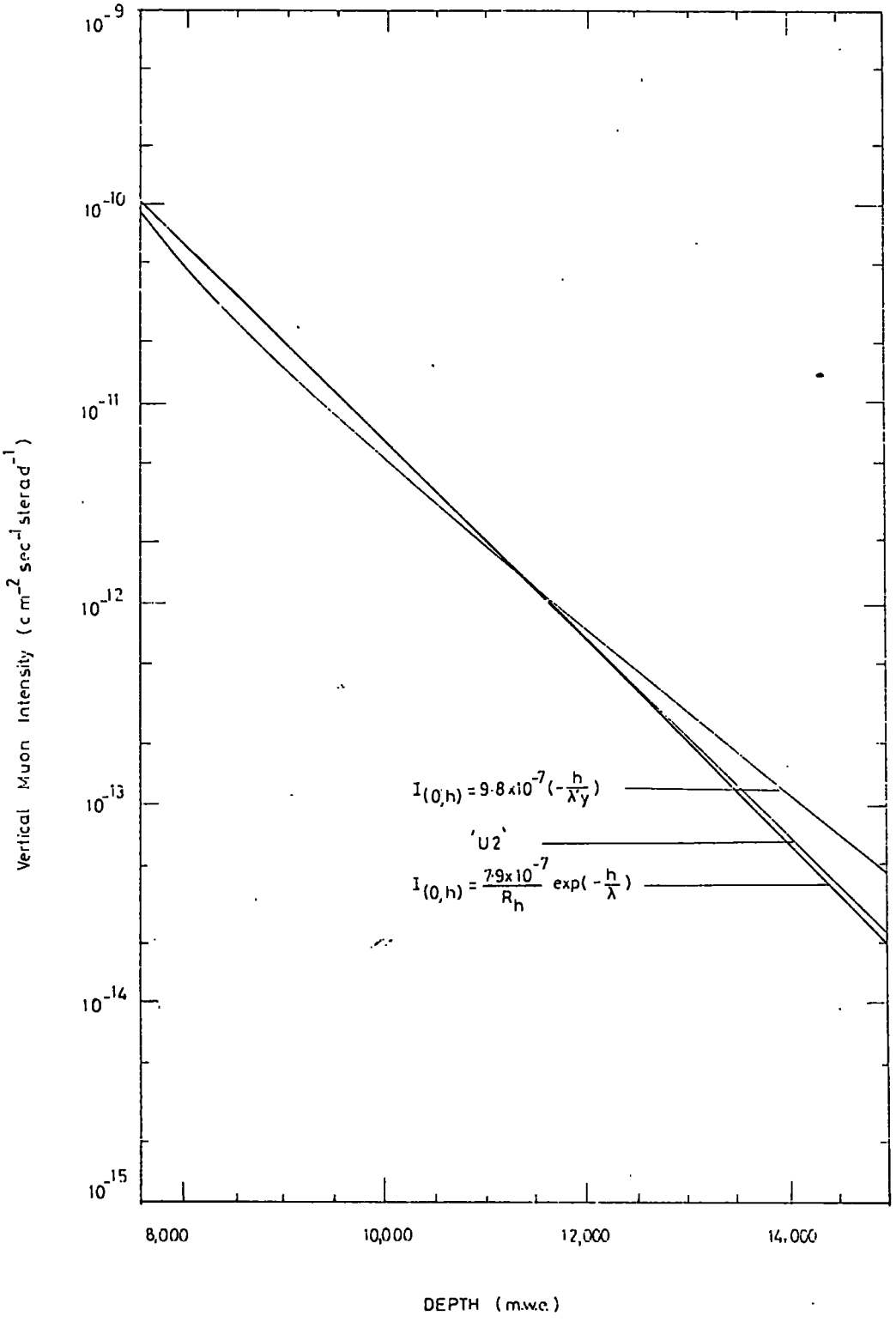

normalised by the authors at 7500 m.w.e. to have constants as follows,

$$I\ (0,h) = 9.8 \times 10^{-7}\ \exp\left(-\frac{h}{810}\right)\ \text{cm}^{-2}\ \text{sec}^{-1}\text{st}^{-1}$$

where h is in m.w.e. standard rock.

The value of B, 9.8×10^{-7}, already incorporates the fluctuations correction factor as it is based upon experimental evidence.

To extend this depth intensity relation to greater depths incorporating the relevant fluctuations correction, B may be replaced by A/R_h where A is constant and R_h is the correction factor at the depth h. The depth intensity curve for > 7500 m.w.e. has been predicted using the above method, from the angular distribution observed in Tels. 1 & 2 and is,

$$I\ (0,h) = (A/R_h)\ \exp\ (-h/\lambda) \qquad 6.21$$

where $A = 7.9 \times 10^{-7}$ and $\lambda = 781$ m.w.e.

This is shown in fig. 6.8 using the enhancement factors of Osborne et al. (1968) for values of γ taken from the U2 sea level spectrum at appropriate energies. It can be seen in the figure and in table 6.3 that this leads to similar values of intensity to those predicted by equation 6.18 for depths between 7500 m.w.e. and 12000 m.w.e., the latter being about the maximum effective depth used in establishing equation 6.20.

Table 6.3 Comparison of Depth Intensity relations

Depth Intensity relation	Intensity (cm^{-2} sec^{-1} $sterad^{-1}$)		
	8500 m.w.e.	11000 m.w.e.	15000 m.w.e.
From U2 primary spectrum	3.4×10^{-11}	2.0×10^{-12}	2.3×10^{-14}
$I(o,h) = 9.8 \times 10^{-7} \exp(-h/\lambda)$ - Menon et al.	2.3×10^{-11}	1.2×10^{-12}	8.9×10^{-15}
$I(o,h) = 9.8 \times 10^{-7} \exp(-\frac{h}{\lambda' y})$ - equn. 6.18	2.7×10^{-11}	2.0×10^{-12}	4.8×10^{-14}
$I(o,h) = \frac{7.9 \times 10^{-7}}{Rh} \exp(-h/\lambda)$ - equn. 6.21	3.5×10^{-11}	2.1×10^{-12}	2.1×10^{-14}

Although the slope of the U2 spectrum was used to obtain the fluctuations correction factor in equation 6.21, the intensities given by the latter are not very sensitive to γ and their similarity to those from the U2 spectrum is not primarily a consequence of using the correction factors for the same slope.

6.4 : 4 The Nature of the 30° - 50° Events Excess

To investigate the possibility of a process other than $\pi - \mu$ decay being responsible for the excess of events at 30° - 50°, additional information, about the events, is required. The effect is virtually non-existent in the spectrograph results, quite obvious in the Tels. 1 & 2 results and possibly more obvious in Tels. 3, 4 & 5 O.S.T. $\geqslant$ 2 layer

results. The extent of the effect may be roughly correlated with the reduction in thickness of the telescope absorbers. To further investigate this possible correlation, the angular distribution of O.S.T. 1 layer events has been calculated for comparison with the observed events on the assumption that they are all muons. (fig. 6.9).

Using Tels. 1 & 2 and Specs. 1 & 2 results as a guide, it might be expected that an excess of events would be detected in the 30° - 50° region in Tels. 1 & 2 on account of the reduction of absorber thickness presented at those angles. Similarly, in general, Specs. 1 & 2 present less absorber (i.e. path length in magnet) at smaller angles. Thus, taking any excess of muons in Tels. 1 & 2 in the 30° - 50° region and in Specs. 1 & 2 in the $< 30^{\circ}$ region to be of different origin, the intensity and angular distribution can be estimated using Tels. 1 & 2 $< 30^{\circ}$ data and Specs. 1 & 2 30° - 50° data. This gives a vertical intensity of 9.4×10^{-11} cm^{-2} sec^{-1} st^{-1} and an angular distribution (of the form of equation 6.4) of,

$$I(o,h) = 9.4 \times 10^{-7} \sec\theta \cdot \exp.(-8.5(\sec\theta - 1)) \qquad 6.22$$

The variation of the ratio of observed to expected intensity against absorber thickness is shown in fig. 6.10. Although there are quite large errors on the points, the general tendency does seem to be towards a higher intensity of particles in detecting bands with less absorber.

The possibility of the excess of events being a result of muon pair production from the decay of the heavy intermediate particle proposed to explain the results of muon less air showers by Maze et al. (1969), has been considered. However the survival probability of a particle of rest mass 10 GeV and lifetime 10^{-9} sec increases so rapidly with energy that muons detected from its decay would be of high mean energy in contrast with

FIG. 6.9: O.S.T. 1-Layer Events Angular Distribution

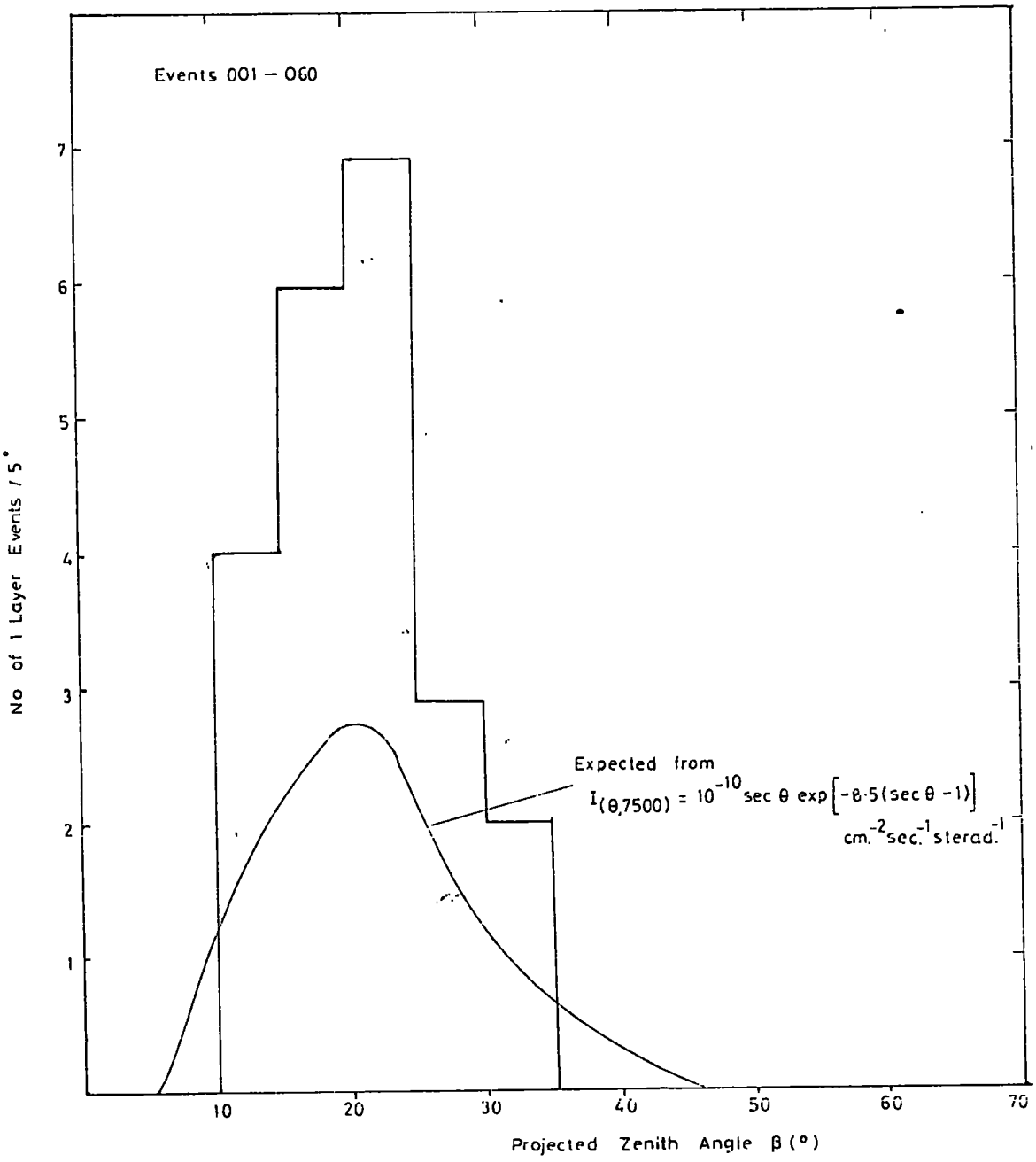

FIG. 6.10: Variation of Observed to Expected Intensity with Absorber Thickness.

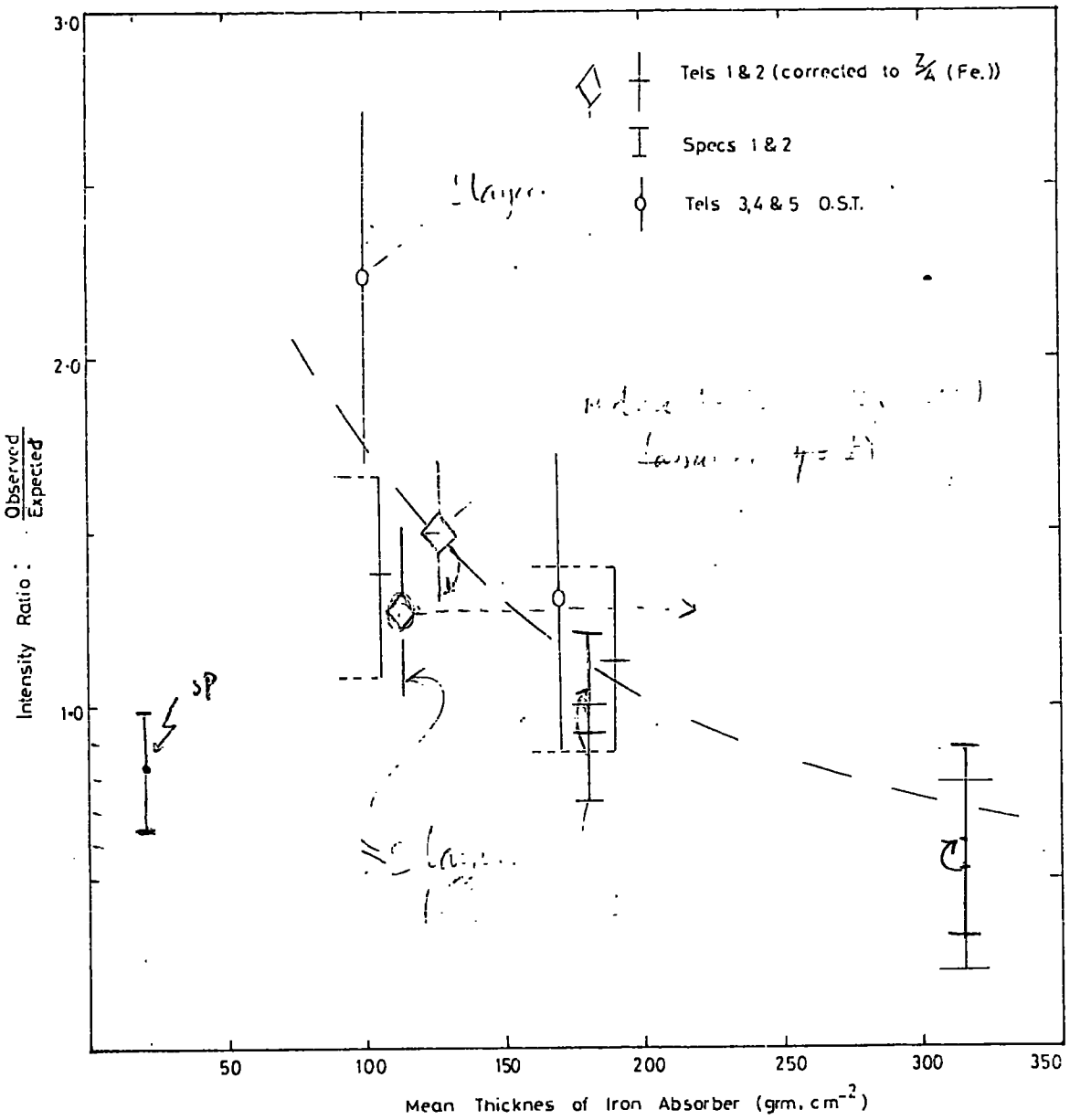

the probably low energy of the detected excess muons.

Another possibility is that of a resonance in the neutrino interaction cross section. However a low energy resonance would be needed to explain the results and no such resonance has been observed in machine experiments to 10 GeV.

It thus seems that although there may be some evidence for a low energy component in the observed events, no satisfactory explanation is readily available.

6.5 The Energy of Atmospheric Muons.

The experiment was not designed to investigate the energy of atmospheric muons but a study of the electromagnetic accompaniment, particularly that produced by muons in the lead absorber of Tels. 1 & 2, can be of use in estimating the mean energy.

6.5 : 1 Shower Events.

Seven useful shower events have been recorded in Tels. 1 & 2. Two of these showed two stages of the shower development in different flash tube trays. It was, therefore, possible to fit the numbers of electrons present (as estimated from the flash tube photographs) on either side of a lead absorber to the cascade shower curves shown in fig. 3.15 so as to obtain an estimate of the shower initiating primary energy. In the other five events, the shower was visible in only one layer of flash tube trays and the approximation was made that the shower maximum was observed so as to estimate the energy of the shower primary.

The results of the analysis are shown in Table 6.4.

Table 6.4 Tels. 1 & 2 Shower Events.

Event No.	Number of electrons (Ne) at shower max.	Ne at depth t_1	Ne at depth t_2	Absorber Thickness $t_2 - t_1$ (rad.lengths)	Shower primary energy(GeV)
8	8	-	-	-	0.4
9	30	-	-	-	1.7
19	4	-	-	-	0.2
14		10	6	15	4
26	4	-	-	-	0.2
32	18	-	-	-	1
41		5	12	8	2

6.5 : 2 Frequency of Shower Observation

Following the theoretical analysis in Chapter 3, the observed events may be studied with regard to the frequency of observation of showers of greater than a given number of electrons.

For all 'in geometry' atmospheric muons detected in Tels 1 & 2, the thickness of absorber traversed has been estimated. The 44 muons used in the analysis traversed a total of 5.4×10^3 grms/cm^2 of lead in the telescopes. In all cases, by virtue of the scintillator coincidence arrangement, the muon passed through two layers of lead flanked by layers of flash tubes.

Table 6.5 shows the total number of showers observed, the distance in lead absorber traversed by the muons and the consequential frequency of

observing a shower per grm.cm^{-2} of absorber traversed per lead layer. The relative contributions of muons with projected zenith angles $< 30^{\circ}$ and 30° - 50° are also given.

Table 6.5 Frequency of Showers detected in Tels. 1 & 2

	Total Showers - all muons	Showers from muons $\beta < 30^{\circ}$	Showers from muons 30° - 50°
No. of showers of > 2 electrons observed leaving a lead layer	9	4	5
Total absorber traversed by detected muons (grm.cm^{-2} lead)	5.39×10^{3}	3.24×10^{3}	2.15×10^{3}
Probability of shower observation per grm.cm^{-2} traversed	1.67×10^{-3}	1.23×10^{-3}	2.33×10^{-3}
E_{μ} effective(GeV)	460	310	710

(N.B. The 2 showers visible in 2 flash tube tray layers are each included twice.)

6.5 : 3 The Effective and Mean Energies

The shower frequency observations for showers of more than 3 electrons may be applied to the predicted frequency distributions of fig. 3.7. In this way a unique 'effective' energy may be attributed to the muons

detected. Values of this energy, $E_{\mu\,eff}$ are shown in table 6.5.

As the observations do not permit the measurement of the mean energy $\bar{E}_\mu$, $E_{\mu\,eff}$ must be calculated for comparison with the observed energies. From section 3.7 4, if $Pn(E_\mu) = \int \varepsilon P_\varepsilon \, . \, d E_p$ 6.23

then the effective probability of observing a shower of $>$ n electrons from a muon traversing a lead absorber layer, per grm. cm.$^{-2}$, is given by

$$Pn_{eff} = \frac{Pn(E_\mu)\, n(E_\mu)\, d E}{n(E_\mu)\, d E} \qquad 6.24$$

(where $n(E_\mu)$ is the differential muon spectrum)

and the effective energy is obtained from fig. 3.17 from the variation of $\int \varepsilon P_\varepsilon \, . \, dE_p$ with E.

Using the D^{-9}, U2 and EXP spectra derived for 7500 m.w.e. in sections 3.2 and 3.3, $E_{\mu\,eff}$, calculated using $Pn(E_\mu)$ for $n > 4$, has the values shown in table 6.6.

Table 6.6 Mean and Effective Energies

Spectrum	Mean Energy $\bar{E}_\mu$ (GeV)	$E_{\mu\,eff}$ (GeV)	
		Predicted	Observed
D^{-9}	393	355	
U2	336	310	430^{+330}_{-180}
'EXP'	287	285	

(N.B. The observed $E_{\mu\,eff}$ is derived from the 7 observed showers consisting of $>$ 4 electrons).

The errors on the observed effective energy do not permit a distinction to be made between the different spectra but, in any case, it must be remembered that the predicted values are for vertical muons whereas the observed value was recorded for muons over the range 15° - 50° p.z.a. $E_{\mu\,eff}$ for two angular ranges is given in table 6.5 as observed from showers of $>$ 2 electrons. However, of the 9 shower sections observed 3 were produced by muons from projected zenith angles between 30° and 31°. If these had been included in the $< 30^{\circ}$ group, the result would have been reversed. Clearly, then it would be unsatisfactory to base any firm conclusions on these energies.

If the ratio of mean to effective energy for the actual spectrum is taken to be the same as for the U2 spectrum, the mean energy of detected atmospheric muons may be taken as $450\ ^{+330}_{-180}$ GeV corresponding to an equivalent vertical depth of 8900 ± 200 m.w.e.

6.5 : 4 Total Electromagnetic Accompaniment

As a final means of estimating the underground muon energies, a method based on the spectrograph observations of Said (1966) has been applied.

The observations made were on the frequency of electron events produced by muons in the momentum range 5 - 1000 GeV/c. The results, also shown by Menon et al. (1967), show a rapid increase in shower frequency with energy above $\sim$ 100 GeV. A less rapid increase in single electron production and an almost constant probability of δ - ray production with energy.

A quantity R has been defined such that,

$$R = 1 + 0.7\,F_1 + F_2 + 3\,F_3 \qquad 6.25$$

where F_1, F_2 and F_3 are the probabilities of observing, per flash tube tray from one muon traversal, δ - rays produced in the flash tube trays, knock on electrons and showers.

The co-efficients of F have been established empirically from previous experiments. The first term represents the traversing muon.

In the analysis made by Menon et al. the observations in all 3 flash tube tray layers were included and the F parameters had values of 0, 1/3, 2/3 or 1. This method has been maintained for the Tels. 1 & 2 analysis but only accompaniment produced in the iron absorber has been included in the Tels. 3, 4 & 5 analysis so that the F parameter derived from the data of Said are directly applicable.

Fig. 6.11 shows the R values calculated for the 'in geometry' $< 50^{\circ}$ events which are probably atmospheric muons. Also shown is the mean R for the O.S.T. $\geqslant$ 2 layer events. The continuous line is that predicted by Menon et al. for Tels. 1 & 2 at 7500 m.w.e. and the dotted line is that predicted for the B.D. experimental points (Creed et al., 1965) which are also, shown. The points are plotted at the mean energies calculated in Chapter 3, sections 3.5 and 3.6, and the estimated R value for O.S.T. events has been corrected for the fact that the accompaniment was produced in iron and not lead as in the other cases.

This data has also been divided into the $< 30^{\circ}$ and 30° - 50° regions and the points plotted on the expected curve at the respective values of R. The results indicate an increase of energy at larger zenith angles. This may not be as significant as it seems since the expected curve is for muons at the mean zenith angle of about 30°. The increased acceptance of the telescopes to large zenith angle particles must increase the probability

FIG. 6.11: Variation of Accompaniment Parameter with Muon Energy

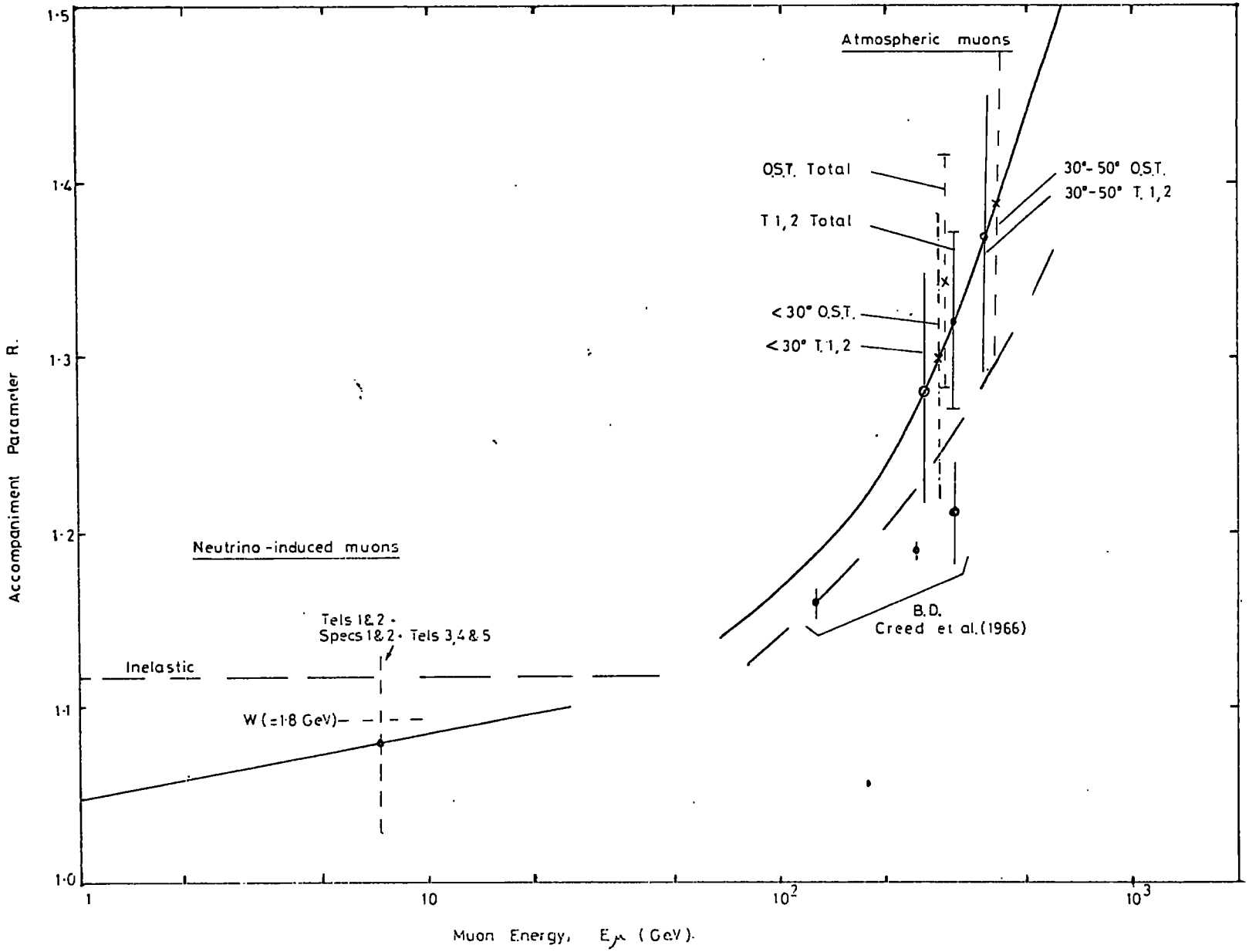

of observing accompaniment produced in the surrounding rock. This, however, can only be the case for the Tels. 1 & 2 data as the Tels. 3, 4 & 5 events accompanied by rock showers were not included.

The analysis indicates that the mean energy continues to increase with effective depth underground greater than 7500 m.w.e.

6.6 Conclusions

The similarity between the depth intensity relations, equations 6.18 and 6.21, suggests that the excess of events could well be at least partly explained as a result of energy loss fluctuations. Consequently, assuming all muons detected at zenith angles less than 50° to be of atmospheric origin, other than those which are clearly neutrino-initiated, the best expression for the angular distribution of atmospheric muons deep underground is

$$I(\theta, h) = I(o,h) \left(Rh/Rh_{eff}\right) \sec\theta \exp\left(-\frac{h}{\lambda}(\sec\theta - 1)\right)$$

where h_{eff} is the effective depth at an angle θ .

The best estimate vertical intensity of atmospheric muons at 7500 m.w.e. standard rock is,

$$I(0,7500) = (1.0 \pm 0.2) \times 10^{-10} \text{ cm}^{-2} \text{ sec}^{-1} \text{ sterad}^{-1}$$

and the best estimate angular distribution of atmospheric muons is

$$I(\theta,7500) = 5 \times 10^{-11} \frac{\sec\theta}{Rh_{eff}} \exp\left(-9.6\,(\sec\theta - 1)\right) \text{cm}^{-2}\text{sec}^{-1}\text{sterad}^{-1}$$

(i.e. $\lambda = 781$ m.w.e.)

Poor statistics do not permit firm conclusions to be drawn about the variation of mean energy with depth greater than 7500 m.w.e. from the present shower analysis. The observed showers, however, suggest a mean

energy of $450\ ^{+330}_{-180}$ GeV at an effective depth of 8900 ± 200 m.w.e.

The total electromagnetic accompaniment suggests that the mean energy at 8200 m.w.e. is $\sim$ 270 GeV and continues to increase to at least 9500 m.w.e. effective depth where it is of the order of 400 GeV. This is in quite good agreement with the shower analysis and is taken to be the best estimate from the present experiment.

CHAPTER 7

Analysis of the Neutrino Events.

The number of neutrino-induced muons expected in all detectors from the different neutrino interactions has been listed in table 4.1. These predictions were made using the angular intensity variations of muons from the different interactions as given by Osborne (1966) (see fig. 7.1). The reasons for the increased intensities of neutrinos at large zenith angles have already been described and the extent to which this angular variation is passed on to the muons is governed by the energy dependence of the cross-sections.

The differential effective apertures $I_\beta/I_{90}\left(d\Omega/d\beta\right)$ or $I_\theta/I_{90}\left(d\Omega/d\theta\right)$ according to the detector concerned) have been integrated over all zenith angles for each type of detector and are given in table 7.1.

Table 7.1 : Effective apertures for neutrino-induced muons.

	Aperture (m^2 sterad)			
Interaction	Tels 1 & 2	Specs 1 & 2	Tels.3, 4 & 5(4-fold)	Tels.3, 4 & 5 (O.S.T.)
Elastic	15.4(13.4)	30.1(25.1)	6.7(6.4)	6.7(5.1)
Inelastic (i) + (ii)(A)	12.2(10.8)	23.7(20.4)	5.5(5.3)	5.2(3.9)
Inelastic (i) + (ii)(B)	13.6(11.9)	26.5(22.5)	6.1(5.8)	5.9(4.5)

Figures in brackets are for large zenith angles only i.e. Tels. 1 & 2 and Specs. 1 & 2 – $>45^\circ$ p.z.a. Tels. 3, 4 & 5 – $>50^\circ$ s.z.a.

FIG. 7.1 : Angular Variation of Neutrino-induced Muon Intensity

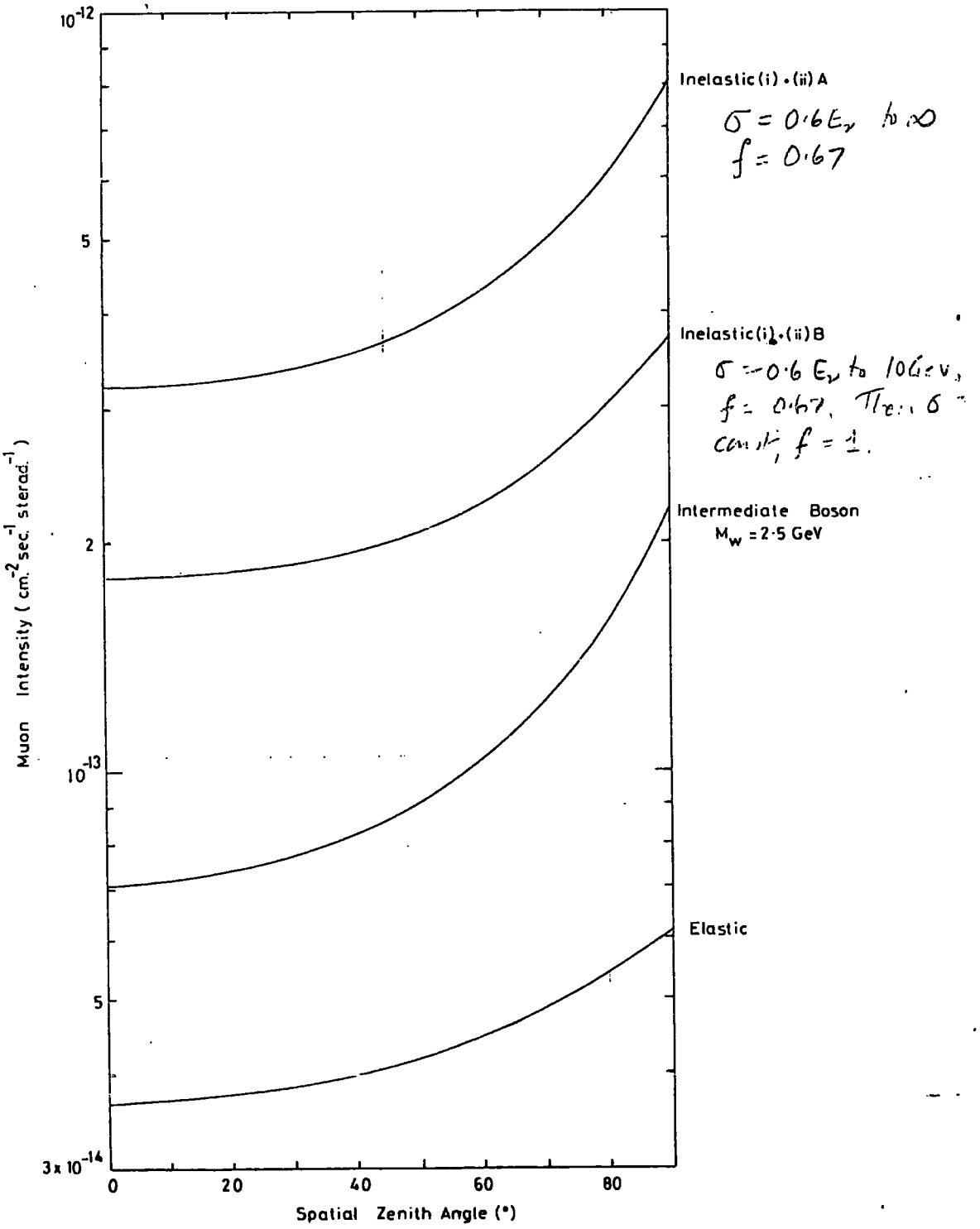

7.1 Neutrino-induced Muon Intensities

In table 7.1, it can be seen that the aperture presented to neutrino-induced muons varies according to the interaction and, as the exact proportion of events detected from each type of interacting is not known, an effective mean aperture must be estimated for the calculation of the horizontal intensity.

From the observed neutrino-induced events described in Chapter 5, when allowance is made for the O.S.T. detection efficiency, about 33% of the events can be recognised as being from non-elastic interactions. This is a high proportion and represents those in which more than one of the charged interaction products passed through the detectors. Of the remainder, several may well be from non-elastic interactions also. Thus, as a reasonable estimate, the apertures presented for the inelastic (i) + (ii)(B) case may be taken. The corresponding exposures for each detector are, therefore, as given in table 7.2 and the intensities of horizontal neutrino muons are - Tels. 1 & 2, $\left(3.2\ ^{+1.9}_{-1.4}\right) \times 10^{-13}$; Specs. 1 & 2, $\left(1.9\ ^{+1.9}_{-1.0}\right) \times 10^{-13}$; Tels. 3, 4 & 5 (4-fold), $\left(6.8^{+8.8}_{-4.4}\right) \times 10^{-13}$; Tels. 3, 4 & 5 (O.S.T.), $\left(4.9^{+4.6}_{-2.7}\right) \times 10^{-13}$, all in cm.$^{-2}$ sec^{-1} sterad^{-1}, the combined best estimate being $3.2 \pm 0.9 \times 10^{-13}$ cm.$^{-2}$ sec.$^{-1}$ sterad^{-1}.

Fig. 7.2 shows the measured intensity from the present experiment together with the latest intensity given for the Case-Wits. - Irvine Experiment (Reines, 1969) and predicted intensities for different assumptions about the inelastic cross-section and boson mass.

The observed angular distributions at large zenith angles and those expected from the inelastic (i) + (ii)(A) case are shown in fig. 7.3. The poor statistics do not permit any comparison to be made between the

FIG. 7·2 : Comparison of Rates of Neutrino-induced Muons

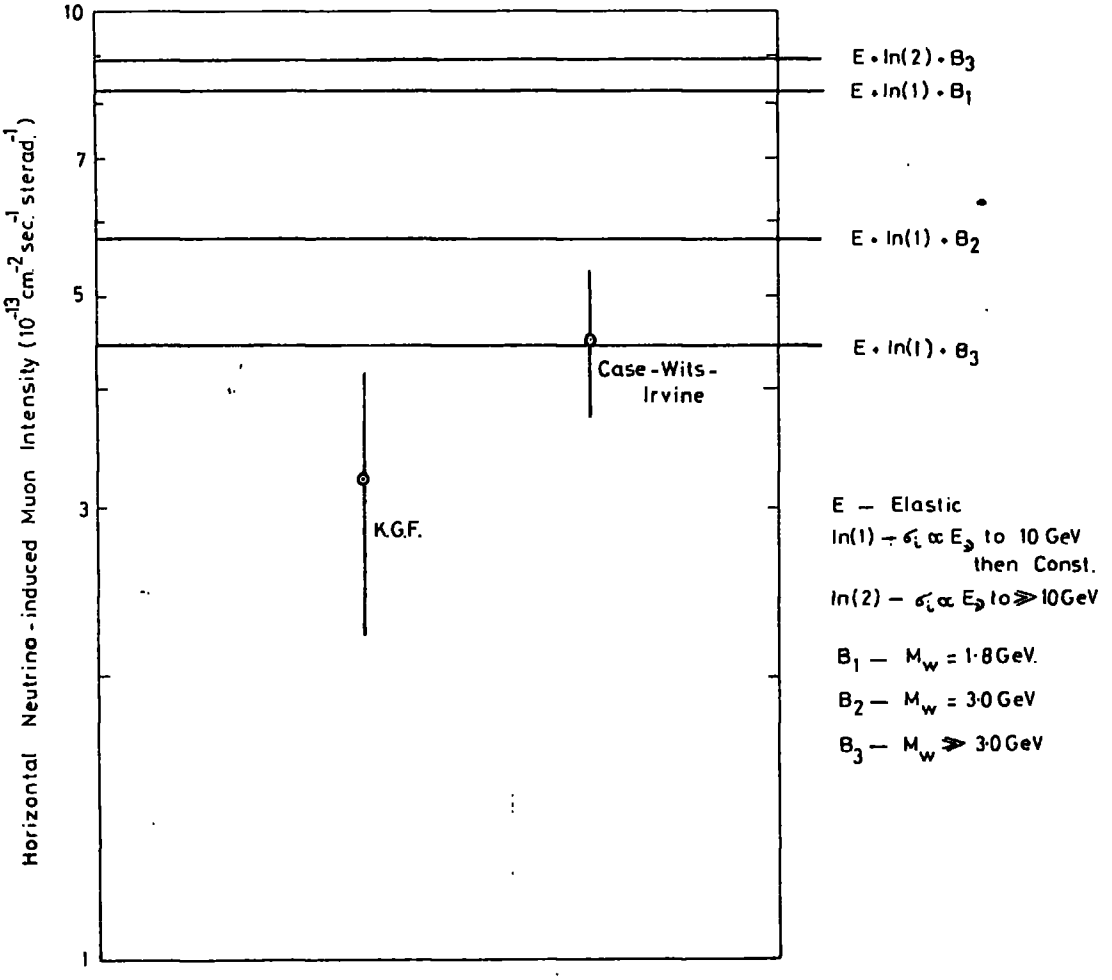

FIG. 7.3: Observed and Expected Angular Distributions of Neutrino-induced Muons

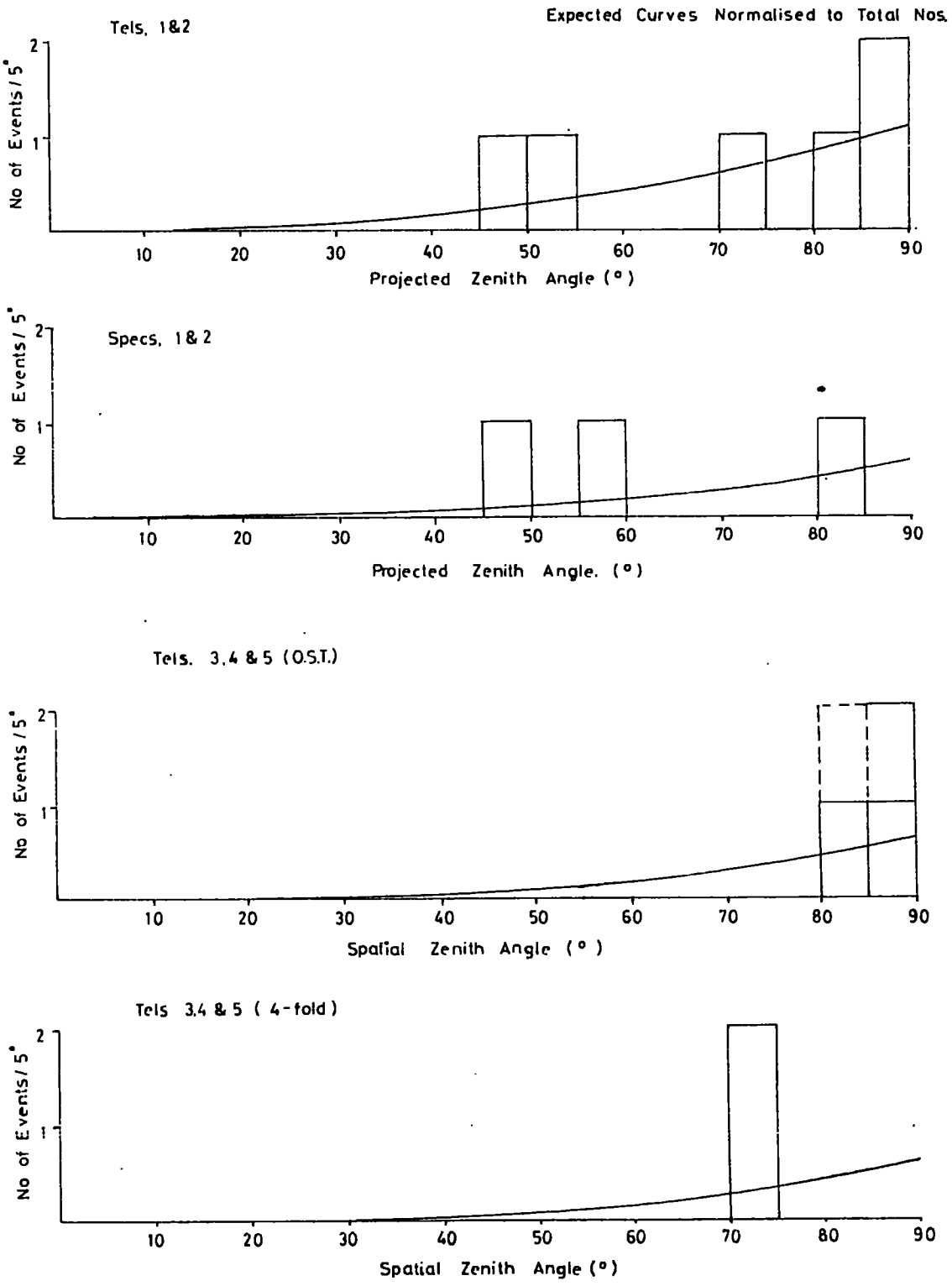

observed distributions and those resulting from different saturation energies of the inelastic cross-section.

Table 7.2 : Exposures to neutrino-induced muons

Interaction	Exposure ($cm.^2$ sec. sterad.)			
	Tels. 1 & 2 (all x 10^{13})	Specs. 1 & 2 (all x 10^{13})	Tels. 3, 4 & 5 (4-fold) (all x 10^{12})	Tels. 3, 4 & 5 (O.S.T.) (all x 10^{12})
Elastic	2.42(2.11)	2.05(1.71)	3.42(3.27)	8.9(6.8)
Inelastic (i) + (ii)(A)	1.92(1.70)	1.62(1.39)	2.81(2.71)	6.9(5.2)
Inelastic (i) + (ii)(B)	2.13(1.87)	1.81(1.55)	3.12(2.96)	7.85(6.0)

Figures in brackets are for large zenith angles only.

7.2 Neutrino-induced Muons at Smaller Zenith Angles

From the observed large angle events, the total number of upward moving neutrino-induced muons at small zenith angles in Tels. 1 & 2 is calculated to be 0.4 on the basis of the predicted angular intensities (see table 7.3). This figure, coupled with the observed probability of knock on production, leads to an expected number of upward moving muons producing knock ons of $\sim$ 0.08. In Chapter 5 the observed number of upward moving muons producing knock ons in Tels. 1 & 2 was estimated to be 2^{+2}_{-1}, however, the poor statistics do not yet permit any significance to be attached to this difference between the observed number and expectation.

Table 7.3 : Expected rates of upward moving muons at small zenith angles

		Tels. 1 & 2	Specs. 1 & 2	Tels.3,4 & 5 (4-fold)	Tels.3,4 & 5 (O.S.T.)
Aperture fraction :	$\left[\frac{\text{Small angles (lower-hemisphere)}}{\text{Total}}\right]$	0.12	0.14	0.05	0.24
Expected rates for lower hemisphere per detector hour	Elastic	2.8×10^{-6}	7.0×10^{-5}	5.0×10^{-6}	2.5×10^{-6}
	Inelastic (i)+(ii)(A)	1.6×10^{-5}	3.7×10^{-5}	3.0×10^{-6}	1.4×10^{-5}
	Inelastic (i)+(ii)(B)	1.0×10^{-5}	2.2×10^{-5}	1.8×10^{-6}	8.0×10^{-6}
No.of upward moving muons expected at small zenith angles to 31/12/68		0.4	0.4	0.03	0.3

7.3 Interpretation of the Neutrino-induced Events

The most interesting feature of the events is the number resulting from interactions close to and in the detectors.

The relatively large angles of divergence of the products in the inelastic interactions may be considered as a part explanation for the 30° - 50° excess discussed in the previous chapter. However, even though the neutrinos are expected to be peaked in the horizontal direction, the angular distribution of product muons produced with even a large transverse momentum would give a much less peaked distribution than is necessary to explain the excess. In particular, several muons from this source would

be expected in the 50° - 70° region which has, in fact, yielded very few events. On the other hand, the number of upward moving muons detected at small zenith angles is greater than that predicted, on the assumption that the muon retains the direction of the neutrino, and is in agreement with large opening angles.

As in section 6.5.4, the electromagnetic accompaniment of the neutrino events has been used to estimate the mean muon energy. Fig. 6.11 shows this to be, very approximately, 7 GeV for the Tels. 1 & 2, Tels. 3, 4 & 5 (4-fold) and Specs. 1 & 2 events. To reduce error the O.S.T. events have not been included as the detection efficiency is biassed towards accompanied events. Even so, the estimated mean energy has a large error as the accompaniment is not very sensitive to energy over the region of interest. Consequently, when the measured rate and mean energy are compared with the predictions in fig. 4.4, a large region is covered by the errors. It can be seen that the observations do not cover the possibilities considered at all, the total rate not even being as high as predicted from the constant elastic cross-section and the inelastic cross-section saturating at 10 GeV. On the other hand, the proximity of several inelastic interactions, mentioned above, is a clear indication of an increasing inelastic cross section above the 10 GeV. limit of the accelerators.

The apparent anomaly is reconciled if the energy taken by the muon, in higher energy interactions, falls. From the available results it is not possible to determine to what energy the cross section continues to increase so that, for instance, the results could be in keeping with a constant cross-section above 10 GeV and $\overline{E}_{\mu}/E_{\nu}$ falling from 0.67 at 10 GeV to 0.15 at 20 GeV and then constant to higher energies. Alternatively,

they could be in keeping with the cross-section saturating at 100 GeV with $\bar{E}_\mu/E_\nu$ falling rapidly from 0.67 at 10 GeV to 0.05 at $\sim$ 20 GeV and constant above. A more gentle fall in $\bar{E}_\mu/E_\nu$ could be accomodated if the cross-section saturates at 10 - 30 GeV with constant $\bar{E}_\mu/E_\nu$ of $\sim$ 0.1 at higher energies.

7.4 O.S.T. A-type Events

In the scanning of the O.S.T. films, many non-event frames have been seen which show either a short track in one tray or a few flashed tubes, in different trays, which can be aligned. Such occurrences have been designated 'A-type events'. The possibility of some of these being caused by charged particles has been investigated and, for this purpose, the A-type events have been subdivided into three types,

(a) Those showing a configuration of 3 flashed tubes which could be of 100% internal efficiency, the particle, if genuine, having passed through an inter-tube gap in one layer.

(b) Those showing configurations with $<$ 100% internal efficiency but still with 3 tubes flashed.

(c) Those involving more than one tray in which, if a charged particle was responsible, the flash tube efficiency was $\ll$ 100%.

The number of occurrences in category (c) was small and could be explained adequately in terms of chance alignment of spurious tubes. The occurrences in category (b) were more frequent, but some degree of scanning error must be allowed for since the unflashed intermediate tubes could be misleading. 'Tracks' in this category are, by definition, confined to small and intermediate zenith angles.

Category (a) is the most useful and the only one fully analysed. Again by definition, events in this category are confined to near-horizontal directions. Using the regularly recorded spurious rates, the expected rate of chance combination of spurious tubes has been calculated to be $\sim$ 40% of the total observed rate in category (a). If it is assumed that some of the remaining 60% is from radioactive decay in the iron absorber, then different rates would be expected in the inner trays, flanked by two layers, than in the outer trays, flanked by one. When this is taken into account, a rate of external radiation, not from the iron or flash tube trays, of $\sim 2 \times 10^{-11}$ cm.$^{-2}$ sec.$^{-1}$ sterad.$^{-1}$ is obtained assuming a detection efficiency of 50%.

The estimated rate is quite high and is most unlikely to be due to a flux of electrons from solar neutrino interactions. It is most probably due to the accompaniment of atmospheric muons since this mechanism could provide particles of sufficient energy to penetrate the scintillator and 3 flash tubes (i.e. $\gtrsim$ 8 MeV).

CHAPTER 8

Celestial Co-ordinates of Event Arrival Directions.

It is possible that some of the detected particles have come from parents produced, not in the Earth's atmosphere, but in extra-terrestrial sources and an analysis has been made of this possibility.

Before looking for anistropy and points of high intensity, however, it is necessary to consider the effect of the detector running times and apertures presented to different regions of the celestial sphere.

Fig. 8.1a shows the differential running time, in 45° segments of right ascension, to the end of 1968. The non-uniformity of the Tels. 1 & 2 distribution is indicative of lost running time during the construction of the other detectors. Fig. 8.1b shows the total differential exposure for all detectors, the deviation over sidereal time amounting to $< \pm 3\%$.

Figs. 8.2 & 8.3 show the projection on the celestial sphere of the Tels. 1 & 2 geometry, each arc representing the azimuthal range scanned at the projected zenith angle indicated. The effect of the site latitude is manifest in the ranges of declination scanned in the two hemispheres during the rotation of the acceptance projections about the pole with sidereal time.

In accordance with the analysis in Chapter 5, the celestial co-ordinates of the neutrino-induced events have been plotted seperately from those of the atmospheric muon events. The distribution of the atmospheric events in right ascension is shown in fig. 8.1c and the celestial co-ordinates in figs. 8.4 & 8.5. In figs. 8.6 & 8.7, the celestial co-ordinates of the neutrino events are shown plotted in the appropriate hemisphere in cases

FIG. 8.1a: Differential Running Time in Right Ascension

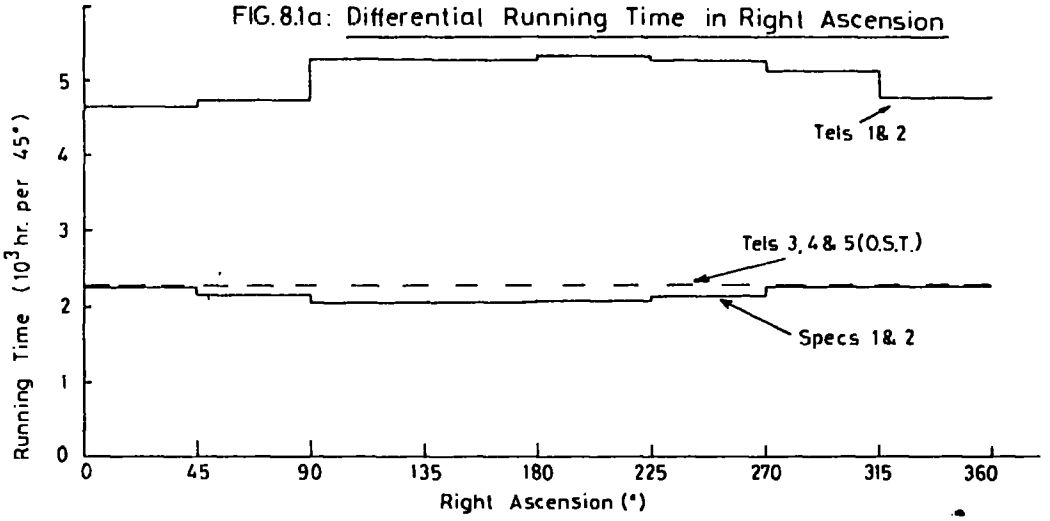

FIG. 8.1b: Total Differential Exposure

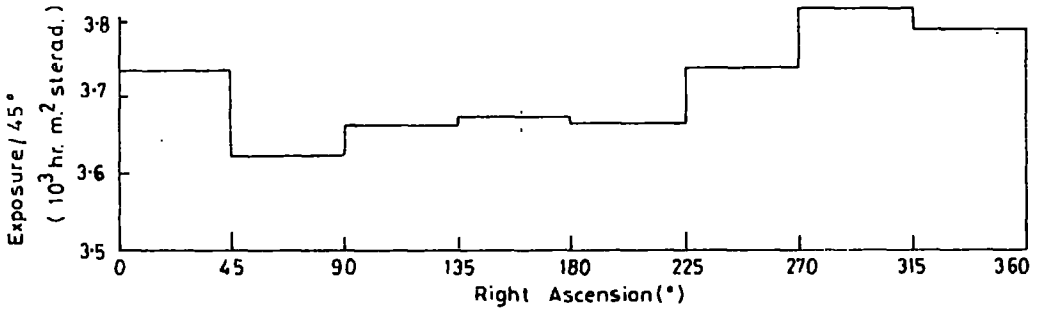

FIG. 8.1c: Distribution of Atmospheric Muon Events in Right Ascension

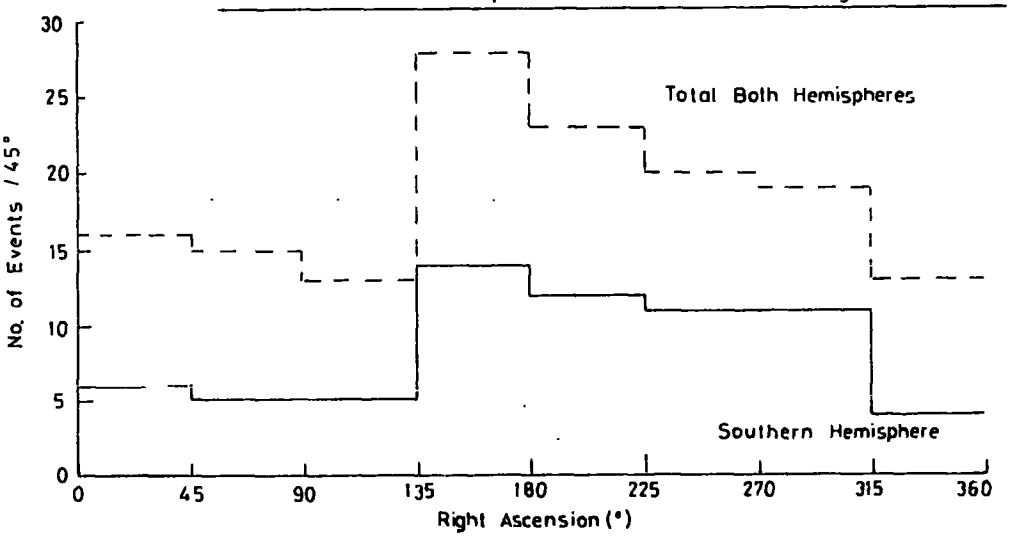

FIG. 8.2: Northern Celestial Hemisphere

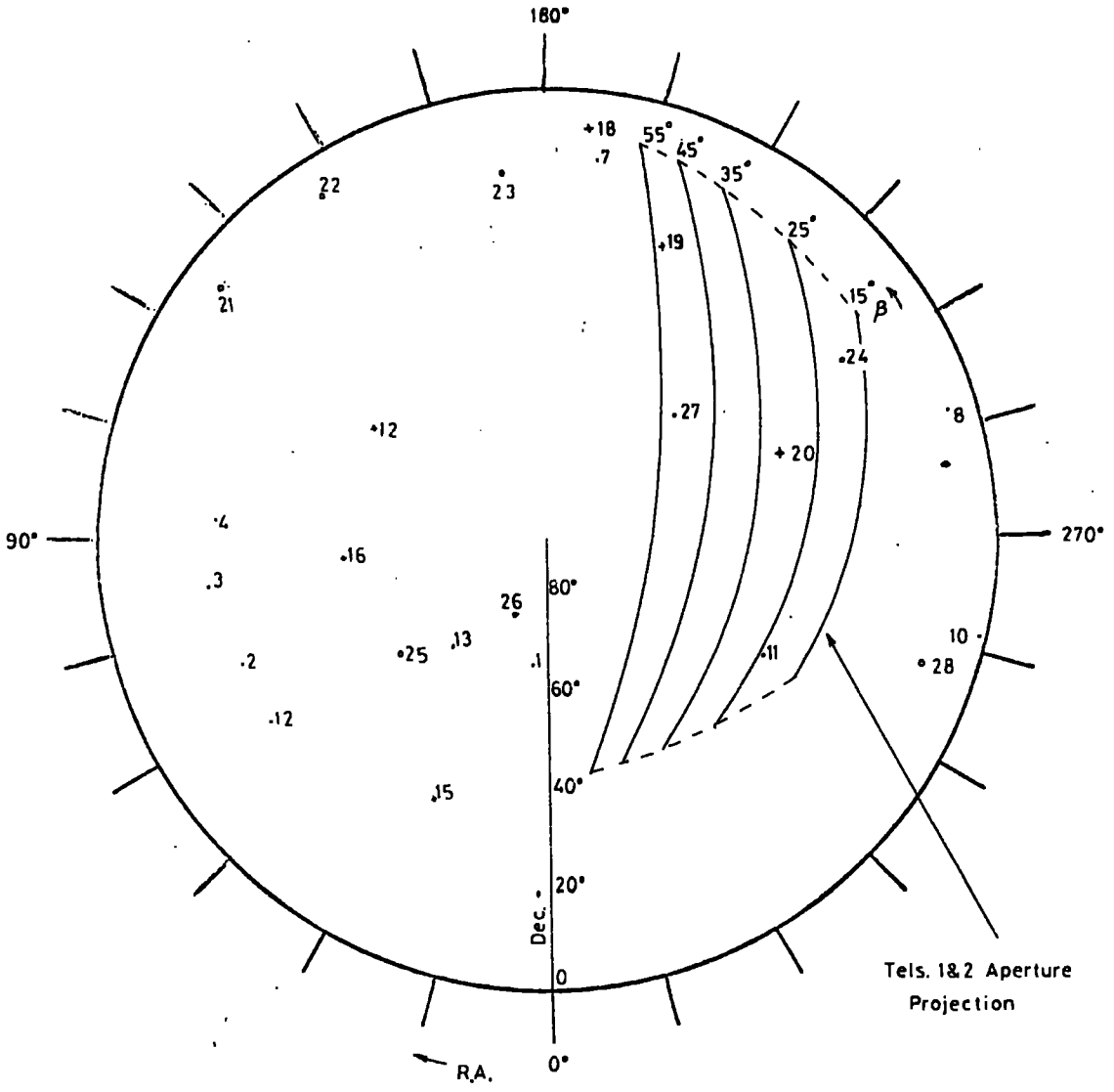

Strong Radio Sources

1. 3C10 (Tycho Brahe's S.N.)
2. 3C123
3. 3C144 (Crab Nebula)
4. 3C147
8. 3C274 (NGC 4486 (M 87))
9. 3C348
10. 3C392
11. 3C405 (Cygnus A)
12. 3C409
13. 3C430
14. 3C461 (Cassiopeia A)

Quasars

15. 3C48
16. 3C147
17. 3C196
18. 3C273
19. 3C286
20. 3C345

Pulsars

21. CP0834
22. CP0950
23. CP1133
24. CP1919
25. CP0328
26. CP0808
27. HP1506
28. PSR 1929+10

FIG. 8.3: Southern Celestial Hemisphere

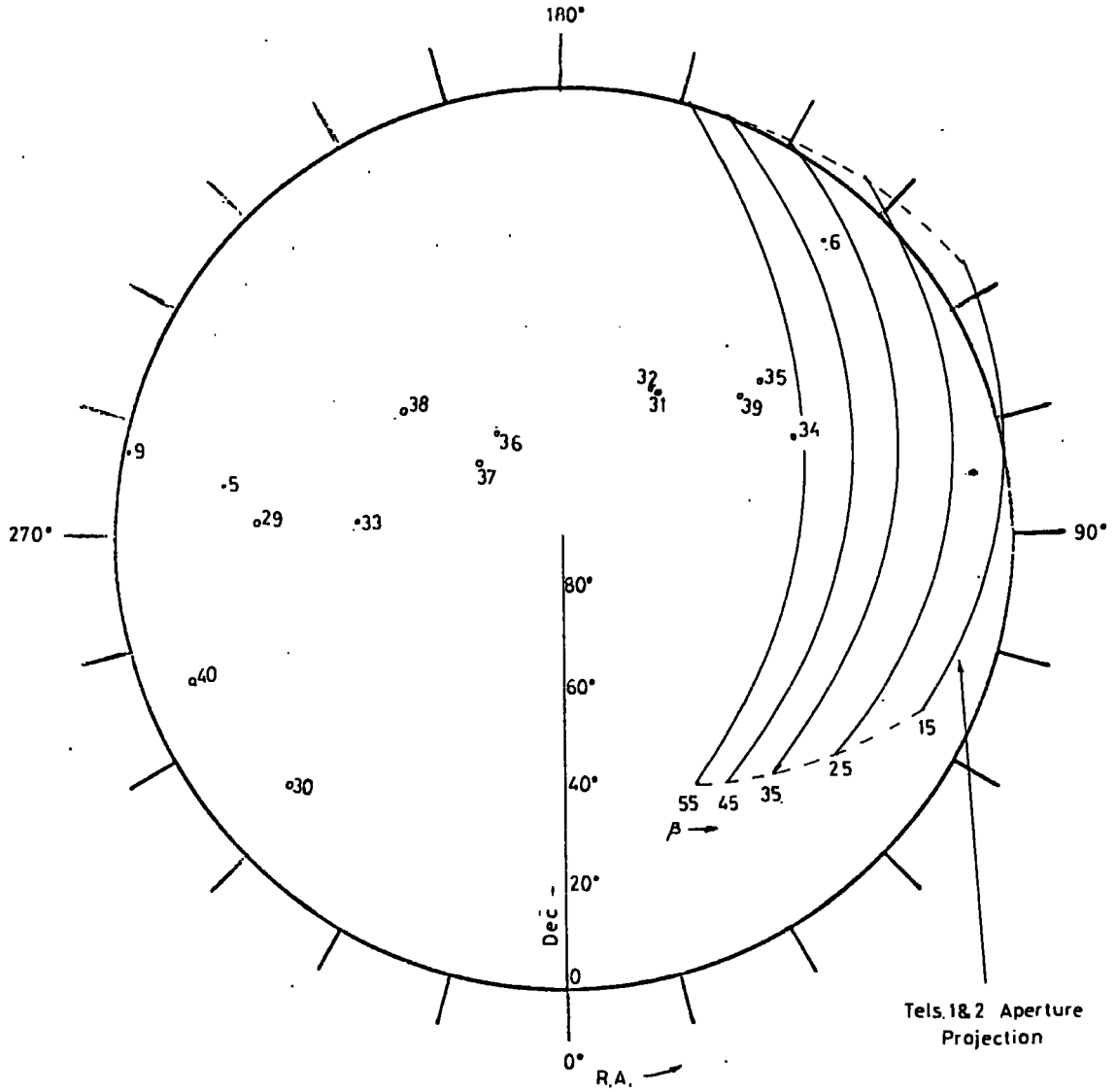

Strong Radio Sources

33. MP 1747		
34. MP 0736	5. 3C 358 (Kepler's SN)	Strong Radio Sources
35. MP 0835	6. 3C 218	
36. MP 1426	7. 3C 353	
37. MP 1451	29. PSR 1749 – 28	Pulsars
38. MP 1727	30. PSR 2045 – 16	
39. PSR 0833-45	31. MP 0940	
40. PSR 1929-10	32. MP 0959	

where the muon direction has been clearly identified and in both hemispheres where there is ambiguity.

As can be seen in figs. 8.2 & 8.3, the poor azimuthal information in Tels. 1 & 2 and Specs. 1 & 2 leads to a large error in the celestial co-ordinates which appears principally in right ascension and to a smaller extent in declination. However, the probability of an atmospheric event being detected at a large zenith angle (i.e. at the extremities of the azimuthal range) is considerably reduced by the rapid fall off of intensity with zenith angle and to a lesser extent by the telescope aperture. The majority of the Tels. 1 & 2 and Specs. 1 & 2 atmospheric events are expected to have traversed the detectors at a small azimuth angle and, to avoid confusion, their celestial co-ordinates have been plotted at the most probable azimuth angle (i.e. zero, in most cases) instead of in the form of arcs as has been done for the neutrino events.

8.1 Atmospheric Muons.

Previous analyses of the early events, made by Menon et al.(1967a), Creed (1967) and Narasimham (1967), revealed anisotropy in both hemispheres for atmospheric muons. The increased numbers recorded since then have removed the anisotropy in the northern hemisphere, but not in the southern hemisphere.

A χ^2 test applied to the two ranges of right ascension, 100° - 280° and 280° - 100° in the southern hemisphere (these being approximately the regions above and below the galactic plane) gives a confidence level of less than 1% that the observed distribution is a statistical fluctuation. This confidence level may be a slight underestimate as the choice of cells,

FIG. 8.4: Celestial Coordinates of Atmospheric Muons

(Northern Hemisphere)

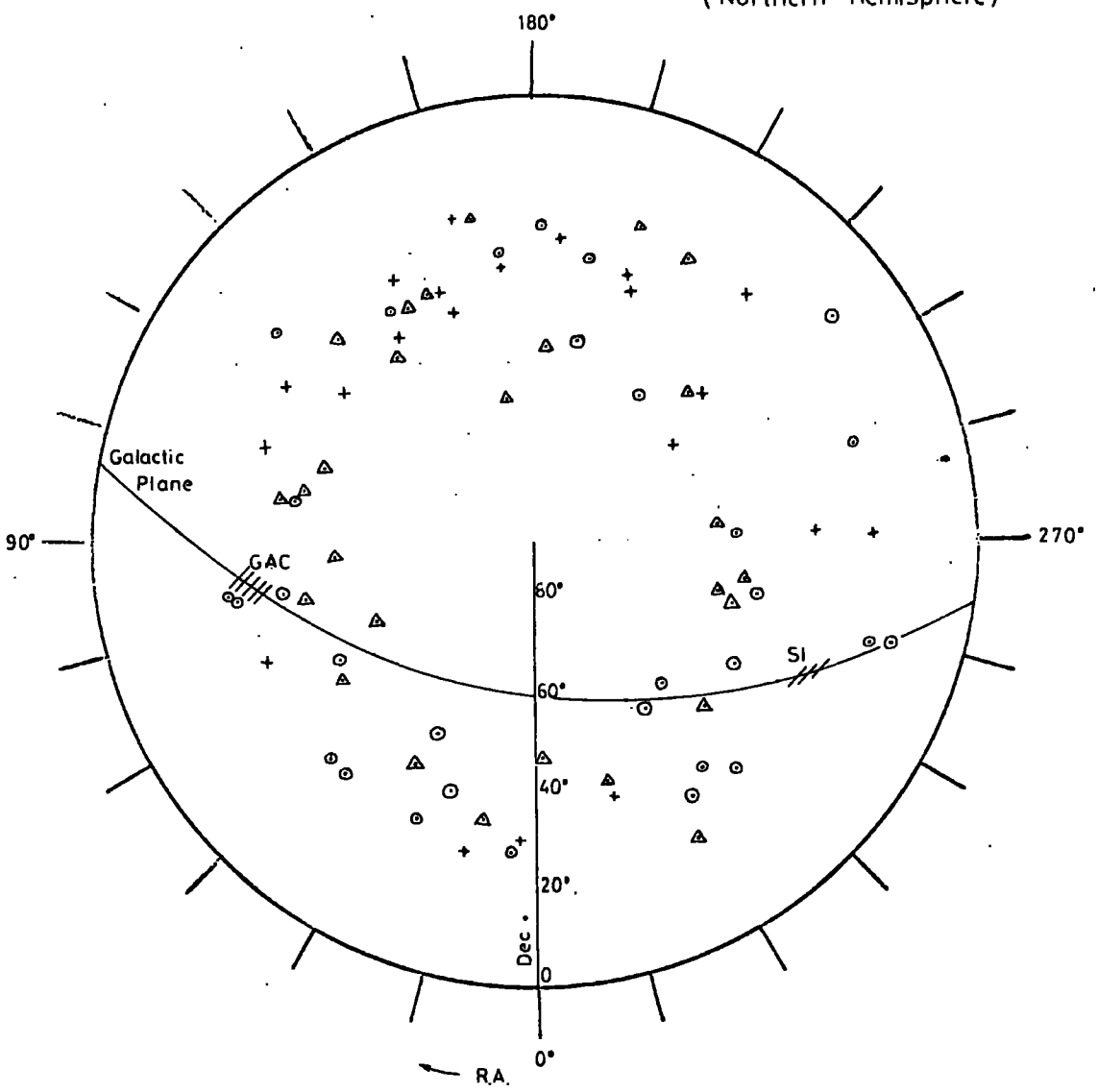

△ Tels 1&2

⊙ Specs 1&2

\+ Tels 3,4&5

GAC Galactic Anticentre : SI — Spiral in (Orion Arm)

FIG. 8.5 : Celestial Coordinates of Atmospheric Muons

(Southern Hemisphere)

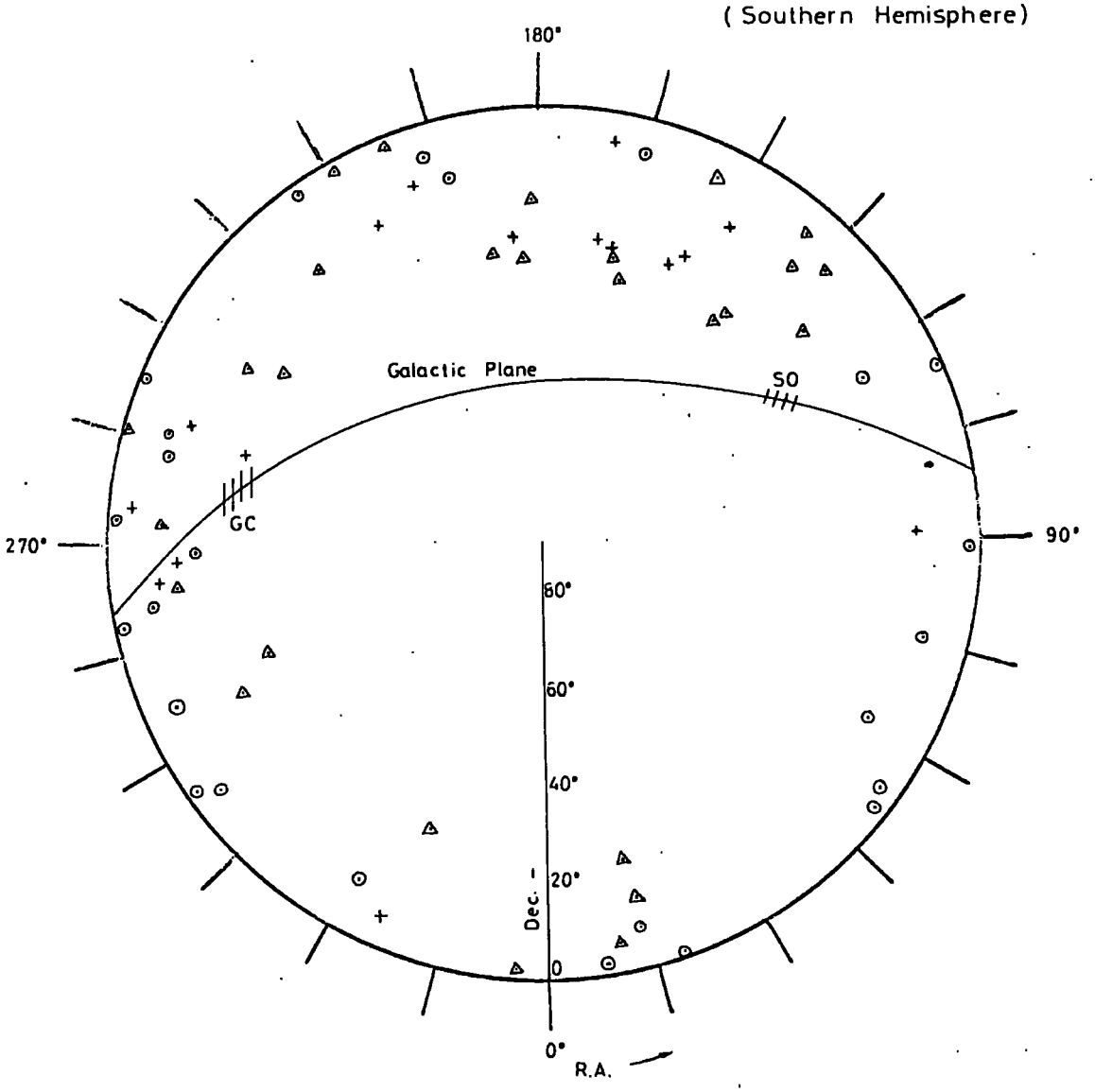

△ Tels 1& 2

⊙ Specs 1& 2

\+ Tels 3,4& 5

GC Galactic Centre : SO'— Spiral Out (Orion Arm)

whilst not made to give a maximum χ^2, was not made entirely at random. A similar test of the northern events shows the difference in intensities in the same two ranges to be within statistical fluctuation with about 90% confidence.

8.1 : 1 Comparison with Previous Investigations

With the few exceptions indicated below, no sidereal variations have been found in extensive air showers from primaries $\lesssim 10^{17}$ eV and possibly higher, the majority of experiments having been carried out in the northern hemisphere. The observed lack of anisotropy in the northern hemisphere in the present experiment is, thus, in accordance with the majority view.

Reports have been given of two experiments carried out near the equator which covered the southern hemisphere to some extent. Chatterjee et al. (1967) at Ootacamund (11° N) have reported a decrease in the intensity of muon rich showers of $\sim 10^{15} - 10^{16}$ eV in the region of $225^\circ - 315^\circ$ right ascension for the declination range -20° to $+40^\circ$ (a result which is in agreement with the observations of Matano et al. (1966) for the declination range $+6^\circ$ to $+66^\circ$). However, the M.I.T. air shower group's experiment at Kodaikanal (10° N), which covered the southern celestial hemisphere to a declination of -40° and responded to primaries of $\sim 10^{15}$ eV, showed isotropy with no deviation from the statistical error of $\sim 1\%$ (Rossi, 1960).

The present results are not necessarily inconsistent with these results for the following reasons,

(i) Chatterjee et al.: As the region of reduced intensity reported by these authors agrees with that of Matano et al., it seems most likely that it is principally, if not all, in the northern celestial hemisphere.

Only 12 events are plotted in the southern hemisphere and it is not possible to attach any significance to their distribution in right ascension.

(ii) M.I.T. group: The χ^2 tests were applied to declination bands and "suspected" areas such as a belt around the galactic plane and a belt around the plane perpendicular to the spiral axis. The group have not reported applying a χ^2 test to regions of right ascension and, from their plot, it cannot be said that isotropy would necessarily have been found had they done so.

A report has also been given of an experiment carried out in the southern hemisphere. Kamata et al. (1967) at Chacaltaya (16° S) have observed, for some time, an excess of muon-poor showers in the range 10^{14} - 10^{16} eV in the right ascension cell 200 - 220° over a declination range from - 60° to + 40°. This right ascension cell falls in the region of excess in the present experiment. (Although at first sight it may seem unlikely, it is possible that there may be a connection between muon-poor showers and high energy muons, particularly if the recently discussed direct production of muons occurs.)

8.1 : 2 The Observed Anisotropy

If genuine, the effect in the present experiment may have some connection with the galactic plane, in view of its large scale nature, and deflection in magnetic fields must be considered, particularly as recent studies indicate that the high altitude field is in opposite sense to the disc field above the galactic plane and in the same sense below (Davis, 1966). However, the dimensions of these fields are thought to be such

that primary cosmic rays, of energies 10^{14} - 10^{15} eV (the energy range thought to give rise to the majority of muons detected in the present experiment), originating from outside the local spiral arm, could only reach the Earth by spiralling along the fields. Also the irregularities of interstellar magnetic clouds might be expected to produce isotropy at these energies. If, however, the sources of a sizeable proportion of the observed events are relatively close within the local spiral arm, the muons could arrive anisotropically.

It seems, then, that the observed anisotropy, which does not seem to be in direct conflict with the observations of other workers, has a possible interpretation in terms of primaries, from nearby sources, deflected in the local magnetic fields.

8.1 : 3 30° - 50° Atmospheric Muons

The arrival directions of atmospheric muons in the 30° - 50° p.z.a. range of Tels. 1 & 2 have been studied seperately for the possibility of their throwing light on the cause of the excess. 18 of the events lie in the northern hemisphere and the other 10 lie in the southern hemisphere. Neither hemisphere shows any inconsistency with an isotropic distribution.

8.2 Neutrino-induced Muons.

In table 8.1, the arrival directions of the neutrino events plotted in figs. 8.6 & 8.7 are compared with the celestial co-ordinates of some important stellar objects (also shown in figs 8.2 & 8.3). Most of the events have an error of $\pm$ 1° p.z.a. which permits their covering the co-ordinates of the events listed.

The most interesting feature of the plot is the linking of events 3,

Table 8.1: Comparison of Celestial Co-ordinates with Stellar Objects

Northern Celestial Hemisphere			Southern Celestial Hemisphere.		
Event No.	Direction	Object	Event No.	Direction	Object
3 +	Up	3C10,3C430,3C461 CP0328, CP0808.	3 +	Down	MP1426,MP1451, MP1727
11	Down	3C10, 3C430	4	Up	-
43	Down	3C10	11	Up	MP0835, PSR0833-45, MP0959,MP0940
48	Down	-			
54	Up	CP1133	29	Up	-
30*	Up	CP0950	43	Up	-
36	Up	3C345	30*	Down	PSR2045-16
S23	Down	3C345	36	Down	-
S40	Down	3C409	S40	Up	-
S71	Down	-	061	Up	-
016	Up	-	073	Down	-
070 +	Up	3C147			

\+ There is a large error in the projected zenith angles of these events

* Correspondence with the object is possible as a result of azimuthal error.

FIG. 8.6: Celestial Coordinates of Neutrino-induced Muons
(Northern Hemisphere)

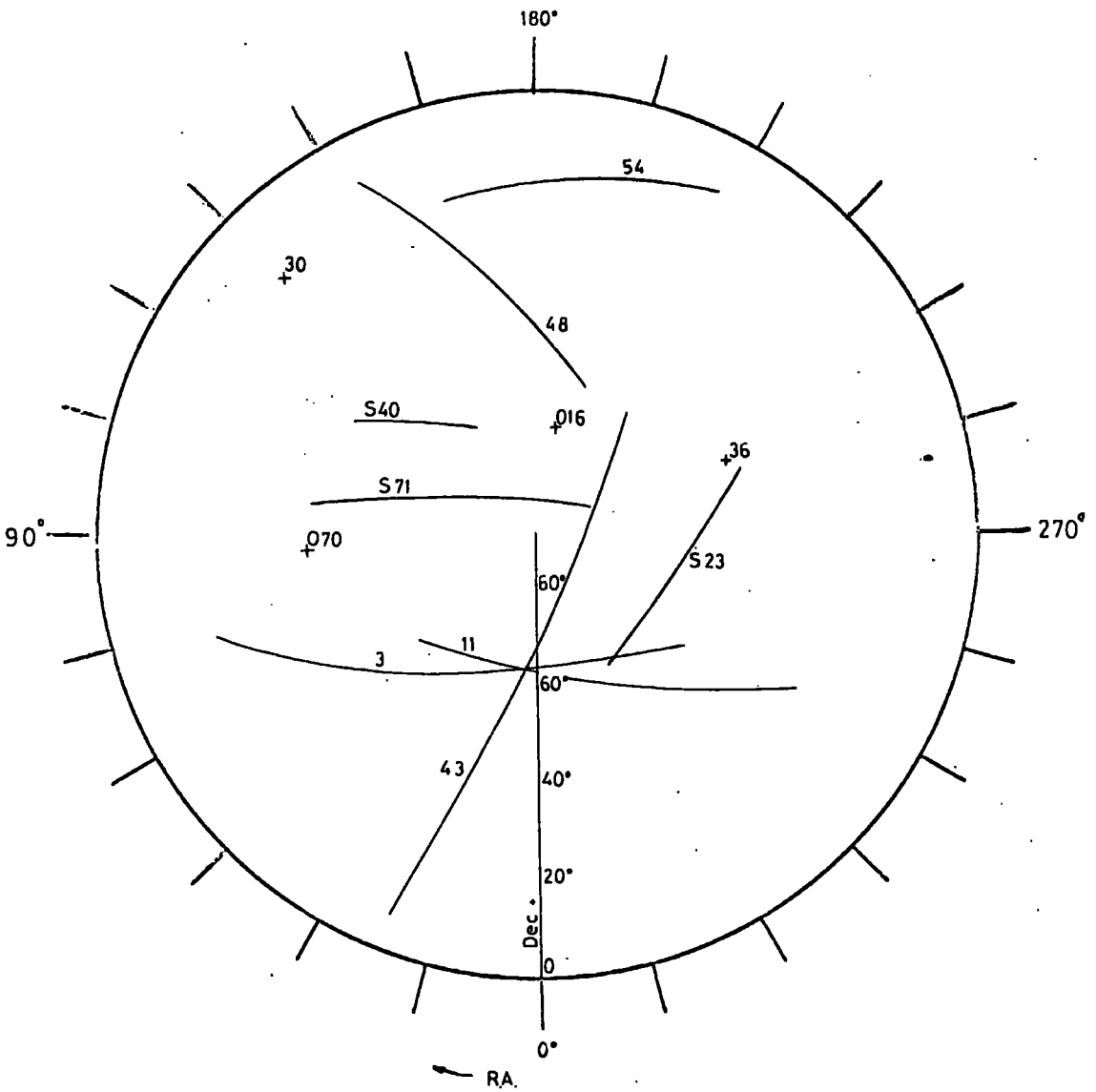

FIG. 8.7: Celestial Coordinates of Neutrino-induced Muons
(Southern Hemisphere)

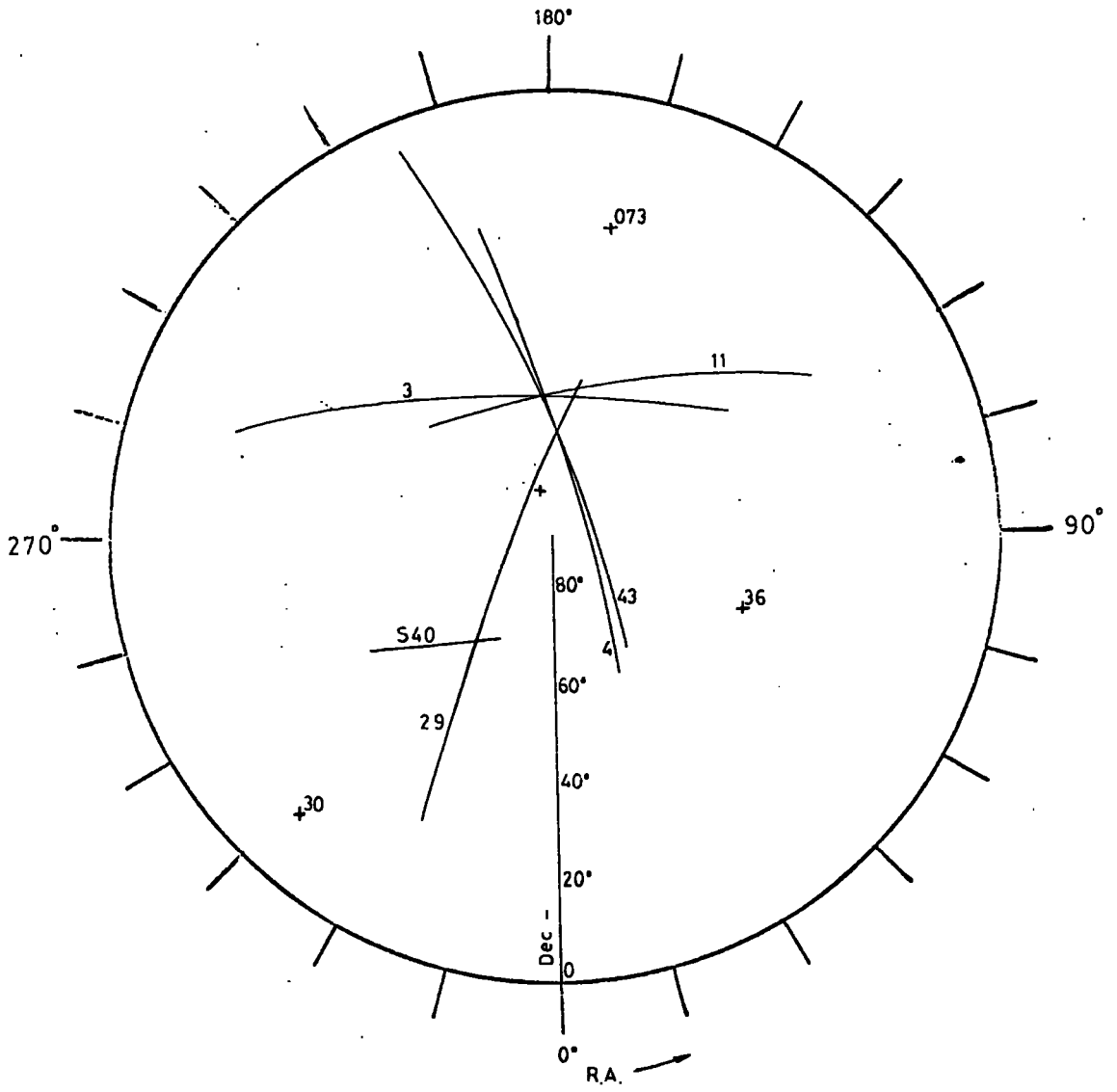

11 & 43 in the northern hemisphere and the same three, together with events 4 & 29, in the southern hemisphere. Event 43 is more likely to be from the northern hemisphere and events 3 & 11 are equally probable from either direction. The vicinity of the southern intersection does not contain any interesting visual or radio sources but the northern intersection, at $\sim 5^{\circ}$ R.A. and 63° Dec., is very close to Tycho Brahe's supernova (3C10) at 5.7° R.A. and 64° Dec. Taking into account the error in the projected zenith angle of event 3, the probability of three of the events in the northern hemisphere intersecting within an area of $(1^{\circ})^2$ is estimated to be not much less than 0.1. However, that the point of intersection should lie in the same cell of $(2^{\circ})^2$ as one of the 4 brightest radio sources in the 3C catalogue covered by the exposure in the northern hemisphere (i.e. those of flux density $\geqslant 10^{-24}$ w.m.$^{-2}$ ($^{c}/_{s}$)$^{-1}$), reduces the probability of chance coincidence to $\sim 10^{-4}$. (Of the three other sources covered, Cygnus A (3C405) is thought to be an exploding galaxy and Cassiopeia A (3C461) the remains of a supernova).

As supernovae are considered to be one of the main sources of cosmic rays, this result is of considerable interest. Muon neutrinos can be produced in the decay of pions which in turn were produced in the interactions of high energy nuclei with the nuclei of local gas atoms. Burbridge (1967) has said that for most radio galaxies with steep spectra, the majority of neutrinos would have fairly low energies (i.e. $\sim$ 100 MeV). However, sources with flat radio spectra, such as the Crab Nebula, would emit predominantly higher energy neutrinos of $\sim$ 100 GeV. However, the high proton fluxes required are not thought to be present during steady state conditions and only violent outbursts could give rise to them.

In the present experiment, the Crab Nebula, which is the most thoroughly studied supernova, receives very poor coverage as it lies in the northern hemisphere at a declination of $\sim 22^{\circ}$. Even if it is a source of detectable neutrinos, their identification would only be possible if the flux was large enough to be seen over the atmospheric muon background. 3C10 (Tycho Brahe's star) receives a much better coverage by the K.G.F. detectors, both in aperture and at large zenith angles, and it is relevant to note that, although not the biggest supernova remains in our galaxy, it is one of the most recent, having been first observed in 1572. It could be that this supernova is still in a position to emit a large enough flux of muon neutrinos with sufficient energy to be detected in the present experiment.

CHAPTER 9

Other Cosmic Ray Neutrino Experiments.

Apart from the K.G.F. Experiment, two other experiments are currently in operation for the detection of neutrino-induced muons. Their experimental details and the results obtained are now described.

9.1 The Case - Wits - Irvine Experiment

9.1 : 1 The Detection System

The original arrangement, built in 1964, for the collaboration experiment between the Case Institute, Ohio and the University of Witwatersrand, now also including the University of California (Irvine), has been mentioned in Chapter 1. Fig. 9.1 is a schematic diagram of the array. Situated at 8800 m.w.e. local rock at 76th level in the East Rand Proprietry Mines, near Johannesburg, the detector array consisted of two parallel walls of Lucite and Plexiglass tanks, each tank being of dimensions 5.5 m. long, .58 m. high and .125 m. thick, containing liquid scintillator and viewed by four 5" photomultipliers, two at each end. Mounted three high, the total of 36 tanks stretched for 37 m. along opposite walls of the tunnel. The length was extended, in 1966, to 67 m., giving a total detecting area of 165 mt^2, and two additional 'bays' including Cerenkov detectors were added.

The system was triggered by a 4-fold coincidence, from any four photomultipliers in one wall, and the event was located along the detector axis from the ratio of the photomultiplier pulses at each end.

9.1 : 2 The Events.

The events are most simply divided into categories according to their

coincidences. These are,

(a) Single tank events - events triggered by four photomultipliers only, all four viewing the same scintillator.

(b) More than one tank vertical events - in which pulses were recorded in tanks mounted above each other in the same bay.

(c) Two tank cross-tunnel events - 8-fold pulses were recorded from two tanks, one on each side of the tunnel.

(d) Three tank cross-tunnel events - two tanks on one side and one on the other, all in the same bay, provided the coincidence.

(e) Multitank events - in which pulses were recorded in a total of more than three tanks from both sides of the tunnel or more than one bay.

Types (a) and (b) could have been caused by both neutrino-induced and atmospheric muons or their secondaries. Type (c) events were mainly caused by single penetrating particles passing through both walls, with a projected zenith angle of $> 43^{\circ}$, and are interpreted as neutrino-induced muons. The type (d) events may have been due to complex neutrino interactions, pairs of near-vertical atmospheric muons and/or their accompaniment.

The results obtained in the experiment from 27/10/64 to 23/8/67 are given in table 9.1

Table 9.1 Case - Wits - Irvine - 76th level Results
(Reines, 1968)

Type of Event	Total No.	Running Time
(a) Single tank events	264	31863 tank days
(b) Two tank vertical events	58	5327 bay days
Three tank vertical events	32	5327 bay days
(c) Two tank cross-tunnel events	34	5417 bay days
(d) Three tank cross-tunnel events	6	4980 bay days
(e) Multiple events	13	4980 bay days

For each event, the pulses from each photomultiplier were displayed on oscilloscopes and measured. A minimum ionising particle traversing a scintillator normal to the detecting plane loses, on average, 20 MeV. Thus, in cases of two tank cross-tunnel events, an energy deposition of this order per detector is confirmation of a neutrino-induced muon. The energy deposited may, sometimes, help to clarify the nature of ambiguous events, however, the method is of very limited use when more than one particle passes through a tank. Also, of the 34 cross tunnel events, type (c), about one third deposited a small energy (i.e. $\sim$ 5 - 10 MeV) in, at least, one of the tanks. This might be an indication of low energy knock-on electrons associated with muons.

It is clear, then, that the analysis of the results of this experiment is not as straightforward as in the K.G.F. Experiment.

9.1 : 3 Intensity of Neutrino-induced Muons

The events listed in categories (c), (d) and (e) may be considered in estimating the total rate of neutrino-induced muons passing through both walls of scintillator. Reines (1969) has taken the total number of these to be 34, presumably on the assumption that the number of type (c) events which were not neutrino-induced equals the number of types (d) and (e) events which were. Consequently, the quoted intensity, assuming an isotropic flux, is $(3.5 \pm 0.6) \times 10^{-13}$ cm.$^{-2}$ sec.$^{-1}$ sterad.$^{-1}$. If allowance is made for the expected angular distribution and effective aperture of the detectors, as has been done in the last chapter for the K.G.F. Experiment, the intensity of horizontal neutrino-induced muons may be derived and is calculated, by the present author, to be, $(4.5 \pm 0.8) \times 10^{-13}$ cm.$^{-2}$ sec.$^{-1}$ sterad.$^{-1}$

9.1 : 4 Intensity of Atmospheric Muons.

The Case - Wits - Irvine group do not appear to have published the atmospheric muon intensity derived from their results. Creed (1967) has made an estimate of the intensity using the data available to 14/10/66 and this estimate can now be revised using the complete data obtained at 76th level.

The effective differential aperture has been calculated assuming a $\cos^{9}\theta$ angular distribution of atmospheric muons in spatial zenith angle and an error of ± 1.5 on the index. Taking the events in categories (a) and (b), the total number of tanks traversed by muons is 476 and the aperture presented to neutrino-induced muons in these categories is 907 m.^{2} sterad. Assuming the isotropic neutrino-induced muon intensity to be $(3.5 \pm 0.6) \times 10^{-13}$ cm.$^{-2}$ sec.$^{-1}$ sterad^{-1}, 97 ± 17 of the 476 tank traversals are estimated

FIG. 9.1: The 76th Level Array.

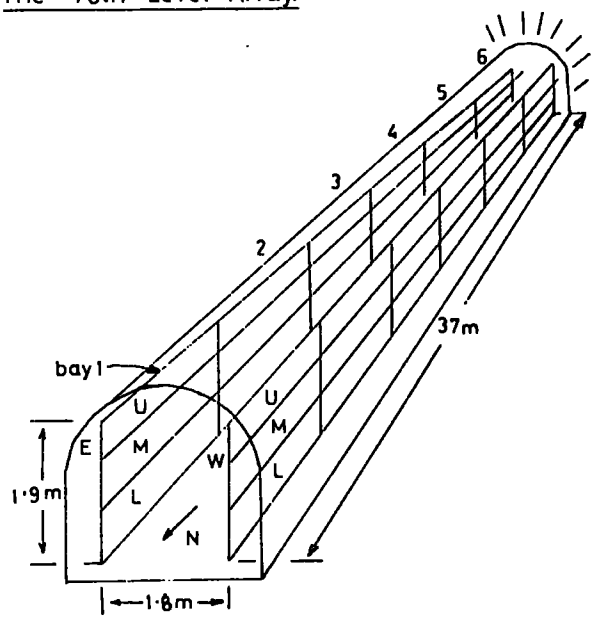

FIG. 9.2: The 77th Level Array.

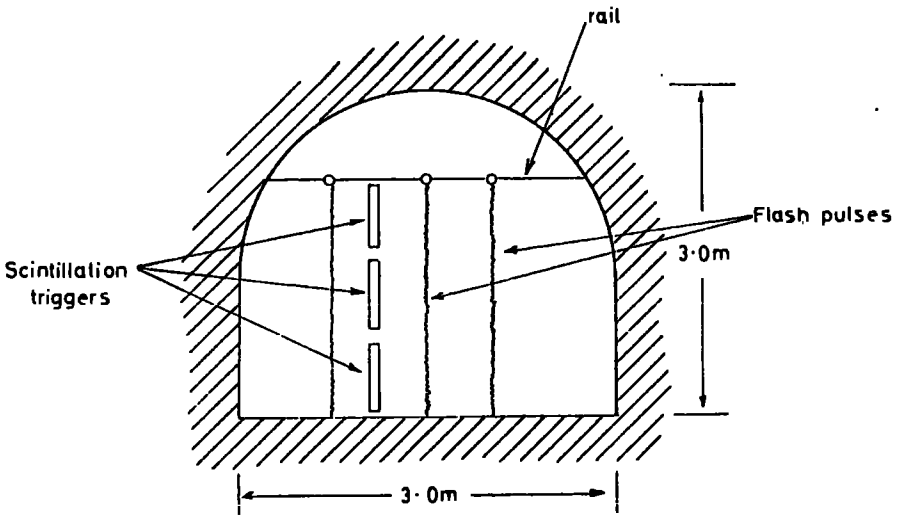

to have been made by neutrino-induced muons and, consequently, 379 $\pm$ 17 were by atmospheric muons. This number may be increased to 392 $\pm$ 17 if half of the multitank events are assumed to have been caused by atmospheric muons involving $\sim$ 2 tank traversals. Applying the differential aperture and a total array running time of 592 days, the vertical intensity of atmospheric muons is found to be $(2.0 \pm 0.4) \times 10^{-11}$ cm.$^{-2}$ sec.$^{-1}$ sterad.$^{-1}$ (including the error in the angular distribution index). This figure is dependent upon the assumptions made in estimating the neutrino-induced muon rate and also on the assumption that no 'out of geometry' events have been recorded.

9.1 : 5 The 77th Level Array

Within the last year, a further development has been undertaken by the Case - Wits - Irvine group. The 76th level apparatus has been dismantled and at least half of a new array at 77th level has been brought into service. The detecting area has been increased to 190 m.^{2} and the geometry altered to give a neutrino-induced muon rate of $\sim$ 75 per year, three times greater than before.

When complete, the new apparatus will incorporate 50,000 flash tubes suspended on rails as shown in fig. 9.2. The variable seperation between the detector layers is to permit the insertion of absorber or magnets. Another feature is the use of light sensors attached to the flash tube viewing windows to obviate the use of many cameras. A display board is arranged as a mimic diagram of the flash tubes and each event is simulated by panel lights, to be recorded on video tape for immediate play back and photographed by a 3.5 m m . camera as a permanent record. This system has the advantage that the apparatus can be operational whilst the laboratory is

illuminated, thus reducing the running time lost during the performance of many routine checks.

No results are available yet from this system.

9.2 The Utah Experiment

A detector designed primarily for the purpose of detecting upward moving muons from neutrino interactions has been constructed, by the University of Utah group, beneath the Wasatch mountains at a vertical depth of 1850 ft. The detector is also useful for studying downward moving muons and, indeed, it is the results obtained in this direction which have aroused the greatest interest in the experiment.

9.2 : 1 The Detector

The detector is shown in fig. 9.3. The coincidence system is composed of four directional Cerenkov tanks made of concrete and filled with water. Two 16 kG solid iron magnets are positioned between the Cerenkov tanks and 15 columns of cylindrical spark counters are incorporated throughout the detector to give a fine angular resolution.

The cylindrical spark counters are geiger-counter like detectors each being constructed of a steel pipe, 37' long and 6" in diameter, filled with 1/3 argon and 2/3 ethylene, at atmospheric pressure, with a central wire, along the pipe axis, which is maintained at 6 kV during operation. The discharge, resulting from the traversal of a charged particle, which is encouraged by an incremental bias pulse triggered by the coincidence system, is a sharply localised corona which is detected sonically, to a precision of a few m.m., by a microphone situated at the front end of the detector.

FIG. 9.3: The Utah Detector.

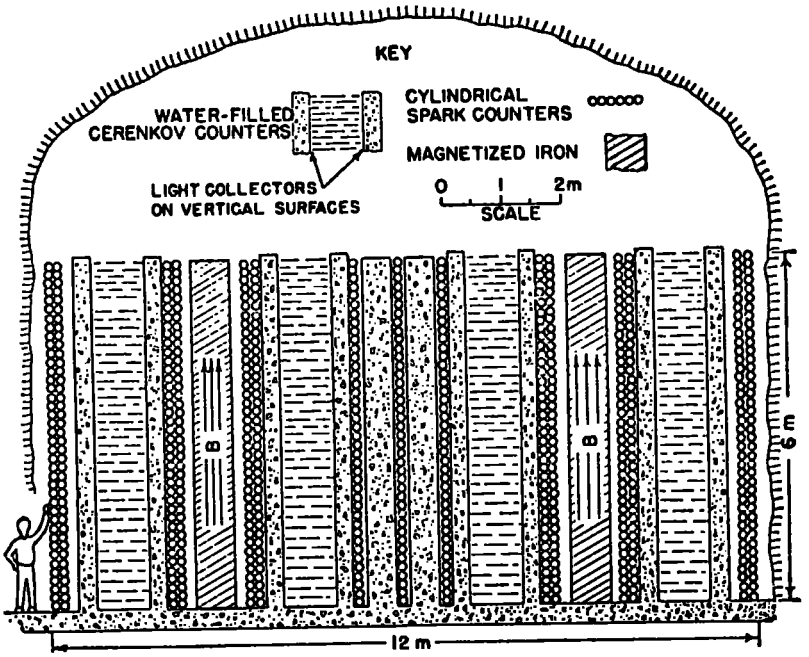

Depth in Line of Sight, 10 m.

Both the acoustical spark counter pulses and the Cerenkov pulses are recorded on magnetic tape. The directional information provided by the Cerenkov counters is vital for the identification of upward moving neutrino induced muons and the whole system should be capable of a maximum detectable momentum of up to 100 GeV/c.

9.2 : 2 The Atmospheric Muon Results

The results of a preliminary study of muon backgrounds, using the detector, were reported by Bergeson et al. (1967). These were obtained using about half of the detector shown in fig. 9.3 for about three weeks and are for 14,500 muons of energy greater than $\sim$ 2 GeV.

The situation beneath a mountainous terrain enabled the compilation of data for a series of depth intensity curves for different zenith angles, as shown in fig. 9.4 (after Keuffel, 1968). The continuous lines are from a world survey of vertical depth intensity measurements and the broken lines are those from the same survey with a zenith angular enhancement of $\sec\theta$. At a given zenith angle, the variation of intensity with depth is of the form expected. However, at a given depth there appears to be no variation in intensity with zenith angle in contradiction to the expected $\sec\theta$ enhancement. (Although in previous chapters the conventional angular variation of intensity of muons from π-μ decay has been referred to as the '$\sec\theta$ enhancement', the actual variation is slightly less than $\sec\theta$).

9.2 : 3 Discussion of the Results

Possible 'trivial' explanations of the effect considered by the authors are topography, rock composition, aperture, triggering efficiency, scanning efficiency and spark counter efficiency. To date, the publications of

FIG. 9.4: The Underground Intensity Results of Bergeson et al. (1967)

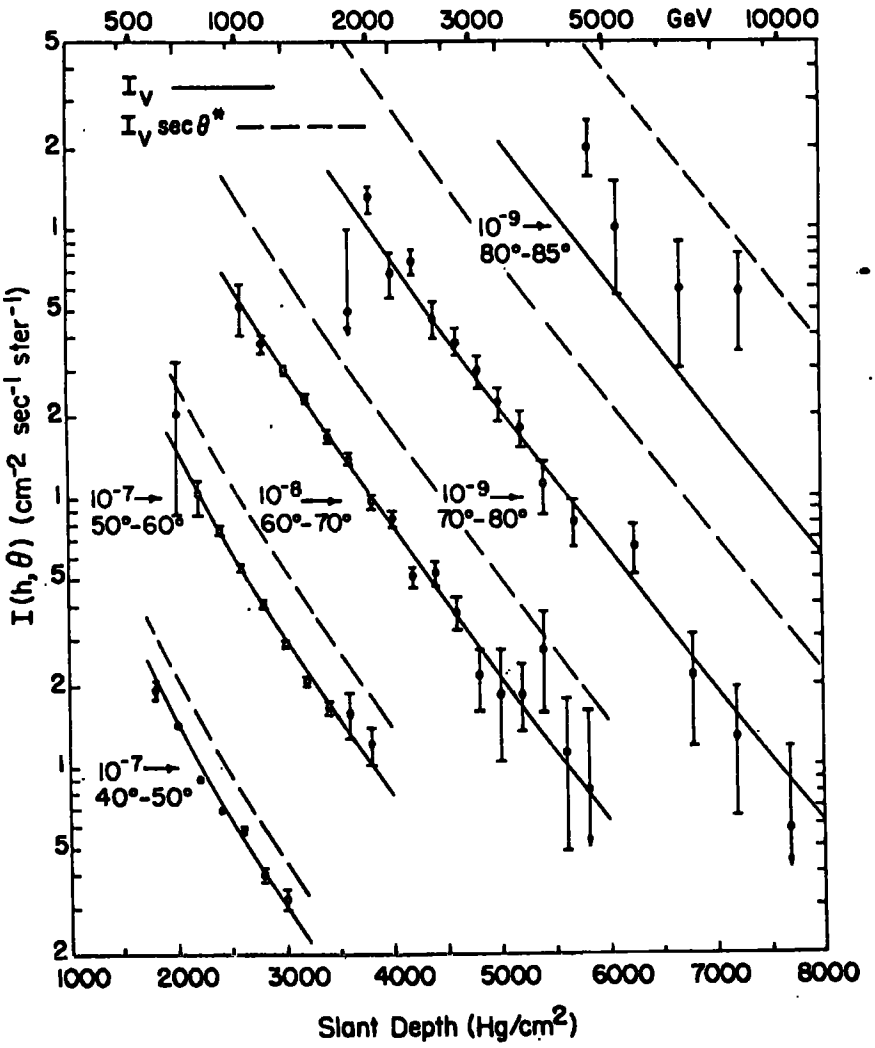

the group show that of these, the only one subsequently found to be in error was the rock composition which has a mean density 5% greater than originally quoted such that the measured intensities are moved closer to the values expected, assuming the sec θ enhancement, than was originally thought (Keuffel, 1968).

In view of the importance of the results, Nash and Wolfendale (1968) have examined the spectrograph measurements of near-vertical and inclined muon spectra at sea level. They have plotted the ratio of observed intensity at 87° to that expected from pions alone as parents and have concluded that the measurements are not in support of the original suggestion that an appreciable fraction of muons with energy below 1000 GeV are produced directly. However, with the new density determination, Bergeson et al. (1968) say that the results appear to indicate that the anomaly does not commence until above 1000 GeV and they have described the effects of the 'X - process' which would produce muons with a suitable intensity independent of zenith angle. A proportion of the pion production intensity, R = 0.01 to 0.04, is suggested as the proportion of secondaries which are X particles. However, the fraction of muons detected from this source is greater than R as not all pions decay to muons and those which do are at a higher energy than the product muons and from a lower intensity part of the spectrum. For the increased rock density data, Bergeson et al. (1968) have established a best fit value of R = 0.02 and they claim that this gives excellent agreement with the three highest energy points given by Nash and Wolfendale. Keuffel (1968) has substantiated this in saying that if there is a threshold energy for the proposed process, then the latter would predict only a slightly different intensity than does the conventional model near the

threshold.

However, several criticisms may be raised about the interpretation of the basic Utah results. Returning to fig. 9.4, if the 5% density increase is applied, the experimental points will be moved to greater depths than plotted. Although the fractional shift is the same for all depths, the absolute shift (in m.w.e.) is greater for greater depths, in a given angular range, so that the best fit curve through the points, which was previously virtually the same as the world survey depth intensity curve, is now less steep and no longer parallel to the latter. Consequently, this suggests that at greater depths, and greater sea level muon energies, the observed angular intensity approaches the secθ enhanced curve. This observed situation is exactly opposite to what would be expected from the proposed X - process which should make a greater contribution to the total muon flux at high energies such that the predicted intensity would approach the non-enhanced curve.

Another difficulty arises when the angular intensity variation is considered at a fixed slant depth (after the approach of Sheldon et al., 1969).

If $I(\theta, h)$ is the intensity at a vertical depth h and zenith angle θ, then $I(o, h \sec\theta)$ is the intensity at a vertical depth h sec θ (i.e. which is the same as $I(\theta, h)$ if there is no angular enhancement). The revised density shifts all observed points at different zenith angles, at that slant depth, to a depth 5% greater and the observed intensity, which could previously be written $I_{obs} = I(0, h \sec\theta)$, can now be written as,

$$I_{obs} = I(o, h' \sec\theta) + \frac{dI}{dH}(h' - h) \qquad 9.1$$

where h' is the revised depth (i.e. $h' = 1.05\ h$) and dI/dH is the slope of the vertical depth intensity curve at the fixed slant depth $h \sec\theta$. As $h' \sec\theta$ is the same for all zenith angles, equation 9.1 is independent of zenith angle and consequently the observations still show no evidence for an angular - dependent enhancement. Furthermore, if equation 9.1 is used to predict the vertical intensity for the slant depth in question, the vertical intensity is found to be,

$$I_{Vert} = I(o,h) + \frac{dI}{dH}\left(h' - h\right) \qquad 9.2$$

which is higher than given by the world survey by an amount $\frac{dI}{dH}\ (h' - h)$.

Clearly, rather than helping to resolve the problem, the increased density has added further complications to the results. The originally published results could perhaps have been explained by a single effect such as, for instance, an angular variation of detection efficiency, if such could exist, whereas now, both the anomalous vertical intensity and the tendency to a $\sec\theta$ enhancement at high energies must be explained.

Finally, the preliminary results of the experiment of Krishnaswamy et al. (1968) performed under a flat earth at K.G.F. do not show the same effect but do suggest, if anything, a greater than $\sec\theta$ enhancement. A direct comparison between the two experiments is possible for the slant depth and zenith angle combinations of the Krishnaswamy et al. experiment, these corresponding to single points on the curves in the Utah plot. The result is that the two experiments are in clear disagreement. Although the threshold muon energy for detection in the two experiments may be different such that the experiment of Krishmaswamy et al. may be recording an increased number of low energy muons which would not be detected in the Utah detector, it seems unlikely that the intensity required of such particles could be present.

With so many problems, the results of the Utah experiment are very much in doubt and are, perhaps, best taken as an investigation into the properties of the system with regard to its future use in the detection of neutrino-induced muons. Assuming these difficulties can be successfully overcome, the detector promises to provide a useful contribution to the study of neutrino interactions.

CHAPTER 10

Conclusions.

The K.G.F. Neutrino Experiment has produced interesting results concerning both atmospheric muons and neutrino-induced muons and the conclusions drawn from these results are as follows.

10.1 Atmospheric Muons

The vertical intensity of atmospheric muons has been established at the 7500 m.w.e. site as $(1.0 \pm 0.2) \times 10^{-13}$ cm.$^{-2}$ sec.$^{-1}$ sterad.$^{-1}$ and the observed angular distribution suggests that the depth intensity relation continues to greater depths somewhat less steeply than predicted by the exponential form of Menon et al. (1967c), i.e. $I(o,h) = 9.8 \times 10^{-7} \exp(-\frac{h}{\lambda})$ cm.$^{-2}$ sec.$^{-1}$ sterad.$^{-1}$ where h is the depth in m.w.e. and $\lambda = 810 \pm 50$ m.w.e. This is supported by the estimates of mean energy made from the electromagnetic accompaniment, which suggests its increase with zenith angle and equivalent vertical depth in contrast to the constant value predicted by the pure exponential form. (The estimates made from the angular distribution are $\sim$ 270 GeV at 8200 m.w.e. increasing to $\sim$ 400 GeV. at 9500 m.w.e.)

The observed angular distribution seems best described by the exponential form modified to include the effects of fluctuations, i.e. $I(\theta, 7500) = 5 \times 10^{-11} \frac{\sec\theta}{R_{h\ eff}} \cdot \exp\left[-9.6(\sec\theta - 1)\right]$ cm.$^{-2}$ sec.$^{-1}$ sterad.$^{-1}$. The increasing effect of fluctuations at greater depths leads to a broader angular distribution which covers most of the observed excess at intermediate zenith angles. There is, however, some slight evidence for a flux of particles of energy $\lesssim$ 1 GeV. and it cannot yet be definitely established

that the observed excess is entirely due to the effects of atmospheric muons range fluctuations and not partly due to charged particles from another source.

10.2 Neutrino-induced Muons.

The intensity of horizontal neutrino-induced muons is estimated to be $(3.2 \pm 0.9) \times 10^{-13}$ cm.$^{-2}$ sec.$^{-1}$ sterad.$^{-1}$ which is in quite good agreement with the 'isotropic' intensity of the Case - Wits - Irvine group of $(3.5 \pm 0.6) \times 10^{-13}$ cm.$^{-2}$ sec.$^{-1}$ sterad.$^{-1}$ (estimated to be equivalent to a horizontal intensity of $(4.5 \pm 0.7) \times 10^{-13}$ cm.$^{-2}$ sec.$^{-1}$ sterad.$^{-1}$). The rate observed is slightly less than predicted by the constant elastic cross section and an inelastic cross section saturating at 10 GeV. for the assumption of $\bar{E}_\mu / E_\nu = 0.67$. It is not possible to establish the upper limit of the energy proportional rise of the inelastic cross section but the detection of several non-elastic interactions near the detectors is a sure indication of its rising beyond the 10 GeV. limit of the accelerators. A limit in the region of 20 - 30 GeV. would seem a reasonable estimate from the present experiment and would be in keeping with the Case - Wits - Irvine results. However, $\bar{E}_\mu / E_\nu$ must begin to fall at energies not much greater than 10 GeV.

The mean energy of neutrino-induced muons is estimated to be no more than a few tens of GeV. The poor statistics lead to a large error on the very approximate estimate of 7 GeV. from the electromagnetic accompaniment. The two spectrograph events in which the energy could be measured were both produced by low energy muons of about 1 - 2 GeV.

No unambiguous evidence has been obtained concerning the existence or

not of the intermediate boson. The overall low rate suggests its mass would be significantly greater than the 2 GeV. limit of the accelerators. Bearing in mind the possible variation of the inelastic cross section and $\bar{E}_\mu/\epsilon_\nu$ above 10 GeV., the results of the present experiment would be in accord with $M_W \gtrsim 3.0$ GeV. The Case - Wits. - Irvine results may not suggest so high a lower limit, perhaps $\gtrsim 2.5$ GeV., but only a limited degree of confidence is put in this figure in view of the unexplained low energy deposition in some of the events. The greater information ensuing from the improved array is expected to give a more reliable figure.

10.3 Celestial Co-ordinates

The celestial co-ordinates of the arrival directions of atmospheric muons appear to show a large scale anisotropy in the southern celestial hemisphere. More than twice as many events have been detected from one half of the hemisphere than from the other. The ratio of the two intensities is found to be 2.2 ± 0.26 which is more than 4 standard deviations from the expected value of unity and has a $\ll 1\%$ probability of chance occurrence. Deflection of primaries from nearby sources in local magnetic fields of the spiral arm would seem to be a possible explanation.

The neutrino-induced events have shown Tycho Brahe's supernova to be a possible point source, the probability of chance intersection of the arcs of error near such a strong radio source having been estimated to be very small.

10.4 Future Plans.

The K.G.F. experiment is planned to be closed down in late June, 1969 and it is unlikely that any more interesting observations will be made

before that date. The improved Case - Wits. - Irvine array, however, is only coming into operation now and should continue to give some of the detailed information which has been a feature of the present experiment. The Utah detector, now in full operation, is beginning to record possible neutrino-induced events (p.c. to A.W. Wolfendale) and should provide enough data to establish the basic form of the neutrino-induced muon spectrum if sufficient running time is accumulated. The celestial co-ordinates of the arrival directions of the events detected in both of these experiments should be of great interest, although neither is in such a good position as the K.G.F. experiment for studying atmospheric muons.

APPENDIX 1

Muon Energy loss Parameters.

The average rate of energy loss by muons in standard rock* has been given by Barrett et al. (1952) as,

$$-\frac{dE}{dx} = 1.88 + 0.077 \ln \frac{E_m}{mc^2} + bE \quad \text{MeV gm.}^{-1} \text{ cm.}^2$$

where E_m is the maximum transferable energy in a μ - e collision and m is the muon mass.

Hayman et al. (1963) have given a best estimate of the energy loss parameter b in the energy proportional term as 4.0×10^{-6} gm.$^{-1}$ cm.^{2} where,

$$b = b_{pp} + b_{brems} + b_{nuc}$$

b_{pp} is the contribution from pair production, b_{brems} from bremmsstrahlung and b_{nuc} from nuclear interaction, all of which processes are taken to give an energy loss proportional to energy.

In calculating the effect of energy loss fluctuations, Osborne et al. (1968) have used the values,

b_{nf} (non fluctuating) = $b_{pp} = 1.6 \times 10^{-6}$ grm.$^{-1}$ cm.^{2}

& b_f (fluctuating) = $b_{brems} + b_{nuc} = 2.4 \times 10^{-6}$ grm.$^{-1}$ cm.^{2}

with $b_{brems} = 1.7 \times 10^{-6}$ grm.$^{-1}$ cm.^{2} & $b_{nuc} = 0.7 \times 10^{-6}$ grm.$^{-1}$ cm.^{2}

The greatest uncertainty is in the value of b_{nuc}. This was given as 0.28×10^{-6} grm.$^{-1}$ cm.^{2} by Fowler and Wolfendale (1958) but is now generally accepted as being higher although Miyake et al. (1964,b) have said that is is less than 0.9×10^{-6} grm.$^{-1}$ cm.^{2}.

In Chapter 3 it was stated that the complete termination of the photo-nuclear cross section might not suffice to explain the observed angular distribution. This is the case for $b_{nuc} = 0.28 \times 10^{-6}$ grm.$^{-1}$ cm.^{2}.

However, if $b_{nuc} > 0.5 \times 10^{-6}$ grm.$^{-1}$ cm.^{2}, then a reduction in it alone at higher energies would be sufficient to explain the results.

* For standard rock, $\bar{Z} = 11$, $\bar{A} = 22$ and $p = 2.65$ grm. cm.$^{-3}$.

APPENDIX 2

Correction for Muon Range Fluctuations

FIG. A2.1: Fluctuations Enhancement Factors F(D,γ) - Osborne et al. (1968).

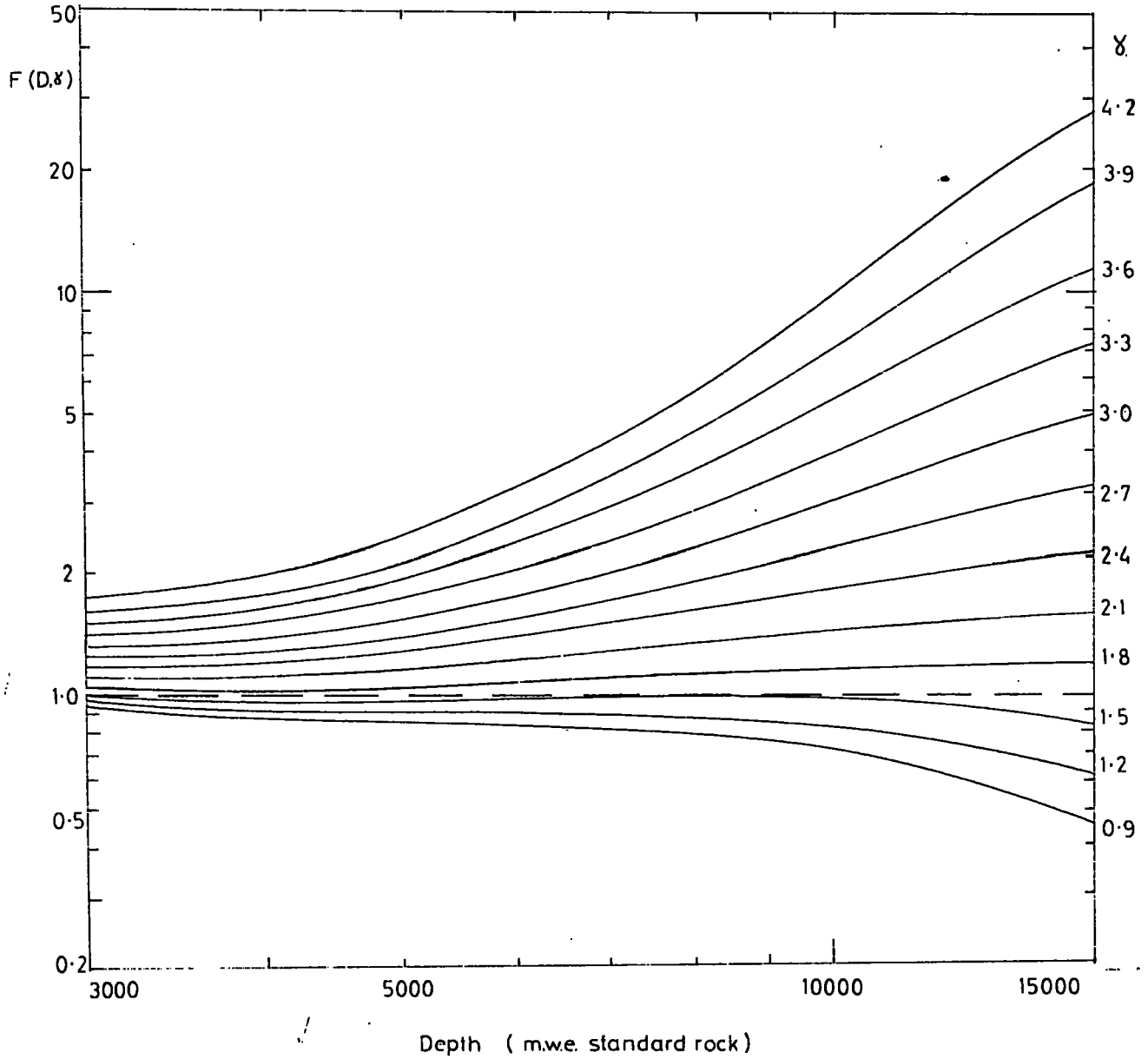

APPENDIX 3

The Apertures of Vertical walled Telescopes.

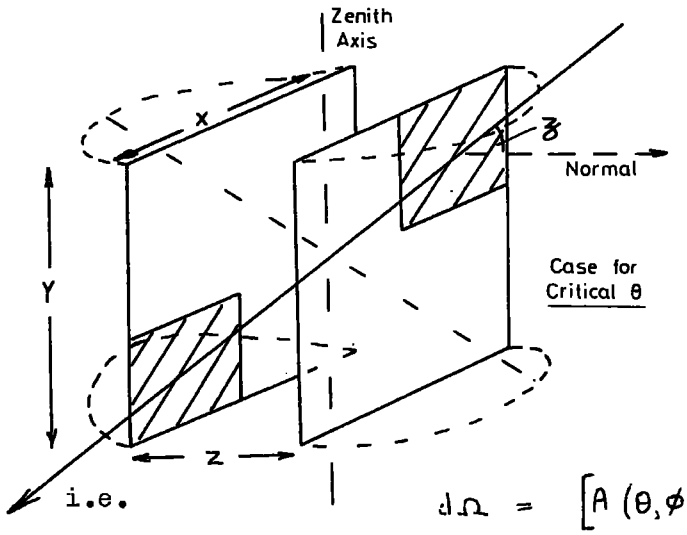

The differential aperture of a particle arriving at an angle ζ to the normal to the detector surface of this type of telescope is given by the product of the solid angle and area of the 'shadow' of the first detector surface on the second at that ζ and where ϕ is the azimuth angle.

$$d\Omega = \left[A(\theta,\phi)\cos\zeta\right]\sin\theta\, d\theta\, d\phi \qquad A3.1$$

is the spatial zenith angle and $A(\theta,\phi)$ is the 'shadow' area governed by θ and ϕ.

Substitution of $\cos\zeta = \cos\phi\sin\theta$ and $\tan\beta = \cos\phi\tan\theta$ in equation A3.1 leads to the differential aperture in terms of β, as given in equations 6.5 & 6.6 or in terms of θ as follows,

$$\frac{d\Omega}{d\theta} = 4\left[\sin\theta^2\left\{Y\left[(X^2+Y^2)^{\frac{1}{2}}-Z\right]\right\} - \sin\theta\cos\theta\left\{XZ\tan^{-1}\frac{X}{Z} - Z^2\ln\left[\frac{(X^2+Z^2)^{\frac{1}{2}}}{Z}\right]\right\}\right] \qquad A3.2$$

for $\pi/2 \geq \theta \geq \theta_c$

$$\frac{d\Omega}{d\theta} = 4\sin\theta\left[XY\left(\sin^2\theta - \frac{Z^2}{Y^2}\cos^2\theta\right)^{\frac{1}{2}} - YZ\sin\theta + \cos\theta\left\{Z^2 - XZ\cos^{-1}\left(\frac{Z}{Y}\cot\theta\right) + Z^2\ln\left(\frac{Y}{Z}\tan\theta\right)\right\}\right] \qquad A3.3$$

for $\theta_c \geq \theta \geq \tan^{-1}\frac{Z}{Y}$

where $\theta_c = \tan^{-1}\left[\frac{(X^2+Y^2)^{\frac{1}{2}}}{Y}\right]$

The need for two cases can be seen in the diagram. For $\theta < \theta_c$ the limits of ϕ are no longer dictated by the intersection of the cones of rotation, of the incident direction through ϕ about the zenith axis, with the side edges of the detector surfaces, but with their intersections with the top and bottom edges.

APPENDIX 4

(a) Total Events Recorded in K.G.F. Neutrino Experiment (1/4/65 to 31/12/68)

(i) Tels. 1 & 2:

Event No.	Run No.	Tel.	Time I.S.T.	Scintillators	p.z.a. (degrees)	Comments
2	55	1	08-30	N1; S1	48	
3	69	2	11-58	N6; S6	75 ± 15	1 layer N.F.T.
4	100	2	06-57	N1; S1	96.2 ± 0.8 & 99.2 ± 0.3	double track
5	106	2	11-21	N4; S3,5,6	45	
6	110	1	22-15	N3,6; S1,2	8.5	O.G.
7	116	2	07-37	N6; S3	37.5	knock on
8	117	1	23-23	N6; S3	29.5	small shower
9	120	2	15-18	N1; S3	32.5	shower
10	122	1	17-23	?; S6	25	O.G.
11	122	1	00-02	N6; S4	47	
12	131	1	14-38	N4; S5	33	rock shower. O.G.
13	132	2	08-43	All	?	large shower
14	143	2	01-12	N5; S1,3	21	shower
15	144	1	07-15	N6; S3	26.5	
16	171	1	13-23	N3; S1	40	
18	208	1	11-40	N4; S5	36	
19	209	1	10-29	- -	33	knock on
20	217	2	13-10	N6; S4	51.5	knock on
21	248	1	17-09	N2,4,6; S5	?	O.G.
23	289	2	08-33	- -	44.6	
24	302	1	15-52	N4; S1,3,5	?	shower O.G.

Event No.	Run No	Tel.	Time M.S.T.	Scintillators	p.z.a. (degrees)	Comments
25	315	2	05-39	N3; S1	44.1	
26	321	2	11-52	N2; S4,5	19.4	small shower
27	329	2	10-09	N4; S6	42.8	
29	331	1	16-27	N1,3,4; S1,2,4,5	96.5	three tracks
31	359	2	13-14	N6; S1,3	21	
32	378	1	04-28	N2,3,4,5,6; S1,3	26	three tracks & shower
34	422	1	21-49	N4,6; S2	30	
35	422	1	10-55	N3,5; S1	26.6	knock on
37	438	2	00-20	N2; S6	19.4	
38	459	2	15-02	N6; S1	19	
40	471	2	08-08	N6; S4	33.7	
41	480	1	06-49	N2; S1,2,4,6	38.5	
42	486	1	05-46	N5; S4,6	18	O.G.
43	501	1	07-25	N3; S1,2,3,4	85.5	
44	554	1	09-32	N5; S1	21.8	
45	562	1	16-17	- -	36	
46	572	2	15-28	N2; S5	19.5	
47	601	1	15-57	N5; S2	22.2	
48	606	1	15-13	N2,3; S2	53.7 & 48.7	multiple track
49	616	1	07-53	N3; S5	35.2	
50	641	1	19-34	N2; S3	21.6	
51	644	2	23-36	N3, S1	27.3	knock on
52	651	1	15-04	N2; S5	28	small shower
53	698	1	20-07	N5; S3	37	

Event No.	Run No.	Tel.	Time E.S.T.	Scintillators	p.z.a. (degrees)	Comments
54	737	1	01-26	N2; S3	24.9	knock ons ?
55	743	2	12-31	N3; S6	28	
56	798	2	12-31	N2; S5	16.9	
57	824	1	20-13	N3; S5	38.4	
58	838	1	04-50	N3; S2	41.9	
59	868	1	09-56	N1; S5	19.5	
60	905	2	08-27	N2; S6	23.5	
61	917	1	20-09	N3; S1	39.8	
62	945	2	10-41	N6; S4	25.5	
63	956	2	21-37	N2; S4	41.5	
64	963	2	01-32	N1; S6	33.8	
65	978	1	19-03	N4; S2	42.5	
66	984	1	23-31	N2; S5	18.1	
67	999	1	19-43	N5; S3	35.2	
68	1027	2	19-05	N2; S4	35	
69	1027	2	04-27	N5; S3	29	

(ii) Tels. 3,4 & 5 (4-fold)

Event No.	Run No.	Tel.	Time E.S.T.	Scintillators	p.z.a. (degrees)	Comments
22	289	5	04-21	N3; S1	46.2	
28	331	3	15-18	N3; S3	-	O.G.
30	344	4&5	16-04	N1(T4.); S1(T5)	72	
33	412	5	03-40	N4; S2	34	O.G.
36	432	5	01-32	N2; S4	74	
39	462	4	09-17	N1; S3	48	small shower

(iii) Specs. 1 & 2

Event No.	Run No.	Spec.	Time M.S.T.	Scintillators	p.z.a. (degrees)	Comments
S2	610	1B	19-06	S4; T2	26 ± 1.5	
S3	614	2F & B	01-20	T3; N2,3	14 ± 5	shower. O.G. ?
S4	615	1F	17-32	T1; N1	17.5 ± 0.2	
S5	624	2F & B	18-20	S2; T3	-	weak shower ?
S6	626	1B	21-56	T4; N3	12	O.G. ?
S7	632	1B	20-18	S3; T3	39.8 ± 1.0	
S8	634	1F	19-29	T2; N1	18.0 ± 1.0	
S9	638	1F	09-35	T1; N2	17.4 ± 0.3	
S10	644	2F	15-15	S2, N2	41.8 ± 0.2	
S11	655	2F & B	03-41	S2, T3	16.7 ± 0.3	
S12	660	1F & B	23-24	S1,2,3,4; T1,2,3,4	-	large shower
S13	663	1F	10-17	S2; T2	23.3 ± 0.3	knock on
S14	667	2F	00-02	S2; T1	12.9 ± 0.3	
S15	669	2F	03-01	S2; T1	28.8 ± 0.2	
S16	669	1F	07-25	T2; N2	12.5 ± 0.3	
S17	684	2F	16-06	S2; T2	27.9 ± 0.3	
S18	685	2B	20-18	T3; N3	19.6 ± 0.2	knock on
S19	691	1B	04-41	T3; N3	22.0 ± 0.3	
S20	693	2F	19-45	S1; T1	22 ± 13 or 14 ± 5	
S21	694	1B	03-39	S3; T3	14.0 ± 0.5	
S22	698	1F	03-43	T1; N1	32.6 ± 0.5 & 31.3 ± 0.8	double track
S23	708	2F	20-04	S2; N2	48.4 ± 0.7	deflected
S24	711	2F	21-22	T2; N1	-	shower O.G.

Event No.	Run No.	Spec.	Time M.S.T.	Scintillators	p.z.a. (degrees)	Comments
S25	725	1F	04-39	S1; T2	13.5 ± 0.4	
S26	726	2B	22-53	S4; T1	-	O.G. ?
S27	737	1B	06-30	T2,3; N2	-	shower
S28	743	1F	05-19	S1; T1	-	O.G.
S29	743	1B	07-17	S4; T4	27.9 ± 0.3	knock on ?
S30	744	1B	17-56	S3; T3	-	weak shower
S31	747	1B	21-10	S3; T4	14.5 ± 0.2	knock on
S32	748	1F	02-39	S2; N2	34.7 ± 0.4	
S33	759	2F	12-37	T2; N2	25 ± 8	
S34	760	1F	21-38	S1; T1	13.7 ± 0.3	
S35	761	1B	08-34	- -	-	
S36	768	1F	05-45	S1; T1; S1	12.2 ± 0.5	
S37	788	1B	00-55	T2; N3	13.5 ± 0.4	
S38	792	2F	05-01	S2; T2	37.2 ± 0.2	
S39	793	1B	01-55	S4; T4	16.5 ± 0.2	
S40	796	1B	12-26	S4; N3	59.1 ± 0.2	knock on
S41	834	1F	13-00	T2; N2	7.3 ± 0.5	
S42	850	2F	07-24	S1; T1	39.0 ± 0.5	O.G.
S43	852	2B	22-54	S3; T4	23.5 ± 0.3	three tracks
S44	855	1F	10-25	- -	-	O.G.
S45	866	1B	17-43	S4; T3	33.6 ± 0.3	
S46	880	2B	19-23	S4; T4	30.9 ± 0.2	
S47	895	1F	00-17	S1; T1	32.0 ± 0.3	O.G.
S48	895	2F	00-46	T1; N1	22.2 ± 0.2	knock on
S49	897	2B	18-40	S3; N3	36.6 ± 0.2	secondaries from magnet

Event No.	Run No.	Spec.	Time M.S.T.	Scintillators	p.z.a. (degrees)	Comments
S50	906	1F	06-32	T2; N1,2	-	weak shower
S51	910	2B	08-21	S4; T3	8.6 ± 0.2	
S52	915	2B	07-32	T4; N4	28.8 ± 0.3	
S53	917	2F	05-29	S1; T1	14.2 ± 1.0	
S54	919	1B	10-42	T?; N4	19.5 ± 0.4	
S55	920	2F & B	16-56	S1; T1; N1	1 - 6	shower
S56	922	2F	17-51	T1; N1	32.4 ± 0.3	knock ons ?
S57	943	1F	17-05	S2; T2	9.5 ± 0.2	
S58	969	1B	12-01	S1; T1	19.8 ± 0.5	
S59	974	1B	13-09	S4; T4	20.0 ± 0.2	
S60	977	1F	20-53	S1; T2	34.5 ± 0.2	
S61	979	1F	18-36	T1; N1	14.5 ± 0.2	
S62	982	2F	08-21	S1; N2	28 ± 1	
S63	984	1B	17-46	T3; N3	16.8 ± 0.3	O.G.
S64	987	1F & B	07-19	S4; T2,3; N2,3	39.3 ± 0.3	rock shower
S65	988	2F	20-36	S2; T2	29.2 ± 0.2	
S66	990	1B	03-08	T4; N4	16 ± 3	
S67	990	1F		S2; T2	-	
S68	997	2F		T1,2; N1	-	shower O.G ?
S69	999	2F	16-38	T1; N2	12 ± 2	
S70	1009	1B	18-40	T3; N4	21 ± 2	
S71	1013	2B	03-22	T4; N4	10 ± 0.5	
S71	1015	2F & B	00-05	S3; N2	83 ± 1	deflected
S72	1016	1B		T3; N3	12 ± 1	shower

Event No.	Run No.	Spec.	Time M.S.T.	Scintillators	p.z.a. (degrees)	Comments
S73	1019	1F	03-38	S3; T2	19 ± 1	
S74	1019	1F		T2; N2	11 ± 0.5	
S75	1025	1F	15-38	T3; N2	29 ± 3	
S76	1026	1B	22-06	T4; N4	2.5 ± 0.5	
S77	1026	1F	19-42	S2; T1	8.5 ± 1	
S78	1026	1F	19-32	T1; N1	7.0 ± 0.5	
S79	1031	1F	19-12	S1; T1	-	shower O.G.

(iv) Tels. 3,4 & 5 (O.S.T.)

Event No.	Run No.	Tel.	Time M.S.T.	p.z.a. (degrees)	az. a.	No.of layers	
001	778	3	21-18	27 ± 2		1	No az.
002	778	3	23-36	22.2 ± 0.5	109-251E	3	No az.
003	778	3	13-14	35.5 ± 2	-	1	No az.
004	778	3	13-18	57 ± 10	-	1	No az.
005	779	4	13-35	22.5 ± 1.5	58 ± 2 W	2	
006	781	3	23-04	21 ± 1.5	-	1	
007	781	3	10-32	-	0 ± 15	1	Az. only
008	787	3	23-06	-	124 ± 2 W	2	
009	788	3	11-46	14.5 ± 1	39 ± 2 E	2	
010	790	4	02-48	-	-	1	
011	792	3	17-39	17 ± 1	173 ± 7 W	2	
012	794	4	10-39	40 ± 0.5	176 ± 5 W	4	
013	800	3	12-00	14 ± 1.5	-	1	
014	802	4	16-33	33 ± 3	147 ± 10 E	2	
015	802	4	04-26	16 ± 1	150 ± 13 W or 173 ± 7 W	2	

Event No.	Run No.	Tel.	Time M.S.T.	p.z.a. (degrees)	as. a.	No.of layers	Comments
016	802	5	10-31	94 ± 0.15	0 ± 12	5	2 knock ons
017	813	4	19-15	35 ± 5	-	1	
018	815	4	14-26		26 ± 20 E	2 or 3	shower
019	818	4	21-27	11.5 ± 0.5		1	
020	822	3	17-14	20.5 ± 0.5	-	3	
021	828	4	06-23	25 ± 2	44 ± 4 W	3	
022	835	4	14-30	23 ± 0.5	70 ± 1 E	3	
023	840	5	12-33	37 ± 0.5	143 ± 13 W	3	
024	844	3	05-39	15.5 ± 1.5		1	
025	851	3	11-54	17 ± 1.5	144 ± 6 W	2	
026	856	4	11-31	31 ± 0.5	-	3	
027	858	4	12-38	41 ± 1	-	3	Small shower
028	861	3	04-24	23 ± 1.5	-	1	
029	863	3	21-33	25 ± 3	-	1	
030	863	4	18-40	35 ± 0.5	44 ± 0.5 W	5	4-fold type. shower
031	872	3	12-06	33.5 ± 0.5	147 ± 10 E	3	
032	878	3	00-34	5.6 ± 0.5	-	1	shower
033	881	5	08-48	30.5 ± 2 & 40.5 ± 2	160 ± 10	2	O.G. 4-fold type
034	883	5	06-00	19.5 ± 1.5	-	1	
035	890	3	15-24	-	-	1	part of shower
036	892	4	14-05	-	-	1	part of shower
037	893	5	22-17	29 ± 2	23 ± 6 W	2	
038	897	5	09-52	25 ± 3	-	1	
039	899	5	10-24	35 ± 0.5	25 ± 1 W	4	

Event No.	Run No.	Tel.	Time M.S.T.	p.z.a. (degrees)	as. a.	No.of layers	Comments
040	903	4	14-07	22.5 ± 2	143 ± 13 W	2	
041	903	5	19-44	38 ± 4	-	1	
042	906	5	12-49	43 ± 0.5	36 ± 3 W	5	4-fold type
043	906	5	16-38	38 ± 1	174 ± 0.5 W	4	
044	915	3	13-38	22 ± 1	0	3	
045	919	4	19-07	21 ± 5	145 ± 9 W	2	shower
046	931	5	16-28	34 ± 0.5	10.5 ± 0.5 W	4	
047	934	4	12-04	12 ± 2	-	2	
048	937	3	19-37	15 ± 2	-	1	
049	939	3	00-24	24.5 ± 1	-	1	
050	941	3	17-34	23.5 ± 3.5	-	1	
051	941	4	09-42	20.5 ± 0.3	56 ± 2 E	3	
052	942	4	13-20	37.7 ± 0.3	150 ± 2 W	5	
053	951	3	05-56	10.5 ± 1.5	-	1	
054	953	3	10-36	23 ± 0.5	8 ± 22 E	3	
055	953	3	20-30	27 ± 1 & 17 ± 1	-	1	
056	953	3	06-42	15 ± 7	-	1	shower
057	955	4	20-47	23.7 ± 0.5	60 ± 2 W	3	
058	956	5	20-07	18 ± 3	-	1	
059	963	3	01-34	19.5 ± 2	-	1	
060	966	4	07-58	30.5 ± 2	-	1	
061	970	5	13-03	-	-	2	interaction in iron
062	976	5	18-12	32.7 ± 0.5	?	3	
063	977	3	16-35	19.0 ± 0.3	51 ± 2 W	3	O.G.

Event No.	Run No.	Tel.	Time M.S.T.	p.z.a. (degrees)	as. a.	No.of layers	Comments
064	987	5	15-29	7.5 ± 0.5	-	1	
065	990	4	08-39	-	-	1	
066	990	5	00-49	26 ± 4	-	1	
067	991	3	10-12	17.5± 1	16 ± 9 E	3	two parallel tracks
068	998	4	08-08	24.7 ± 2.3	16 ± 10 E	2	knock on
069	1007	4	11-05	32 ± 0.5	14 ± 0.5 E	4	
070	1009	4	17-28	89 ± 10	46 ± 1 E	2	interaction product
071	1009	4	23-32	24 ± 3	8 ± 4 W	2	
072	1012	3	20-07	9.4 ± 0.5	?	1	
073	1013	3	16-02	?	?	2	part of shower
074	1013	5	06-10	17 ± 1.5	61 ± 2 E	2	
075	1017	3		12 ± 1	30 ± 9 W	2	shower
076	1019	5	09-25	26 ± 1	38 ± 12 E	2	
077	1021	5	18-22	105 ± 15 & 58 ± 8	-	1	two tracks
078	1022	3	08-22	23 ± 1	22 ± 12 E	3	knock on
079	1023	5	01-21	18 ± 1	30 ± 5 W	3	
080	1024	4	08-50	13 ± 1	-	1	
081	1028	3	12-17	28 ± 2	-	1	
082	1030	3	23-14	18 ± 2	-	1	
083	1031	4	15-36	32 ± 3	35 ± 6 W	2	
084	1033	4	10-03	8 ± 1.5	-	1	knock on

B - Back F - Front O.G. - Out of geometry

All azimuth angles are given with respect to Telescope or Spectrograph North.

(b) Individual Neutrino-induced Events (1/4/65 to 31/12/68)

(i) Tels. 1 - 5	Event No.	p.z.a.	Penetration
Single Muons:	3	75°	6 cm. Pb
	30	60° (Spatial 72°)	45 cm. Fe
	36	73° (Spatial 74°)	32 cm. Fe
	20	51°	cm. Pb
Multiple Events:			
2 diverging particles	4	96°, 99°	6 cm. Pb, 3 cm. Pb.
3 diverging particles	29	96°, 155°, 48°	6 cm. Pb, ?, interaction
Penetrating particle & associated cascade	43	85°	5 cm. Pb
2 penetrating particles 2 associated particles	48	49°, 54°, 60°, 10°	8 cm. Pb, 8 cm. Pb, 3 cm. Pb, ?

(ii) O.S.T.	Event No.	p.z.a.	Penetration
Single Muons:	016	94°	35 cm. Fe
Multiple Events:			
Dense shower	061	at $98 \pm 10^{\circ}$ inside detector	10 cm. Fe, cascade energy 2.5 GeV.
3 diverging particles	070	at $125^{\circ} \pm 30^{\circ}$ inside detector	50 cm. Fe, 9 cm, Fe, ?

(iii) Spectrographs	Event No.	p.z.a.	momentum	sign
Downward muon (losing energy)	S23	48^{o}	2 GeV/c	+
Upward muon (knock on electron)	S40	121^{o}	4 GeV/c	more probably +
Downward muon (losing energy)	S71	83^{o}	1-2 GeV/c	+

FIG. A4.1: Event 43

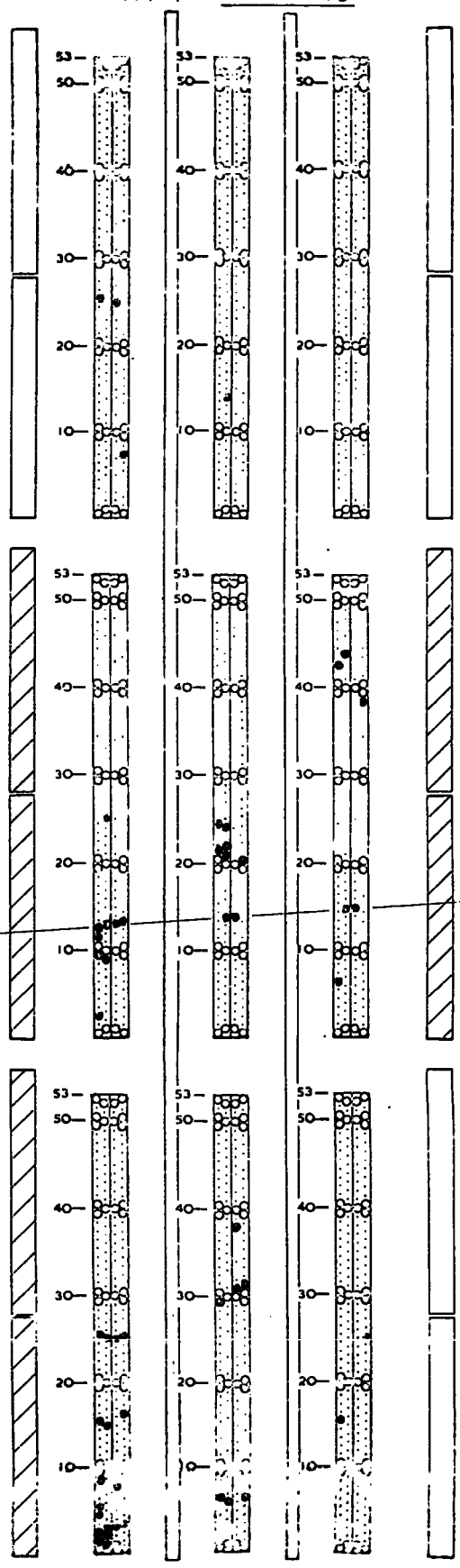

Telescope 1

Scintillators
N S
3 1,2,3,4

Total Running Time for Both Telescopes

19917
Detector Hours

Run No. 2) R 501

Proj. Zen. Ang.
85·5° ± 0·5°

Az. Ang. Range
66° W of Tel N
to 47° E of Tel N

Date
5/2/67

Time
22·41 I.S.T
07·25 M.S.T.

North C.R.O.

South C.R.O.

FIG. A4·2: Event 18

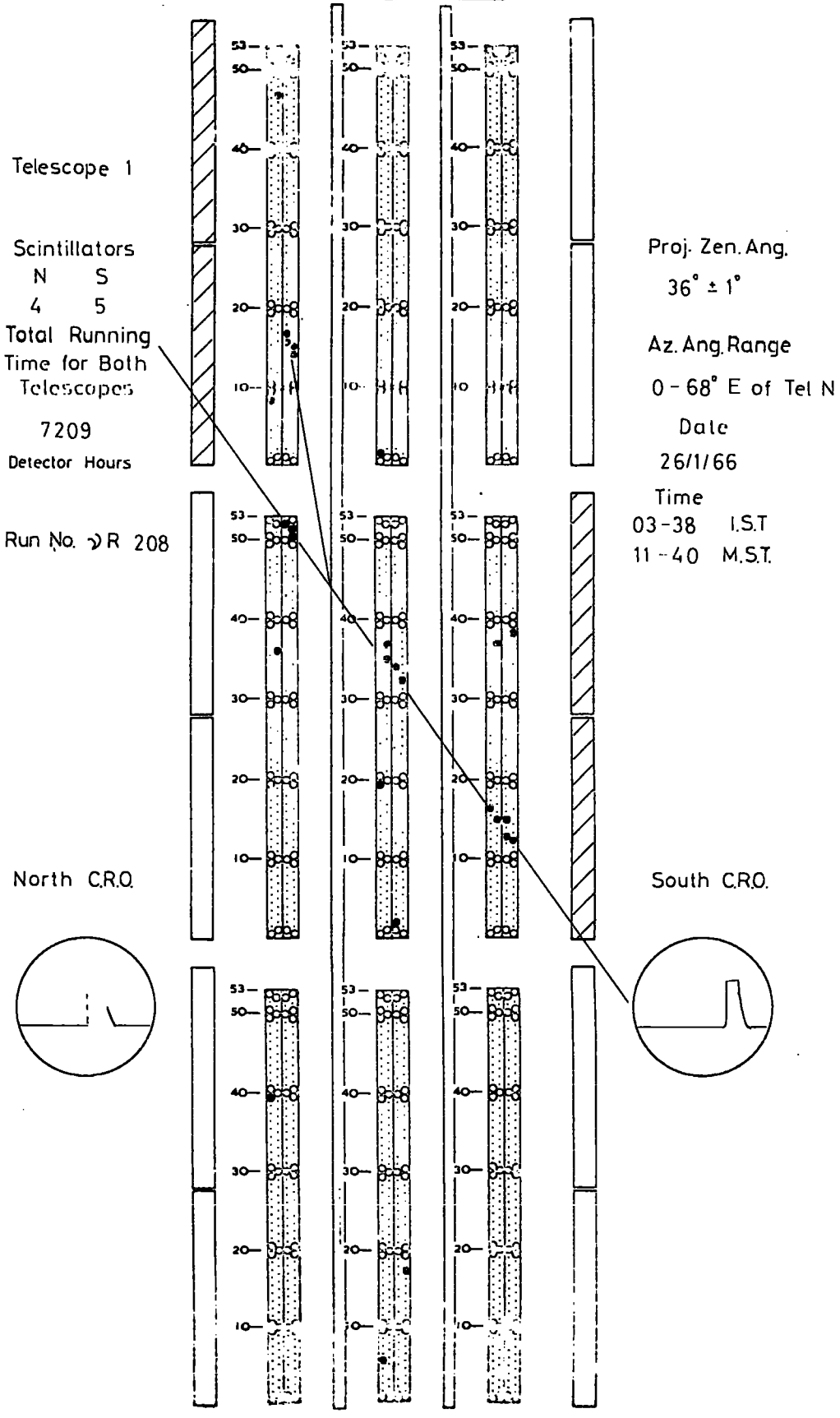

FIG. A4.3: Event 51

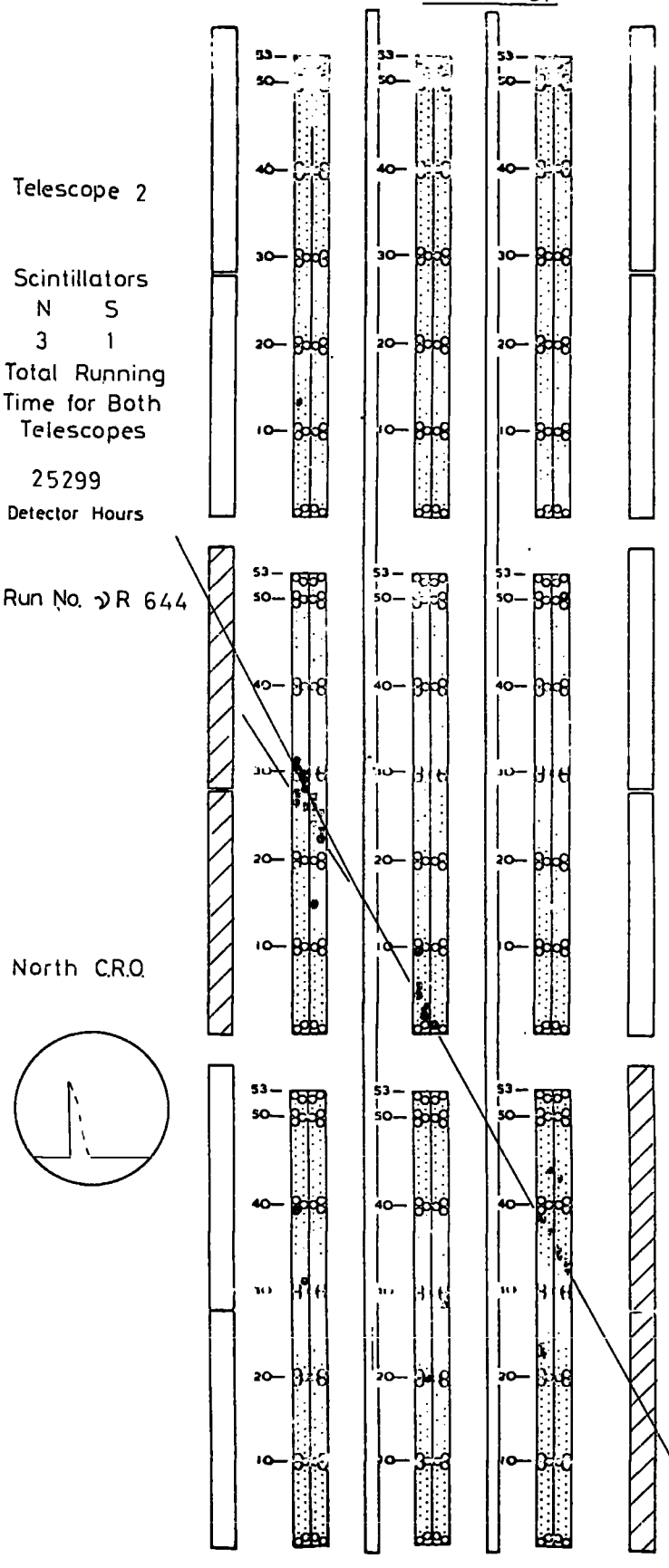

FIG. A4.4

EVENT NO S 12 RUN NO 663 DATE 24/8/67 TIME 01-35 IST 23-24 MST

SPECTROGRAPH
1F & B

SCINTILLATORS
S1234, T1234, N14

S CRO T CRO N CRO

TOTAL RUNNING TIME (SPECTROGRAPHS) 2206 hr.

AZIMUTH ANGULAR RANGE

DIRECTION

PROJECTED ZENITH ANGLE

SPATIAL ZENITH ANGULAR RANGE

MAGNET CURRENT
210 A

MAGNETIC DEFLEXION
—

MOMENTUM

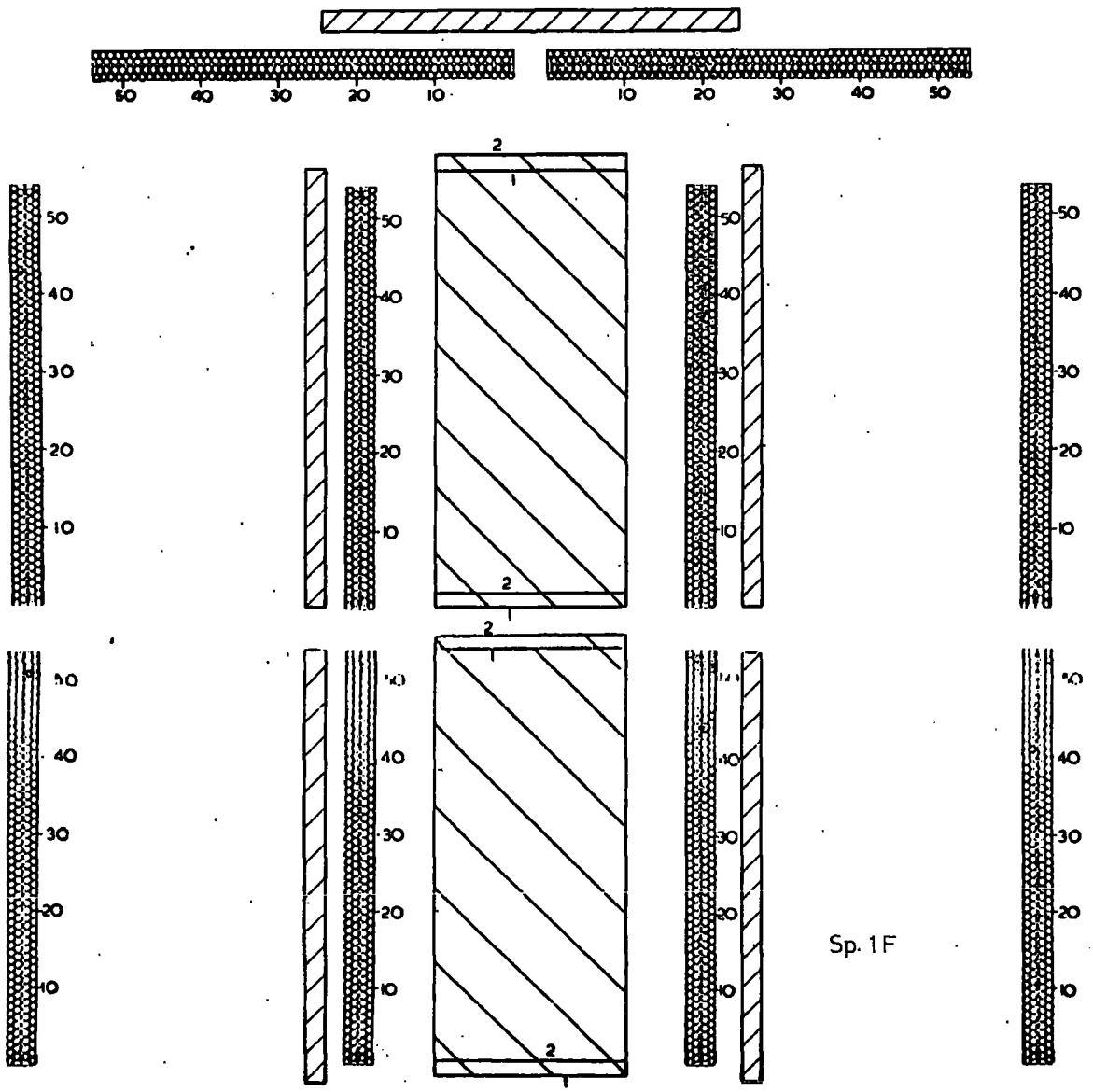

FIG.A4.5

EVENT NO S 48 RUN NO 895 DATE 5/6/68. TIME 08-09 IST 00-46 MST

SPECTROGRAPH
2F

SCINTILLATORS
S- T1 N1

TOTAL RUNNING TIME (SPECTROGRAPHS) 11127 hr.

AZIMUTH ANGULAR RANGE
35°E to 35°W of Spec S (or N)

DIRECTION
?

PROJECTED ZENITH ANGLE
22·2° ± 0·2°

SPATIAL ZENITH ANGULAR RANGE
22°-26

MAGNET CURRENT

MAGNETIC DEFLEXION

MOMENTUM

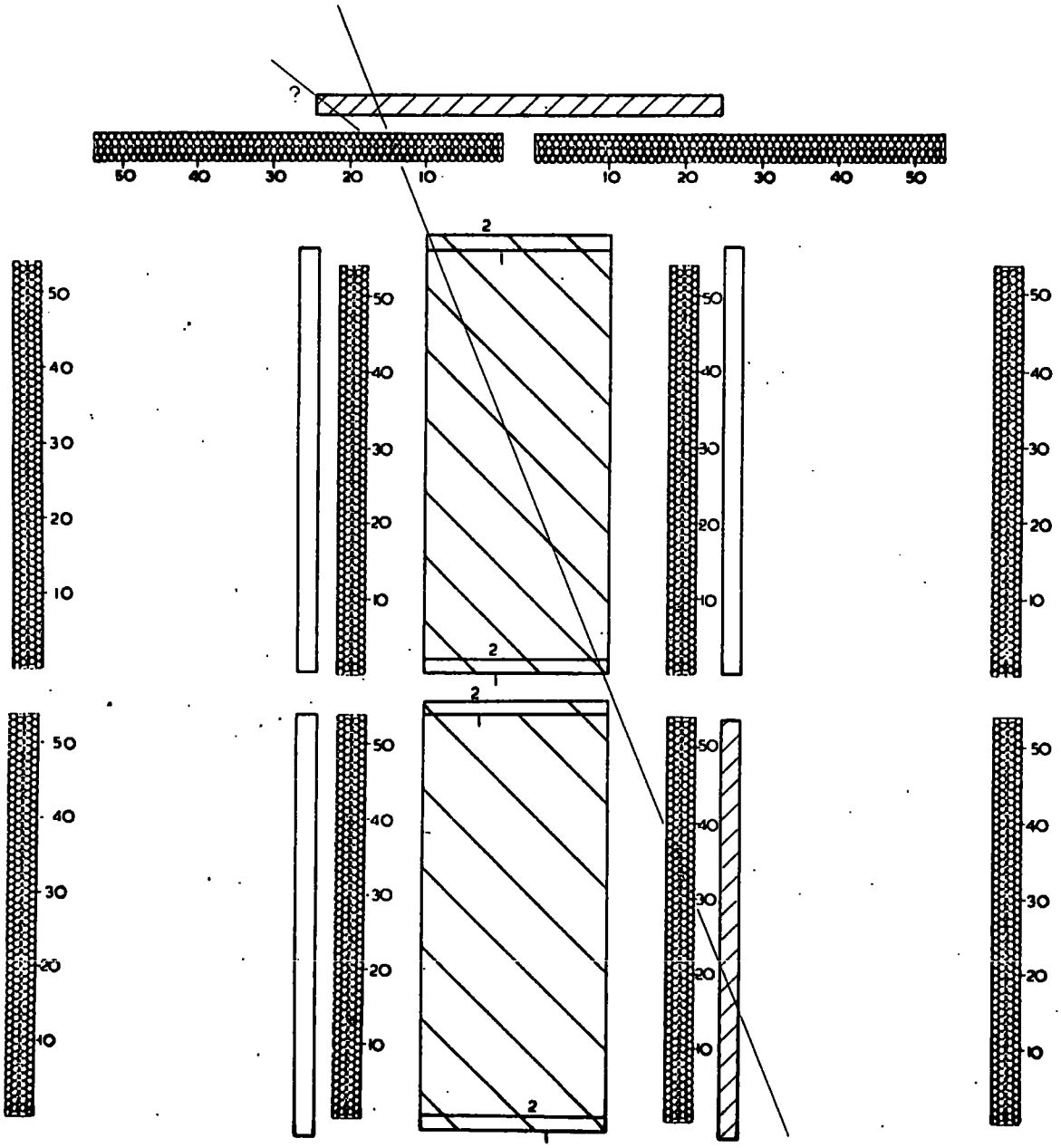

FIG. A4.6 Event 016

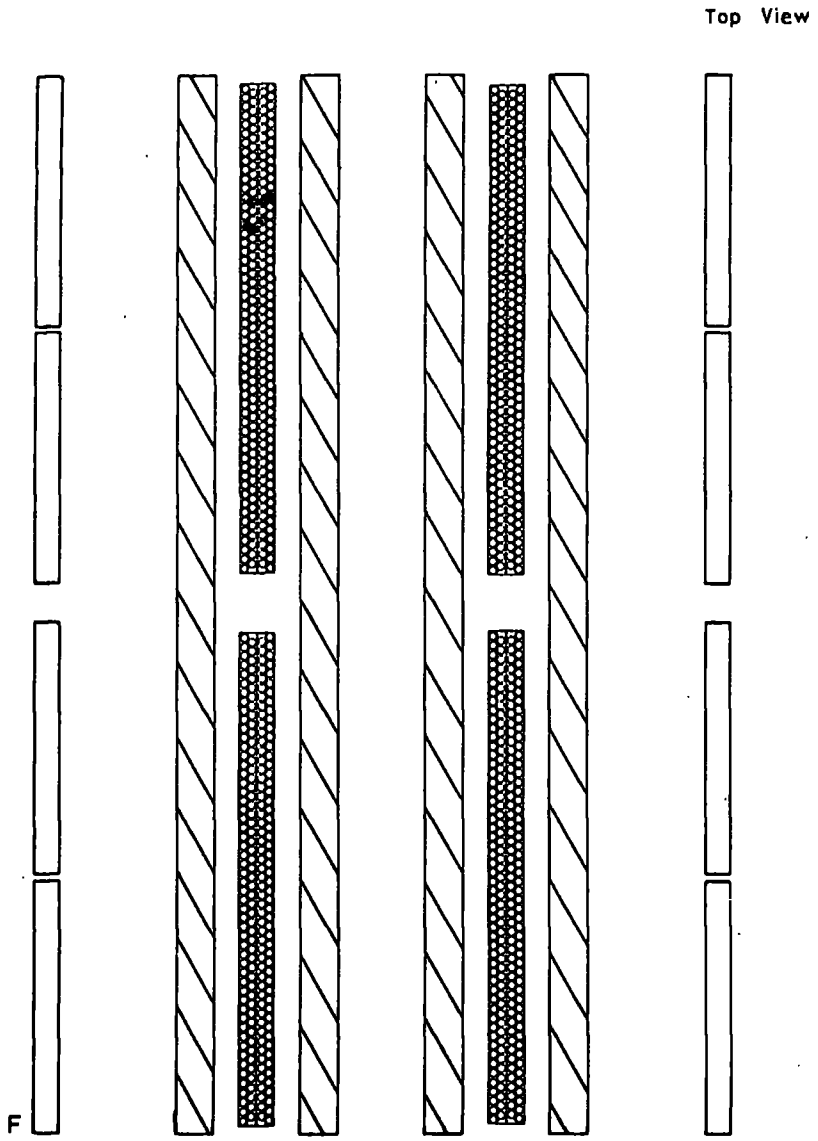
Top View
F

FIG. A4·6 Event 016

Run No. ϑR 802

Telescope 5

Date 14/2/68

Time 01-16 I.S.T.
10-31 M.S.T.

Projected Zenith Angle : $94{\cdot}4^{\circ} \pm 0{\cdot}5^{\circ}$

Azimuth Angle : $\sim 0^{\circ}$

Spatial Zenith Angle : $94{\cdot}4^{\circ} \pm 2^{\circ}$

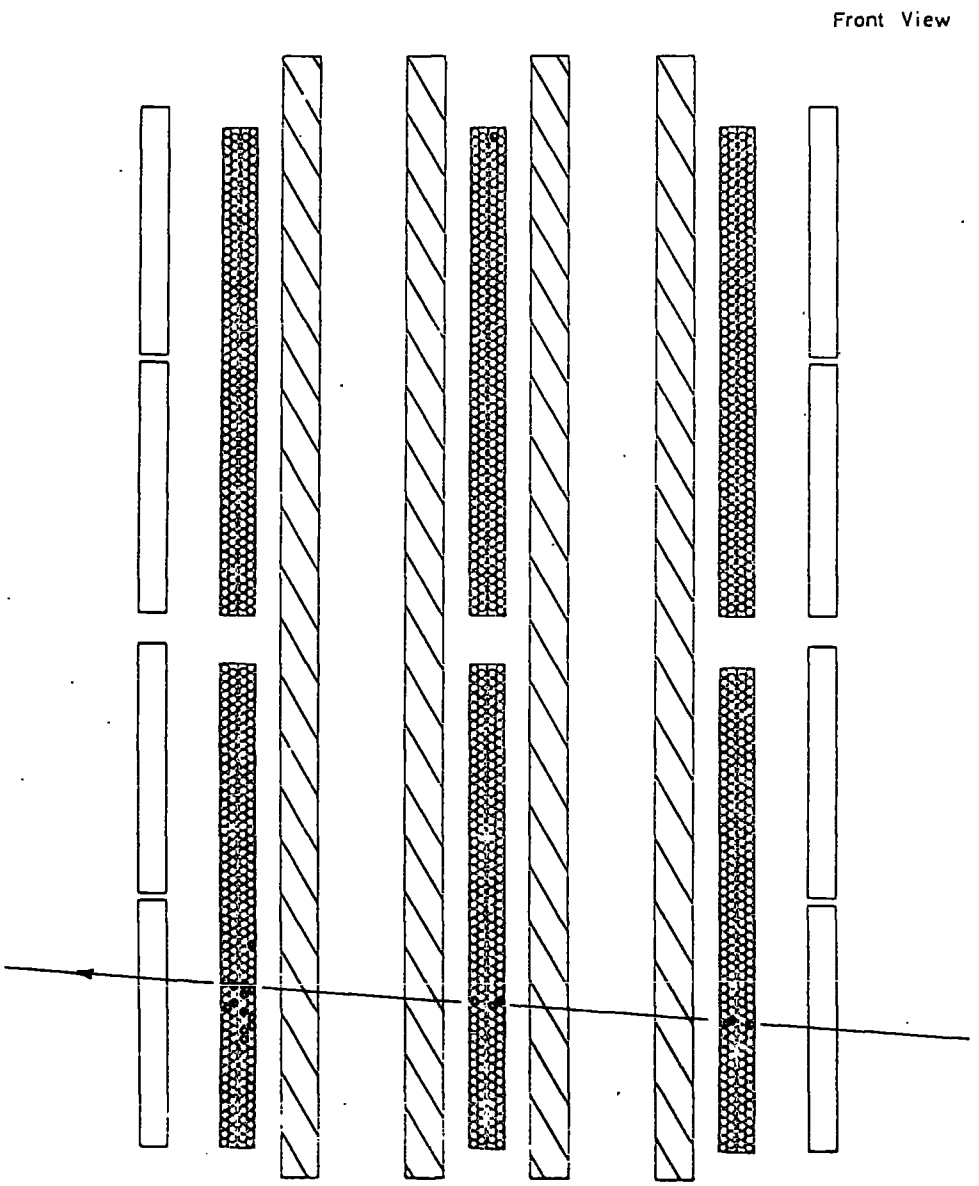

APPENDIX 5

The Possibility of Detecting Neutrino-Induced Muons in Muscovite Mica.

If muscovite mica is examined, decorated lines are seen which seem to fall into two categories, the majority lines, orientated in preferred directions at 30° intervals, and the minority lines, orientated at other angles. Russel (1967a) has made the suggestion that the minority lines are tracks of charged particles (presumably muons produced by neutrinos) which passed through the mica in a direction close to the plane of easy cleavage during its formative period. Heavy charged particles are known to leave tracks, in some insulators, which can be made visible to optical microscopes by chemical etching but that minimum ionising particles could leave tracks, in the form of the minority lines was not known and to check the suggestion, Craig et al. (1968b) made a detailed study of the lines. A brief summary of this work follows.

The measurements were made on ten sheets of mica with at least two lines lying at an angle of 60° to each other (i.e. majority lines). As the crystal structure of muscovite mica is repeated every 60° and each segment is composed of two symmetrical 30° segments, the measurements for all angles 0-360° have been superposed over one 30° range, as shown in fig. A5.1.

The majority lines were found, by definition, to be the most commom and their distribution at 30° intervals clearly suggested their connection with crystal dislocations. The minority lines, in contrast to the random distribution reported by Russel, were also found to be distributed with

some preferred directions, namely at $3 - 4^{\circ}$ and $6 - 7^{\circ}$, the latter being particularly prominent in one sheet. The distribution was not in keeping with an isotropic distribution of neutrino-induced muons or a peaked angular distribution of atmospheric muons as might have been expected deep underground where the mica was formed. Neither do the shapes of the length distribution curves show any difference which might have been expected between the two classes of line if they were from different sources; that for the restricted range $10.5^{\circ} < \theta < 24^{\circ}$, although possibly of different slope, cannot definitely be said to be different either.

The scattering analysis, which was conducted in the standard manner used in emulsion studies, showed that the majority lines were straight within the errors of measurement with only very rare exceptions. The measurements made on minority lines showed evidence for lack of straightness but in 60 cm. of track examined, 12 deflections of greater than 1° were observed and several of these were of 1.5° or 3.0°. The normal distribution fitting the points for small deflections in fig. A5.3 could be the result of measuring errors or a combination of both these and multiple coulomb scattering of particles. The large deflections could be related to the crystal structure or conceivably be examples of single large angle Rutherford scattering if the lines were in fact due to ionising particles. This latter possibility has been considered and the probability of its occurrence was estimated to be $< 3 \times 10^{-4}$ cm.$^{-1}$ of track, for neutrino-induced muons and less for atmospheric muons. The observed probability of such deflections was 0.2 cm.$^{-1}$ which is quite inconsistent with this figure.

Finally a comparison was made between the frequency of observed tracks and that expected from neutrino-induced muons. For the assumption of a

FIG. A5.1: Angular frequency distribution (in 001 plane) of lines having lengh greater than 12 mm.

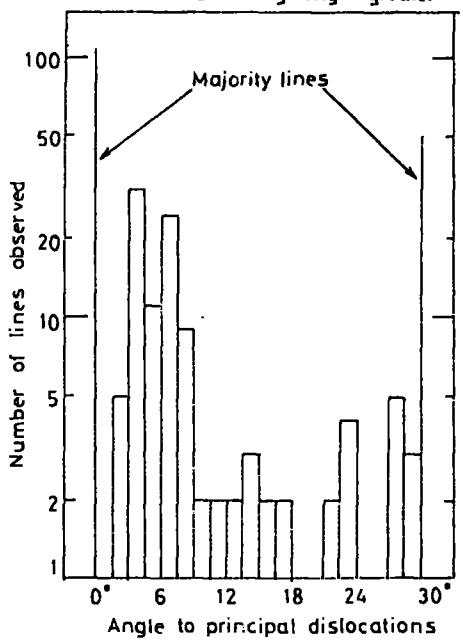

FIG. A5.2: Lengh distributions of the majority and minority lines.

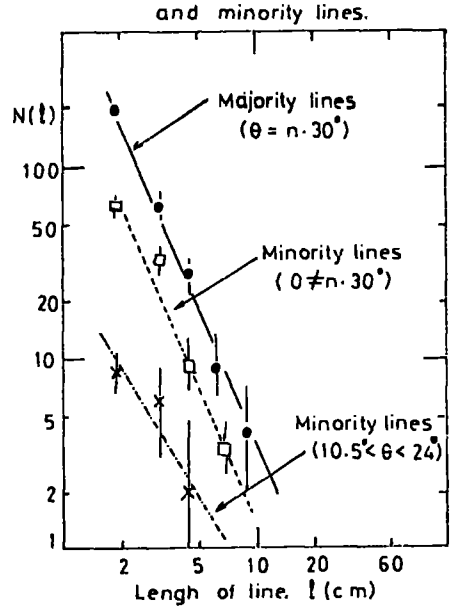

FIG. A5.3: Distribution of second differences of measurements made with 1000 μ cells on lines in the minority class.

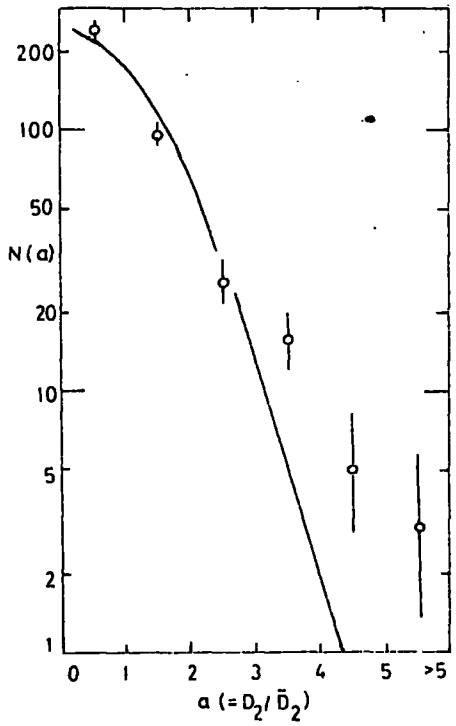

sensitive time of 20 years and the angular acceptance criterion, suggested by Russel, of $\pm$ 0.3 milliradians about the plane of easy cleavage, the expected number has been calculated to be less than the observed number by a factor of $\sim 10^5$. Agreement can be restored if the cosmic ray intensity is assumed to have been higher by this factor when the mica was formed and Russel has suggested that if this was so, it would be in keeping with the 'big bang' theory of the creation of the Universe.

The work of Craig et al., however, did not substantiate Russel's basic suggestion and it was remarked by them that to establish genuine examples of particle tracks, very rigorous selection criteria are needed for their isolation from the multitude of other lines.

A second paper by Russel (1967b) has suggested that electron showers have been recorded in the form of aligned nucleation centres of impurities in the crystal. The reason for the difference between these intermittent tracks and the continuous tracks in terms of different rates of energy loss of electrons and muons is hard to conceive as both are minimum ionising particles, however, Russel has suggested that the phenomena of channelling of particles in specific directions in the crystal lattice could be responsible. In the paper, Russel has given a plot of the gap length distribution (a 'gap' being the distance between nucleation centres) in the 'electron' tracks and the slope is found to be exponential in agreement with measurements of charged particle tracks in emulsions. However, the present author has calculated the effect of a random distribution of impurity atoms in the crystal and has found this to lead to the same result such that the alignment could still be explained in terms of dislocations.

Further studies made by Russel (p.c. to A.W. Wolfendale) have reproduced

the non-isotropic distribution of minority lines measured by Craig et al. and it would seem that there is agreement that at least some of the minority lines were produced by some rarer phenomenon connected with the crystal structure. Channelling of charged particles would seem an unlikely possibility as the ability of muons to leave tracks at all is the greatest uncertainty and that they could do so under the reduced energy loss predicted by channelling would seem to be even less likely.

The conclusion drawn by the present author is, therefore, that the ability of muscovite mica to detect cosmic ray secondaries is by no means proven.

Acknowledgements

Professor G. D. Rochester F.R.S. is thanked for his interest at all stages of the experiment and for making available the facilities at Durham.

The author is most grateful to his supervisor, Professor A. W. Wolfendale, for his invaluable guidance and advice at all times.

Professors M. G. K. Menon and S. Miyake are also thanked for their guidance and advice in India.

Thanks are due to Dr. J. L. Osborne, for his advice on the theoretical aspects of the work, and the other members of the international team whose co-operative effort has lead to the success of the experiment. They are, Drs. S. Naranan and V. S. Narasimham, Messrs. M. R. Krishnaswamy, A. M. Vinze, R. M. Wanker and P. Jayacham of Tata Institute, Professor K. Hinotani, Dr. N. Ito and Mr. S. Kino of Osaka City University and Drs. J. B. M. Pattison, D. R. Creed, P. K. MacKeown and E. C. M. Young of Durham University.

For the provision of the facilities and their ready co-operation, the following officers of the Kolar Gold Mining Undertakings are thanked; Mr. M. H. Parthasarathy I,A.S. (Managing Director), Mr. P.N.V. Raghavan (Champion Reef Mine Superintendent) and M. A. Sitharam (Chief Engineer).

Messrs. Boscoe and Elangoven, the Junior Technicians are also thanked for their continuous efforts along with the many other officers and men of the K.G.M.U. who have given their services at various times.

Messrs. E. W. Lincoln and W. Leslie are thanked for the construction of apparatus in their workshops and advice on its design and operation.

Mrs. J. Lincoln is thanked for her typing of the thesis and my wife for her preparation of many of the diagrams and scanning of much of the film in India.

Finally, the Science Research Council is thanked for its award of a Research Studentship throughout the period of study.

References

Achar, C.V., Narasimham,V.S., Ramana Murthy, P.V., Creed, D.R., Pattison, J.B.M. and Wolfendale, A.W., (1965a) Proc. Phys. Soc., 86, 1305: (1965b) Proc. 9th Int. Conf. Cosmic Rays, London, 2, 989, 1966.

Achar, C.V., Menon, M.G.K., Narasimham, V.S., Ramana Murthy, P.V., Sreekantan, B.V., Hinotani, K., Miyake, S., Creed, D.R., Osborne, J.L., Pattison, J.B.M. and Wolfendale, A.W., (1965c) Phys. Lett., 18, 196, (1965d) Phys. Lett., 19, 78; (1965e) Proc. 9th Int. Conf. Cosmic Rays, London, 2, 1012, 1966.

Ashton, F., and Wolfendale, A.W. (1963), Proc. Phys. Soc. 81, 593.

Barrett, P.H., Bollinger, L.M., Cocconi, G., Eisenberg, Y. and Greisen, K., (1952), Rev. Mod. Phys., 24, 133.

Barton, J.C., (1961), Phil. Mag., 6, 1271.

Bell, J.S., and Veltman, M., (1963), Phys. Lett., 5, 151.

Bergeson, H.E., Keuffel, J.W., Larson, M.O., Martin, E.R., and Mason, G.W., (1967), Phys. Rev. Lett., 19, 1487.

Bergeson, H.E., Keuffel, J.W., Larson, M.O., Mason, G.W., and Osborne, J.L., (1968), Phys. Rev. Lett., 21, 1089.

Berman, S.M., and Veltman, M., (1965), Nuovo Cim., 38, 992.

Bernardini, G., et al., (Cern Spark Chamber and HLBC Groups), (1965), Nuovo Cim., 38, 608.

Bhabha, H.J. (1938) Proc. Roy. Soc., 164, 257.

Block, M.M., et al. (Cern HLBC Group), (1964), Phys. Lett., 12, 281.

Bollinger, L.M., (1951), Ph.D. Thesis, Cornell University.

Brooke, G., Hayman, P.J., Kamiya, Y. and Wolfendale, A.W., (1964), Proc. Phys. Soc., 83, 853.

Buja, Z., (1963), Acta Physica Polonica, 24, 381.

Burbidge, G.R., (1967), T.I.F.R. Summer School Lectures, Bangalore, 1966, p.150.

Burns, R., Goulianos, K., Hyman, E., Lederman, L., Lee, W., Mistry, N., Rettberg, J., Schwartz, M., Sunderland, J., and Danby, G., (1965), Phys. Rev. Lett., 15, 42.

Castagnoli, C., De Marco, A., Longhetto, A., and Penengo, P., (1965), Nuovo Cim., 35, 969.

Chatterjee, B.K., Gopalakrishnan, N.V., Murthy, G.T., Naranan, S., Sreekantan, B.V., Srinivasa Rao, M.V., Tonwar, S.C., and Vatcha, R.H., (1967), Proc. 10th Int. Conf. Cosmic Rays, Calgary; Canad. J. Phys., 46, 5131, 1968.

Cocconi, G, Koester, A., and Perkins, D.H., (1961), Int. Conf. on Theoretical Aspects of Very High Energy Phenomena (Geneva: Cern), p.128.

Coxell, H., (1961), Ph.D. Thesis, University of Durham.

Craig, R., Osborne, J.L., Wolfendale, A.W., and Young, E.C.M., (1967), Proc. 10th Int. Conf. Cosmic Rays, Calgary; Canad. J. Phys., 46, 5352, 1968: (1968a), J. Phys. A. (Proc. Phys. Soc.), (2), 1, 55.

Craig, R., Mamidzhanian, E., and Wolfendale, A.W., (1968), Phys. Lett., 26B, 468.

Crawford, D.F., and Messel, H., (1962), Phys. Rev., 128, 2352.

Creed, D.R., (1967), Ph.D. Thesis, University of Durham.

Creed, D.R., and Wolfendale, A.W., (1967), Nuovo Cim., 47, 786.

Creed, D.R., Pattison, J.B.M., Wolfendale, A.W., Achar, C.V., Narasimham, V.S., and Ramana Murthy, P.V., (1965), Proc. 9th Int. Conf. Cosmic Rays, 2, 980, 1966.

Crouch, M.F., Gurr, H.S., Jenkins, T.L., Kropp, W.R., Reines, F., Smith, F., Meyer, B., and Sellschop, J.P.F., (1966) Proc. Int. Conf. Weak Interactions, Argonne, ANL-7130.

Danby , G., Gaillard, J.M., Goulianos, K., Lederman, L.M., Mistry, N., Schwartz, M., and Steinberger, J., (1962), Phys. Rev. Lett., 9, 36.

Davis, R., Jr., (1964), Phys. Rev. Lett., 12, 303.

Davis, R., Jr., Harmer, D.S., Hoffmann, K.C., (1968), Phys. Rev. Lett., 20, 1205.

Davis, R.M., (1966), Sci. J., 5, 10, p.62.

Fowler, G.N., and Wolfendale, A.W., (1958), Prog. in Elementary Particles and Cosmic Ray Physics, (North-Holland), 4, 107.

von Gehlen, G., Nuovo Cim., (1963), 30, 859.

Ginzburg, V.L. and Syrovatsky, S.I., (1964), (Pergamon Press).

Glashow, S.L., (1960), Phys. Rev., 118, 316.

Greisen, K., (1960), Proc. Int. Conf. Inst. for High Energy Physics, Berkeley (Inter Science Publishers), p.209: (1965), Proc. 9th Int. Conf. Cosmic Rays, London, 2, 609, 1966.

Hayman, P.J., Palmer, N.S., and Wolfendale, A.W., (1963), Proc. Roy. Soc., A 275, 391

Higashi, S., Kitamura, T., Mishima, Y., Mitani, S., Miyamoto, S., Oshio, T., Shibata, H., Watanabi, K., and Watase, Y., (1962), J. Phys. Soc. Japan, (Supp. A III), 17, 362.

Kamata, K., Shibata, S., Saavedra, O., Domingo, V., Suga, K., Murakami, K., Toyoda, Y., La Pointe, M., Gaebler, J., and Escobar, I., (1967), Proc. 10th Int. Conf. Cosmic Rays, Calgary; Canad. J. Phys., 46, S72, 1968.

Keuffel, J., (1968), Proc. Utah Acad. Sci., 45, 1.

Khristiansen, G.B., Abrosimov, A.T., Atrashkevitch, V.B., Kulikov, G.V., Solovieva, V.I., Fomin, Yu. A., Khrenov, B.A., (1965), Proc. 9th Int. Conf. Cosmic Rays, London, 2, 799, 1966.

Kinoshita, T., (1960), Phys. Rev. Lett., 4, 378.

Kobayakawa, K., (1967), Nuovo Cim., 47B, 156.

Krasilnikov, D.D., (1964), Proc. Int. Conf. Cosmic Rays, Jaipur, 6, 124.

Krishnaswamy, M.R., Menon, M.G.K., Narasimham, V,S., Ito, N., Kino, S., Miyake, S., Craig, R., and Wolfendale, A.W., (1968), Proc. Moscow Conf. on Neutrinos, Lebedev Inst. (In the Press): (1969), Cern Informal Neutrino Conf., Geneva, (In the Press).

Krishnaswamy, M.R., Menon, M.G.K., Narasimham, V.S., Kawakami, S., Kino,S., and Miyake, S., (1968), Phys. Letts., 27B, 535.

Lamb, R.C., Lundy, R.A., Novey, T.B., Yovanovitch, D.D., Good, M.L., Hartung, R., Peters, M.W., and Subramanian, A., (1965), Phys. Rev. Lett. 15, 800.

Lee, T.D., Markstein, P., and Yang, C.N., (1961), Phys. Rev. Lett., 7, 429.

Lee, T.D., and Yang, C.N., (1960), Phys. Rev., 119, 1410: (1960), Phys. Rev., 126, 2239.

Markov, M.A., and Zheleznykh, I.M., (1961), Nuc. Phys., 27, 385.

Matano, T., Miura, I., Nagano, M., Shibata, S., Suga, K., and Hasegawa, H. (1965), Proc. 9th Int. Conf. Cosmic Rays, London, 2, 637, 1966.

Maze, R., Wdowczyk, J., Wolfendale, A.W., Zawadzki, A., (1969), Phys. Rev. Lett., 22, 899.

Menon, M.G.K., Naranan, S., Narasimham, V.S., Hinotani, K., Ito, N., Miyake, S., Craig, R., Creed, D.R., Osborne, J.L., and Wolfendale, A.W., (1966) Proc. 13th Rochester Int. Conf. on High Energy Physics, Berkeley: (1967a), Proc. Roy. Soc., A301, 137.

Menon, M.G.K., Naranan, S., Narasimham, V.S., Hinotani, K., Ito, N., Miyake, S., Creed, D.R., Osborne, J.L., Pattison, J.B.M., and Wolfendale, A.W., (1967c), Proc. Phys. Soc., 90, 649.

Menon, M.G.K., Naranan, S., Narasimham, V.S., Hinotani, K., Ito, N., Miyake, S., Creed, D.R., Osborne, J.L., and Wolfendale A.W., (1967), Proc. 10th Int. Conf. Cosmic Rays, Calgary; Canad. J. Phys, 46, 5344, 1968.

Menon, M.G.K., and Ramano Murthy, P.V., (1967), Prog. in Elementary Particle and Cosmic Ray Physics, (North-Holland), 9, 163.

Miyake, S., Narasimham, V.S., and Ramana Murthy, P.V., (1962), J. Phys. Soc. Japan, (Supp. A.III), 17, 318: (1964a), Nuovo Cim., 32, 1505: (1964b) Nuovo Cim., 32, 1524.

Miyazaki, Y., (1949), Phys. Rev., 76, 1733

Murota, T., Ueda, A., and Tanaka, H., (1956), Prog. Theor. Phys., 16, 482.

Narasimham, V.S., (1967), Ph.D. Thesis, University of Bombay.

Nash, W.F., and Wolfendale, A.W., (1968), Phys. Rev. Lett., 20, 698.

Oda, H., and Murayama, T., (1965), J. Phys. Soc. Japan., 20, 1549.

Osborne, J.L., and Wolfendale, A.W. (1964), Proc. Phys. Soc., 84, 901.

Osborne, J.L., Wolfendale, A.W., and Palmer, N.S., (1964), Proc. Phys. Soc., 84, 911.

Osborne, J.L., Said, S.S., and Wolfendale, A.W., (1965), Proc. Phys. Soc., 86, 93.

Osborne, J.L., (1966), Ph.D. Thesis, University of Durham.

Osborne, J.L. (1968), J. Phys. A (Proc. Phys. Soc.), (2), 1, 55.

Pattison, J.B.M., (1965), Ph.D. Thesis, University of Durham.

Perkins, D.H., (1969), Proc. Topical Conf. on Weak Interactions, CERN Report 69-7, p.1.

Price, P.B., and Walker, R.M., (1962), Nature, 196, 732: (1963), J. Geophys. Res. 68, 4847.

Reines, F., (1967), Proc. Roy. Soc., A301, 022: (1969), Proc. Topical Conf. on Weak Interactions, CERN Report 67-7, p.101.

Reines, F., Crouch, M.F., Jenkins, T.L., Kropp, W.R., Gurr, H.S., Smith, G.R., Sellschop, J.P.F., and Meyer, B., (1965), Phys. Rev.Lett., 15, 429.

Reines, F., Crouch, M.F., Jenkins, T.L., Kropp, W.R., Gurr, H.S., Smith, G.R., Sobel, H.W., Sellschop, J.P.F., and Meyer, B., (1965), Proc. 9th Int. Conf. Cosmic Rays, London, 2, 1051.

Reines, F., Kropp, W.R., Gurr, H.S., Lathrop, J., Crouch, M.F., Sobel, H.W., Sellschop, J.P.F., and Meyer, B., (1967), Proc. 10th Int. Conf. Cosmic Rays, Calgary; Canad. J. Phys., 46, 5350, 1968.

Roe, B.P., (1959), Ph.D. Thesis, Cornell University.

Rogers, I.M.R., (1965), Ph.D. Thesis, University of Durham.

Rossi, B., (1952), High Energy Particles, (Prentice-Hall): (1960), Proc. Moscow Cosmic Ray Conf., II, p.18.

Russell, F.M., (1967a), Phys. Lett., 25B, 298: (1967b), Nature, 216, p.907.

Said, S.S., (1966), Ph.D. Thesis, University of Durham.

Sheldon, W.R., Cantrell, W.G., and Duller, N.M., (1969), Phys. Rev. Lett., 27, p.312.

Silk, E.C.H., and Barnes, R.S., (1959), Phil. Mag., 4, 970.

Sternheimer, R.M., (1952), Phys. Rev., 88, 851.

Stokel, C.T., (1967), Ph.D. Thesis, University of London.

Uberall, H., (1964), Phys. Rev., 133, B444.

Veltman, M., (1963), CERN Report, 63-37, p.21.

Yamaguchi, Y., (1961), CERN Report 61-2.

Young, E.C.M. (1967), CERN Report, 67-12.

Zatsepin, G.T. and Kuz'min, V.A., (1962)., Sov. Phys. JETP, 14, 1294.

Zatsepin, G.T. and Mikhalchi, E.D., (1961), J. Phys. Soc. Japan, (Supp.AIII), 356; (1965), Proc. 9th Int. Conf. Cosmic Rays, London, 2, 997.